Generation of the Complex Spike in Cerebellar Purkinje Cells

Thesis submitted for the degree of
Doctor of Philosophy

Jennifer Thorpe Davie

University College London
2008

ProQuest LLC
789 East Eisenhower Parkway
P.O. Box 1346
Ann Arbor, MI 48106-1346

I, Jennifer Davie, confirm that the work presented in this thesis is my own. Where information has been derived from other sources, I confirm that this has been indicated in the thesis.

1st July, 2008

Abstract

Each neuron of the nervous system is a machine specialised to appropriately transform its synaptic inputs into a pattern of spiking output. This is achieved through the combination of specialisations in synaptic properties and location, passive cell geometry and placement of particular active ion channels. The challenge presented to the neuroscientist is to, within each cell type, identify such specialisations in input distribution and resulting active events, and assess their relative importance in the generation of action potential output patterns.

The Purkinje cell, in particular its response to climbing fibre (CF) input, is an excellent setting in which to attempt to meet this challenge. The Purkinje cell receives a single, easily isolated CF axon, which makes hundreds of synapses across the cell's highly branched, active dendritic tree, resulting in the generation of prominent dendritic calcium spikes and a distinctive, reproducible burst of fast action potentials (the complex spike) at the soma. In this thesis I have separated out the importance of the size of this input, its location and the active dendritic spikes it triggers in the generation of the complex spike.

I have found that, to a large extent, the complex spike pattern is determined by the size of the CF input alone. I have characterised the complex spike (its number of spikes, their timing, height and reliability) at both constant physiological frequency and across a range of paired-pulse depression causing intervals. By alternating between whole cell current and voltage clamp in the same cell, I have recorded both the complex spikes and EPSCs generated at certain paired pulse intervals. In this way I have been able to construct the EPSC - complex spike 'input - output' relationship. This demonstrated that there is a straightforward linear transformation between the EPSC input amplitude and the number and timing of spikes in the complex spike. This applies across cells, explaining a large amount of the inter-cell variability in complex spike pattern.

Input location and dendritic spikes have surprisingly little influence over the Purkinje cell complex spike. I found that complex spikes generated by dendritically distributed CF input can be reproduced by using conductance clamp to inject CF-like synaptic conductance at the soma. Both CF input and somatic EPSG injection produced complex spike waveforms that can only be easily explained by a model in which spikelets are initiated at a distant site and variably propagated to the soma. By using simultaneous somatic and dendritic recording I have demonstrated that this distant site initiation site is not in the dendrites. Somatic EPSG injection reproduced complex spikes independently of dendritic spikes, and extra dendritic spikes triggered by CF stimulation were associated with only 0.24 ± 0.09 extra somatic spikelets in the complex spike.

Rather, I have found that dendritic spikes, generated reliably by the dendritic location of CF inputs, have a role in regulating the post-complex spike pause. An extra dendritic spike generates a 3.4 ± 0.7 mV deeper AHP and a 52 ± 11 % longer pause before spontaneous spiking resumed.

In this way, I have identified specialisations that encode the size, and thus timing, of CF inputs in the complex spike burst, whilst allowing the dendritic excitation of Purkinje cells (which is strongly associated synaptic and intrinsic plasticity) to be simultaneously encoded in the post-complex spike pause. This may reflect the complex spike's proposed dual role in both controlling ongoing movement and correcting for motor errors.

Acknowledgements

This thesis is for Matt, without whom I wouldn't have wanted to do it.

I am also greatly indebted to:

Michael Häusser, for all his support throughout the many years of my PhD, from providing me with a lovely high spec rig, engaging in late night scientific debate, through to getting me to some excellent conferences.

Beverley Clark and Arnd Roth for all their detailed advice and consideration.

Ede Rancz, Paul Chadderton and Wolfgang Mittmann, my PhD brothers, for providing many and varied forms of mental stimulation.

Ikuko Smith, Spencer Smith and Tiago Branco for letting me invade their office and helping me figure out all the finer details of writing this thesis.

Latha Ramakrishnan, Kate Powell and Arifa Naeem, for all the ways they made lab life easier, and especially for their processing of biocytin filled cells.

Alanna Watt, Ian Duguid, Mickey London, Peter Latham, Julian Jack, Troy Margrie, Severine Mahon, Kamilla Angelo, Pablo Monsivais, Kazuo Kitamura, Alex Mathy, Benjamin Judkewicz, Matteo Rizzi, Sara Ho, Kate Powell, Sarah Rieubland, Jan Gruendemann, James Cottam, Lisa Beeren, Ingrid Van Welie, Jesper Sjöström, Taro Ishikawa, Misa Shimuta, Hermann Cuntz, Christian Wilms and Takayuki Michikawa for excellent discussion, warm friendship and donation of excess food during lunch.

Contents

Jan Evangelista Purkyně (1787 – 1869)
Eminent and pioneering physiologist.
Identified cerebellar Purkinje cells, cardiac Purkinje fibres and sweat glands. His work ranged from the formative study of the psychophysics of vision, through the description of the configuration of finger prints and the observation of the protein digesting power of pancreatic secretions, to the development of cell theory.

Introduction

The principle role of a neuron is to appropriately transform its synaptic inputs into a pattern of spiking output. This is achieved like clockwork through the combination of specialisations in passive geometry and active ion channels. Current flowing in through synaptic conductances changes the membrane potential of the neuron in a temporally and spatially graded manner. This is amplified, curtailed, spatially restricted or propagated by active and passive ion channel conductances. Through the specific location of ion channels of particular permeabilities, voltage sensitivities and kinetics, current input is moulded and manipulated until ultimately a distinct pattern of output action potentials is produced, abstractly representing a transformation of the input pattern.

Although many of the principles underlying this transformation have been elucidated (reviewed in many articles, including Häusser et al., 2000; Segev and London, 2000; Migliore and Shepherd, 2002; Häusser and Mel, 2003; Williams and Stuart, 2003; Gulledge et al., 2005; London and Häusser, 2005; Magee and Johnston, 2005 and outlined in the following introduction), we are not yet at the point where the spiking out pattern of a chosen neuron can be predicted given its inputs. This is an essential step if we are to achieve neuroscience's basic goal of understanding how sensory input is received, pondered upon by the brain and transformed into a pattern of muscle output.

In this thesis I have aimed to elucidate the principle factors that determine the Purkinje cell's pattern of complex spike burst production in response to its giant, distributed, dendritic spike evoking, excitatory climbing fibre input. I shall first outline what has so far been understood about how synaptic inputs are integrated in neurons, focusing in particular on excitatory input, and the generation of dendritic spikes and of bursts. I shall then highlight what is known about Purkinje cells and their climbing fibre input. Finally, I shall outline the aims of this thesis.

Single neuron computation

Passive properties

Current injected into a neuron does not uniformly alter the cell's voltage, either immediately after injection or at steady state. The cable equation, initially developed to describe propagation of electrical signals through transatlantic telegraphic cables, was first applied to dendrites by Rall (1959) and describes the manner in which current is distributed through the neuron, and the voltage changes that result.

At steady state, the local voltage change at the point of current injection is determined by the local input resistance. Steady state current flow is divided across the relatively low, lateral axial resistance of the cytoplasm and the higher resistance, short circuit, routes to earth through ion channels in the cell membrane. This results in an exponential decay of transmembrane voltage along the length of the cell which, in a cable of uniform diameter and infinite length, follows the equation:

$$V_m(x) = \frac{2I_0R_i\lambda}{\pi d^2}e^{x/\lambda}$$

(plotted in Intro. Fig. 1a), where λ, the electrotonic length constant (the distance in which voltage decays to 1/e of its initial value) is determined by both the membrane resistance and axial resistance:

$$\lambda = \sqrt{\frac{d}{4}\frac{R_m}{R_i}}$$

During transient changes in current injection, current flow is additionally divided to flow onto the cell membrane capacitance; as this capacitance charges, greater proportions of the current flows across membrane resistances and the local membrane potential approaches its steady state value. The mathematical description of this process results in the cable equation:

$$\lambda^2\frac{\partial^2V_m(x,t)}{\partial x^2} - \tau_m\frac{\partial V_m(x,t)}{\partial t} - V_m(x,t) = 0$$

where λ is, as before, the cable's length constant and τ_m is the membrane time constant, r_mc_m. This equation can be solved to describe the voltage trajectory towards steady state at any chosen distance, x, from the injection site. This trajectory takes the form of an infinite sum of multiple exponentials:

$$V(x,t) = \sum_{i=0}^{\infty}C_ie^{-t/\tau_i}$$

where the time constants τ_i are however independent of location (x), time (t) and current injection (I_0) (the slowest τ is, in fact, the membrane time constant, and faster τs depend on the length of the cable relative to λ), but the coefficients C_i are dependent on the recording location, x, and the current injection amplitude. The further the recording location, x, is from the injection site, the slower its response to a step change in current injection (Rall, 1969; Johnston and Wu, 1995).

These analytical equations were shown by Rall to apply to branched cables (Rall, 1959, 1964, 1969), so long as the total length of all branches is equal and the diameter of the branches (from the point of view of the injection site) follows the '3/2' rule:

$$d_{parent} = \sum d_{daughter}^{3/2}$$

such that the total membrane and axial resistances remain constant. Where this rule is not obeyed, or cable diameter alters, the local input impedance is changed; at such impedance mismatches the relationship of the current in the cable to the transient or steady state voltage is altered. For example, current flowing from a narrower branch to a wider branch (as is often the case as synaptic current flows from dendrites to soma) will result in a smaller depolarisation of the wider branch. In such cases, or when non-uniform distributions of passive and active, voltage and time dependent conductances are to be considered (as is the case in most neuronal processes, be they dendrites or axons), analytical solutions are usually no longer feasible. In these circumstances, the neuron can be modelled as a tree of connected isopotential compartments consisting of membrane capacitance and resistances (in parallel) and connected via resistors representing the axial resistance between compartments (Intro. Fig. 1b). The voltage trajectory can then be solved numerically (Rall, 1964); the NEURON and GENESIS modelling programmes have been developed specifically for this purpose (Hines and Carnevale, 1997, www.neuron.yale.edu, Bower and Beeman, 1998). In cases where analytical solution exists, it can be shown that as the size of these compartments reduces to 0, the solution to the continuous cable model approaches the numerical solution (Rall, 1964; Segev and Burke, 1998) .

Importance of synapse distribution

Passive cable theory predicts that the result of the neurons combined resistances and capacitances is that the voltage change at a site distant from current injection (e.g. the EPSP recorded at the soma due to dendritic EPSC) will be attenuated in amplitude and filtered in timecourse. The degree of attenuation and filtering should depend on the location of the input (distant inputs in highly branched dendrites should be most affected), the time course of the current injection (brief, rapidly rising events being most affected) and the specific properties of the dendrites. This is borne out by direct dendritic and somatic recordings (e.g. in layer V pyramidal cell apical and basal dendrites, Williams and Stuart, 2002; Nevian et al., 2007)

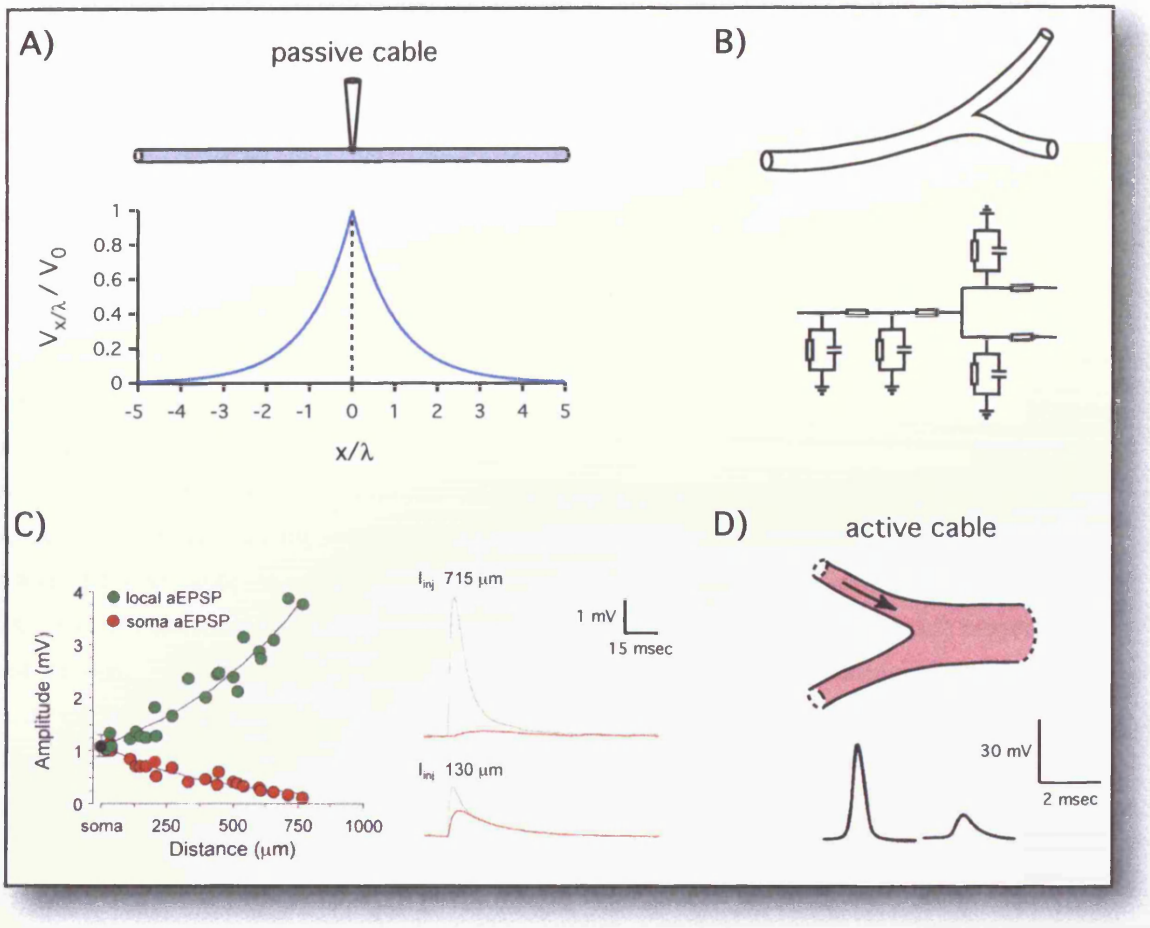

Intro. Figure 1: Passive cable properties

A) Illustration of the steady state distribution of voltage in an infinite cable (adapted from Johnston & Wu 1999).
B) Illustration of the way in which neuronal morphologies (top) can be abstractly modelled as a series of connected compartments with associated membrane capacitances, membrane resistances and axial resistances (bottom).
C) Amplitude of artificial EPSPs evoked by dendritic current injection at 0 - 800 μm from the soma (from Williams & Stuart, 2002). The local (green) and somatic (red) voltage changes are shown.
D) Illustration of failure of propagation of an active spike (generated by Hodgkin Huxley conductances) across a branch point where the geometric ratio = 10 (from Parnas & Segev 1979). Geometric ratio = $((\Sigma\ d_2^{2/3}) / d_1^{2/3})$, where d_1 is the diameter of the branch the spike is propagating from and d_2 the diameters of the branches it is propagating to.

(Intro. Fig. 1c), but can also be somewhat compensated for by synaptic and active properties (see Magee, 2000; Williams and Stuart, 2003 for a review).

Passive modelling further predicts that synapse location influences local and distant voltage change in a number of other important ways (reviewed in Segev and Rall, 1998; Spruston et al., 2008). For example, the placement of a synapse on a spine, a small (=> high resistance and low capacitance) compartment, with only a narrow, high axial resistance neck connecting it to the dendrites, should cause a much larger local voltage change in the spine head (voltage dye recordings have demonstrated this: Palmer and Stuart, 2007). Although this cannot on its own increase the voltage change at the soma (Rinzel and Rall, 1974), it may recruit active conductances in the spine head that amplify the input (Segev and Rall, 1988, 1998). As synaptic input applies conductance changes rather than current injection to, large voltage deflections in high input resistance compartments can have the disadvantage of approaching the synaptic reversal potential, so reducing the driving force for current (Intro. Fig. 2a). This is especially pertinent for inhibitory inputs, as resting Vm is usually much closer to their reversal; in these cases the main effect of the synapse is to increase the local conductance 'shunt', attenuating voltage change caused by other current sources (Intro. Fig. 2b). Synaptic shunt should similarly affect summation of both excitatory and inhibitory input to multiple synapses at electrotonically close locations. This should lead to sublinear passive summation of spatially and temporally clustered synaptic input (evidence for this is seen in Cash and Yuste, 1998, 1999; Gasparini et al., 2004; Losonczy and Magee, 2006) (Intro. Fig. 2b). Conductance shunt can also shape synaptic input once propagated to the soma. Axosomatic action potentials are associated with a brief yet large increase in conductance; this can dissipate a significant proportion of the current that reaches the soma, greatly curtailing that available to generate the EPSP (Häusser et al., 2001) (Intro. Fig. 2c).

Active dendrites

Dendritic active properties can compensate for or enhance many of the features of passive integration; the generation of supralinear active events also adds considerably to the computational power of dendrites.

Dendritic Ih, for example, has been shown to normalise the width of synaptic potentials, filtered to differing degrees by their path from different locations in the dendritic tree, and so standardise temporal integration (Magee, 1999; Berger et al., 2001; Angelo et al., 2007). Similarly, dendritic I_A can be modulated to alter the attenuation of EPSPs propagating to the soma (Hoffman et al., 1997; Cash and Yuste, 1999; Ramakers and Storm, 2002; Kim et al., 2007). An opposite 'boosting' of EPSPs can occur through activation of voltage and glutamate gated NMDA channels (Schiller et al., 2000; Polsky et al., 2004; Losonczy and Magee, 2006; Nevian et al., 2007), which, in combination with I_A and other active conductances, appears to be used to compensate for passive shunting effects in cultured hippocampal pyramidal cells,

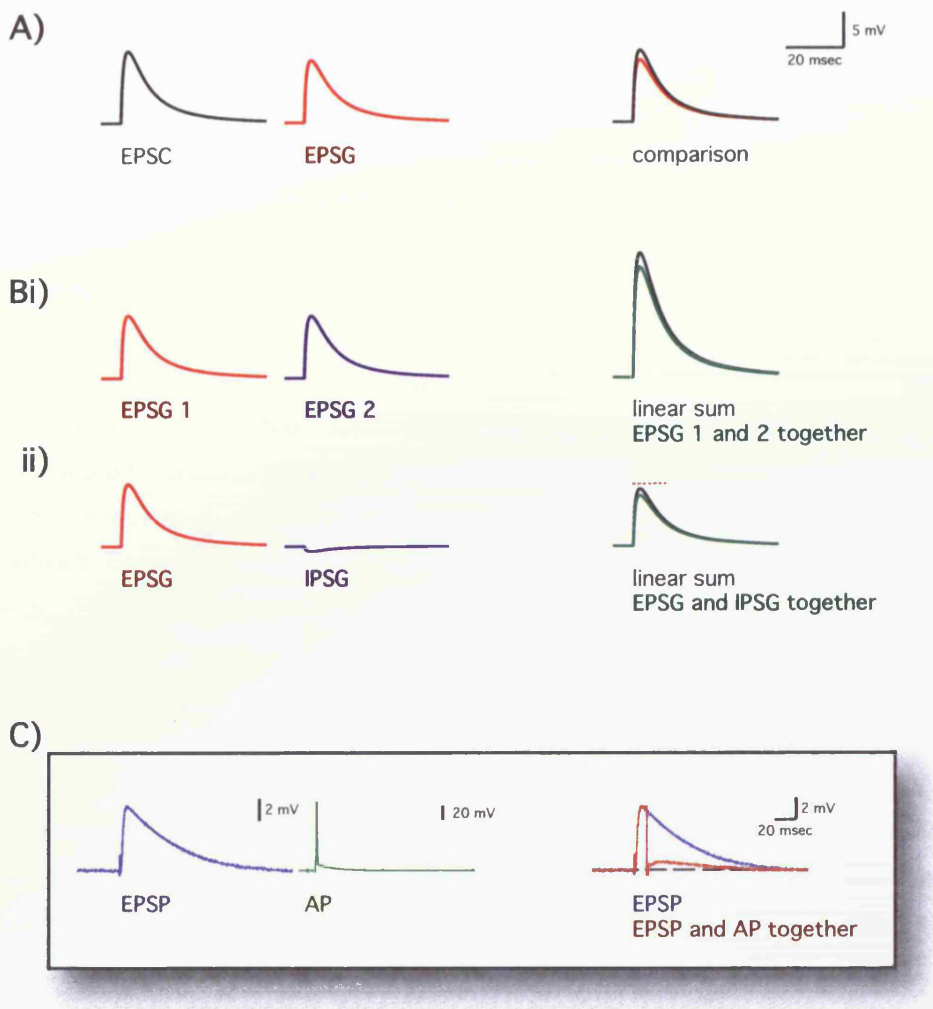

Intro. Figure 2: Effects of conductance on synaptic integration

A) EPSPs evoked by injecting a synaptic-like current waveform (left) and a synaptic-like conductance waveform (middle); overlay for comparison on right. (EPSPs recorded 200 µm from the site of injection in a 2 µm wide cable, synaptic-like waveform was biexponential with a τ_{rise} of 0.3 msec and τ_{decay} of 3 msec.)
Bi) EPSPs recorded at the same distant site following injection of an EPSG to the same site as in A (left), a second EPSG to a nearby site (2 µm distant, middle) or to both together (green trace, right). The linear sum of EPSG 1 and 2 applied separately is shown in black (right).
ii) PSPs recorded as in (Bi) except that an IPSP was injected to site 2 (middle). The black trace (right) again shows the linear sum of the two events, green, the actual combined PSP; the red dotted line marks the amplitude of the EPSP alon
C) Data (taken from Hausser, Major & Stuart, 2001) illustrating the shunting of somatic EPSPs by the somatic action potentials conductance. The somatic voltage is shown following activation of either dendritic synaptic input (left), of a somatic action potential (middle, 2 msec, 1.4 nA current pulse) or stimulation of the action potential 10 msec after the EPSP (right, shown together with the EPSP alone, for comparison).

tuning summation to linearity (Cash and Yuste, 1998, 1999, similar active compensations are seen in Gasparini et al., 2004).

Temporal and spatial summation is greatly enhanced by the presence of regenerative channels, through the generation of dendritic spikes. The rapid activation a large number of synapses clustered within the same dendritic branch can cause sufficient depolarisation to open these channels, thus generating active events and a supralinear increase in voltage, promoting axo-somatic action potential firing. These mechanisms allow individual compartments in the dendrites to report the coincident activation of synapses, and provide the elements for the neuron to behave as a 'two layer neural network', increasing the range of computations it can perform on its inputs (Poirazi et al., 2003; Polsky et al., 2004; London and Häusser, 2005). In addition, dendritic active events can be promoted by the coincidence of synaptic inputs and backpropagating action potentials (Larkum et al., 1999, 2001; Stuart and Häusser, 2001; Letzkus et al., 2006; Sjostrom and Häusser, 2006) (the extent of which can also be modulated; Spruston et al., 1995; Colbert et al., 1997; Hoffman et al., 1997; Jung et al., 1997; Xiong and Chen, 2002; Christie and Westbrook, 2003; Loftis et al., 2003; Gentet and Williams, 2007), providing a further substrate for coincidence detection.

Dendritic spikes

So far, 3 classes of dendritically initiated spikes have been observed: local NMDA spikes; rapid dendritic sodium spikes that can, given favourable circumstances, forwards propagate and prolonged dendritic calcium spikes that can support/trigger a burst of firing at the soma.

NMDA spikes have been observed in finely branched terminal dendrites: in the basal and apical oblique dendrites of layer 5 pyramidal cells (Schiller et al., 2000; Nevian et al., 2007) (Polsky et al., 2004) and the basal, radial oblique and distal tuft dendrites of CA1 pyramidal cells (Wei et al., 2001; Ariav et al., 2003; Losonczy and Magee, 2006; Losonczy et al., 2008). They occur when strong, spatially and temporally clustered synaptic stimulation, often boosted by a local dendritic sodium spike (Schiller et al., 2000; Schiller and Schiller, 2001; Polsky et al., 2004; Losonczy and Magee, 2006), provides sufficient depolarisation to relieve the Mg^{2+} block of glutamate bound NMDA receptors, triggering supralinear current influx (Schiller et al., 2000) and a local voltage plateau. This is often further prolonged by the recruitment of dendritic calcium channels (Schiller et al., 2000; Wei et al., 2001; Losonczy and Magee, 2006). Such spikes are usually confined to individual branches by the inherently local nature of the glutamate bound NMDA receptor contribution, by dendritic morphology and by potassium and K_{Ca} channel activation (Schiller and Schiller, 2001; Wei et al., 2001; Cai et al., 2004; Losonczy et al., 2008). Similarly local, calcium (non-NMDA), spikes can be generated by strong parallel fibre input to the spiny branchlets of Purkinje cells, and are again restricted by dendritic branching and BK channel activation (Vetter et al., 2001; Rancz and Häusser,

2006). In pyramidal cell, these local spikes do not often trigger axo-somatic spiking (Schiller et al., 2000) (Losonczy et al., 2008); input to selected, particularly regenerative, electrically well connected branches can reliably trigger one well timed action potential, while input to weaker branches can increase the precision of timing of spikes triggered by concomitant stimulation elsewhere in the dendrites (Ariav et al., 2003; Losonczy et al., 2008).

In contrast, fast, largely sodium current dependent spikes, often observed in larger 'trunk' dendrites, are capable of forward propagation, directly transforming into axo-somatic spikes (Stuart et al., 1997a). Their success of forward propagation is variable and depends strongly on dendritic morphology; as with other active events, they are susceptible to failure at impedance mismatched branch points (Goldstein and Rall, 1974; Parnas and Segev, 1979; Segev and Schneidman, 1999; Vetter et al., 2001) (Intro. Fig. 1d). In the apical branches of layer V and CA1 pyramidal neurons, isolated dendritic sodium spikes are often observed (Stuart et al., 1997a; Golding and Spruston, 1998; Gasparini et al., 2004), with somatic failures occurring in ~40% of the 83% of CA1 pyramidal cells where dendritic spikes could be evoked (Golding and Spruston, 1998; Gasparini et al., 2004). In the unbranched principle dendrite of olfactory bulb mitral cells, somatic propagation of dendritic spikes triggered by strong distal stimulation is highly secure (Chen et al., 1997). It is worth noting that, in all these cases, it is likely that the dendritic spike propagates forwards to trigger a spike in the low threshold axonal initiation zone, which then backpropagates to the soma (Stuart et al., 1997a; Shen et al., 1999).

The third class of dendritic spike, prolonged dendritic calcium spikes, have the most dramatic effect on axo-somatic spiking, triggering up to ~2.5 extra spikes at the soma in layer V pyramidal neurons (Williams and Stuart, 2002). Such spikes have been most heavily studied in the apical dendrites of layer V pyramidal neurons, though similar mechanisms appear to exist in e.g. inferior olive neurons (Llinas and Yarom, 1981a, b). Strong, synchronous distal synaptic input can trigger these powerful dendritic spikes (Larkum et al., 1999; Williams et al., 2002). Alternatively, the coincidence of weaker distal synaptic input and a backpropagating action potential can trigger a long lasting calcium spike, which in turn promotes further rapid somatic spiking (Larkum et al., 1999, 2001); a sequence termed 'BAC firing'. The success of BAC firing depends on coincidence of synaptic input (Williams and Stuart, 2002), depolarisation of the proximal dendrites (Larkum et al., 1999, 2001) and dendritic morphology (Schaefer et al., 2003), with both forward propagation of any initial dendritic sodium spike and backpropagation of axo-somatic action potentials being liable to fail in the proximal apical dendrite (Larkum et al., 2001; Vetter et al., 2001; Schaefer et al., 2003).

Burst generation

Bursts of somatic spikes can, however, be produced by a range of mechanisms. In its simplest form, bursting is produced by the interaction of a slowly changing process with the more rapidly cycling, spike generating mechanism (Rinzel and Ermentrout, 1998). The slow process modulates the system between a stable quiescent state, stable repetitive firing state and back again. Burst generation can thus act as a 'feature detector' signalling the occurrence of events that recruit the slow process, such as inputs of rapidly rising slope (Kepecs et al., 2002). The generation of the 'slow process' is achievable in neurons in a number of different ways. Many involve the use of a dendritic compartment and/or the slow currents generated by calcium channels, but similar effects can also be achieved by many combinations of parameters in single compartment neurons (Goldman et al., 2000; Izhikevich, 2003, 2004; Taylor et al., 2006) or in networks of recurrent excitatory and inhibitory neurons (Prinz et al., 2004).

Reduced compartmental models show that bursting can be produced by a fast spiking 'somatic' compartment partially coupled to a more slowly spiking dendritic compartment (Pinsky and Rinzel, 1994; Mainen and Sejnowski, 1996) (Intro. Fig. 3a, b). Current from the somatic spike spreads to the dendrite, triggering a slower spike, which feeds current back to the soma, supporting a burst of spiking; the limits of this mechanism have been analysed (Pinsky and Rinzel, 1994; Mainen and Sejnowski, 1996; Doiron et al., 2002). This, or a comparable, mode of bursting occurs in layer V and CA1 pyramidal cells following tonic somatic current injection (Magee, 1999; Williams and Stuart, 1999; Larkum et al., 2001), and BAC firing has strong similarities (Intro. Fig. 3c). In an interesting variation, in pyramidal cells of the electrosensory lateral line lobe, repetitive firing is terminated when backpropagation into the dendrite fails to follow the frequency of firing built up in the soma, so ceases to proved the depolarising after potential that supports somatic firing (Doiron et al., 2002; Turner et al., 2002).

One method of bursting that does not rely on dendritic spikes is that caused by T-type calcium channels. If these channels are relieved of inactivation, depolarisation can evoke a 'rebound burst' of spiking, riding on the transient T-type current (reviewed in Perez-Reyes, 2003) (Intro. Fig. 3d). This mechanism is observed in a diverse group of cells (including, curiously, many in the cerebellar circuit), such as CA1 pyramidal cells (Higashima et al., 1998), thalamic relay neurons (Deschenes et al., 1984; Jahnsen and Llinas, 1984), inferior olive cells (Llinas and Yarom, 1981a, b), cells of the deep cerebellar nucleus (Aizenman and Linden, 1999; Molineux et al., 2006), unipolar brush cells (Diana et al., 2007) and even in Purkinje cells in culture (Cavelier et al., 2002a).

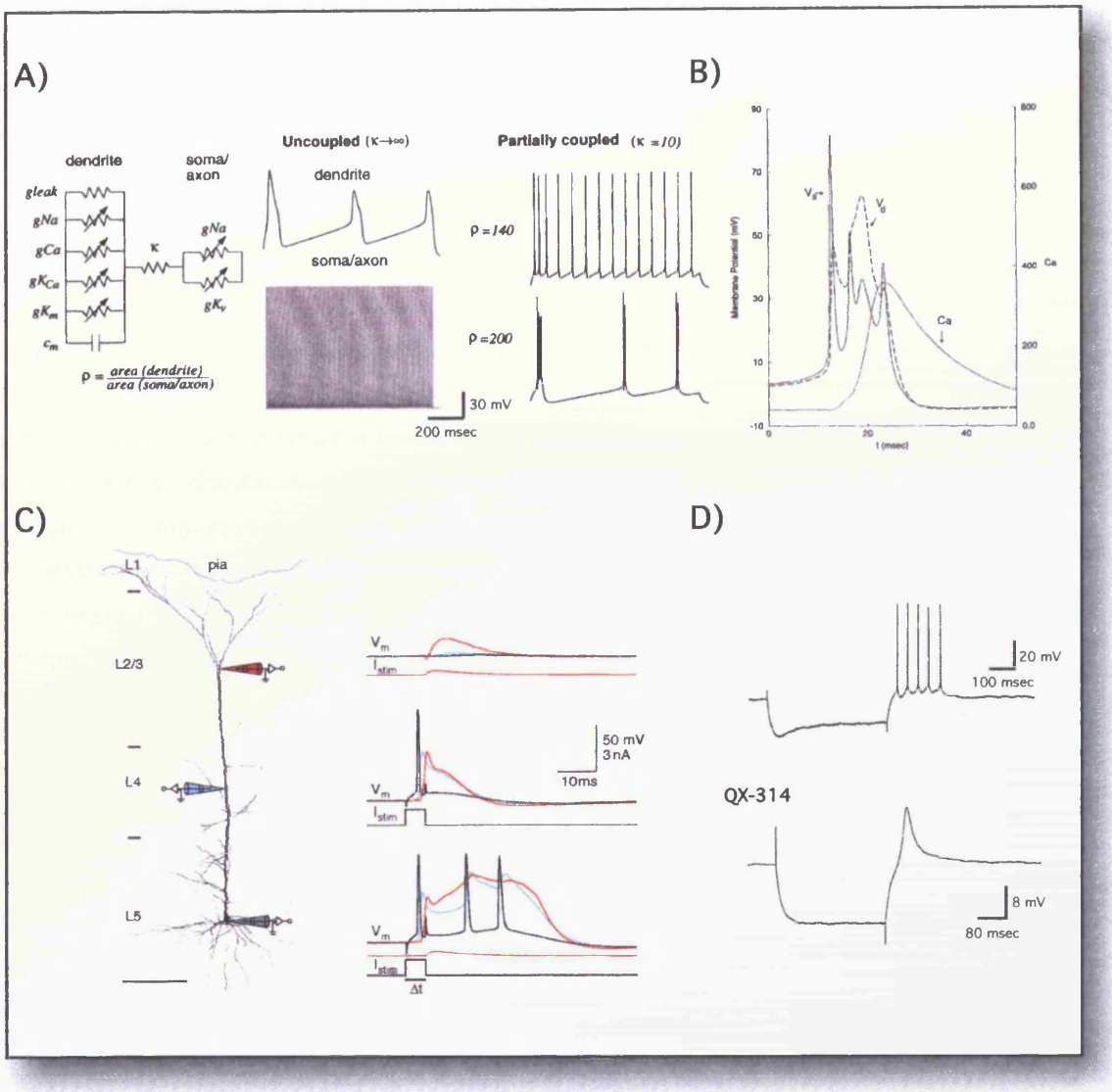

Intro. Figure 3: Neuronal Bursting

A) Illustration (from Mainen & Sejnowski, 1996) of a reduced neuronal model that, with the correct parameters, produces bursts of spikes. Model consists of two compartments, soma and dendrite (left), that, when uncoupled and allowed to fire on their own, generate fast and slow action potentials, respectively (middle). When partially coupled, tonic spiking or bursting can be produced in the soma (in response to current injection), depending on the ratio of somatic and dendritic active membrane area (right).
B) Close up of bursting produced by a similar model (from Pinsky & Rinzel, 1994), showing the somatic sodium spike burst (V_s), the dendritic calcium spike (V_d) and the calcium concentration (Ca, note different y axis, right), which terminates the burst through its activation of KCa channels.
C) Coupling of distal synaptic-like current injection (right, top) with a backpropagating action potential (right, middle) generates a dendritic spike and a burst of somatic action potentials (bottom, right) in a layer V pyramidal cell (left) (from Larkum & Sakmann, 1999). Simultaneous recordings from the soma (black electrode and traces), and apical dendrite, 400 µm (blue) and 770 µm (red) from the soma.
D) Example of a rebound burst in a DCN cell (from Aizenman & Linden, 1999) produced following relief from a hyperpolarising current step (top). The t-type calcium spike that drives this type of bursting is revealed (bottom) after block of sodium

intrinsic plasticity (Loftis et al., 2003; Losonczy et al., 2008). Physiologically relevant cha
in the way in which input is distributed and synchronised can also alter output e.g. the ch
from theta state distributed input to sharp wave clustered input in hippocampal CA1 cells
switch the cell from linear integration to coincidence detection mode (Gasparini and Ma
2006); increased perisomatic (basal dendrite) conductance can separate apical dendritic
somatic synaptic integration in pyramidal cells (Williams, 2004). Even changes in the stati
of tonic synaptic bombardment (as occurs *in vivo* Destexhe et al., 2003) can alter the sh
of the relationship between input and output. Increasing input conductance a
subtractively shifts the relationship between input current and output firing frequency (th
curve'), whereas co-varying input variance divisively alters the gain of the relationship (
and Koch, 1997; Chance et al., 2002; Mitchell and Silver, 2003). This malleability of ir
output relationships allows the same, fixed network of neurons to function in different v
(Gellman et al., 1985; Grammer, 1993; Nusbaum et al., 2001; Dean et al., 2005), extrac
different features from its input, depending on e.g. the context in which stimuli are receive
the behavioural state of the animal.

The aim of this thesis is to understand the subcellular processing that results in complex spike production following climbing fibre activation of the cerebellar Purkinje cell. Having introduced the principles of dendritic integration derived from a range of neuronal types, I shall now describe the specific properties of the system in with the complex spike is generated. I shall outline

- the position of the CF – Purkinje cell connection in the cerebellar anatomy
- the patterns of CF input activation seen *in vivo*
- the distribution and release properties of the CF synapse
- the post-synaptic receptors properties and other factors that shape the CF EPSC
- the passive behaviour of the Purkinje cell
- the firing properties of compartments within the Purkinje cell
- the active ion channels expressed that determine these firing properties
- the functional roles of CF input and complex spike generation.

These provide the building blocks of knowledge necessary to begin to question how climbing fibre input might result in the somatic complex spike burst of action potentials, and what the functional implications of this mechanism might be.

The anatomy of the cerebellum

The cerebellum is the large, horizontally foliated structure at the back of the brain, above the brainstem. It consists of a central midline structure, the vermis, paired with two lateral hemispheres and the flocculonodular lobe tucked underneath. The upper, folded surface of the cerebellar cortex surrounds a number of deep cerebellar nuclei. Inputs to and outputs from the cerebellum are made through the three connecting cerebellar peduncles.

Purkinje cells are at the heart of the cerebellar circuit (Intro. Fig. 4a). They receive the two main excitatory inputs to the cerebellum, monosynaptically through the powerful climbing fibre (CF) - Purkinje cell synapse and disynaptically through the distributed mossy fibre - granule cell - Purkinje cell connections. They are also the sole output of the cerebellar cortex, summing the excitatory and inhibitory processing of the cerebellar cortex and projecting the result to the deep cerebellar nuclei (DCN), where it makes robust inhibitory connections (Palay and Chan-Palay, 1974). Principal DCN neurons then project excitatory axons out of the cerebellum to innervate brainstem motor control areas, collectively termed the mesodiencephalic junction (De Zeeuw et al., 1998).

The cerebellar circuit is not, however, an open loop. CF axons arise from the inferior olive (IO) in the brainstem, but these axons also project collaterals to the DCN; mossy fibres make a similar branching to innervate the DCN. The DCN, in turn make connections back to the IO, with inhibitory DCN neurons projecting monosynaptically, and excitatory DCN projections feeding back disynaptically to the IO via some of the mesodiencephalic junction nuclei

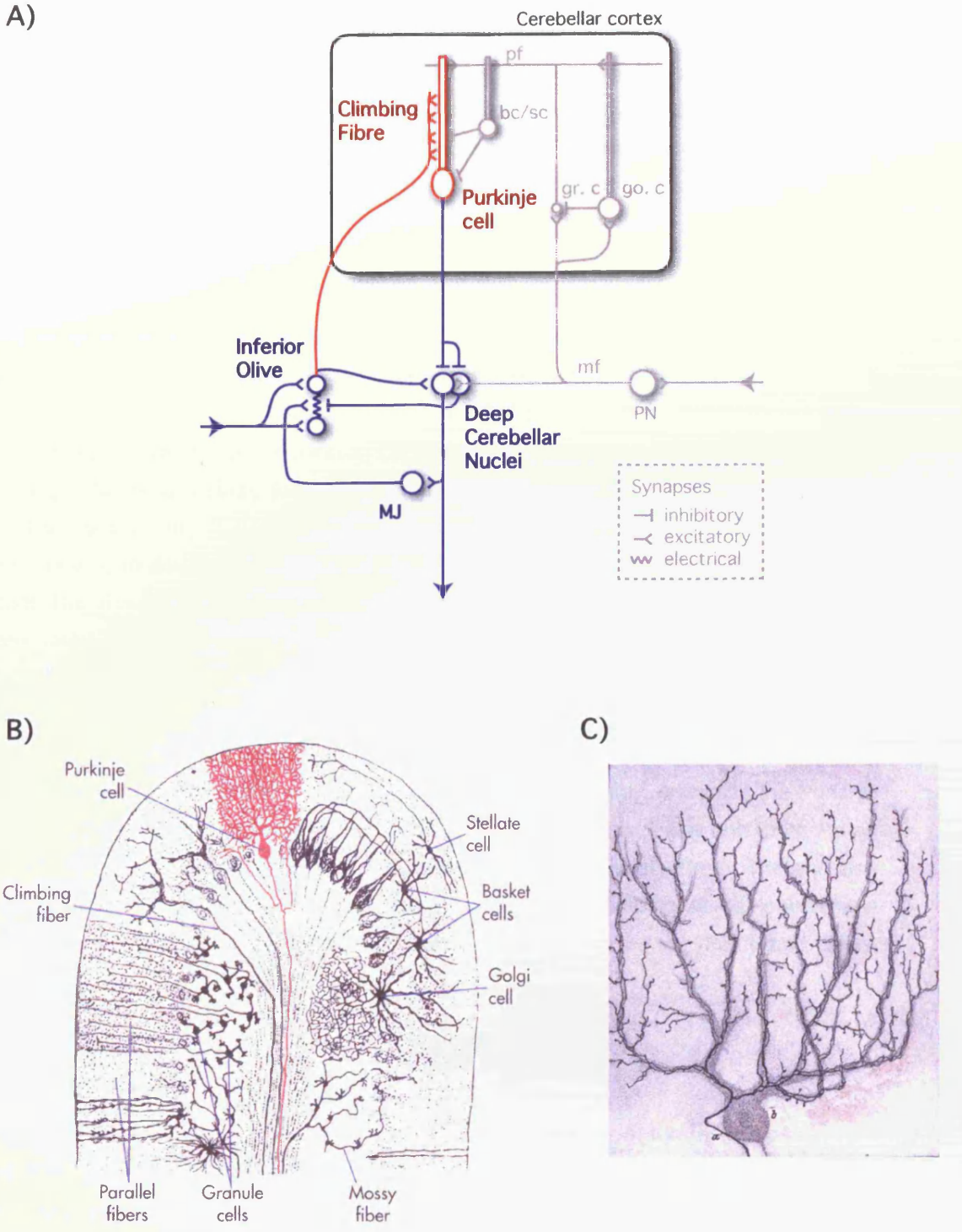

Intro. Figure 4: The anatomy of the cerebellum

A) Diagram of the olivocerebellar circuit (blue), with climbing fibre input to the Purkinje cell highlighted in red. The parallel circuit formed by mossy fibre (mf) input to the cerebellar cortex shown in gray. External sensory input (to inferior olive and pontine nuclei (PN)) highlighted by bold arrows. Abreviations: MJ – mesodiencephalic junction; PN – pontine nuclei; mf – mossy fibre; gr. c – granule cell; go. c – golgi cell; pf – parallel fibre; sc/bc – stellate cell or basket cell.
B) Illustration of the cell types of the cerebellar cortex, as revealed by Golgi staining (modified from Ramón y Cajal (1909) by Nolte (1999)).
C) Drawing by Ramón y Cajal of the tendrils of the CF axon wrapping round the Purkinje cell (drawing held by the Instituto de Neurobiología "Ramón y Cajal", Madrid, Spain).

(reviewed in Ruigrok, 1997; De Zeeuw et al., 1998; Bengtsson and Hesslow, 2006). Some DCN neurons have also been suggested to project excitatory connections back to the pontine nuclei sources of mossy fibres (reviewed in Kistler and De Zeeuw, 2003). Similarly, in the cerebellar cortex, local interneurons (mostly inhibitory) project backwards and forwards to control the excitation of granule cells and Purkinje cells (Voogd and Glickstein, 1998).

Climbing Fibre input

The neurons of the inferior olive, which project CF axons to Purkinje cells, are electrically coupled and show synchronous intrinsic oscillations (Llinas and Yarom, 1981b; Devor and Yarom, 2002b, a; Leznik et al., 2002; Long et al., 2002; De Zeeuw et al., 2003). Neighbouring IO cells project topographically to parasagittal bands of Purkinje cells, demarcated laterally by alternating aldolase C (zebrin) expression (Llinas and Sasaki, 1989; Sugihara and Shinoda, 2004; Sugihara et al., 2007; Sugihara and Quy, 2007). Their collaterals also project topographically, innervating the region of the DCN to which their Purkinje cell targets also connect. The olivocerebellar loop is closed by the topographic projection of these same DCN regions back to the appropriate IO regions (Bengtsson and Hesslow, 2006).

Individual IO axons branch, when mature, to innervate ~7 Purkinje cells each (Sugihara et al., 2001), some within the same folium, others projecting into other regions of the cortex, again orienting in a parasagittal direction. Each climbing fibre branch, again when mature, innervates only a single Purkinje cell, and does so incredibly strongly, entwining the Purkinje cell proximal dendritic tree and making hundreds of synaptic contacts (Palay and Chan-Palay, 1974), resulting in a ~200 nS peak synaptic conductance (Silver et al., 1998). There is also anatomical and increasing physiological data that suggests climbing fibres innervate a number of glial cells and inhibitory interneurons in the cerebellar cortex (Palay and Chan-Palay, 1974).

The Purkinje cell

Purkinje cells form a distinct monolayer of several millions of cells in the mature cerebellum (Palay and Chan-Palay, 1974), 200-300 μm below the surface of the cortex (Intro. Fig. 4b). They extend their dendrites upwards into the 'molecular layer', which also contains inhibitory interneurons, excitatory axons and numerous glia. Their myelinated axons project through a densely packed layer of small granule cells to the white matter tracts in the centre of the folia, and out to the DCN. In addition, CF axonal collaterals are seen to branch within the granule cell layer and project back up to the Purkinje cell layer, innervating Purkinje cells (Orduz and Llano, 2007; Watt et al., *In review*) and potentially other Purkinje layer structures (Ramón y Cajal, 1911; Chan-Palay, 1971).

The mature Purkinje cell is a planar structure, orienting its dendrites in the parasagittal plane. Usually, a single primary dendrite extends from the soma; the dendrites then branch

recursively producing first thicker main dendritic trunks and then finer 'spiny branchlets'. It is the smoother main dendritic trunk which receives CF input (in fact onto small stubby spines), and the spiny branchlets, which as their name suggests have abundant synaptic spines, which receive the axons of granule cells. These are both the ascending axons of granule cells, projecting upwards with the Purkinje cell, and their later perpendicularly bifurcated collaterals/branches, termed parallel fibres because of their striking parallel alignment in the molecular layer, projecting several mm horizontally across the planes of many hundred Purkinje cell's dendrites. It is estimated that the parallel fibre synaptically contacts every second Purkinje cell, and that, in the rat, each Purkinje cell receives ~200,000 granule cell synapses (Palay and Chan-Palay, 1974; Napper and Harvey, 1988). These synapses are all either weak (< 30 pA), or functionally silent (Isope and Barbour, 2002).

Cerebellar cortex interneurons

A number of interneurons interpose between the mossy fibre – granule cell – Purkinje cell connection, forming feedforward and feedback loops that shape excitatory input (Voogd Glickstein 1998). Golgi cells, which inhibit granule cells, receive feedforward mossy fibre and feedback parallel fibre input. Stellate cells, which inhibit Purkinje cell dendrites and basket cells, which inhibit Purkinje cell somata and axons, both receive feedforward parallel fibre input. A number of other, rarer interneurons exist, such as the unipolar brush cells that amplify mossy fibre input to the granule cell layer, and Lugaro cells which inhibit Purkinje cells (Dean et al., 2003).

The DCN

Purkinje cells project, again topographically, to a number of distinct deep cerebellar nuclei, including the dentate, fastigius, interpositus and lateral vestibular nuclei (Chan-Palay, 1977). These amorphous structures contain both inhibitory and excitatory projection neurons, as well as local interneurons. Work is ongoing to identify the subtypes of neurons present in the DCN (Sekirnjak and du Lac, 2002; Sekirnjak et al., 2003; McKay et al., 2006; Molineux et al., 2006; Gittis and du Lac, 2007, 2008).

At least 30 Purkinje cell axons are estimated to converge onto one DCN cell (Chan-Palay, 1977). These form large, multirelease site synapses, mostly at the DCN cell somata (Chan-Palay, 1977; Telgkamp and Raman, 2002).

The monosynaptic and disynaptic connections from the DCN to the inferior olive are made onto the gap junction containing dendritic spines which connect IO neurons, thus providing an excellent mechanism whereby the general level of input excitation and the coupling of groups of IO neurons might be controlled (De Zeeuw et al., 1998; Devor, 2002; Bengtsson and Hesslow, 2006). The excitatory projections from the DCN are the principle output of the cerebellum.

Climbing Fibre input patterns

The *in vivo* rate of CF input to individual Purkinje cells is low. Complex spikes are triggered at a frequency of ~1 Hz, on average, though this can vary from cell to cell, and there is considerable intracell irregularity (Eccles et al., 1967; Bell and Grimm, 1969; Armstrong and Rawson, 1979). Inter complex spike intervals can typically be as low as 50 - 100 ms or as long as 3 s (Eccles et al., 1967; Bell and Grimm, 1969; Armstrong and Rawson, 1979). Although Purkinje cells are mono-innervated by single CFs, and Eccles et al. (1966a) demonstrated that a single presynaptic CF action potential/stimulation is sufficient to trigger a complex spike, CF input is not always received as discrete, single spikes. As IO cells can intrinsically generate bursts (Crill and Kennedy, 1967; Llinas and Yarom, 1981a, b), CF input often consists of a burst up to 6 spikes at interspike intervals of ~2 ms (Armstrong et al., 1968; Armstrong and Rawson, 1979; Maruta et al., 2007). This bursty input can be seen in the bursts of EPSPs that remain once *in vivo* Purkinje cell sharp electrode recordings degrade beyond spike generation capability (Eccles et al., 1966a; Armstrong and Rawson, 1979; Maruta et al., 2007). Estimates of the fraction of IO output that is bursty vary from ~1/3 (Armstrong and Harvey, 1966) to >70 % ((Maruta et al., 2007), see also (Armstrong and Rawson, 1979)). This fraction has also been found to vary with sensory stimulation, and with the interval between CF events (Maruta et al., 2007), with bursts been less common and composed of fewer spikes at short inter-event intervals. Armstrong and Rawson (1979) found that the variance of the number spikelets in the complex spike was usually less than the variation in the number of EPSPs that remained in a decayed sharp electrode recording. The direct relationship between the number of CF inputs in a burst, or the interval between CF events and the Purkinje cell complex spike has not been fully explored.

The Climbing Fibre to Purkinje cell synapse

The mature CF to Purkinje cell synapse is a remarkable connection, in terms of its strength, its distribution and its singularity. After the ~P15 (in both rats and mice), most Purkinje cells are innervated by only a single axon from the inferior olive. This branches, following and entwining the dendritic arborisations of the postsynaptic Purkinje cell, making hundreds of synaptic contacts in the dendrites. These synapses release, with a high probability, glutamate onto postsynaptic AMPA receptors, generating an enormous excitatory post synaptic potential (EPSC).

Development of the CF synapse

The unitary, closely entwined, dendritic distribution of the CF - Purkinje cell connection is the result of dynamic axonal and dendritic outgrowth together with synapse formation and pruning

during their co-development. Differentiating Purkinje cells migrate into the cerebellar anlage from the metencephalic neuroepithelium to meet axons from the nascent inferior olive (Hatten and Heintz, 1995). From as early as embryonic day 19, they are multiply innervated by a large number of widely ramifying inferior olive axons, which synapse perisomatically on the short, thin dendrites that radiate in all directions from the Purkinje cell somata (Morara et al., 2001; Lohof et al., 2005; McKay and Turner, 2005). In the early postnatal days (P2 - P5) electrophysiological measurements resolve at least 3 - 4 CF separate inputs to a Purkinje cell (Mariani and Changeux, 1981; Hashimoto and Kano, 2003; Scelfo and Strata, 2005), and anatomical evidence suggests that there are as many as 14 CFs per Purkinje cell (Sugihara, 2005). Between the 5^{th} to 10^{th} postnatal days, multiple innervation is greatly reduced and a single CF input begins to dominate in strength over its competitors (Mariani and Changeux, 1981; Hashimoto and Kano, 2003; Scelfo and Strata, 2005). Anatomically, there is a reduction of the number of CFs in the cerebellum, and 'nest' like specialisations of CF ramifications and swellings form around Purkinje cell somata during the second postnatal week (O'Leary et al., 1970; Sugihara, 2005, 2006). During this period, the developing Purkinje cell retracts its multiple, unoriented dendrites and extends a single primary dendrite into the molecular layer; CF innervation follows, moving into the dendrite (Ramón y Cajal, 1911; O'Leary et al., 1970; Mason et al., 1990). Multiple innervation initially persists, with at least two CFs synapsing in overlapping areas in the dendrites (Scelfo and Strata, 2005), but as some CFs become strengthened to cause calcium entry across the dendrites, the weaker input's Ca^{2+} influx becomes confined to the very proximal dendrites and soma (Hashimoto and Kano, 2003). From ~P10 onwards, elimination of the remaining few weaker inputs continues in a distinct second stage, which is dependent on the presence of parallel fibres, NMDA receptor triggered activity presumably in these presynaptic cells, and the on the mGluR1 to PKC pathway downstream of parallel fibre activity in Purkinje cells (reviewed in Hashimoto and Kano, 2005). By the beginning of the third postnatal week, in both rats and mice, the majority of Purkinje cells are innervated by a single CF (Mariani and Changeux, 1981; Scelfo and Strata, 2005). From this stage onwards the CF shows its mature distribution, wrapping around the main Purkinje cell dendritic branches in the proximal ~2/3rds of the molecular layer, with few remaining functional contacts at the soma (Palay and Chan-Palay, 1974; Mason et al., 1990; Chedotal and Sotelo, 1992; Nishiyama and Linden, 2004; Scelfo and Strata, 2005) (Intro. Fig. 5a). Even in adulthood, however, some form of plasticity of this synapse remains, as high levels of stimulation of the CF itself can depress CF input amplitude (Hansel and Linden, 2000).

CF distribution

Throughout this development, the Purkinje cell has extended and elaborated its highly branched, planar dendritic tree (Altman, 1972; Berry and Bradley, 1976; Roth and Häusser, 2001; McKay et al., 2005). A mature rat Purkinje cell dendritic tree reaches >200 μm to the

surface of the cerebellar folium and >200 μm horizontally, branching recursively within this area (Berry and Bradley, 1976; Roth and Häusser, 2001; McKay and Turner, 2005). The spines of its fine terminal spiny branchlets are occupied by ~200,000 parallel fibre synapses (Palay and Chan-Palay, 1974; Napper and Harvey, 1988), confining the ~300-500 climbing fibre contacts to the thicker dendritic trunks, the proximal ~2/3 of the dendrites (Palay and Chan-Palay, 1974) (Intro. Fig. 5a). The large (~2 μm diameter) CF axon follows the main Purkinje dendrites, with fine axonal 'tendrils' extending to ensheath the main dendrites in a network of varicosities (Ramón y Cajal, 1888; Palay and Chan-Palay, 1974; Xu-Friedman et al., 2001). Eccles et al. (1966) have estimated, from their recordings at different depths of the molecular layer, that the CF action potential spreads through its terminal arbour at 150-500 μm/ms. The CF axonal varicosities are packed with hundreds of excitatory synaptic vesicles (Intro. Fig. 5b), and are invaded by clusters of 1-6 short, stubby 'thorn' like spines extending from the Purkinje cell dendrite, onto which the CF synapses are made (Palay and Chan-Palay, 1974; Xu-Friedman et al., 2001). Anatomical estimates indicate that the average separation of these clustered thorns is 7μm, and that ~300 synaptic contacts are made (Llinas et al., 1969b); quantal analysis suggests this is an underestimate, calculating ~500 functional release sites (Silver et al., 1998).

CF synaptic release

Each of the several hundred CF synaptic contacts has an extremely high release probability, estimated by quantal analysis to be ~0.9 in physiological extracellular calcium concentrations (Silver et al., 1998). This is due to both a high release probability for each vesicle (Foster et al., 2002) and a large number of readily releasable vesicles (on average 7 vesicles are docked at the presynaptic membrane, (Xu-Friedman et al., 2001)) (Intro. Fig. 5c). Together, these factors also combine to result in multivesicular release (Wadiche and Jahr, 2001) and a high concentration of glutamate in the synaptic cleft, usually sufficient to cause postsynaptic receptor saturation (Foster et al., 2002; Harrison and Jahr, 2003; Foster and Regehr, 2004). This mature, adult situation develops through an increase in multivesicular release at synapses with already high individual vesicular release probability (Hashimoto and Kano, 2003). Multivesicular release causes both highly reliable transmission and, to some extent, mitigates the high level of paired pulse depression seen at this synapse (Eccles et al., 1966d; Latham and Paul, 1971; Konnerth et al., 1990; Perkel et al., 1990; Dittman and Regehr, 1998; Hashimoto and Kano, 1998; Silver et al., 1998). Paired pulse depression, where a second stimulation of the synapse closely following the first results in a smaller postsynaptic EPSC, is a common feature of many high release probability synapses, due to depletion of their readily releasable pool of vesicles (Betz, 1970; Dittman et al., 2000; Foster and Regehr, 2004; Xu-Friedman and Regehr, 2004). At CF synapses, under physiological temperature and calcium, EPSC paired pulse depression of >40% is seen at interstimulus intervals of <40 ms (Dittman and Regehr, 1998; Hashimoto and Kano, 1998) (Intro. Fig. 5d). Although this reduction is

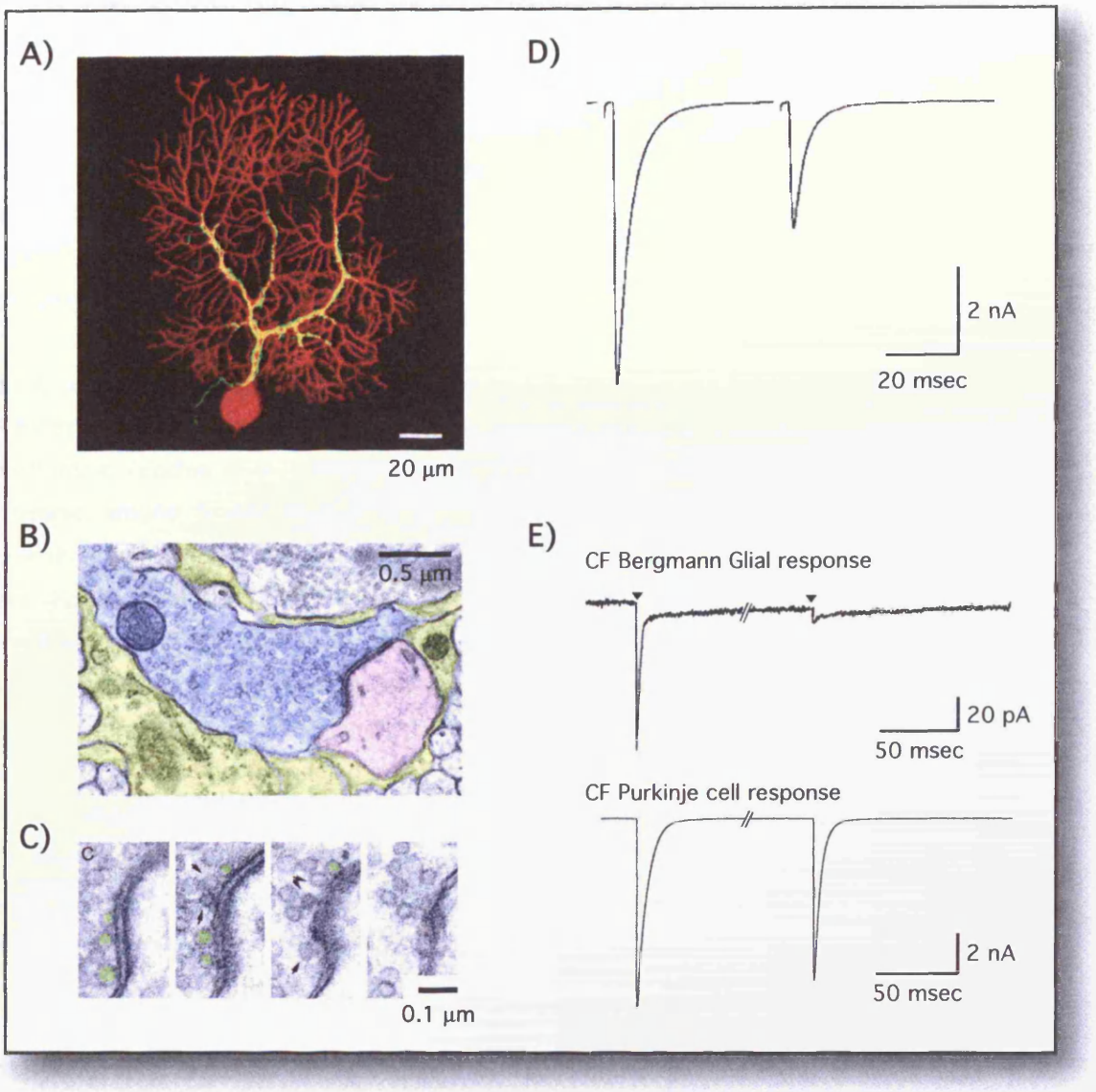

Intro. Figure 5: The Climbing Fibre - Purkinje cell synapse

A) Image (taken from Kreitzer et al., 2000) of a fluorescently labelled Purkinje cell (red) and its innervating climbing fibre (green). Purkinje cell labled by Alexa Fluor 568 hydrazide via a patch pipette, climbing fibre labled by calcium green dextran injection into the inferior olive.
B) Electron microscope image (taken from Xu-Friedman et al., 2001) illutrating the large number of vesicles in a CF presynaptic bouton (shaded blue) where it synapses onto a Purkinje cell spine (pink). Surrounding astrocytic processes shaded yellow.
C) Serial EM sections of the active zone of the synapse shown in (B) (from Xu-Friedman et al., 2001). Docked vesicles (directly touching the presynaptic membrane) are highlighted in green, nondocked vesicles labelled with arrows.
D) Example (taken from Silver et al., 1998) of the prominent paired pulse depression of CF – Purkinje cell EPSCs (interstimulus interval 50 msec, recording made at room temperature).
E) An experiment (taken from Harrison & Jahr, 2003) illustrating the effect of Purkinje cell post-synaptic receptor saturation in response to multivesicular release at the CF synapses. The incredibly large degree of depression of glutamate release from the CF is seen in extrasynaptic Bergmann Glial responses (top), but is partially masked by AMPA receptor saturation in the Purkinje cell response (bottom).

substantial, it is considerably less than the synapse's >75% depression of glutamate release, as postsynaptic AMPA receptor saturation following the first stimulation masks the full presynaptic effect (Foster et al., 2002; Harrison and Jahr, 2003; Foster and Regehr, 2004) (Intro. Fig. 5e). Recovery from paired pulse depression occurs with a triple exponential time course at the CF synapse, the fast component of which has a time constant of ~40 ms (though this rate, and its amplitude, is calcium dependent) and the intermediate component of ~1.2 s at 35 °C (the third, even slower component was not quantified at this temperature) (Dittman and Regehr, 1998).

CF post-synaptic receptors

The large concentrations of glutamate released by CF synapses are received principally by AMPA receptors. Initial investigations had shown that CF EPSPs have a linear current voltage (IV) relationship (Eccles et al., 1966a); voltage clamp later confirmed this and showed that they reverse around 0 mV (Perkel et al., 1990; Llano et al., 1991). Pharmacological experiments have demonstrated that the bulk of the CF EPSC is sensitive to AMPA receptor blockers (Konnerth et al., 1990; Perkel et al., 1990). It was thought that functional NMDA receptors were not present in Purkinje cells (Perkel et al., 1990; Farrant and Cull-Candy, 1991; Llano et al., 1991), however, recently it has been found that, in mice, a small NMDA receptor current appears with development (becoming observable at 3 weeks, and increasing to a few 100 pA in adulthood), adding an after-depolarisation to the CF response (Piochon et al., 2007). Further, immunocytochemistry and electrophysiology has shown the presence mGluR1 metabotropic glutamate receptors at the CF synapse (Nusser et al., 1994; Petralia et al., 1998), though these contribute at most only a few 10s of pA of current to the normal CF response, only becoming significant when glutamate uptake is blocked (Dzubay and Otis, 2002).

The AMPA receptor subunits of the Purkinje cell have been identified and characterised though a combination of PCR, immunocytochemistry, calcium imaging and electrophysiology. Single cell PCR has found that, of the four AMPA receptor subunits that can combine to form a functional ion channel, GluRs 1, 2 and 3, but not 4, are expressed in Purkinje cells, both in culture (Lambolez et al., 1992; Brorson et al., 1999) and in acute slices (Tempia et al., 1996). Light and electron microscopy of immunostaining has confirmed the presence of GluR 1, 2 and 3 in the Purkinje cell at both parallel fibre and CF synapses, and has found no evidence of the presence of GluR 4 (Baude et al., 1994; Bergmann et al., 1996; Petralia et al., 1998; Ripellino et al., 1998). Of these subunits, the highest expression levels (~70%, Lambolez et al., 1992; Brorson et al., 1999) are of GluR2. The result of this is to ensure that most Purkinje cell AMPA receptors contain a GluR2 subunit, giving the CF EPSC its linear, non-rectifying IV relationship (Bowie and Mayer, 1995; Kamboj et al., 1995). More pertinently, it gives the net response to glutamate a very low level of calcium permeability (Jonas and Burnashev, 1995),

as assessed by Ca^{2+} imaging (Tempia et al., 1996) and electrophysiological measurement of reversal potential during ion substitution experiments (Häusser and Roth, 1997b; Brorson et al., 1999). CF EPSCs have similar properties (linear IV, low Ca^{2+} permeability) throughout development, indicating that their postsynaptic receptor composition is likely to be similar (Tempia et al., 1996; Momiyama et al., 2003). The low Ca^{2+} permeability of the CF synapse, due to low levels of NMDA receptor expression and the high levels of GluR2, have important implications for the manner in which CF excitation causes associative synaptic plasticity, which will be discussed later.

Purkinje cell AMPA receptor kinetics and density have been characterised electrophysiologically. Measurements of the macroscopic current in outside-out patches pulled from the soma or dendrites of P12-18 Purkinje cells have been used to create a kinetic model of the AMPA current, firstly at room temperature (Häusser and Roth, 1997b) and later at more physiological temperatures (Wadiche and Jahr, 2001). Among other features, the model reflects the channels' rapid desensitisation and their single channel conductance of ~8pS; AMPA receptors *in situ* in the post-synaptic membrane may however show different properties (e.g. slower desensitisation and faster recovery from desensitisation (DiGregorio et al., 2007)). Analysis of spontaneous and miniature EPSCs in whole cell recordings of P2-4 Purkinje cells reports a quantal synaptic conductance of ~300 pS, due to glutamate acting on postsynaptic densities containing >66 AMPA receptors (Momiyama et al., 2003). Similar numbers of AMPA receptors have been counted at immature (10 – 207 receptors) and mature (69 ± 43 receptors) CF synapses using sensitive immunogold labelling of freeze fractured sections (Tanaka et al., 2005; Masugi-Tokita et al., 2007). This, together with the observation that the concentration of glutamate released by a single vesicle remains constant from at least P3 onwards (Hashimoto and Kano, 2003), is in accord with quantal conductance remaining similar at ~0.55 nS (Silver et al., 1998). Although the later number may be an underestimate of the synaptic conductance, due to poor voltage clamp of distant synaptic events (the 'space clamp' problem, Spruston et al., 1993; Williams and Mitchell, 2008), it is approximately consistent with the ~200 nS conductance (also measured somatically, with similar associated errors) caused by activation of the whole CF axon, releasing glutamate at ~500 contacts with a synaptic release probability of ~0.9 (Silver et al., 1998).

The CF EPSC

The result of the near coincident, high probability, multivesicular release of saturating concentrations of glutamate onto these hundreds of AMPA receptor containing synapses is an enormous post-synaptic current. Although the ability to faithfully record such large, distributed currents is limited both by the quality and speed of somatic voltage clamp and by the poor space clamp of the highly branched Purkinje cell dendritic tree (Roth and Häusser, 2001; Spruston, 2003; Williams and Mitchell, 2008, discussed further in the discussion of Chapter 1), the CF input is estimated to be ~ 200 nS, resulting in EPSCs of several nA at

resting membrane potentials. Reports of amplitude measured under slightly differing conditions range from ~2-4 nA (Konnerth et al., 1990; Hashimoto and Kano, 1998; Hansel and Linden, 2000), through ~6-12 nA (Llano et al., 1991; Silver et al., 1998; McKay et al., 2005) up to ~10-20 nA (Dittman and Regehr, 1998; Wadiche and Jahr, 2001) (all values normalised to -70 mV). Thus, the CF-Purkinje cell connection is one of the largest in the nervous system. Its kinetics have been most accurately characterised using voltage jump experiments (Häusser and Roth, 1997a; Wadiche and Jahr, 2001), in which the sensitivity of the recorded EPSC to step changes in voltage made throughout its timecourse is used to infer the continued activation of the synaptic conductance. A rise time of 0.22 ± 0.7 ms and a biexponential decay time course of τ_{fast} 1.3 ± 0.7 ms (57.4 ± 25 %) τ_{slow} 5.0 ± 0.9 ms was reported at 32-35 °C (Wadiche and Jahr, 2001). This gives a weighted mean single exponential decay (2.9 ms) slightly faster than that reported under voltage clamp at similar temperatures (Hashimoto and Kano, 1998; McKay et al., 2005), and parameters around twice as fast as recorded at room temperature (Silver et al., 1998 (double exponential decay), Perkel et al., 1990; Llano et al., 1991; Barbour et al., 1994; Takahashi et al., 1995; Dittman and Regehr, 1998).

The relatively slow time course of the CF EPSC is determined both by the desensitisation of the postsynaptic AMPA receptors and by the timecourse of glutamate in the synaptic cleft (Barbour et al., 1994; Takahashi et al., 1995). Addition of drugs which slow the desensitisation of AMPA receptors, prolongs the CF EPSC (Barbour et al., 1994; Takahashi et al., 1995; Takayasu et al., 2005), confirming that the desensitisation measured in outside out patches (Häusser and Roth, 1997b; Wadiche and Jahr, 2001), while not necessarily accurately reflecting synaptic AMPA receptor kinetics (DiGregorio et al., 2007), does play a role in sharpening CF EPSC decay. This prolongation of the EPSC also suggests that glutamate may be present long enough in the cleft to cause continued AMPA receptor activation in the absence of desensitisation (though this is complicated by the drugs' additional effects on AMPA receptor deactivation and glutamate affinity (Patneau et al., 1993; Yamada and Tang, 1993; Barbour et al., 1994)). The clearance of glutamate from the synaptic cleft is not left only to diffusion; glutamate transporters in the perisynaptic Purkinje cell membrane (Takahashi et al., 1996; Otis et al., 1997; Tanaka et al., 1997) and in the ensheathing Bergmann glial membrane (Chaudhry et al., 1995; Bergles et al., 1997; Clark and Barbour, 1997) increase the rate of removal of the neurotransmitter. Either pharmacologically blocking or genetically knocking out these transporters slows the CF EPSC (Barbour et al., 1994; Takahashi et al., 1995; Takayasu et al., 2005; Takatsuru et al., 2006). Purkinje cell EAAT4 transporters operate more slowly, determining the slow tail of the EPSC, while Bergmann glial cell GLAST and GLT-1 transporters operate on a similar timescale to AMPA receptor desensitisaion (Otis et al., 1997; Auger and Attwell, 2000; Brasnjo and Otis, 2004; Takayasu et al., 2005; Takatsuru et al., 2006).

The CF - Purkinje cell synapse: a uniquely specialised connection

The CF - Purkinje cell synapse is remarkable in terms of its size, distribution, release probability, receptor expression and kinetics. Throughout the nervous system, there are relatively few examples of such large, reliable synapses. These, often labelled "detonator synapses", tend to occur where the faithful, temporally accurate transmission of information is required, and can be seen as little more than an effective 'relay' between cells. Examples of such high release probability, effective synapses include the calyx of Held (which accurately relays high frequency auditory input to higher brain areas (Borst et al., 1995; Taschenberger and von Gersdorff, 2000)), the neuromuscular junction (which causes the rapid, dependable contraction of the muscle, end effector of all prior neuronal processing (Katz, 1966; Ruff, 2003)) and the Drosophila olfactory receptor neuron – projection neuron synapse (which creates a sharp onset, high signal to noise olfactory signal (Kazama and Wilson, 2008)). In most of these cases, unambiguous binary transmission is achieved by the precise triggering of a single spike. In the calyx of Held, for example, this may be aided by the location of the synaptic input, clasped around the postsynaptic cell's soma, electrotonically close to the spike generation site, together with especially brief EPSCs (Taschenberger and von Gersdorff, 2000). In contrast, the CF 'detonator synapse' reliably amplifies presynaptic input into a burst of precisely timed spikes, generating a salient 'feature' in the Purkinje cell's spike train, which has the potential to encode (through modification of the burst) more than just the occurrence of the input. Potentially, features of the Purkinje cell's passive and distributed active properties, outlined in the next section, help it achieve this amplification.

Purkinje cell properties

The complex spike is the result of the combination of the giant, distributed CF input with the active and passive properties of the Purkinje cell. Decades of study have created a wealth of data (outlined below) describing the Purkinje cell. Its highly branched geometry and passive characteristics have been detailed. A large amount is known about the ion channels it expresses, their biophysical properties and how they are distributed. Together, these equip the Purkinje cell to spontaneously fire axosomatic sodium spikes and to be capable, giving suitable current stimuli, of firing at very high axosomatic firing frequencies, of intrinsically generating bursts and of generating prominent dendritic calcium spikes. However, this information, which has been incorporated into some of the most biophysically accurate models developed to date, has failed to provide a complete understanding of how the complex spike is generated (Schmolesky et al., 2002).

Purkinje cell passive structure

The timecourse and amplitude of the EPSC recorded at the soma, and of the resulting depolarisation in the soma and dendrites is determined in part by the geometry of the Purkinje cell dendritic tree. With development, Purkinje cells become progressively more branched, increase in dendritic surface area (to >12,000 um^2) and decrease in somatic input resistance (to <20 MΩ), reaching near adult levels after P18 (Roth and Häusser, 2001; McKay and Turner, 2005). As CF synapses are distributed across these highly branched dendritic trees, the synaptic current must be transmitted along the leaky electrical cable of the dendrites towards the soma (see cable theory section earlier).

Although even mature Purkinje cells are electrically compact at steady state, the large capacitance of the dendritic tree and the many points of impedance mismatch created by its highly branched structure mean that brief inputs are greatly attenuated and slowed in time course by their propagation to distant sites (Rall, 1964; Rapp et al., 1994; Roth and Häusser, 2001; Vetter et al., 2001). At P21, the distal tips of Purkinje cell dendrites are ~0.3 λ from the soma, meaning that the leak of the relatively short, high membrane resistance dendrites causes a maximum tonic voltage attenuation from soma to dendrites to only 74% (Roth and Häusser, 2001). However, steady state attenuation from dendrites to soma is worse (due to impedance mismatch being worse when viewed from points in the dendrites), with <25% of the voltage at the distal tips of the dendrites propagating to the soma (though from the main dendrites, attenuation is to only >75%). Transient voltage changes are far more poorly propagated to distant sites. In these cases, it is the capacitance increase at branch points that is particularly unfavourable to propagation. Membrane capacitance causes voltage changes at distant sites to occur more slowly (Rall, 1969, see also earlier cable theory section), so that, if not fully charged before the end of the transient, their peak (steady state) voltage is not reached i.e. their voltage change is attenuated. The increase in membrane area at most branch points makes this charging particularly slow, and passive attenuation of transients in Purkinje cells particularly great (Vetter et al., 2001). Further, because of these factors, branch points are particularly unfavourable to propagation of active events, as, past the branch point, voltage changes are often not fast enough or large enough to cross threshold for continued spike generation (Goldstein and Rall, 1974; Parnas and Segev, 1979; Segev and Schneidman, 1999; Vetter et al., 2001). In the case of Purkinje cells, parallel fibre EPSPs from the spiny dendrites are greatly attenuated in their propagation to the soma (Roth and Häusser, 2001), fast axo-somatic spikes are poorly and passively propagated into the dendrites (Stuart and Häusser, 1994; Vetter et al., 2001), and brief action potentials in the dendrites are predicted to forwards propagate to the soma poorly (Vetter et al., 2001).

Although similar constraints apply to the CF EPSC, the wide distribution of many synapses in the larger, more proximal dendrites may help mitigate these effects through the rapid, local charging of the dendritic capacitance, the reduction of axial current flow at branch points due to distributed depolarisation and their favourable location on electrotonically close, low axial

resistance dendrites. In fact, voltage jump measurements of the time course of the EPSG give decay time constants (of τ_{fast} 1.3 ± 0.7 ms (57.4 ± 25 %) and τ_{slow} 5.0 ± 0.9 ms (Wadiche and Jahr, 2001)) that do not differ significantly from those of the EPSC measured by somatic voltage clamp. This suggests that dendritic filtering does not significantly alter the recorded EPSC time course; the resulting EPSP will of course be filtered by the time constants of the cell from the viewpoint of the soma. The distributed nature of CF synapses and their location on stubby spikes is also suggested to reduce somewhat the conductance shunt and reduction in driving force that might be experienced by more clustered synaptic input (Palay and Chan-Palay, 1974), increasing the size of the EPSC. Further, the dendritic distribution of inputs also provides a more effective depolarisation of the dendrites than somatic input would (Segev and Rall, 1988; Vetter et al., 2001) . This would aid the recruitment of dendritic active events by the CF input. The site of action potential generation is also influenced by Purkinje cell geometry, with small capacitance, high input impedance, high axial resistance isolated compartments, such as the axon or the central region of spiny branchlet dendritic clusters being favoured (Stuart and Häusser, 1994; Khaliq et al., 2003; Roth and Häusser, 2004; Clark et al., 2005). Thus, it appears that the synaptic distribution of CF input is perfectly placed to globally depolarise the dendrites and provide a massive current input to the soma, triggering both dendritic and axonal spikes.

Purkinje cell firing patterns

The passive properties of the Purkinje cell dendrites serve to compartmentalise the cell, separating the dendrites and the soma. The cell's active properties (first thoroughly described using sharp electrode recording in slice (Llinas and Sugimori, 1980b, a; Hounsgaard and Midtgaard, 1988)) emphasise the distinction.

Purkinje cell somata fire narrow (< 0.2 ms), fairly small (reaching ~0 mV) TTX sensitive sodium action potentials at high frequencies, both *in vitro* (Llinas and Sugimori, 1980a; Hounsgaard and Midtgaard, 1988; Clark and Barbour, 1997) and *in vivo* (Granit and Phillips, 1956; Eccles et al., 1967; Bell and Grimm, 1969; Latham and Paul, 1971; Armstrong and Rawson, 1979; Nitz and Tononi, 2002) (Intro. Fig 6a). The Purkinje cells characteristic tonic high frequency 'simple spike' firing (~50 Hz) is intrinsically generated, continuing (indeed becoming more regular) in the absence of synaptic input (Häusser and Clark, 1997). Paired axonal and somatic whole cell recording demonstrated that fast action potentials (both simple spikes and the first spike of the complex spike) are, at room temperature, initiated in the axon before propagating into the soma (Stuart and Häusser, 1994). This was confirmed for simple spikes at physiological temperatures using paired cell-attached axonal and somatic recordings (Clark et al., 2005), though whether the initiation site is at the first node of Ranvier (Clark et al., 2005) or in the axonal initial segment (Khaliq and Raman, 2006) has been contested.

These spikes backpropagate poorly into the Purkinje cells highly branched dendrites (Llinas and Sugimori, 1980b, a; Hounsgaard and Midtgaard, 1988; Stuart and Häusser, 1994) (Intro. Fig 6a and b). Indeed, the dendrites act as a passive capacitative brake on spiking, which continues at a higher rate after dendrotomy (Bekkers and Häusser, 2007). The dendrites are, however highly electrically excitable; tonic depolarisation generates trains of gradualy rising, rapidly repolarising Ca^{2+} spikes, insensitive to TTX, but blocked by cadmium (Llinas and Sugimori, 1980b; Hounsgaard and Midtgaard, 1988) (Intro. Fig 6c). These can be seen at the soma if sodium channels are blocked (Llinas and Sugimori, 1980a) and underlie the bursting of sodium spikes seen with somatic depolarisation in the absence of sodium channel block (Llinas and Sugimori, 1980b, a; Womack and Khodakhah, 2004; Bekkers and Häusser, 2007).

This pattern of excitability develops over the first 3 postnatal weeks in rats. At P0 the majority of Purkinje cells are silent (McKay and Turner, 2005; Fry, 2006). With development, somatic sodium channel density increases, their voltage activation becomes more negative and a greater proportion of resurgent current (see later) is expressed (Fry, 2006), resulting in spontaneous spiking, higher firing frequencies and faster rising, lower threshold, narrower action potentials and (McKay and Turner, 2005; Fry, 2006). Initially, current injection leads to a transient 'low threshold burst' pattern of firing. This develops into the mature pattern of steady firing of linearly increasing frequency with increasing current injection, followed by Na-Ca^{2+} spike bursting, which acts to 'clamp' the average firing frequency at a maximum around 200-300 Hz (McKay and Turner, 2005; Rancz and Häusser, 2005). Also, it was found that, in slices, Na^{+}- Ca^{2+} bursting can occur spontaneously, as part of a cycle of bursting, silence and tonic spiking (Womack and Khodakhah, 2002a; Womack and Khodakhah, 2004) which increases in prevalence with age and size of the dendritic tree (McKay and Turner, 2005). As these patterns indicate a more depolarised state, and are not seen *in vivo* (unless the cell is damaged by microelectrode impalement (Granit and Phillips, 1956; Eccles et al., 1966c), or CF input is prevented (Cerminara and Rawson, 2004)), it is possible that they might reflect either slicing damage to the Purkinje cell, or the acute result of CF input removal.

In vivo, Purkinje cells fire repetitively at frequencies that are modulated by parallel fibre and interneuron sensory input (e.g. Granit and Phillips, 1956; Gilbert and Thach, 1977; Loewenstein et al., 2005; Schonewille et al., 2006; Barmack and Yakhnitsa, 2008). Whole cell recording (under anaesthesia) has demonstrated that Purkinje cells *in vivo* are bistable, and that CF input can trigger the cell to switch from tonic firing to silence and vice versa (Loewenstein et al., 2005, though see Schonewille et al., 2006), illuminating the bistable behaviour recorded by extracellular electrodes (Bell and Grimm, 1969; Latham and Paul, 1971; Armstrong and Rawson, 1979; Nitz and Tononi, 2002, among others). This bisability can be seen *in vitro*, where the firing rate to a current input depends on whether increasing or

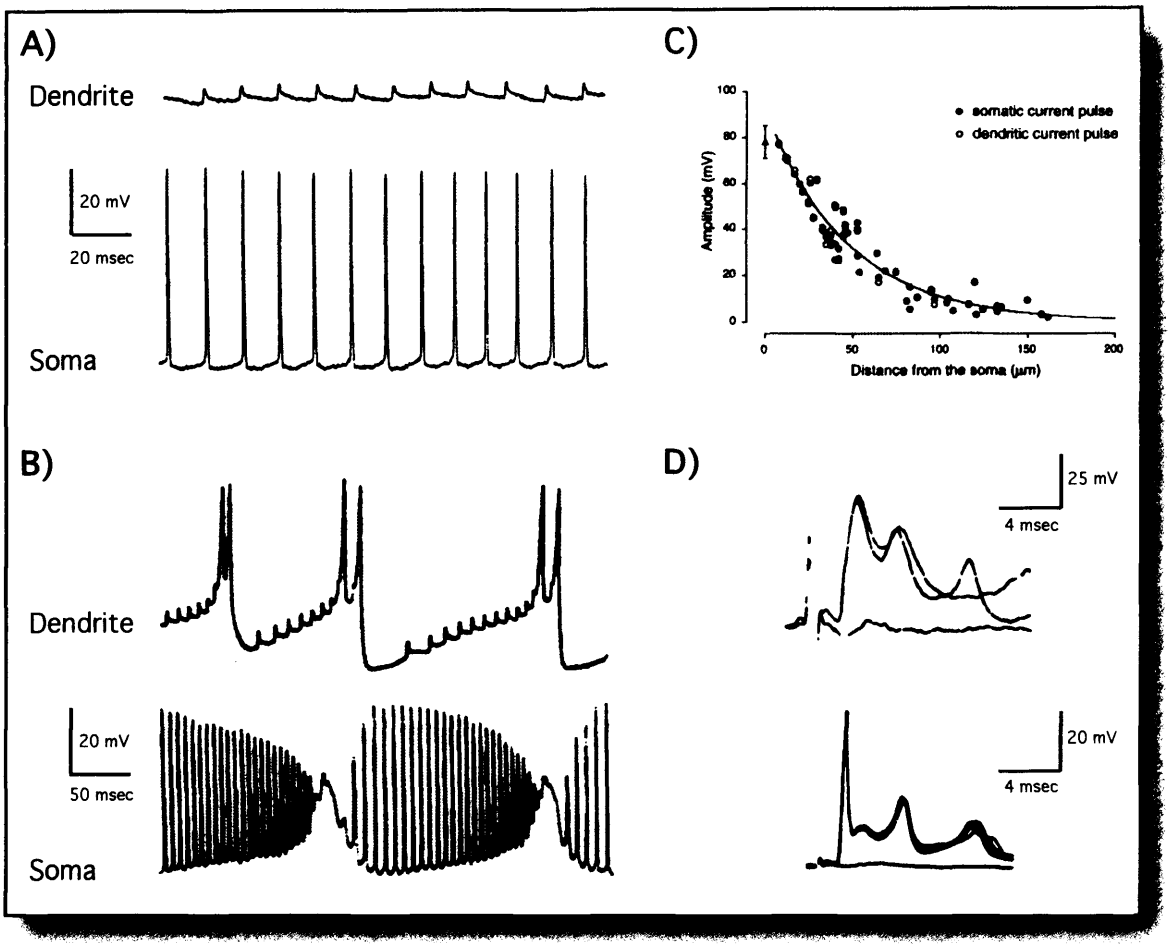

Intro. Figure 6: Firing behaviour of the cerebellar Purkinje cell

A) Example (taken from Hounsgaard & Midtgaard, 1988) of the axosomatic sodium spiking (bottom) that is barely visible in dendritic recordings (top), due to its lack of active backpropagation.
B) Examples of Na-Ca bursting produced by intense current injection (also from Hounsgaard & Midtgaard 1988). In dendrites (top) rhythmic calcium spikes are generated; somata (bottom) generate cycles of rapid spiking that increase in frequency and decreases in amplitude before complete inactivation.
C) Measurement (from Stuart & Häusser 1994) of the rapidly diminishing amplitude of axosomatic spikes as they backpropagate into the dendrites.
D) Example responses (from Crepel et al., 1981) to CF stimulation. Prominent calcium spikes are seen in a dendritic recording (top), and a highly reproducible complex spike is seen at a soma (bottom). A single stimulation failure is shown in both dendrites and soma.

decreasing amounts of current are being injected, and is enhanced by blockers of Ih, where similar rapid switches between silent and tonic firing can be made (Williams et al., 2002).

The CF evoked firing pattern- the complex spike

The result of strong, distributed CF input to the Purkinje cell dendrites is to evoke electrical responses in both somatic and dendritic compartments (Eccles et al., 1966a). 1-3 dendritic spikes are triggered together with the somatic complex spike burst, composed of an initial fast spike followed by a number of high frequency spikelets of varying height generated on top of an envelope of depolarisation (Intro. Fig 6d) (Eccles et al., 1966a; Fujita, 1968; Martinez et al., 1971; Llinas and Sugimori, 1980b, a; Crepel et al., 1981; Campbell and Hesslow, 1986a; Chan et al., 1989; Hashimoto and Kano, 1998; Schmolesky et al., 2002; Khaliq and Raman, 2005; Monsivais et al., 2005). The somatic complex spike is 'all-or-none', being highly reproducible when evoked repeatedly in the same cell (Eccles et al., 1966a; Crepel, 1971; Puro and Woodward, 1977; Armstrong and Rawson, 1979; Llinas and Sugimori, 1980a). The complex spike is often followed by a pause in the simple spike firing of the cell (Bloedel and Roberts, 1971; Latham and Paul, 1971; Armstrong and Rawson, 1979; Sato et al., 1992). The simple spike firing rate following this pause can be modulated both up and down following this pause (Sato et al., 1992; Bloedel and Bracha, 1998).

The adult characteristics of this response develop early on in the maturation of the Purkinje cell and its CF input. By P3 a burst of spikes is seen (Crepel, 1971, 1974; Puro and Woodward, 1977), though these last longer, are of lower frequency and have fewer spikes than in the adult complex spike (Crepel, 1971). The adult number of spikes in the complex spike is reached by P7 and adult frequency reached by P16 (Crepel, 1971), neatly paralleling the development of the CF input and Purkinje cell excitability (Hashimoto and Kano, 2005; McKay and Turner, 2005; Fry, 2006; Sugihara, 2006). It has also been noted that before P11 the spontaneous and evoked CF response is more variable and sensitive to stimulus intensity (Puro and Woodward, 1977); this is again consistent with CF maturation and the major pruning of multiple innervation that occurs in this period (Hashimoto and Kano, 2005; Sugihara, 2006).

The initial fast spike of the complex spike is, at room temperature, generated in the axon (Stuart and Häusser, 1994) and is usually faithfully propagated down the axon (physiological temperature, Khaliq and Raman, 2005; Monsivais et al., 2005). The origin of later spikelets in the complex spike, in particular the role of dendritic calcium spikes in their generation, is unclear, and often small spikes generated at short interspike intervals fail to propagate down the axon (Khaliq and Raman, 2005; Monsivais et al., 2005).
Although the complex spike observed in any one Purkinje cell is highly reproducible, a large variety is generated across cells (Eccles et al., 1966a; Armstrong and Rawson, 1979;

Campbell and Hesslow, 1986a; Schmolesky et al., 2002; Khaliq and Raman, 2005). It is not, as yet, clear how this variety of spikes is generated. The relationship between the strong, yet modulable (Dittman and Regehr, 1998; Hashimoto and Kano, 1998; Silver et al., 1998; Hansel and Linden, 2000) dendritic CF input, the intrinsic properties of the Purkinje cell and the eventual somatic complex spike production is not understood, and will be explored in this thesis.

The output spiking patterns generated in response to input current, both synaptic or artificially injected by the experimenter, are the product of the interact between geometry and channel expression. The following is an outline of what is known about Purkinje cell ion channel expression and what is understood of the specialisations that produce the distinct dendritic and somatic patterns of firing observed.

Purkinje cell voltage gated ion channel expression

The principle distinction in ion channel distribution between the somatic and dendritic Purkinje cell compartments is the lack of sodium channels in the dendrites. In the axon and soma, sodium channels specialised for high frequency repetitive firing are expressed, but these are absent from the dendrites. Both compartments contain calcium channels of a subtype more usually responsible for the discrete presynaptic calcium events that cause rapid neurotransmitter release, together with a compliment of potassium and calcium activated potassium channels specialised to produce brief active events and a dynamic range of high frequency firing.

Sodium channels and fast spiking initiation

Outside-out patches pulled from the soma and dendrites of Purkinje cells has demonstrated that there are very low densities of sodium current in Purkinje cell dendrites, but high levels at the soma (Stuart and Häusser, 1994). This, together with the unfavourable dendritic geometry, prevents sodium spike initiation and active backpropagation into the dendrites (Stuart and Häusser, 1994; Vetter et al., 2001); passive attenuation ensures that action potential height diminishes rapidly with distance (47 μm exponential decay constant (Stuart and Häusser, 1994)).

The sodium currents measured in acutely dissociated Purkinje cell somata have three notable features: rapid activation and inactivation that gives a transient current; a resurgent current, briefly generated following depolarising, inactivating steps (~10 % of the peak transient current), and a persistent, noninactivating current (0 - 3 % of the peak transient current) (Raman and Bean, 1997; Kay et al., 1998; Raman and Bean, 1999, 2001; de Ruiter et al., 2006; Fry, 2006). These currents are due to the combined expression of high levels of $Na_v1.6$

and $Na_v1.1$ channels, potentially some $Na_v1.2$ (Felts et al., 1997; Vega-Saenz de Miera et al., 1997; Shah et al., 2001; Schaller and Caldwell, 2003; Kalume et al., 2007) together with the effects of the auxiliary β4 subunit (Grieco et al., 2002; Grieco and Raman, 2004; Grieco et al., 2005). There is now good evidence to suggest that the resurgent current is due to recovery of sodium channels from inactivation via an open state, due to a blocking particle entering the pore in its open state (Raman and Bean, 2001). Disruption of the β4 peptide (through proteolysis, later rescued by β4 resubstitution) abolished the resurgent current, indicating that it might act as the open pore blocking particle (Grieco et al., 2005). Further, lack of expression of the relatively slowly inactivating $Na_v1.6$ subunit results in a great reduction of resurgent current (Raman et al., 1997; Khaliq et al., 2003; Levin et al., 2006). However, slowing of inactivation of the remaining sodium channels (with β-Pompilidotoxin) allows a β4 sensitive resurgent current to develop (Grieco and Raman, 2004). The source of the persistent sodium current is hypothesised be similar to that of resurgent (Kay et al., 1998; Raman and Bean, 2001; Fry, 2006), and it appears to develop in parallel with upregulation of resurgent current, but independently of total transient current (Fry, 2006).

These subthreshold sodium currents play an important role in the generation of high frequency spontaneous action potential in Purkinje cells. Reduction of resurgent current through lack of $Na_v1.6$ expression prevents spontaneous spiking (Raman et al., 1997; Khaliq et al., 2003; Levin et al., 2006) while knockout of $Na_v1.1$, which reduces sodium current density by a similar amount (~60%) but does not affect the characteristics of resurgent current, only slows spontaneous spiking (Kalume et al., 2007). This is supported by modelling of lack of the resurgent component (Khaliq et al., 2003). Further, voltage clamp of dissociated Purkinje somata to an action potential train waveform demonstrates that the principle inward current flowing between spikes is resurgent current, with some small component of persistent current (Raman and Bean, 1997, 1999; Fry, 2006). In intact Purkinje cells, this may be augmented by capacitative and active currents from the dendrites (Jaeger et al., 1997; Clark et al., 2005; Fernandez et al., 2007). The loss of spontaneous spiking through Purkinje cell specific $Na_v1.6$ knockout shows the distinct phenotype of cerebellar ataxia (Levin et al., 2006).

While rapid sodium channels are important for rapid firing, burst generation and thus for complex spike generation (Raman and Bean, 1997; Khaliq et al., 2003; Swensen and Bean, 2003, 2005; Levin et al., 2006; Kalume et al., 2007), burst generation is maintained after sodium channel reduction, through the compensatory balance of other ion channel activation (Swensen and Bean, 2005), and vastly different complex spike patterns are produced across species with very similar sodium channel properties (de Ruiter et al., 2006).

Calcium channels and dendritic excitability

While the low levels of sodium channels in the dendrites of Purkinje cells cannot support sodium spikes, they have been known for many years to have a prominent, calcium dependent electrical excitability (Llinas et al., 1968; Calvin and Hellerstein, 1969; Llinas et al., 1969c; Llinas et al., 1969a; Llinas and Nicholson, 1971; Nicholson and Llinas, 1971; Llinas and Sugimori, 1980b, a; Hounsgaard and Midtgaard, 1988; Rancz and Häusser, 2006). The calcium channels responsible were, in fact, first identified in Purkinje cells and were thus named 'P-type' (Llinas et al., 1989), and are now known to correspond to $Ca_v2.1$, or the alpha1A subunit (Dolphin, 2006). P-type channels form the bulk of calcium channels expressed, although some lower levels of L, N, R and T type channels exist in Purkinje cells (Ahlijanian et al., 1990; Regan, 1991; Mintz et al., 1992; Westenbroek et al., 1992; Yokoyama et al., 1995; McDonough and Bean, 1998; Chung et al., 2002; Yunker et al., 2003; Gruol et al., 2006; McKay et al., 2006; Molineux et al., 2006), and low threshold spikes generated by T-type excitability have been reported in young animals, perhaps localised to the distal, spiny dendrites (Mouginot et al., 1997; Pouille et al., 2000; Cavelier et al., 2002b; Cavelier et al., 2002a; Isope and Murphy, 2005).

P-type channels have been characterised as high voltage activating channels present at a high conductance density in both the soma and larger dendrites amenable to patching (Regan, 1991; Usowicz et al., 1992), and immunocytochemistry and the Ca^{2+} influx recorded by imaging suggests they are also present in the distal spiny branchlets (Ross and Werman, 1987; Miyakawa et al., 1992; Westenbroek et al., 1995; Rancz and Häusser, 2006), though lack of direct electrical measurement does not preclude that their channel characteristics or excitability might differ somewhat (Ekerot and Oscarsson, 1981; Tank et al., 1988; Isope and Murphy, 2005; Rancz and Häusser, 2006). The Cav2.1 subunit exists as a number of different splice variants in Purkinje cells (Kanumilli et al., 2006), the expression of which changes during development (Chaudhuri et al., 2005). Pertinently, this leads to increased expression of subunits that display Ca-calmodulin dependent facilitation (Chaudhuri et al., 2004; Chaudhuri et al., 2005), which suggests a positive feedback mechanism whereby prior excitation can increase e.g. the number calcium spikes in the CF response (Christensen, 2002). Further, it might underlie the slightly altered pharmacology of P-type channels in mature rat Purkinje cells (Tringham et al., 2007).

The lack of functional Cav2.1 subunits, due to block, mutation or knockout, prevents the generation of dendritic calcium spikes and the resulting Na^+- Ca^{2+} bursting of spikes seen at the soma, but also leads to more irregular simple spiking due to the consequent lack of activation of K_{Ca} channels (Cavelier et al., 2002b; Hoebeek et al., 2005; Donato et al., 2006; Walter et al., 2006; Ovsepian and Friel, 2008). The behavioural phenotype of these mice is ataxia, apparently due to the lack rhythmicity in Purkinje cell firing, but the potential role in altered synaptic plasticity due to altered calcium influx does not seem to have been explored

(Jun et al., 1999; Hoebeek et al., 2005; Dolphin, 2006; Walter et al., 2006; Ovsepian and Friel, 2008).

Potassium channels and fast spiking

Excitable channels carrying inward current, such as sodium and calcium channels, are only part of what determines the firing capabilities of a neuron. The outward current carrying channels of the large, diverse voltage gated potassium channel family display a large variety of voltage sensitive and kinetic properties that control neuronal excitability in a number of different ways (Coetzee et al., 1999). In Purkinje cells potassium channels (both voltage and calcium dependent) make a strong contribution to fast somatic spiking and dendritic calcium spike generation. Recently, a large amount of progress has been made to identifying and characterising the conductances responsible. In 1991, it was known from single channel recordings that at least 6 separate potassium channel conductances were expressed (in slice culture, Gruol et al., 1991). It is now known that Purkinje cells prominently express K_V3 and K_V1 channels and have some properties consistent with K_V4 channels, together with the expression of BK and SK calcium activated potassium channels, most with an apparently uniform somatodendritc distribution. The following outlines what is known about the expression and functional role of these subunits.

K_V3

In general, K_V3 channels are high threshold activating (>-20 mV), rapidly activating and rapidly deactivating (Rudy and McBain, 2001). As such, they are usually only activated by action potentials, curtailing spike height and width, so limiting sodium channel inactivation. This, together with their rapid kinetics, which avoid prolonged potassium conductance between spikes, serves to increase the firing frequency of the neuron (Rudy and McBain, 2001). Purkinje cells express high densities of $K_V3.3$ and 3.4 channels ($K_V3.1$ expression is negligible and $K_V3.2$ appears to be absent, (Goldman-Wohl et al., 1994; Weiser et al., 1994; Rashid et al., 2001; Martina et al., 2003; McMahon et al., 2004; Sacco et al., 2006)).

The properties of potassium channels in outside-out patches from the soma and dendrites are consistent with a high density of K_V3 channels (Martina et al., 2003); TEA (in the absence of Ca^{2+} and presence of internal and external EGTA, to avoid K_{Ca} currents) has been used to separate out and characterise the high voltage activated ($V_{1/2}$ ~-5 mV), rapidly activating and deactivating (1-8 ms, depending on Vm) K_V3 component (Sacco et al., 2006). These currents are activated at the soma during action potentials, carrying most of the potassium current during the spike (Martina et al., 2007), and are activated in the dendrites by action potential backpropagation and CF-stimulus-like depolarisations (Martina et al., 2003). They are largely responsible for the Purkinje cell somatic action potentials' characteristic brief duration and

small amplitude (McKay and Turner, 2004; Akemann and Knopfel, 2006; Martina et al., 2007), and also limit the amplitude and duration of calcium spikes (McKay and Turner, 2004).
Their removal (either pharmacologically or genetically) causes an increase in somatic and dendritic spike width, slower spontaneous simple spiking or evoked calcium spiking, and longer post-complex spike pauses (McKay and Turner, 2004; McMahon et al., 2004; Akemann and Knopfel, 2006; Hurlock et al., 2008). They may promote rapid tonic firing in a novel manner in Purkinje cells, by causing an accumulation of the Nav1.6 resurgent current acting between spikes (Akemann and Knopfel, 2006). The rapid transient burst of spiking during the complex spike relies on somatic $K_V3.3$ channels for interspike repolarisation; their removal results in a plateau of depolarisation in place of the complex spike secondary spikelets (Hurlock et al., 2008; Zagha et al., 2008). The knockout of $K_V3.3$ channels across the whole mouse brain causes ataxia; interestingly this can be rescued (together with rescue of the Purkinje cells electrophysiological phenotype) by Purkinje cell specific rescue of $K_V3.3$ expression (Hurlock et al., 2008). This illustrates the importance of appropriate ion channel expression and demonstrates that Purkinje cell spike width, spontaneous spike rate and/or the number of spikelets in the complex spike have an important role to play in motor coordination.

K_V1

In contrast to K_V3 channels, K_V1 channels tend to have low activation thresholds. In addition, many do not show inactivation (Coetzee et al., 1999). In other neuron types they have been seen to determine sodium spike threshold, width, timing and frequency and can influence the site of calcium spike initiation (Storm, 1988; Brew and Forsythe, 1995; Trussell, 1997; Golding et al., 1999; Kupper et al., 2002; Rothman and Manis, 2003). Purkinje cells express some K_V1 channels, in particular having strong $K_V1.5$ and $K_V1.1$ staining across their soma and dendrites (Veh et al., 1995; Chung et al., 2001). McKay and Turner (2005) have found margatoxin (a K_V1 blocker) sensitive K_V1 currents in outside-out patches from Purkinje cell somata. They found K_V1 current to be active both during and between action potentials, and its block to cause faster spiking, more rapid accumulation of spike inactivation, a greater propensity to fire Na^+-Ca^{2+} bursts at an increased interburst rate (McKay et al., 2005; Haghdoust et al., 2007). These effects are consistent with the removal of a repolarising conductance between spikes (Fernandez et al., 2005). K_V1 action on the complex spike is to curtail the burst; their block increases spikelet frequency, number and total burst duration (McKay et al., 2005)). The somatic presence of K_V1 has been contested, however; Southan and Robertson (2000) did not find dendrotoxin (another K_V1 blocker) sensitive currents in outside out patches from Purkinje soma, and Khavandgar et al., (2005) argue that the effect of K_V1 blockers, at concentrations at which they are specific, is at the dendrites, where they increase calcium spiking, promoting high frequency bursts in a background of unaltered steady state firing. Overall, the effects of K_V1 channels appears to be to dampen tonic excitability, in opposition to K_V3 channels, which promote higher frequency firing and allow

rapid bursts of spikes. These may act together to increase the dynamic range of Purkinje cell responses, keeping the cell at rest below its high maximum firing frequency, but above zero firing frequency.

I_A

A-type currents are inactivating potassium currents and have been found to have a role in controlling the spread of synaptic and active events within neuronal dendritic arbours (Hoffman et al., 1997; Ramakers and Storm, 2002; Cai et al., 2004; Kim et al., 2007). In turtle Purkinje cells, Midtgaard has reported the slow development of depolarisation with dendritic current injection, characteristic of the inactivation of an A-type current (though other factors may account for this (Fernandez et al., 2007)), which influences the number of dendritic calcium spikes generated in response to CF or strong parallel fibre stimulation ((Midtgaard, 1995)). He also found that 4-AP (an I_A blocker) greatly increases the degree and spatial spread of dendritic excitability (Midtgaard et al., 1993; Midtgaard, 1995, see also Cavelier et al., 2002a). However, identification of I_A in Purkinje cells is controversial. A-type inactivating current can be generated by a number of potassium channels, given the appropriate cellular environment (e.g. some K_V1 subunits, especially in combination with β subunits (Rettig et al., 1994)), but is usually ascribed to K_V4 channels. However, there does not appear to be prominent $K_V4.1$ or 4.2 mRNA or protein expression in Purkinje cells, and although there is $K_V4.3$ in the molecular layer (Tsaur et al., 1997; Serodio and Rudy, 1998; Wang and Schreurs, 2006), this may be due to expression in interneurons at sites opposed to the CF (Kollo et al., 2006), as it reported that Purkinje cell $K_V4.3$ expression is lost with development (Hsu et al., 2003). Further, some groups report failing to find evidence for an I_A current at the classically expected range of voltage sensitivities (Martina et al., 2003; McKay and Turner, 2004; Fernandez et al., 2007). Other groups, however, have reported I_A, which is TEA insensitive and has some 4AP sensitivity, in the Purkinje somata of P3-9 rats (Sacco and Tempia, 2002), developed rats (Wang et al., 1991; Southan and Robertson, 2000) and in the soma and dendrites of mature rabbit Purkinje cells (Wang and Schreurs, 2006). It has even been suggested that a change in I_A underlies the change in dendritic excitability that accompanies parallel fibre plasticity and classical conditioning in rabbits (Schreurs et al., 1997; Schreurs et al., 1998), altering the spiking pattern following parallel fibre input.

K_{Ca} and rhythmogenesis

Both strong dendritic input (e.g. CF stimulation) and spontaneous tonic spiking or bursting causes some level of calcium influx through voltage gated channels (Raman and Bean, 1999; Swensen and Bean, 2003, 2005). The calcium influx through P-type channels (Edgerton and Reinhart, 2003; Womack et al., 2004) during both modes of activity activates calcium dependent potassium channels, and in fact, during spontaneous spiking, calcium conductances lead to a net outward current (Raman and Bean, 1999; Williams et al., 2002; Edgerton and Reinhart, 2003). Purkinje cells express both BK and SK calcium activated

potassium channels, each of which have distinct, important roles in controlling dendritic and somatic spike repolarisations, and in regulating rhythmic firing, all of which have consequences for electrogenesis in response to CF stimulation.

BK

BK, so called after its "big" single channel conductance channels are both voltage and calcium sensitive (reviewed in Salkoff et al., 2006). Purkinje cells stain for BK in both their somata and dendrites (Knaus et al., 1996) and its levels of expression are upregulated during the first two weeks of development (Muller et al., 1998). Its voltage and calcium dependent properties (characterised from single channel recordings in outside-out patches (Jacquin and Gruol, 1999; Womack and Khodakhah, 2002b)) are such that there is little conductance at rest. Open probability can, however, be regulated by PKA or PKC dependent phosphorylation (Widmer et al., 2003). BK channels are activated by both somatic sodium spikes and dendritic calcium spikes and play a prominent role in generating both their AHPs (Edgerton and Reinhart, 2003; Sausbier et al., 2004); this fast hyperpolarisation also serves to restrict the spread of dendritic calcium spikes (Rancz and Häusser, 2006). As the voltage sensitivity of the BK conductance restricts its activating stimuli to spikes, it plays only a weak role in dampening spontaneous firing frequency, but this role becomes more important when SK channels are absent (Edgerton and Reinhart, 2003). The knockout of BK channels leads to reduced AHP generation, reduced spontaneous firing due to inactivation of sodium spiking and increased paired pulse depression and the Purkinje cell-DCN synapses (Sausbier et al., 2004). These properties are thought to underlie the cerebellar motor coordination and eye-blink conditioning abnormalities seen in the BK knockout mice (Sausbier et al., 2004).

SK

SK channels have a smaller conductance than BK and are calcium, but not voltage sensitive (reviewed in Stocker, 2004). They are formed by homo- or heteromultimers of SK 1, 2 or 3 subunits (Stocker, 2004). Purkinje cells express only SK2 subunits (Stocker and Pedarzani, 2000), which are highly calcium sensitive. Staining for both mRNA and protein shows that its levels decrease during development, reducing to nearly nothing in adulthood (following the opposite trend to BK expression) (Cingolani et al., 2002). SK block (by apamin) causes faster, more irregular spontaneous Purkinje cell firing, and increases the occurrence of spontaneous spike bursting, with each burst being of shorter duration but composed of higher frequency sodium spikes (Cingolani et al., 2002; Edgerton and Reinhart, 2003; Womack and Khodakhah, 2003, 2004). SK block does not significantly alter sodium or calcium spike AHPs, except in the absence of BK channels, where a slower SK dependent AHP becomes apparent (Edgerton and Reinhart, 2003). Interestingly, the effect of apamin block is similar if it is applied only to the dendrites, where somatic action potentials do not backpropagate to cause significant calcium influx (Womack and Khodakhah, 2003). This suggests that SK is activated by resting levels of calcium in the cell, and thus is probably the K_{Ca} conductance

reported at rest by Crepel and Penit-Soria (1986). It has been suggested that SK conductance, modulated by Purkinje cell spiking and the consequent calcium influx to the proximal dendrites, might act as a conductance 'gate' controlling the electrical coupling of the soma and dendrites (Womack and Khodakhah, 2003). Enhancement of SK conductance with the drug EBIO can rescue spiking irregularities and the propensity to burst caused by block of SK channels or indeed by loss of function of calcium channels (Cingolani et al., 2002; Walter et al., 2006). This has been found to rescue the ataxic phenotype of the calcium channel mutants (Walter et al., 2006), again suggesting a role for accurate Purkinje cell spiking in motor coordination.

I_h and bistability

The final prominent conductance in the Purkinje cell's repertoire is the hyperpolarisation activated mixed cation conductance, I_h. This is responsible for the 'sag' in membrane potential visible following hyperpolarising or subthreshold depolarising current injection steps, rectifying Vm back towards its initial value (Crepel and Penit-Soria, 1986; Roth and Häusser, 2001). It has been characterised by whole cell recordings at room temperture (Roth and Häusser, 2001), or, more accurately by cell attached dendritic recording at physiological temperature (Angelo et al., 2007). In Purkinje cells, as in other neurons (Magee, 1999; Williams and Stuart, 2000; Berger et al., 2001), this conductances serves to make synaptic integration independent of dendritic input location, in a manner that is independent of its dendritic distribution. The block of I_h *in vitro* emphasises the Purkinje cell's bisability, where brief current pulses, synaptic inhibition, or indeed CF stimulation, can switch the cell from silence to tonic firing and back again. A similar phenomenon occurs in vivo, as observed by whole-cell patch clamp recording (under anaesthesia, Loewenstein et al., 2005), but in the absence of I_h block. Curiously, conductances with properties similar to I_h may be responsible for this bistability (Loewenstein et al., 2005), though other combinations of conductance and capacitance parameters can generate a similar phenomenon (Fernandez et al., 2007). The whole brain knockout of I_h leads to deficits including reduction of cerebellar motor coordination and classical conditioning, which has been ascribed to the inconsistencies introduced into input-output behaviour of the Purkinje cell (Nolan et al., 2003).

Ion channels acting in consort

The ion channels expressed by Purkinje cells result in a beautifully balanced system, capable of generating repetitive fast spiking at the soma, rapid bursts of somatic spikes and also brief, repetitive dendritic calcium spikes. This balanced system has been particularly elegantly revealed in experiments that isolated, pharmacologically, the currents underlying action potential generation by voltage clamping dissociated Purkinje cell somata to the waveforms of action potential trains or of spontaneous bursts (Raman and Bean, 1999; Swensen and Bean, 2003, 2005). These illuminate the sequence of current activation during somatic spiking;

showing the rapid activation of inward sodium currents, coloured with regenerative calcium influx, followed rapidly by high voltage potassium channels activation, together with calcium activated potassium currents. It also demonstrated that, during interspike intervals within both tonic spiking and spontaneous bursting, there is a careful balance of low voltage activated potassium current, calcium activated potassium current and resurgent sodium current, the kinetics and voltage sensitivities of which ensure that there is usually only a small net inward current triggering the next spike.
The importance of appropriate ion channel expression in this elegantly balanced system is made apparent the numerous knockout and mutation studies that result in disrupted Purkinje cell spiking together with cerebellar ataxias.

Modelling

A number of biologically realistic models have attempted to capture the essence of active and passive interactions. In 1994, the available biophysical data was combined into Purkinje cell morphologies and tuned to successfully reproduce Purkinje cell patterns of somatic simple spiking (which backpropagate poorly to the dendrites, although are not spontaneously generated) and Na^{+}-Ca^{2+} somato-dendritic bursting in response to strong current injection (De Schutter and Bower, 1994c). Synaptic responses are also reproduced; the response to strong CF distributed input is a single dendritic spike and a burst of somatic spikes, followed by a pause (De Schutter and Bower, 1994a). Details of the complex spike waveform (height and timing) and dendritic response (timing and variable number of spikes) were not matched. The model has been used, however, to make interesting predictions and interpretations of Purkinje cell response to parallel fibre and inhibitory input (De Schutter and Bower, 1994b; Jaeger et al., 1997; Steuber et al., 2007). The family of conductance densities that reproduce Purkinje cell behaviour to a similar degree of accuracy has also recently been explored (Achard and De Schutter, 2006).

A more recent biophysically accurate model of the Purkinje cell soma has been described, that incorporates accurate descriptions of ion channel behaviour taken from recordings in dissociated cell bodies (Khaliq et al., 2003). This accurately reproduces the details of simple spiking at room temperature, and has been used to explore the contribution of resurgent sodium channels to spontaneous firing (Khaliq et al., 2003), and the interactions between persistent sodium and high voltage activated potassium conductances that produce high frequency firing (Akemann and Knopfel, 2006). It has also been integrated into a full Purkinje cell model which reproduces the initiation of simple spikes at the first branch point (Clark et al., 2005) (dendritic electrogenesis or complex spike production was not explored or accurately matched in this study).

The dynamics of Purkinje cell firing has also recently been analysed with a reduced model based on physiological behaviour (Fernandez et al., 2007). It explores the parameters that are necessary to explain the Purkinje cell's bistability (triggered by strong inputs such as the CF), its inability to begin firing at a non-zero firing frequency and its hysteresis of firing frequency response to increasing or decreasing current injection (Llinas and Sugimori, 1980a; Williams et al., 2002; Fernandez et al., 2007). Much of this can be achieved through the combination of brief spike inactivation (due to e.g. rapidly deactivating potassium channels or resurgent sodium current) with a long membrane time constant (due to e.g. extensive dendrites), which together lead to a spike after-depolarisation that drives repetitive firing once spiking is initiated. Details of the complex spike waveform were not investigated.

So far, these models most successfully capture simple spiking, especially at room temperature. The difficulty of gathering good voltage clamp data of rapidly activating channels at more physiologicial temperatures, together with the difficulty of capturing physiological dendritic calcium channel behaviour, limit these models. Thus, none have been able to completely reproduce the complex spike rapid burst of spikes of differing amplitudes and the burst of 1-3 dendritic spikes that accompany it.

Functions of CF input

Despite abundant and well-trodden evidence on the anatomy and physiology of the cerebellum, the exact function of the cerebellar system, and of CF signalling within it, is difficult to pin down.

There is now good evidence that Purkinje cell spike timing precision is required for accurate motor coordination. Ablation or damage to the cerebellum have been known for over 200 years to cause ataxias (Rolando, 1809; Flourens, 1824; Holmes, 1917), typically involving lack of muscle tone, imprecise, decomposed movements, disrupted fine motor coordination and timing (Hore et al., 2002), and tremor. Similar ataxias are also caused by knock out or mutation of specific ion channels that lead to disruptions to Purkinje cell firing, such as $Na_V1.6$, $K_V3.3$, HCN1 (Ih), $Ca_V2.1$ (the P-type calcium channel), BK and also the calcium buffer calbindin (Nolan et al., 2003; Sausbier et al., 2004; Hoebeek et al., 2005; Servais et al., 2005; Donato et al., 2006; Levin et al., 2006; Hurlock et al., 2008). Further, the rescue of spiking precision in the $Ca_V2.1$ mutant *Ducky* through the pharmacological enhancement of SK (Walter et al., 2006), and the similar rescue of Purkinje cell spiking by the Purkinje specific reexpression of $K_V3.3$ in the $K_V3.3$ knockout background (Hurlock et al., 2008), both lead to the restoration of motor performance. These mutations strongly indicate a role for accurate Purkinje firing in motor coordination, though as, between them, the simple spike rate, post complex spike pause and complex spike pattern is also altered, the exact contribution of each is hard to demarcate.

Motor timing

Many investigators have suggested way in which the cerebellum might be involved in controlling motor timing. One of the first was posed theoretically by Braitenberg, (1961), based on the anatomy of the cerebellar cortex. He proposed that the 'delay lines' formed by parallel fibre axons could convert distance in the cerebellum into a timing delay between signals, with the coincidence of climbing fibre and parallel fibre input (or of two parallel fibre pathways) triggering activity in the appropriate Purkinje cell.

More recently, a role has been suggested for synchrony of CF input across Purkinje cells (Llinas and Sasaki, 1989; Welsh et al., 1995), which is proposed to aid coordination of synergistically acting muscle groups within movements. This idea also has anatomical support. Cells within the olive are electrically coupled to their neighbours via gap junctions and show synchronous subthreshold 2-12 Hz oscillations that are supported by a combination of intrinsic and network properties (Llinas and Yarom, 1981a, b, 1986; De Zeeuw et al., 1998; Devor and Yarom, 2002b, a; Leznik et al., 2002; Long et al., 2002; De Zeeuw et al., 2003). Distinct regions of the inferior olive (IO) project topographically into parasagittal bands in the cerebellar cortex, aligning with, and causing gap junction dependent synchrony within, the intriguing aldolase C (zebrin) staining bands (Llinas and Sasaki, 1989; Sugihara and Shinoda, 2004; Blenkinsop and Lang, 2006; Sugihara et al., 2007; Sugihara and Quy, 2007). This synchrony can be seen powerfully when inferior olive oscillations are potentiated by harmaline (Llinas and Sasaki, 1989), is also observed at rest under anaesthesia (Llinas and Sasaki, 1989), in awake recordings (Lang et al., 1999) and has been reported to occur during the generation of rhythmic movements in rats (Welsh et al., 1995). However, Purkinje cell synchrony could not be detected during isolated movements in monkeys or following visual stimulation in rabbits (Keating and Thach, 1995; De Zeeuw et al., 1998), and the uniform CF conduction time required for IO driven synchrony across the rat cerebellum has been questioned (Baker and Edgley, 2006).

The completion of the olivocerebellar loop (see earlier cerebellar anatomy section), has been proposed to have a feedback role in controlling CF synchrony (De Zeeuw et al., 1998). Convergence onto DCN cells of synchronous Purkinje cell complex spike inhibition and post-complex spike pause inhibitory relief should provide an apt stimulus for rebound bursting (Aizenman and Linden, 1999). This subsequent topographic projection of inhibition and excitation from the DCN to the area of the IO that innervated the original Purkinje cell group has been shown to theoretically support a synchronous, self regenerating oscillation throughout the olivocerebellar loop, which can be disrupted by externally generated CF or mossy fibre impulses (Kistler et al., 2000; Kistler and De Zeeuw, 2003). Indeed inhibitory input from the DCN to the IO has been found to damp oscillations and control the generation of CF

activity in a manner that increases with development (Llinas and Sasaki, 1989; Nicholson and Freeman, 2003a, b), perhaps helping the selection of appropriate, well timed CF activity in response to salient external stimuli (De Zeeuw et al., 1998; Devor, 2002, though see Bengtsson and Hesslow, 2006).

Currently, the clearest evidence that synchrony within the IO and the control of oscillatory CF input to Purkinje cells is crucial to well timed motor control comes from mice in which connexin-36, the IO gap junction protein, is knocked out (Kistler et al., 2002; Van Der Giessen et al., 2008). These animals shown no ataxia and have no prominent general motor deficits, but are impaired in performance and learning of new movements that require accurate timing. Purkinje cell complex spike responses to sensory stimulation showed abnormal timing, with an increased tendency towards firing of doublets due to the compensatory increase in intrinsic oscillation of uncoupled DCN cells (De Zeeuw et al., 2003; Van Der Giessen et al., 2008). Thus, it appears that while well timed, synchronous CF input is required for accurate motor control, and plasticity of motor output (discussed in the next paragraph), the appropriate damping of intrinsic oscillations of the circuit is also required.

Motor learning

There is also good evidence that the complex spike can carry a sensory, error signal. CF input can be triggered by unexpected stimuli, such as gentle touch of the skin while at rest or interruption of a step by the presence of a barrier or the absence of a support, but is not produced by expected stimuli, such as touch of the skin to a surface during an accurate, voluntarily made movement (Gilbert and Thach, 1977; Gellman et al., 1985; Andersson and Armstrong, 1987, reviewed in Bloedel and Bracha, 1998). In the influential models of cerebellar motor learning proposed by Marr and Albus (Marr, 1969; Albus, 1971), such an error signal is proposed to 'teach' parallel fibres their appropriate weights such that the appropriate Purkinje cell output is produced without the CF error signal and later movements are executed more accurately. This has been supported by the finding that CF input, and more specifically the calcium influx caused by dendritic spike activation, causes LTD of concomitantly activated parallel fibre inputs (Ito and Kano, 1982, reviewed in Ito, 2002).

Such models have been used to understand the acquisition of well timed motor responses during tasks such as classical eye-blink conditioning (reviewed in Medina and Mauk, 2000) but appear to apply equally well to other cerebellar cortex dependent motor learning tasks, such as the vestibulo-occular reflex (reviewed in Raymond et al., 1996). In the classical eye-blink conditioning paradigm, parallel fibres active at the end of the unconditioned stimulus (e.g. a tone) presentation are depressed by the occurrence of the CF, signalling the conditioned stimulus (e.g. air puff to the eye). When combined with CF independent LTP of the parallel fibres activated earlier in the unconditioned stimulus, this can explain the

acquisition of a pause in Purkinje cell firing just before the expected conditioned stimulus presentation, mimicking the post-complex spike pause and thus reproducing the CF triggered motor output (e.g. eyeblink) (Medina and Mauk, 2000). That a Purkinje cell may operate in such a manner as a 'perceptron', recognising patterns of parallel fibre input, is supported by the finding that parallel fibre weights appear to be distributed in a similar manner to that predicted for the optimal perceptron, with many silent synapses (Isope and Barbour, 2002; Brunel et al., 2004). There is good evidence from lesion studies that motor learning does occur within the cerebellum, and that mossy fibre and climbing fibre stimulation can replace the conditioned and unconditioned stimuli, respectively (Raymond et al., 1996). However, the site, within the cerebellar system, where learning initially occurs and where the motor memory might finally reside, is less easy to dissect (Raymond et al., 1996; Attwell et al., 2002). The conjunction of mossy and climbing fibre input at the DCN and the plasticity induced there, perhaps under the instruction of Purkinje cell input, may also be responsible for controlling the updated motor output (Raymond et al., 1996; Attwell et al., 2002).

These two, apparently opposite viewpoints of the CF signal as an impetus for ongoing motor signalling and as a sensory signal for motor plasticity, are not mutually exclusive. As a concept, this is elegantly synthesised by the work of Kitazawa et al., (1998). They showed that CF input contains information about both intended movement direction (if active at the beginning of the task) and actual movement error (if active at the end of the task), but in opposite directions (e.g. active before movements to the left and after errors to the right). Thus, as movement is initiated, the complex spike can signal an error appropriate to ongoing motor control ("hand is too far right: move left to target") and after the movement ends can signal a similar error appropriate to updating future movements ("hand went too far right: move further left next time").

Despite these two elegant and well supported theories (and many more besides; Bloedel and Bracha, 1998; De Zeeuw et al., 1998), it is still difficult to interpret or predict the behaviour of most cerebellar cells *in vivo*. For example, the modulation of Purkinje cell simple spiking does not seem to follow mossy fibre input, as conceptualised in the Marr-Albus-Ito model, but appears to be driven by the inhibitory interneurons of the cerebellar cortex (Barmack and Yakhnitsa, 2008). More importantly for theories of how CF input might influence motor output, the post- complex spike pause is not a consistent phenomenon (Murphy and Sabah, 1970; Bloedel and Roberts, 1971; Latham and Paul, 1971; Armstrong and Rawson, 1979), the regulation of simple spiking following the complex spike - pause sequence is not consistent *in vivo* (Bloedel and Roberts, 1971; Latham and Paul, 1971; Armstrong and Rawson, 1979; Sato et al., 1992), and the response of the DCN is not simply correlated to complex spike activity (McDevitt et al., 1987). Thus a more thorough understanding of the firing dynamics and the input-output functions of these cells, both *in vivo* and in more carefully controlled *in vitro* situations, are required.

Aims of the thesis

This thesis aims to understand the manner in which cerebellar Purkinje cells transform their CF input into the distinctive complex spike waveform. It examines the relative importance of the CF's amplitude, its widespread distribution across the dendrites and its triggering of dendritic calcium spikes in the generation of the burst of somatic spikes that form the complex spike. The contribution of the intrinsic excitability of Purkinje cell; its variety across cells, its voltage sensitivity and roles of distant sites of action potential generation, is also described. Finally, a new role for dendritic calcium spikes in controlling the Purkinje cell's spiking output is presented.

This work is divided across three chapters:

Chapter 1: The relationship between CF input size and the complex spike.
The complex spike is first characterised in whole cell recordings from Purkinje cells in slice at physiological temperature. The effect on the complex spike of paired-pulse depression of the CF synapse is described, together with the effect of *in-vivo*-like bursts of CF stimulation. Through the alternate recording of CF EPSCs in voltage clamp and of complex spikes in current clamp, the relationship between the complex spike and its underlying EPSC amplitude is drawn.

Chapter 2: The relationship between Purkinje cell geometry and the complex spike.
The importance of the dendritic distribution of CF input to the generation of the complex spike is addressed by using conductance clamp to artificially apply CF-like synaptic conductances directly to the soma. This is also used as a tool to assess inter-cell differences in Purkinje cell excitability. The complex spike waveform is described in detail by quantifying the relationship between spike height and interspike interval. Compartmental modelling is used to demonstrate that these patterns can only be easily explained as the result of variable spike propagation from a site distant to the soma.

Chapter 3: The relationship between CF triggered dendritic calcium spikes and the complex spike.
Dendritic whole cell recording is used to record and manipulate the number of dendritic spikes made during complex spike generation. The effect of the absence of dendritic spikes and of additional dendritic spikes is described. The influence of dendritic spikes on the resulting burst is quantified and understood through an analysis of its attenuation and timing. A new role for dendritic spikes is revealed by examining the post- complex spike pause.

A general discussion of the contribution of this work to the understanding of Purkinje cells follows.

Methods

Electrophysiological data in this thesis was obtained from whole cell patch clamp recordings of the somata and dendrites of rat Purkinje cells in acute slices maintained at 34-35 °C. Experiments involved the use of current, voltage and/or conductance clamp. Most current and conductance clamp data was obtained from Purkinje cells in slices from P18-24 rats; dual voltage and current clamp recordings were made in P12-16 cells. Slices and recordings were made according to standard techniques (Stuart et al., 1993; Silver et al., 1998; Geiger et al., 2002; Williams, 2004; Davie et al., 2006), which are outlined below.
In addition, modelling was carried out using NEURON simulation software (Hines and Carnevale, 1997), using parameters outlined below.

Solutions

Slices were bathed in artificial cerebrospinal fluid (ACSF) bubbled to saturation with carbogen (95% oxygen, 5% carbon-dioxide, BOC, UK) in order to maintain tissue oxygenation and pH buffering.
ACSF contained (in mM): NaCl 125, KCl 2.5, $NaHCO_3$ 26, NaH_2PO_4 1.25, glucose 25, $MgCl_2$ 1, $CaCl_2$ 2.
Internal solution (280-285 mOsm) contained (in mM): $KMeSO_4$ 133, KCl 7.4, $MgCl_2$ 0.3, HEPES 10, EGTA 0.1, Na_2ATP 3, Na_2GTP 0.3, pH adjusted to 7.2 with KOH. 0.5 % biocytin was added during some experiments. All chemicals were purchased from Sigma (Dorset, UK). Although the internal solution was prepared with the minimisation of disruption to cell metabolic processes in mind (Ca^{2+} buffering was, for example, chosen with the high levels of mobile and immobile Ca^{2+} buffering in Purkinje cells in mind (Maeda et al., 1999; Schmidt et al., 2003)), most patch-clamp internal solution principle anion are associated with some effects on neuronal physiology (Zhang et al., 1994; Vargas et al., 1999) and dialysis of the neuron's ionic and the more mobile cytoplasmic contents is an inevitable drawback of the technique.

Slice Preparation

P12-24 Sprague-Dawley rats were anaesthetised by isoflourane inhalation (Baxter Healthcare Ltd, Thretford, UK) and decapitated, in accordance with UK Animal Scientific Procedures Act (1996). Under ice cold, carbogen saturated ACSF, the scalp was retracted, the top of the skull lifted off and the brain quickly removed. After securing the brain (with dissecting needles through the forebrain) to a sylgard based dish filled with ACSF (again ice cold, carbogen saturated), the meninges covering the cerebellum were carefully peeled away using fine forceps (Dumont No. 5). The vermis of the cerebellum was then dissected with one coronal

cut behind the forebrain, one transverse cut above the brainstem and two parasagittal cuts on either side of the vermis. One of these parasagittal surfaces was attached to a pre-cooled slicing stage using cyanoacrylate glue and transferred to the cooled, ACSF filled slicing chamber. 150-300 μm thick slices were made using either a Leica VT1000S or VT1200S (Nussloch, Germany) and transferred to a carbogen bubbled, ASCF filled slicing chamber (Gibb and Edwards, 1994) heated to 35 °C for 1 hour. Slices were then kept at room temperature until being transferred to the microscope chamber and recorded from within the next 3-5 hours. It should be noted that apart from the obvious physical damage that slicing imposes on the *in vitro* brain slice, the number of dendritic spines can be increased by the procedure (Kirov et al., 1999), possibly due to reduced synaptic activity (as axonal inputs have been severed), which itself can lead to alterations in neurons' intrinsic properties (Desai et al., 1999; Cerminara and Rawson, 2004; McKay et al., 2007).

Patch clamp recording

A diagram of a recording setup analogous to the one used is shown in Methods Fig. 1. The slice chamber was perfused at 5 - 10 ml/min (to ensure good oxygenation of the tissue, Hajos 2004) with carbogen bubbled ACSF heated to 34-35 °C. Slices were held flat in the chamber by a 'harp' with a U-shaped frame made of platinum and strings made of fine threads pulled from nylon tights. Slices were imaged using IR-DIC optics on an AxioSkop microscope (Zeiss, Göttingen, Germany) with a 40x, 0.75 NA lens which projected, through a 2x magnifier, to a Hamamitsu C2400-7 Vidicon tube camera transmitting to a video monitor. The surface of the slice was scanned for clearly visible, 'healthy', smooth, connected somata and dendrites, the microscope being moved by a XY table that allowed the field of view to be manipulated without moving the slice or the recording pipettes. The pipette-holder-headstage assemblies movement was also controlled remotely, using motorised micromanipulators (LN SM1, Luigs and Neumann, Germany). This equipment was mounted on a pneumatic vibration-isolation table (Technical Manifacturing Corporation). Pipettes were connected, via silver chloride coated silver electrodes, to either Axoclamp 2B or 2A amplifiers (Molecular Devices, Palo Alto, CA) (current and conductance clamp recordings) or to an Axopatch 200B amplifier (Molecular Devices, Palo Alto, CA) (voltage clamp recordings), and recordings were made with reference to a silver/silver chloride earth pellet placed in the recording bath. Junction potential (~7 mV) was not corrected. Recordings were preamplified (10 x) and low-pass filtered at 3 kHz before being sampled at 20 - 50 kHz using Axograph 4.9 software (Axograph Scientific) and an ITC-18 interface (Instrutech).

Pipettes were pulled from thick walled, filamented borosilicate glass capillaries (GC150F, Harvard Apparatus, Edenbridge, UK) using a two-stage, vertical puller (PC-10, Narishige, Japan) to a resistance of 7-10 MΩ (dendritic pipettes), 4-5 MΩ (somatic current and conductance clamp pipettes) or 1-2 MΩ (somatic voltage clamp pipettes) when filled with

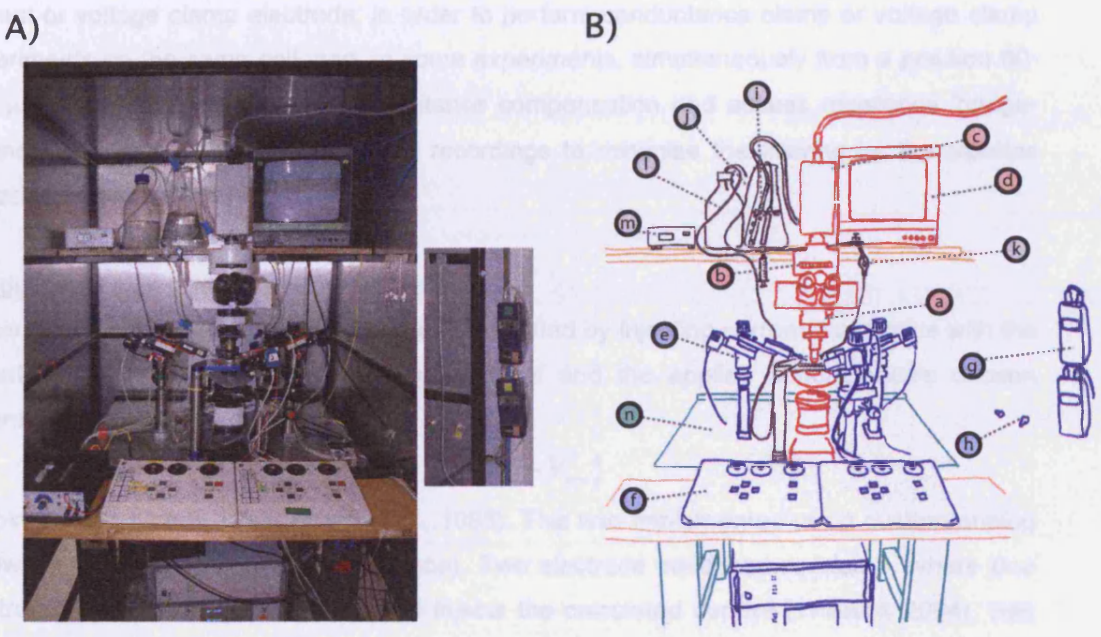

Methods Fig 1: Patch-clamp setup

A) Composite photograph of a typical patch-clamp setup (in a Faraday cage) used for dendritic recording.
B) Schematic sketch of the image in a. Red, imaging equipment; blue, electrode manipulators and pressure controlling equipment; black, perfusion system; green, vibration isolation table. **(a)** an upright microscope equipped with a40 objective and IR-DIC optics, mounted on an XY stage; **(b)** magnifier; **(c)** video camera; **(d)** black and white video monitor; **(e)** three micromanipulators (oriented so that each pipette can be changed independently); **(f)** micromanipulator remote control panels, mounted on a bench which is well separated from the vibration isolation table (boxes containing micromanipulator controller electronics are below the vibration isolation table); **(g)** manometers; **(h)** switchable pressure valves; **(i)** reservoir of carbogen-bubbled ACSF; **(j)** oxygen-impermeable Teflon tubing providing inflow to the recording chamber (heating jacket prior to chamber inflow not visible); **(k)** dripper, interrupting solution inflow; **(l)** outflow from chamber, connected to suction via a collection reservoir; **(m)** temperature monitor (connected to a thermocouple element placed in the recording chamber, not illustrated); **(n)** vibration isolation table.

internal solution. Gigaohm seals between cell and pipette were achieved using standard techniques (Stuart et al., 1993; Davie et al., 2006) before using suction to rupture the cell membrane. This resulted in initial whole cell access/series resistances of ~30 MΩ (dendritic pipettes), 10-15 MΩ (somatic current and conductance clamp pipettes) and 5-10 MΩ (somatic voltage clamp pipettes).

Current clamp

Current clamp recordings were made from the soma, usually together with a second somatic current or voltage clamp electrode, in order to perform conductance clamp or voltage clamp experiments on the same cell, and, in some experiments, simultaneously from a position 60-155 μm distant in the dendrites. Capacitance compensation and access resistance 'bridge-balance' compensation was used in all recordings to minimise the filtering by the pipettes capacitance and resistance.

Conductance clamp

In this method, a membrane conductance is simulated by injecting current that scales with the potential difference between membrane potential and the applied conductance's chosen reversal potential:

$$I = G \times (V_m - V_{rev})$$

(Robinson and Kawai, 1993; Sharp et al., 1993). This was implemented using custom analog hardware (SM-1, Cambridge Conductance). Two electrode conductance clamp, where one electrode records voltage and a second injects the calculated current (Williams 2004), was used in order to ensure voltage measurements were not contaminated by poor bridge balance and thus to prevent oscillation of the command circuitry.

Voltage clamp

All voltage clamp recordings were made from the soma and were performed together with a simultaneous somatic current clamp recording from a second electrode connected to an Axoclamp 2B amplifier. This allowed somatic voltage to be monitored and thus the quality of the somatic voltage clamp to be optimised (Silver et al., 1998). It also allowed the climbing fibre EPSC and the resulting complex spike at the soma to be recorded within the same cell.

EPSCs were clamped at between -70mV and -90mV. Series resistance and cell membrane capacitance compensation were used (compensation lag 7-10 μs). Their values were initially set by eye, while examining a 5 mV hyperpolarising step. During CF stimulation, series resistance compensation was adjusted (usually to ~80 %) so that minimal voltage escape, either in the depolarising or hyperpolarising direction, was seen at the soma with the current clamp electrode (this method is illustrated further in Chapter 1). Only records with < 2 mV somatic escape were analysed. This small escape was then compensated for offline (Silver et al., 1998) using the equation:

$$I_{corrected} = I_{uncorrected} \times \left(\frac{V_{actual} - V_{rev}}{V_{command} - V_{rev}} \right)$$

The resulting EPSC amplitude was normalised to -70 mV. V_{rev} of the AMPAergic CF EPSC was taken to be 0 mV (Perkel et al., 1990; Llano et al., 1991; Häusser and Roth, 1997b).

The voltage clamp amplifier was switched into I=0 mode to allow current clamp recording (from the second somatic electrode, connected to an Axoclamp 2B amplifier) of the complex spike.

CF stimulation

CF input was stimulated by placing a patch electrode filled with ACSF in the granule cell layer (0.2 ms, 20-80 V square pulses; 1 Hz stimulation frequency). The location of the stimulation electrode and the stimulation intensity were adjusted until an isolated CF input was excited without evoking an antidromic action potential in the Purkinje cell axon. Recordings Purkinje cells innervated by multiple CF axons (as evidenced by step increase in the voltage clamp EPSC or a step change in the complex spike waveform) were rejected (~5% of P12-16 cells, less in P18-24 cells). Complex spikes preceded by a simple spike within ~1.5 ms were excluded from analysis (typically ~5-10 % of all recorded complex spikes) as these were found to have a disrupted complex spike pattern.

Protocols

Paired pulse depression

Pairs of stimuli at intervals of 20-3000 ms were given every 5 seconds in alternate voltage and current clamp recording periods. In purely current clamp experiments, pairs of stimuli at intervals of 20-300 ms or of 1-20 ms were given every 1 s.

Burst stimulation

Bursts of 1, 2, 3, 5 or 7 CF stimulations at interstimulus intervals of 1, 2 or 3 ms were given every 1 s. Alternatively, physiological burst patterns (3, 4 or 5 stimuli), as recorded from inferior olive axons in slice, at 35 °C, were applied. Interstimulus intervals were

3 stimuli: 2.7, 2.5 ms

4 stimuli: 2.5, 2.1, 3 ms

5 stimuli: 2.6, 2.4, 2.6, 3.4 ms

Voltage dependence

Somatic average membrane potential, as recorded by one current injection electrode, was altered by tonic hyperpolarising or depolarising current injection through a second, non-recording, current clamp electrode. Periods of tonic calcium spiking were followed by periods of hyperpolarisation, without recording. In some experiments, tonic somatic current was

adjusted until the dendritic CF response was, by chance, either 1 or 2 (or in some cases 2 or 3) calcium spikes.

Synaptic-like conductance injection

Conductance waveforms were biexponential, with τ_{rise} 0.3 ms and τ_{decay} 3 ms, and peak amplitude 100 - 500 nS and a reversal potential of 0 mV. Unless otherwise specified, these were given every 1 s. In some experiments the effect of conductance time course was investigated, varying τ_{rise} from 0.2 - 0.5 ms and τ_{decay} from 2 - 5 ms.

In some experiments, dendritic spikes were evoked during somatic conductance clamp; these spikes were triggered by dendritic current injection (biexponential current waveform, τ_{rise} 0.5 ms and τ_{decay} 5 ms, peak amplitude of 2 - 5 nA together with tonic current of 0 - 330 pA).

Analysis

Data were analysed using custom programs, together with NeuroMatic data analysis software (http://www.neuromatic.thinkrandom.com/), in Igor Pro (Wavemetrics, Lake Oswego, Oregon). Curves were fitted with the Igor 'curvefit' function.

Spikelets in the complex spike were detected using a height or dV/dt threshold adjusted until all spikes identified by eye were captured. Spikelet times were measured at their peak and amplitudes were measured with respect to baseline membrane potential (averaged over 50 ms before the complex spike). The resulting amplitudes were sometimes normalised to the amplitude of the first spike in the complex spike. Where somatic spike threshold was measured, it was taken as the point at which the 2nd derivative of the spike reached 10% of its peak value during the rising phase of the spike; threshold amplitude was measured as the voltage at this point minus the minimum voltage reached in the preceding trough.

Propagation of complex spike spikelets down the Purkinje cell axon was predicted using the separatrix based on spikelet height and interspike interval derived in Monsivais et al. (2005).

Dendritic spike width was measured at half the height of the spike peak above the preceding trough in membrane potential. Attenuation was measured in records in which extra dendritic spikes did not trigger extra somatic spikelets, allowing the depolarisation due to the propagated dendritic spike to be seen in isolation. The amplitude of the propagated event was found by subtracting from these records the average somatic waveform of corresponding responses of a similar somatic spiking pattern but without the extra dendritic spike (see Fig. 3.5 in Chapter 3). Analogously, the amplitude of the dendritic spike was found by subtracting the average dendritic waveform of the same dataset from the individual records with extra dendritic spikes. Attenuation was calculated as the somatic event amplitude as a percentage of the dendritic event amplitude.

The dendritic integral was calculated between where the response crossed 3 mV above baseline membrane potential on its rising and falling phases.

The post complex spike pause was measured as the interval between the last spike of the complex spike and the next simple spike. Spontaneous interspike intervals (ISIs) were

calculated as the average of 3 consecutive intervals between simple spikes occurring in the same trace as the post-complex spike pause. Post-complex spike after-hyperpolarisations were quantified by finding the minimum voltage during the post-complex spike pause in spontaneous firing and subtracting mean baseline membrane potential (as measured above). Data was tested for statistical significance using Student's t-test (paired or unpaired as appropriate). Data were reported as the mean (in some cases weighted by the number of observations in each dataset (Bland and Kerry, 1998)) ± S.E.M unless otherwise indicated.

Modelling

NEURON simulation software ((Hines and Carnevale, 1997), www.neuron.yale.edu) was used to simulate the waveform of spikes in single compartments, spikes propagated from a distant site in a simplified multicompartmental model and of spikes propagated from the axon of a biologically realistic model of a Purkinje cell (Clark et al., 2005).

Single compartment model

Spikes waveform was investigated in a 20 μm diameter sphere (C_m 1μF/cm^2, R_m 20,000 Ωcm^2, R_i 150 Ωcm) furnished with either standard Hodgkin Huxley Na^+, K^+ and leak channels (www.neuron.yale.edu) or channels modelled on those recorded in Purkinje cells (Khaliq et al., 2003) (full channel descriptions given below). Densities of these channels was varied from 0 - 8 times 'standard' density, together with an additional tonic (linear, reversal 0 or -60 mV) conductance of 0 - 30 nS. The voltage deflections caused by brief current (0.5 - 1 ms) injection were analysed.

Multicompartment model of distant spike initiation site

Waveforms were recorded in a 1.2 μm diameter cable (C_m 1μF/cm^2, R_m 20,000 Ωcm^2, R_i 150 Ωcm). The recording site ('soma') was 10000 μm from the cable's sealed end and 100 μm (in the other direction) from the 'hotspot' of spike initiation. A symmetrical length of cable followed the 'hotspot' on the other side. The 'somatic' compartment (20 μm long) was either of uniform diameter (1.2 μm) with the rest of the cable, or varied to 20 μm. The 'hotspot' was made to initiate voltage deflections through either (i) voltage clamp to a square pulse (2 ms, 65 mV), a sample Purkinje cell somatic simple spike or sample Purkinje cell somatic complex spike spikelets (ii) brief current injection to an active compartment, with Hodgkin Huxley active channels at 16 times standard density. The somatic spike waveform was recorded under varying somatic active Hodgkin Huxley channel densities (0 - 16 times standard density; the 16x condition, where the compartment fired 80 mV action potentials was considered 1x 'full' channel density), and varying tonic somatic conductance (0 - 100 nS, -60 mV reversal).

Purkinje cell model

The Purkinje cell model developed by Dr Mickey London (Clark et al., 2005) was adapted for these simulations. In this model, the dendritic, somatic and axonal morphology was reconstructed from a representative P19 Purkinje cell and given passive parameters of R_m 20,000 Ωcm^2, R_i 150 Ωcm and C_m 1$\mu F/cm^2$ (or 0.21 $\mu F/cm^2$ in myelinated sections). In the simulations presented in this thesis, axon collaterals were removed to improve simulation speed. Nodes of Ranvier were placed at the main axon branchpoint and then at 350 μm from the soma, and thereafter in 350 μm intervals. Juxtaparanodal sections (5 μm) were placed between each myelin and node sections. Dendritic spines were incorporated by scaling membrane capacitance (scaling factor in spiny branchlets 5, in main trunk 1.2 (Roth and Häusser, 2001).

The Purkinje cell ion channel models of Khaliq et al., 2003 were inserted to the soma and initial segment, with densities scaled as by 8 and 16, respectively. Nodes of Ranvier contained only Na channels at a density 14 fold higher than the soma. Myelinated sections were passive, and juxtaparanode sections were identical to myelinated sections, except for additional delayed-rectifier K current at 1.6-fold the somatic density. In contrast to the model used in Clark et al., 2005, Ih was not present in the dendrites, preventing spontaneous axonal spike initiation. Spikes were initiated at the first node (as occurs spontaneously in the full model) by either voltage clamping the site to an action potential or injecting a brief current step. Waveforms were recorded at the soma; the density of active channels varied from 0 - 1 times full density and passive conductance (-60 mV) reversal was varied from 0 - 2000 nS.

Hodgkin Huxley channel parameters

The parameters of the standard Hodgkin Huxley channels (Hodgkin and Huxley, 1952b), as provided by NEURON, were:

Channel	gates	G_{max} (S/cm^2)	E_{rev} (mV)
Na^+	m^3h	0.120	50
K^+	n^4	0.036	-77
Leak	1	0.0003	-54.3

where each gate approached its equilibrium value of (substituting m or h for n as appropriate):

$$n_\infty(V) = \frac{\alpha_n(V)}{\alpha_n(V) + \beta_n(V)}$$

with the time course:

$$\tau_n(V) = \frac{1}{\alpha_n(V) + \beta_n(V)}$$

and α and β for each gate were given by:

$$\alpha_m = 0.1(-V - 40) \Big/ \left(exp\left(\frac{-V - 40}{10}\right) - 1\right)$$

$$\beta_m = 4exp\left(\frac{-V - 65}{18}\right)$$

$$\alpha_h = 0.07exp\left(\frac{-V - 65}{20}\right)$$

$$\beta_h = 1 \Big/ \left(exp\left(\frac{-V - 35}{10}\right) + 1\right)$$

$$\alpha_n = 0.01(-V - 55) \Big/ \left(exp\left(\frac{-V - 55}{10}\right) - 1\right)$$

$$\beta_m = 0.125exp\left(\frac{-V - 65}{80}\right)$$

Khaliq et al. 2003 Purkinje soma model parameters

Ion channel behaviours, based on voltage clamp data from isolated Purkinje cell somata, were modelled using the Hodgkin-Huxley gate formalisation (Hodgkin and Huxley, 1952b), except in the case of the resurgent sodium channels, which required a more complex state model (Khaliq et al., 2003).

For the sodium current, the following state model and parameters were used:

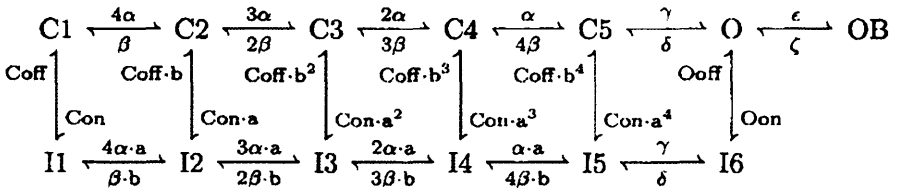

where C, I, O and OB represent closed, inactivated, open and open-blocked states, respectively.

Parameter	Value
α	$150\ e^{(V/20)}\ ms^{-1}$
β	$3\ e^{(V/20)}\ ms^{-1}$
γ	$150\ ms^{-1}$
δ	$40\ ms^{-1}$
ε	$1.75\ ms^{-1}$
ζ	$0.03\ e^{(-V/25)}\ ms^{-1}$
Con	$0.005\ ms^{-1}$
Coff	$0.5\ ms^{-1}$
Oon	$0.75\ ms^{-1}$
Ooff	$0.005\ ms^{-1}$
a	$Oon/Con^{1/4}$
b	$Ooff/Coff^{1/4}$
G_{max}	$0.015\ S/cm^2$
E_{Na}	+60 mV

Models for other currents were based on the Hodgkin-Huxley formalisation for each activation or inactivation gate (m or h). The steady state value of m was expressed as:

$$m_\infty = y_0 + \frac{1 - y_0}{1 + exp\left(-\frac{V_m - V_{1/2}}{k}\right)}$$

and was approached with the time course:

$$m = m_\infty - \left(m_\infty - m_0\right) exp\left(-\frac{\Delta t}{\tau_m}\right)$$

which combine to give a conductance of:

$$G = G_{max} m^x h^y$$

resulting a current flow determined by ohms law:

$$I = G \times \left(V - E_{rev}\right)$$

or, in the case of calcium current, by the Goldman-Hodgkin-Katz equation:

$$I = 4P_{Ca^{2+}} \frac{VF^2}{RT} \frac{\left[Ca^{2+}\right]_i - \left[Ca^{2+}\right]_0 exp\left(-2FV/RT\right)}{1 - exp\left(-2FV/RT\right)}$$

The following channels and parameters were used:

				m		h		
Channel	**gates**	**G_{max}** (S/cm^2)	**E_{rev}** (mV)	**$V_{1/2}$** (mV)	**k** (mV)	**y_0** (S/cm^2)	**$V_{1/2}$** (mV)	**k** (mV)
K^+_{fast}	m^3h	0.04	-88	-24	15.4	0.31	-5.8	-11.2
K^+_{mid}	m^4	0.02	-88	-24	20.4			
K^+_{slow}	m^4	0.04	-88	-16.5	18.4			
P-type Ca^{2+}	m	see below		-19	5.5			
BK	m^3z^2h	0.07	-88	-28.9	6.2	0.085	-32	-5.8
I_h	m	0.01	-30	-90.1	-9.9			
Leak	1	0.005	-60					

For all activation gates (m), y_0 was 0.

For the P-type calcium current, $P_{Ca^{2+}}$ = 5 x 10^{-5} cm/s, $\left[Ca^{2+}\right]_i$ = 100 nM, $\left[Ca^{2+}\right]_o$ = 2 mM, T = 295 K. F and R had their usual values.

The activation and inactivation time constants (τ_m and τ_h) were as follows:

K^+_{fast}

$$\tau_m = \begin{cases} 0.000103 + 0.0149\exp(0.035V_m) & V_m < -35\text{mV} \\ 0.000129 + 1\Big/\left(\exp\left(\frac{V_m + 100.7}{12.9}\right) + \exp\left(\frac{V_m - 56}{-23.1}\right)\right) & V_m \geq -35\text{mV} \end{cases}$$

$$\tau_h = \begin{cases} 1.22\times10^{-5} + 0.012\cdot\exp\left(-\left(\frac{V_m + 56.3}{49.6}\right)^2\right) & V_m \leq 0\text{mV} \\ 0.0012 + 0.0023\cdot\exp(-0.141V_m) & V_m > 0\text{mV} \end{cases}$$

K^+_{mid}

$$\tau_m = \begin{cases} 0.000688 + 1\Big/\left(\exp\left(\frac{V_m + 64.2}{6.5}\right) + \exp\left(\frac{V_m - 141.5}{-34.8}\right)\right) & V_m < -20\text{mV} \\ 0.00016 + 0.0008\cdot\exp(-0.0267V_m) & V_m \geq -20\text{mV} \end{cases}$$

K^+_{slow}

$$\tau_m = 0.000796 + 1\Big/\left(\exp\left(\frac{V_m + 73.2}{11.7}\right) + \exp\left(\frac{V_m - 306.7}{-74.2}\right)\right)$$

P-type Ca^{2+}

$$\tau_m = \begin{cases} 0.000264 + 0.128\cdot\exp(0.103V_m) & V_m \leq -50\text{mV} \\ 0.000191 + 0.00376\cdot\exp\left(-\left(\frac{V_m + 41.9}{27.8}\right)^2\right) & V_m > -50\text{mV} \end{cases}$$

BK

$$\tau_m = 0.000505 + 1\Big/\left(\exp\left(\frac{V_m + 86.4}{10.1}\right) + \exp\left(\frac{V_m - 33.3}{-10}\right)\right)$$

$$\tau_h = 0.0019 + 1\Big/\left(\exp\left(\frac{V_m + 48.5}{5.2}\right) + \exp\left(\frac{V_m - 54.2}{-12.9}\right)\right)$$

I_h

$$\tau_m = 0.19 + 0.72\cdot\exp\left(-\left(\frac{V_m + 81.5}{11.9}\right)^2\right)$$

The calcium dependent gate (z) of the BK channel had a time constant (τ_z) of 1 ms. Its steady state value was determined by

$$z_\infty = \frac{1}{1 + \frac{z_{coef}}{[Ca^{2+}]_i}}$$

where z_{coef} = 0.001 mM. Internal calcium concentration was modelled as uniform entry to a 100 nm shell beneath the cell membrane, and was calculated as

$$[Ca^{2+}]_t = [Ca^{2+}]_{t-1} + \Delta t\left(\frac{-100}{2F}\frac{I_{Ca}}{dA} - \beta[Ca^{2+}]_{t-1}\right)$$

where β = 1ms^{-1}. $[Ca^{2+}]$ is in mM, Δt is in ms, d is depth in μm, A is area in μm^2, and I_{Ca} in nA. $[Ca^{2+}]$ was constrained to be ≥ 100 nM.

Abbreviations used in this thesis

4-AP	4-Aminopyridine
ACSF	artificial cerebrospinal fluid
AMPA	α-Amino-3-hydroxy-5-methylisoxazole-4-propionic acid
Ca	calcium
Cd	cadmium
CF	climbing fibre
CV	coefficient of variation
DCN	deep cerebellar nuclei
EPSC	excitatory post synaptic potential
EPSG	excitatory post synaptic conductance
EPSP	excitatory post synaptic potential
f-I curve	relationship between firing frequency and injected current
IO	inferior olive
IPSC	inhibitory post synaptic current
IPSG	inhibitory post synaptic conductance
IPSP	inhibitory post synaptic potential
K_{Ca}	calcium activated potassium channel
Na	sodium
NMDA	N-Methyl-D-aspartic acid
PCR	polymerase chain reaction
QX-314	N-(2,6-Dimethylphenylcarbamoylmethyl)triethylammonium
SD	standard deviation
SEM	standard error of the mean
TTX	tetrodotoxin
Vm	membrane potential

Chapter 1:

Relationship between CF input size and the complex spike

Introduction

The high frequency burst of spikes known as the complex spike is a salient signal amongst the spontaneous spiking of a Purkinje cell, thought to represent sensory and motor timing signals (Gilbert and Thach, 1977; Gellman et al., 1985; Andersson and Armstrong, 1987; Llinas and Sasaki, 1989; Welsh et al., 1995; Bloedel and Bracha, 1998; Van Der Giessen et al., 2008). Within cells the complex spike waveform is highly reproducible (Eccles et al., 1966a; Crepel, 1971; Puro and Woodward, 1977; Llinas and Sugimori, 1980a), but across cells a wide variety of complex spike patterns are seen (Eccles et al., 1966a; Armstrong and Rawson, 1979; Campbell and Hesslow, 1986a; Schmolesky et al., 2002; Khaliq and Raman, 2005). Further, by stimulating the CF at high frequencies, or by blocking a proportion of the CF's AMPA receptors with NBQX (Foster et al., 2002), complex spikes composed of fewer, larger spikes spikes can be generated (Eccles et al., 1966d; Bloedel and Roberts, 1971; Campbell and Hesslow, 1986a; Hashimoto and Kano, 1998; Servais et al., 2004; Khaliq and Raman, 2005, though see also Campbell and Hesslow, 1986b). However, the exact relationship between the complex spike pattern and its underlying CF input and, consequently, the degree to which this can account for inter and intra- cell diversity of the complex spike is not yet understood.

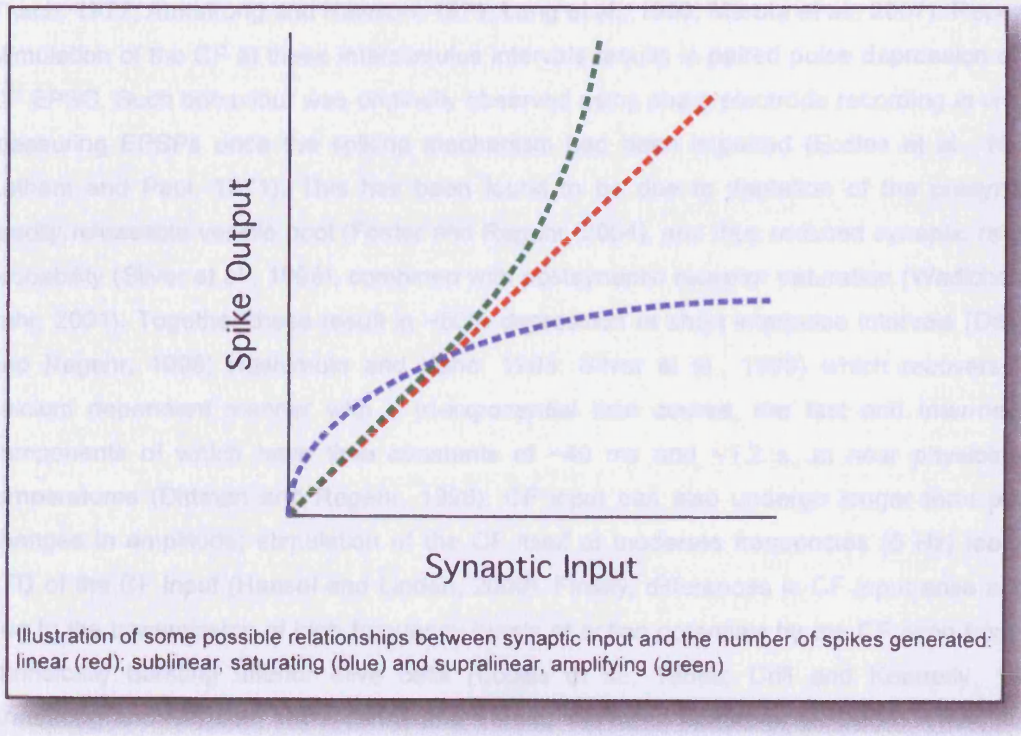

Illustration of some possible relationships between synaptic input and the number of spikes generated: linear (red); sublinear, saturating (blue) and supralinear, amplifying (green)

The nature of the transformation between CF synaptic input and complex spike bursting output is not easy to predict. Although the Purkinje cell displays a linear input-output relationship in response to tonic current injection (even after the removal of its dendrites, Bekkers and Häusser, 2007) and to parallel fibre stimulation (both clustered and distributed, Walter and Khodakhah, 2006; Mittmann and Häusser, 2007), this relationship can alter with the appearance of dendritic calcium spikes (Womack and Khodakhah, 2004; McKay et al., 2005; Rancz and Häusser, 2005). Further, the CF synaptic conductance is extremely large, orders of magnitude larger than even strong parallel fibre input (Konnerth et al., 1990; Llano et al., 1991; Dittman and Regehr, 1998; Hashimoto and Kano, 1998; Silver et al., 1998; Wadiche and Jahr, 2001). Thus, increasing the amplitude of this conductance may lead to a sublinear increase in synaptic current as conductance shunt increases and the resulting EPSP approaches the AMPA receptor reversal potential of 0 mV. This could lead to a saturating, sublinear 'input - output' relationship (see Fig. above). In contrast, the relationship might become supralinear (Fig. above), through amplification of the synaptic input by the recruitment of the active properties of the Purkinje cell, such as the prominent dendritic spikes activated by CF input (Eccles et al., 1966a; Fujita, 1968; Llinas and Sugimori, 1980b; Crepel et al., 1981; Chan et al., 1989; Callaway et al., 1995), or the intrinsic bursting mechanisms of the axon and soma (Raman and Bean, 1997; Swensen and Bean, 2003, 2005; Bekkers and Häusser, 2007)

The size of CF input is modulated by short and long term synaptic plasticity. *In vivo* CF input occurs at ~1 Hz, but with a large standard deviation such that intervals of 50-100 ms to >3 s are observed during normal activity (Eccles et al., 1967; Bell and Grimm, 1969; Gilbert and Thach, 1977; Armstrong and Rawson, 1979; Lang et al., 1999; Maruta et al., 2007). Repeated stimulation of the CF at these interstimulus intervals results in paired pulse depression of the CF EPSC. Such behaviour was originally observed using sharp electrode recording *in vivo* by measuring EPSPs once the spiking mechanism had been impaired (Eccles et al., 1966d; Latham and Paul, 1971). This has been found to be due to depletion of the presynaptic readily releasable vesicle pool (Foster and Regehr, 2004), and thus reduced synaptic release probability (Silver et al., 1998), combined with postsynaptic receptor saturation (Wadiche and Jahr, 2001). Together these result in ~50% depression at short interpulse intervals (Dittman and Regehr, 1998; Hashimoto and Kano, 1998; Silver et al., 1998) which recovers in a calcium dependent manner with a tri-exponential time course, the fast and intermediate components of which have time constants of ~40 ms and ~1.2 s, at near physiological temperatures (Dittman and Regehr, 1998). CF input can also undergo longer term plastic changes in amplitude; stimulation of the CF itself at moderate frequencies (5 Hz) leads to LTD of the CF input (Hansel and Linden, 2000). Finally, differences in CF input arise *in vivo* due to the transmission of high frequency bursts of action potentials by the CF axon from the intrinsically bursting inferior olive cells (Eccles et al., 1966a; Crill and Kennedy, 1967; Armstrong and Rawson, 1979; Llinas and Yarom, 1981a, b; Maruta et al., 2007). Thus, the *in*

vivo stimulus driving the complex spike is likely to be widely modulated during normal behaviour.

In this chapter, I have addressed the effect that such input modulation has on the Purkinje cell complex spike. I have, firstly, described the range and reproducibility of complex spikes evoked in Purkinje cell's by isolated CF input *in vitro*. I have then explored the effect of paired pulse CF stimulation and of rapid bursts of CF stimulation on the somatic complex spike and the CF evoked dendritic calcium spikes. Finally, through the recording of both EPSCs and complex spikes in the same cell at a variety paired pulse intervals, I have characterised the input-output relationship between CF EPSC size and the complex spike waveform. This has revealed surprisingly linear relationships between the CF input and both the number and timing of spikelets in the complex spike. Across cells, this accounts for a large proportion of the variability of the complex spike waveform.

Chapter 1: Results

Characteristics of the Purkinje cell complex spike

The complex spike is a reproducible high frequency burst of spikes that can be evoked by a single activation of a Purkinje cell's climbing fibre (Eccles et al., 1966a; Thach, 1967; Crepel, 1971, 1974; Llinas and Sugimori, 1980a) . A broad range of complex spike waveforms have been recorded in Purkinje cells (Eccles et al., 1966a; Crepel, 1971; Puro and Woodward, 1977; Armstrong and Rawson, 1979; Llinas and Sugimori, 1980a; Campbell and Hesslow, 1986a; Schmolesky et al., 2002; Khaliq and Raman, 2005); however, the intracellularly recorded, *in vitro*, isolated waveform has not been fully characterised. Fig. 1.1a shows example complex spikes from 12 cells together with the concomitant dendritic calcium spike (Llinas and Sugimori, 1980b) responses to CF stimulation (when simultaneously recorded). The examples are ordered by the number of spikes in the complex spike, and are representative of the range of complex spikes I recorded from Purkinje cells at rest, in slices from P 12-24 rats (34-35 °C), in response to repeated CF stimulation given at a 1 s interstimulus-interval.

I found that the complex spike was, on average, composed of 3.64 ± 0.93 spikes (mean ± SD, n = 38, Fig. 1.1b), and ranged between 2 ± 0 and 6.2 ± 0.4 somatic spikelets (within cell averages: maximum observed = 8). The number of spikes in the complex spike did not depend on age, within the range used (r = -0.17, p = 0.31, P12-24), or on baseline membrane potential (averaged over 50 ms, including spikes, r = 0.03, p = 0.87, bVm = - 54.1 ± 4.8 mV (mean ± SD), range -66 to -45 mV) and depended only weakly on spontaneous firing rate (r = 0.36, p = 0.03, rate = 53 ± 22 Hz (mean ± SD), range 17 - 110 Hz). Concomitantly with the complex spike at the soma, Purkinje cells fire dendritic calcium spikes (Llinas and Sugimori, 1980b; Crepel et al., 1981; Chan et al., 1989; Rancz and Häusser, 2006); I recorded on average 1.7 ± 0.5 dendritic spikes (mean ± SD, n = 24 cells, age P18-24, range 1 ± 0 to 2.97 ± 0.17, maximum observed = 3, Fig. 1.1c). The number of spikes in the complex spike was not correlated with the number of spikes in the dendritic response (r = -0.12, p = 0.59). I found that the complex spike burst of spikes lasted on average 4.8 ± 2.0 ms (mean ± SD, range 1.4 ± 0.05 to 11.1 ± 1.2 ms, n = 38, Fig. 1.1d), and indeed was high frequency; average instantaneous firing rate was 620 ± 96 Hz (mean ± SD) and the average maximum and minimum firing rates were 448 ± 114 Hz and 801 ± 184 Hz, respectively.

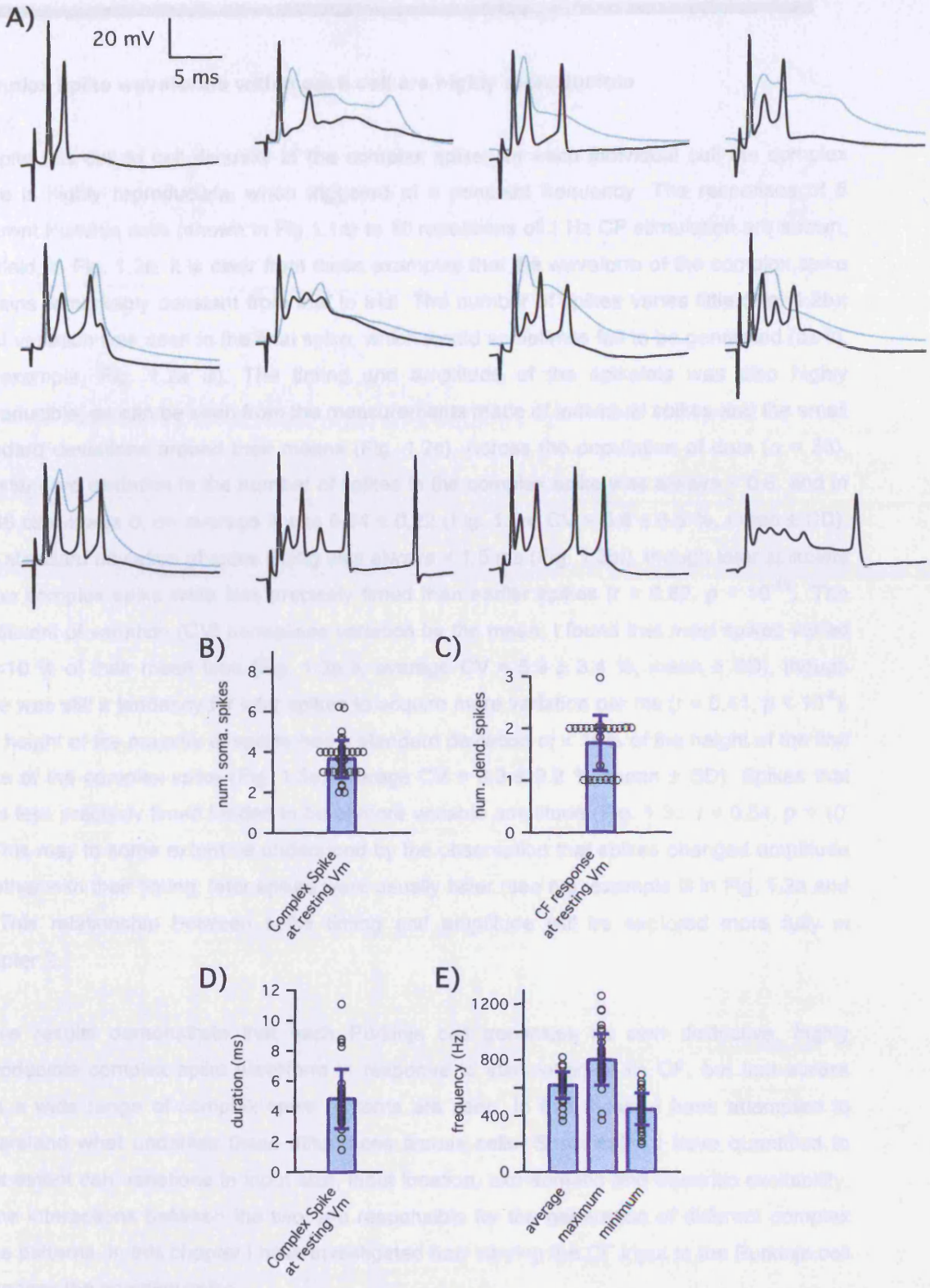

Fig 1.1 Characteristics of Complex Spikes across Purkinje cells

A) Example somatic complex spike responses of 12 different Purkinje cells to 1 Hz climbing fibre stimulation at resting membrane potential (black), together with, where recorded, concomitant dendritic calcium spike responses (blue). Responses are ordered by the number of spikes in their complex spike, and were chosen to reflect the range of complex spikes seen across cells. **B)** Somatic complex spike responses to 1 Hz CF stimulation were composed of between 2 and 7 spikes (population mean ± SD, blue bar, 3.7 ± 1.1, n = 38 cells). Individual cell's averages shown as black circles (places side by side where many cells showed the same or similar numbers of spike).
C) Purkinje cells displayed between 1 and 3 dendritic spikes in response to 1 Hz CF stimulation. Mean ± SD: 1.7 ± 0.5, n = 24 cells. Symbols as in B. **D)** Average duration of the complex spike (interval between first and last spike peaks) ranged between 1.4 and 13.9 ms; mean ± SD: 5.0 ± 2.4 ms (n = 38 cells). **E)** All complex spikes were high frequency bursts, though mean, maximum and minimum instantaneous firing frequencies (illustrated) varied across cells.

Complex spike waveforms within each cell are highly reproducible

Despite this cell to cell diversity of the complex spike, for each individual cell the complex spike is highly reproducible, when triggered at a constant frequency. The responses of 5 different Purkinje cells (shown in Fig 1.1a) to 10 repetitions of 1 Hz CF stimulation are shown, overlaid, in Fig. 1.2a. It is clear from these examples that the waveform of the complex spike remains remarkably constant from trial to trial. The number of spikes varies little (Fig. 1.2b); most variation was seen in the final spike, which would sometimes fail to be generated (as in, for example, Fig. 1.2a iii). The timing and amplitude of the spikelets was also highly reproducible, as can be seen from the measurements made of individual spikes and the small standard deviations around their means (Fig. 1.2c). Across the population of data (n = 38), the standard deviation in the number of spikes in the complex spike was always < 0.6, and in 15/38 cases was 0; on average it was 0.24 ± 0.22 (Fig. 1.3a, CV = 6.6 ± 6.5 %, mean ± SD). The standard deviation of spike timing was always < 1.5 ms (Fig. 1.3bi), though later spikelets of the complex spike were less precisely timed than earlier spikes ($r = 0.82$, $p < 10^{-16}$). The coefficient of variation (CV) normalises variation by the mean; I found that most spikes varied by <10 % of their mean time (Fig. 1.3b ii, average CV = 5.9 ± 3.4 %, mean ± SD), though there was still a tendency for later spikes to acquire more variation per ms ($r = 0.41$, $p < 10^{-5}$). The height of the majority of spikes had a standard deviation of < 10% of the height of the first spike of the complex spike (Fig. 1.3c, average CV = 8.3 ± 9.2 %, mean ± SD). Spikes that were less precisely timed tended to be of more variable amplitude (Fig. 1.3c, $r = 0.54$, $p = 10^{-9}$). This may to some extent be understood by the observation that spikes changed amplitude together with their timing; later spikes were usually taller (see e.g. example iii in Fig. 1.2a and c). This relationship between spike timing and amplitude will be explored more fully in Chapter 2.

These results demonstrate that each Purkinje cell generates its own distinctive, highly reproducible complex spike waveform in response to stimulation of its CF, but that across cells a wide range of complex spike patterns are seen. In this thesis, I have attempted to understand what underlies these differences across cells. Specifically, I have quantified to what extent can variations in input size, input location, axo-somatic and dendritic excitability, or the interactions between the two, are responsible for the generation of different complex spike patterns. In this chapter I have investigated how varying the CF input to the Purkinje cell influences the complex spike.

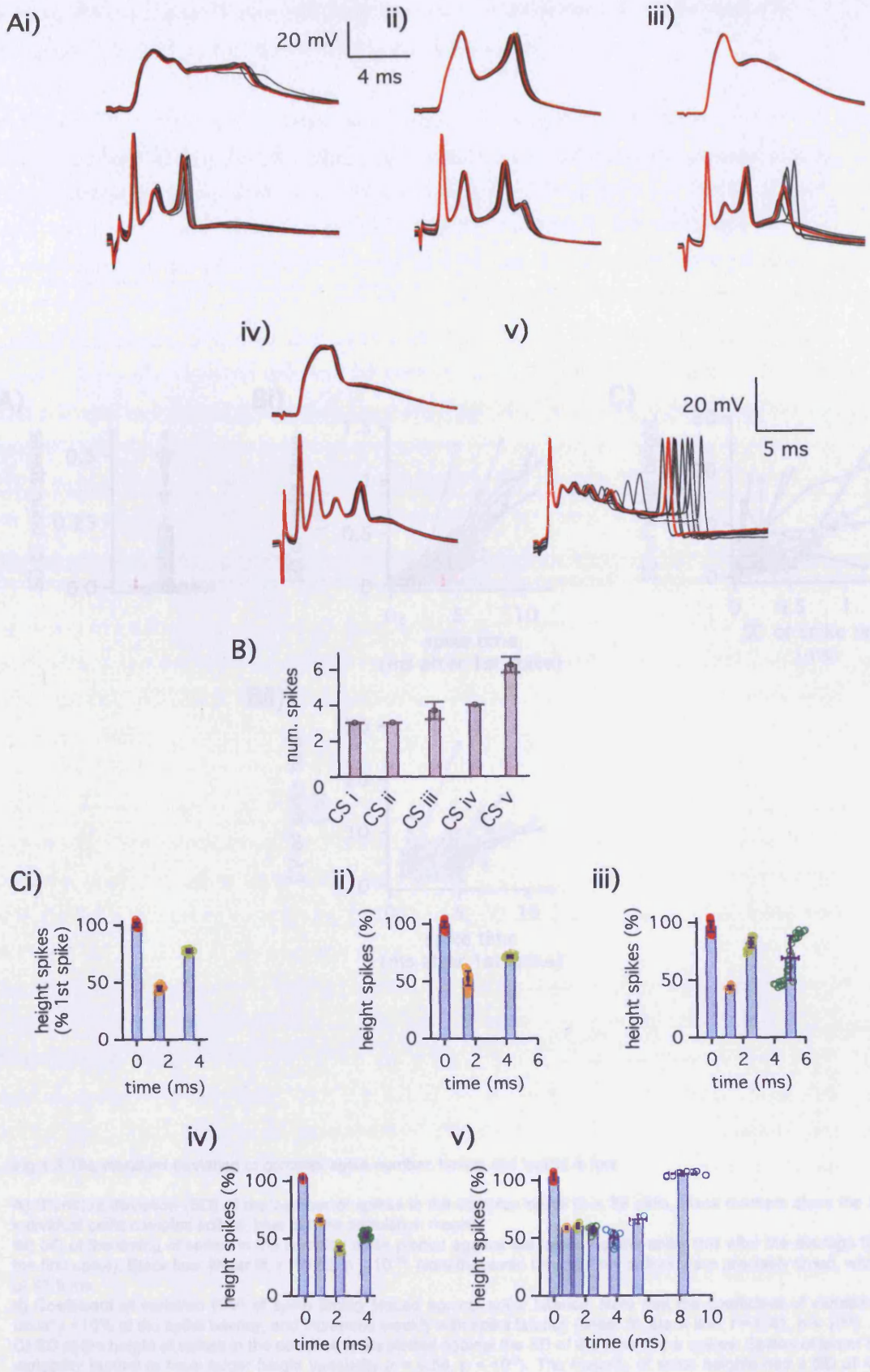

Fig 1.2 Complex spikes are highly reproducible

A) 10 repetitions of 1 Hz CF stimulation of 5 example Purkinje cells (responses overlayed, a single trace highlighted in red). Lower traces: somatic complex spikes, upper traces: dendritic calcium spike responses (no dendritic recording was made of the 5th Purkinje cell). **B)** Mean and SD of the number of spikes and **C)** spike timing and height in the complex spikes illustrated in A, demonstrating the low variability of the response. Coloured circles indicate the measurements of individual spikes. (Total number of complex spikes in the analysed data sets are 28, 77, 49, 34 and 25 respectively).

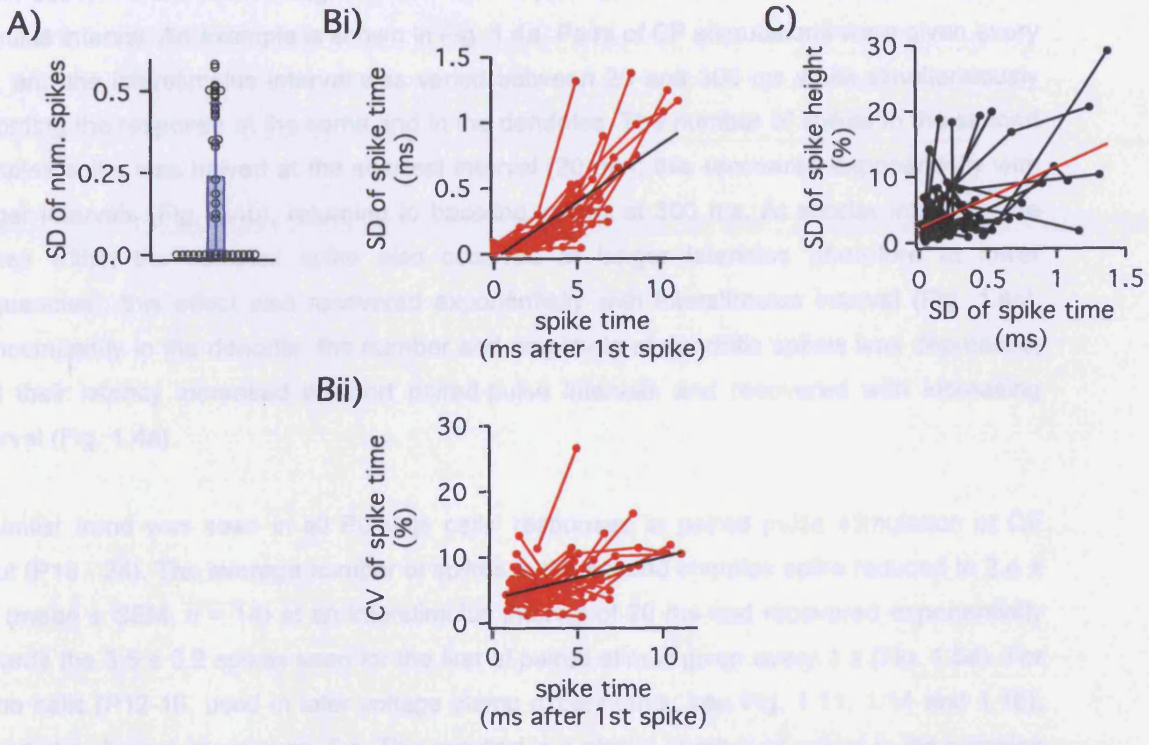

Fig 1.3 The standard deviation of complex spike number, timing and height is low.

A) Standard deviation (SD) of the number of spikes in the complex spike (n = 38 cells, black markers show the SD of individual cell's complex spikes, blue bar the population mean).
Bi) SD of the timing of spikes in the complex spike plotted against the latency of the spike (ms after the average time of the first spike). Black line: linear fit, $r = 0.82$, $p < 10^{-16}$. Note that even long latency spikes were precisely timed, with SDs of <1.5 ms.
ii) Coefficient of variation (CV) of spike timing plotted against spike latency. Note that the coefficient of variation was usually <10% of the spike latency, and increased weakly with spike latency (linear fit: black line, $r = 0.41$, $p < 10^{-5}$).
C) SD of the height of spikes in the complex spike plotted against the SD of the time of the spikes. Spikes of larger timing variability tended to have larger height variability ($r = 0.54$, $p < 10^{-9}$). The majority of spike heights had a SD of <10 % (relative to the height of the first spike in the complex spike).

Influence of CF paired-pulse interval on the complex spike

As discussed in the introduction, the CF to Purkinje cell synapse shows strong paired-pulse depression (Eccles et al., 1966d; Latham and Paul, 1971; Dittman and Regehr, 1998; Hashimoto and Kano, 1998; Silver et al., 1998), resulting in ~ 50% smaller CF EPSCs at short interstimulus intervals, recovering significantly over tens to hundreds of milliseconds. *In vivo*, while complex spikes are observed on average at 1 Hz, there is considerable irregularity in the occurrence of complex spikes, with inter-complex spike intervals of <50 ms or >3 s being observed (Eccles et al., 1967; Bell and Grimm, 1969; Armstrong and Rawson, 1979; Maruta et al., 2007). I therefore investigated how the complex spike waveform depended on inter CF stimulus interval. An example is shown in Fig. 1.4a. Pairs of CF stimulations were given every 1 s, and the interstimulus interval was varied between 20 and 300 ms while simultaneously recording the response at the soma and in the dendrites. The number of spikes in the second complex spike was halved at the shortest interval (20 ms); this recovered exponentially with longer intervals (Fig. 1.4b), returning to baseline values at 300 ms. At shorter intervals, the spikes within the complex spike also occurred at longer latencies (therefore at lower frequencies); this effect also recovered exponentially with interstimulus interval (Fig. 1.4c). Concomitantly in the dendrite, the number and amplitude of dendritic spikes was depressed, and their latency increased at short paired-pulse intervals and recovered with increasing interval (Fig. 1.4a).

A similar trend was seen in all Purkinje cells' responses to paired pulse stimulation of CF input (P18 - 24). The average number of spikes in the second complex spike reduced to 2.4 ± 0.1 (mean ± SEM, n = 14) at an interstimulus interval of 20 ms and recovered exponentially towards the 3.5 ± 0.2 spikes seen for the first of paired stimuli given every 1 s (Fig. 1.5a). For some cells (P12-16, used in later voltage clamp experiments; see Fig. 1.11, 1.14 and 1.15), paired stimuli were given every 5 s. This resulted in a similar number of spikes in the complex spike at an interstimulus interval of 1 s ($p > 0.99$); however this recovered even further to 3.8 ± 0.5 spikes (first stimulus of the pair given every 5 s, Fig. 1.5a ii) and depressed even more strongly at shorter intervals (down to 1.9 ± 0.2 at 20 ms interstimulus intervals). This may reflect the lower level of tonic of depression of the synapse at 0.2 Hz, and perhaps the speeding of fast recovery from depression at 1 Hz due to its calcium dependence (Dittman and Regehr, 1998), or perhaps an age dependence of recovery from PPD.

Across cells, the latency of all spikes in the complex spike increased at short paired-pulse intervals, with the largest change occurring for the later spikes (Fig. 1.5b). For cells in which the 1 Hz inter-sweep interval protocol was used, the first spike latency following CF stimulation was increased on average by 0.12 ± 0.02 ms at the shortest interstimulus interval, the second spike by 0.39 ± 0.05, the third by 1.5 ± 0.5 and the fourth by up to 4.9 ms (there were insufficient numbers of occurrences of later spikes to record the change in

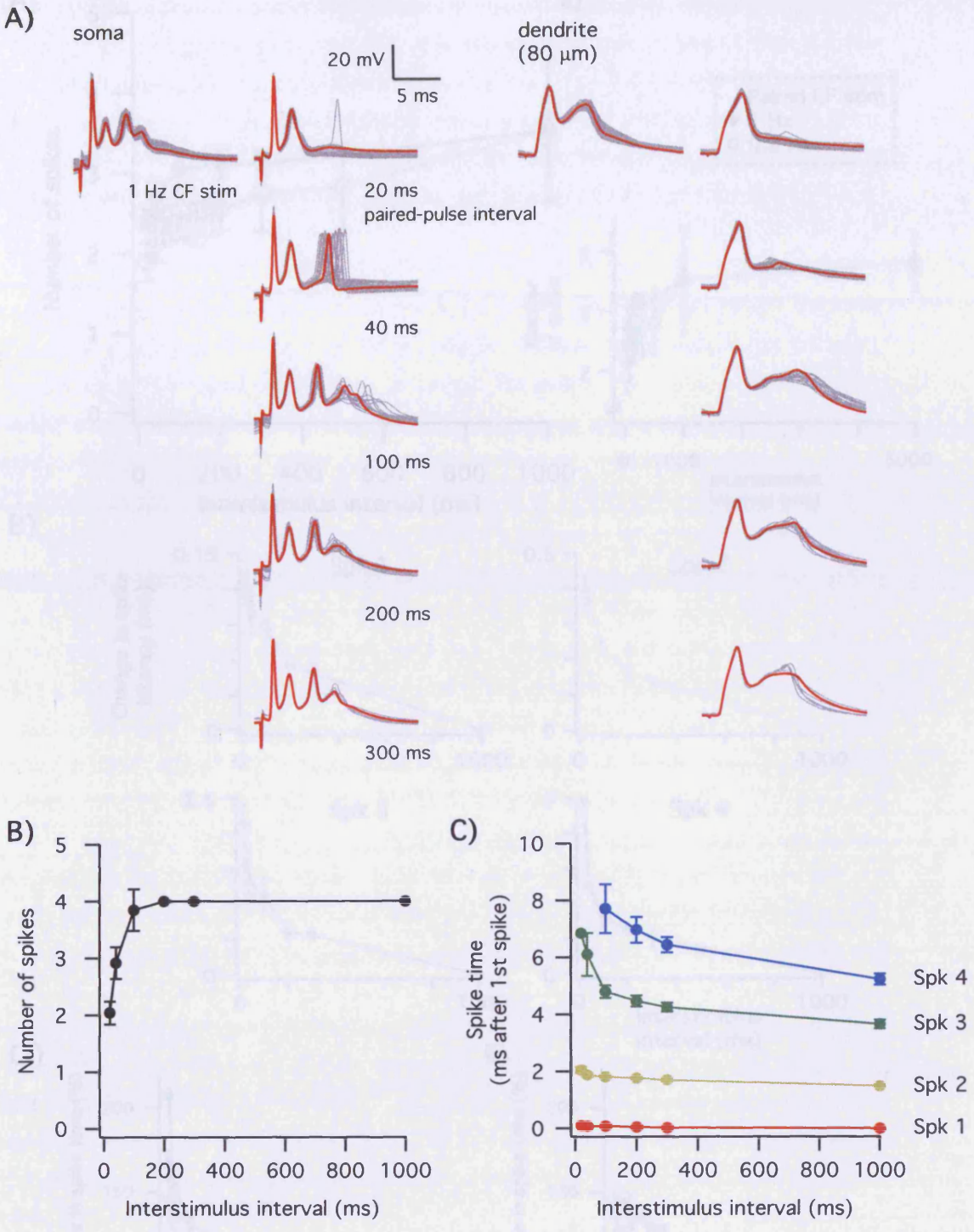

Fig 1.4 Paired-pulse stimulation of the CF reduces the number and increases the latency of spikes in the complex spike.

A) Example of responses to paired stimulation of the CF, recorded in the soma and concomitantly in the dendrite (80 µm from the soma). Every 1 s a pair of CF stimulations was given; the interval between these two stimulations was varied between 20 and 300 ms. The Purkinje cell's responses to the first and second stimulations are shown in the upper and lower panels respectively.
B) Relationship between the number of spikes in the complex spike and the paired-pulse stimulation interval (markers show mean ± SD). The values measured for the complex spike following the first stimulation (which occurred at a baseline rate of 1 Hz) are plotted at the 1000 ms interval.
C) Relationship between spike time and paired-pulse stimulation interval (markers show mean ± SD). The time of each of the spikes (spikes 1 – 4, coloured red, yellow, green and blue respectively) was measured relative to the average latency of the first spike of the complex spike following the first CF stimulation. Note that although the complex spike pattern is changed with stimulation frequency, it remains reliable.

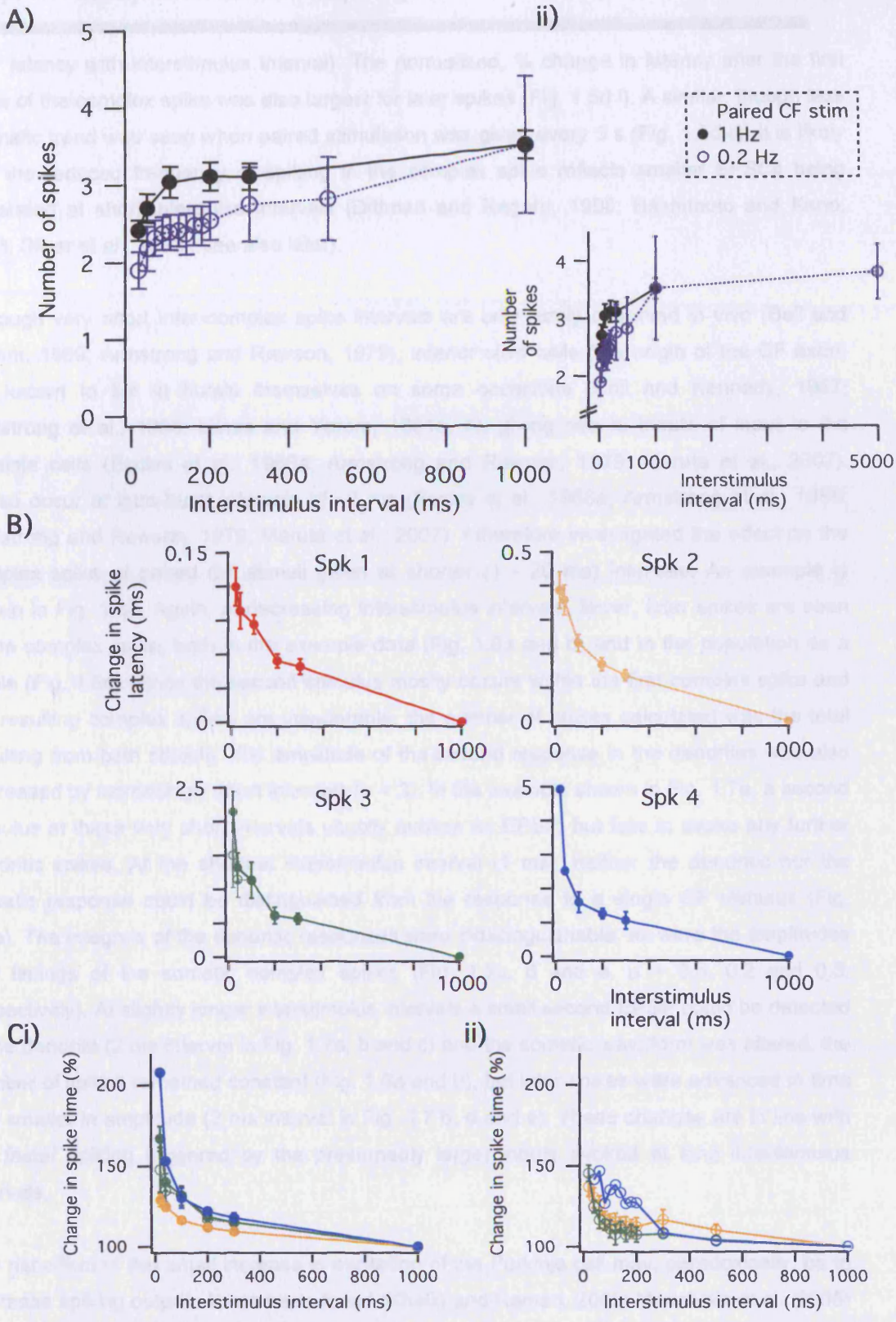

Fig 1.5 Average effect of paired pulse-stimulation on the complex spike.

Ai) Population average (± SEM) number of spikes in CS at different paired-pulse stimulation intervals. Data where pairs of CF stimulation were given every 1 s are shown in black (n = 14); a further data set where pairs were given every 5 s is shown in blue (n = 8). **ii)** The same expanded time scale to illustrate the full recovery in the number of spikes when pairs were stimulated every 5 s. **B)** Average change in spike timing with paired-pulse stimulation interval. The times of spike 1 – 4 of the complex spike are calculated relative to the times of spike 1 – 4 (respectively) of the complex spike response to the first CF stimulation. For spike 3, outliers with decreases in spike latency (see D) were either included (open circles) or excluded (filled circles) from the average). **Ci)** Change in spike timing expressed as a % of the latency of the spike after the first spike of the first complex spike. Pairs stimulated every 1 s. **ii)** Change in spike timing expressed as %, as in (i), but where CF stimulated every 5 s.

their latency with interstimulus interval). The normalised, % change in latency after the first spike of the complex spike was also largest for later spikes (Fig. 1.5d i). A similar, though less dramatic trend was seen when paired stimulation was given every 5 s (Fig. 1.5d ii). It is likely that the reduced frequency of spiking in the complex spike reflects smaller EPSCs being generated at short interpulse intervals (Dittman and Regehr, 1998; Hashimoto and Kano, 1998; Silver et al., 1998 , see also later).

Although very short inter-complex spike intervals are only rarely observed in vivo (Bell and Grimm, 1969; Armstrong and Rawson, 1979), inferior olive cells (the origin of the CF axon) are known to fire in bursts themselves on some occasions (Crill and Kennedy, 1967; Armstrong et al., 1968; Llinas and Yarom, 1981a, b), giving rise to bursts of input to the Purkinje cells (Eccles et al., 1966a; Armstrong and Rawson, 1979; Maruta et al., 2007). These occur at intra-burst intervals of ~2 ms (Eccles et al., 1966a; Armstrong et al., 1968; Armstrong and Rawson, 1979; Maruta et al., 2007). I therefore investigated the effect on the complex spike of paired CF stimuli given at shorter (1 - 20 ms) intervals. An example is shown in Fig. 1.6a. Again, at decreasing interstimulus intervals, fewer, later spikes are seen in the complex spike, both in the example data (Fig. 1.6a and b) and in the population as a whole (Fig. 1.6c) (since the second stimulus mostly occurs within the first complex spike and the resulting complex spikes are inseparable, the number of spikes calculated was the total resulting from both stimuli). The amplitude of the second response in the dendrites was also decreased by increasingly short intervals (n = 3). In the example shown in Fig. 1.7a, a second stimulus at these very short intervals usually evokes an EPSP, but fails to evoke any further dendritic spikes. At the shortest interstimulus interval (1 ms), neither the dendritic nor the somatic response could be distinguished from the response to a single CF stimulus (Fig. 1.7b). The integrals of the dendritic responses were indistinguishable, as were the amplitudes and timings of the somatic complex spikes (Fig. 1.7c, d and e, $p > 0.5$, 0.2 and 0.3, respectively). At slightly longer interstimulus intervals a small second EPSP could be detected in the dendrite (2 ms interval in Fig. 1.7a, b and c) and the somatic waveform was altered; the number of spikes remained constant (Fig. 1.6a and b), but later spikes were advanced in time and smaller in amplitude (2 ms interval in Fig. 1.7 b, d and e). These changes are in line with the faster spiking triggered by the presumably larger inputs evoked at long interstimulus intervals.

The net effect of this small increase in excitation of the Purkinje cell may, paradoxically, be to decrease spiking output. It has been found (Khaliq and Raman, 2005; Monsivais et al., 2005) that not all of the spikelets in the complex spike are successfully propagated down the Purkinje cell axon; small spikelets at short interspike intervals tend to fail at some point in the axon. Propagating and non-propagating spikes (as assessed by paired somatic and axonal recording) can be predicted with a high degree of accuracy, according to a combination of somatic interspike interval (ISI) and spike height or rate of rise (Khaliq and Raman, 2005;

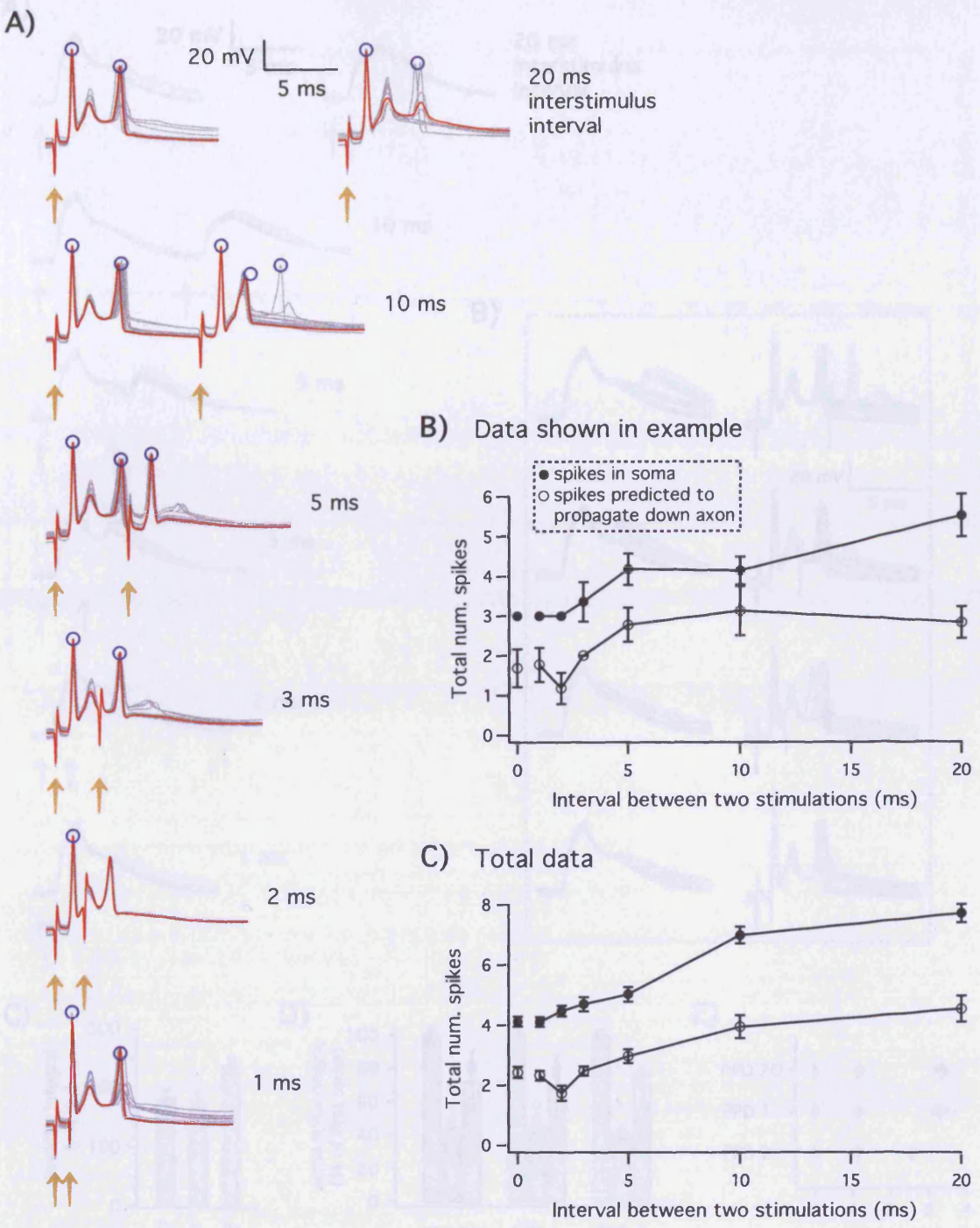

Fig 1.6 Paired-Pulse stimulation of the complex spike at short intervals

A) Example of CF stimulation at short intervals, starting at 20 ms and decreasing to the within the range of the interspike interval within bursts of CF activity seen in vivo. Yellow arrows indicate stimulation times, blue circles encapsulate the peaks of spikes that are predicted to propagate down the axon.
B) Quantification of the number (mean ± SD) of spikes in the example shown in A. Filled circles indicate spikes recorded in the soma, open circles indicate spikes predicted to propagate down the axon (see fig 1.8). Note that at 2 ms interstimulus intervals the number of somatic spikes remains unchanged but the number predicted to propagate down the axon is reduced due to the decrease in interspike interval and spike height at the soma.
C) Quantification of the average number of spikes following paired-pulse stimulation in the population of data (mean ± SEM, n = 11). As in B, filled circles indicate spikes actually recorded in the soma, open circles indicate spikes predicted to propagate down the axon.

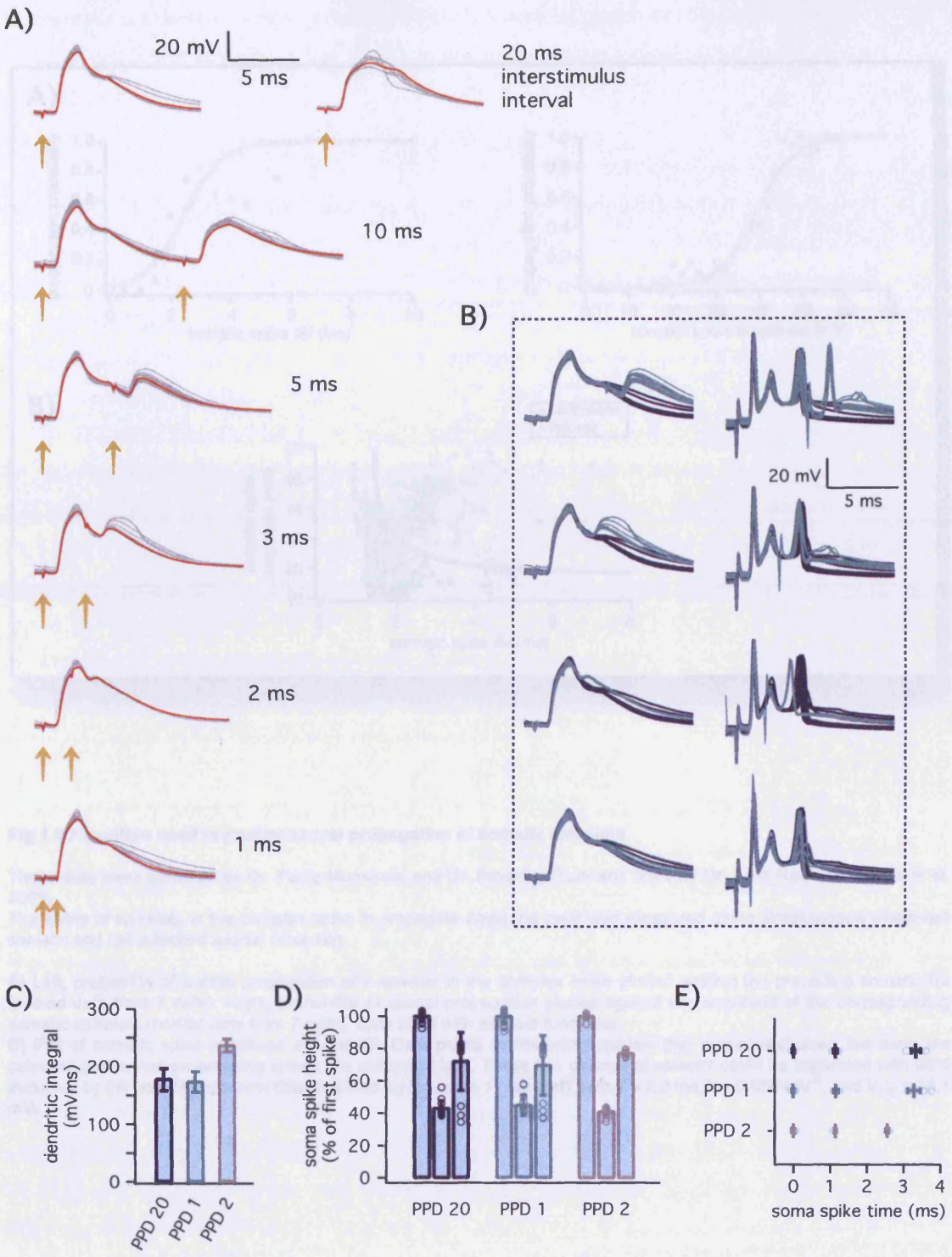

Fig 1.7 Dendritic response to CF stimulation at short interpulse intervals reveals temporal limit of effective synaptic transmission.

A) Illustration of dendritic recordings made simultaneously with the somatic recordings shown in Fig 1.6a. **B)** Overlay of the responses in dendrite (left) and soma (right) to the isolated first response to paired stimulation at 20 ms interstimulus intervals (dark blue traces in the background) and to paired stimulation at 5 – 1 ms interstimulus intervals. **C)** Integral of dendritic voltage responses to the first CF stimulation at 20 ms interstimulus intervals and to the response to both stimulations at 1 and 2 ms interstimulus intervals. The integral at 1 ms interstimulus interval is indistinguishable from the isolated first CF stimulation ($p > 0.5$), whereas the response at 2 ms interstimulus interval is significantly larger ($p < 10^{-5}$). **D)** Height of somatic spikes in response to the 3 stimulation paradigms detailed in (C). Heights of each spikelet are not significantly different between any of the data sets ($p > 0.2$). **E)** Time of somatic spikes in response to the same 3 stimulation paradigms. The timing third spikelet of the response to paired stimulation at a 1 ms interval is not distinguishable from the response to isolated first CF stimulation ($p > 0.3$), but following paired stimulation at a 2 ms interval is significantly earlier ($p < 10^{-4}$).

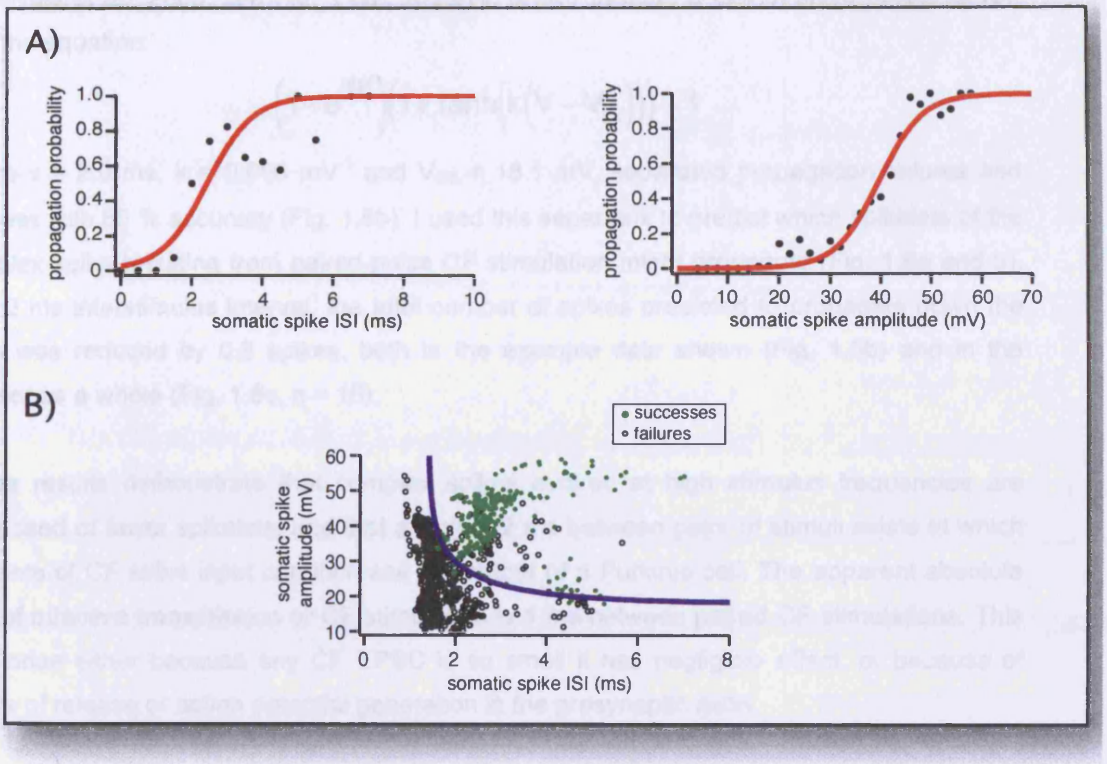

Fig 1.8 Algorithm used to predict axonal propagation of somatic spikelets

These data were gathered by Dr. Pablo Monsivais and Dr. Beverley Clark and fitted by Dr. Arnd Roth (Monsivais et al. 2005).
The ability of spikelets in the complex spike to propagate down the axon was measured using simultaneous whole-cell somatic and cell-attached axonal recording.

A) Left; probability of axonal propagation of a spikelet in the complex spike plotted against the preceding somatic ISI (pooled data from 7 cells). Right; probability of axonal propagation plotted against the amplitude of the corresponding somatic spikelets (pooled data from 7 cells). Data fitted with sigmoid functions.
B) Plot of somatic spike amplitude against ISI. Data points representing spiklets that propagated down the axon are coloured green, non-propagating spikes are coloured black. These two classes of spikelet could be separated with 85% accuracy by the best-fit separatrix (blue) defined by Equation 1 (see text), with τ = 2.0 ms, k = 0.056 mV^{-1}, and $V_{1/2}$ = 18.1 mV.

Monsivais et al., 2005; see Fig. 1.8a). A curve, drawn through a plot of spike height vs ISI, with the equation:

$$\left(1-e^{ISI/\tau}\right)\left(1+\tanh\left(k\left(V-V_{1/2}\right)\right)\right)=1$$

where τ = 2.0 ms, k = 0.056 mV^{-1} and $V_{1/2}$ = 18.1 mV, separated propagation failures and success with 85 % accuracy (Fig. 1.8b). I used this separatrix to predict which spikelets of the complex spike resulting from paired-pulse CF stimulation might propagate (Fig. 1.6a and b). At a 2 ms interstimulus interval, the total number of spikes predicted to propagate down the axon was reduced by 0.6 spikes, both in the example data shown (Fig. 1.6b) and in the dataset as a whole (Fig. 1.6c, n = 16).

These results demonstrate that complex spikes evoked at high stimulus frequencies are composed of fewer spikelets, and that a limit of 2 ms between pairs of stimuli exists at which doublets of CF spike input can increase the output of a Purkinje cell. The apparent absolute limit of effective transmission or CF stimulation is 1 ms between paired CF stimulations. This may arise either because any CF EPSC is so small it has negligible effect, or because of failure of release or action potential generation in the presynaptic axon.

Influence of bursts of CF input on the complex spike

CF axons do not fire only one or two spikes, but can generate bursts of up to 6 spikes (Eccles et al., 1966a; Armstrong et al., 1968; Armstrong and Rawson, 1979; Maruta et al., 2007). I therefore investigated the effect of these bursts on the Purkinje cell response. An example of bursts of 1 – 7 stimuli given every 1, 2 or 3 ms, recorded simultaneously in the soma and dendrite, is shown in Fig. 1.9 a, b and c, respectively. It can be seen that, while two stimuli given at an interstimulus interval of 1 ms do not elicit any change in Purkinje cell voltage trajectory (as detailed above), trains of 3 – 7 stimuli given every 1 ms do further depolarise the dendrites and alter somatic spiking (Fig. 1.9 a and di). Extra dendritic spikes are, however, only triggered by ≥ 5 stimuli at 2 or 3 ms interstimulus intervals. Bursts of >3 inputs at all interstimulus intervals increased the firing frequency of the complex spike and, in some cases, triggered additional spikes (Fig. 1.9a, b, c, di). The number of spikes in the soma increases by 0.9 per additional CF stimulus for stimuli given every 2 ms, and by 1.3 per stimulus for stimuli given every 3 ms (the slopes in this example are similar to the average population data values of 0.4, 1.1 and 1.6 spikes per stimulus for 1, 2 and 3 ms interstimulus intervals). Note, however, that the patterns evoked by bursts of ≤ 3 inputs still appear very similar to complex spikes evoked by single spikes, and might not be easily distinguished by a post-synaptic cell.

Again, as above, the increase in firing frequency and the small amplitude of the spikelets evoked are predicted to reduce the number of spikes propagated down the Purkinje cell axon

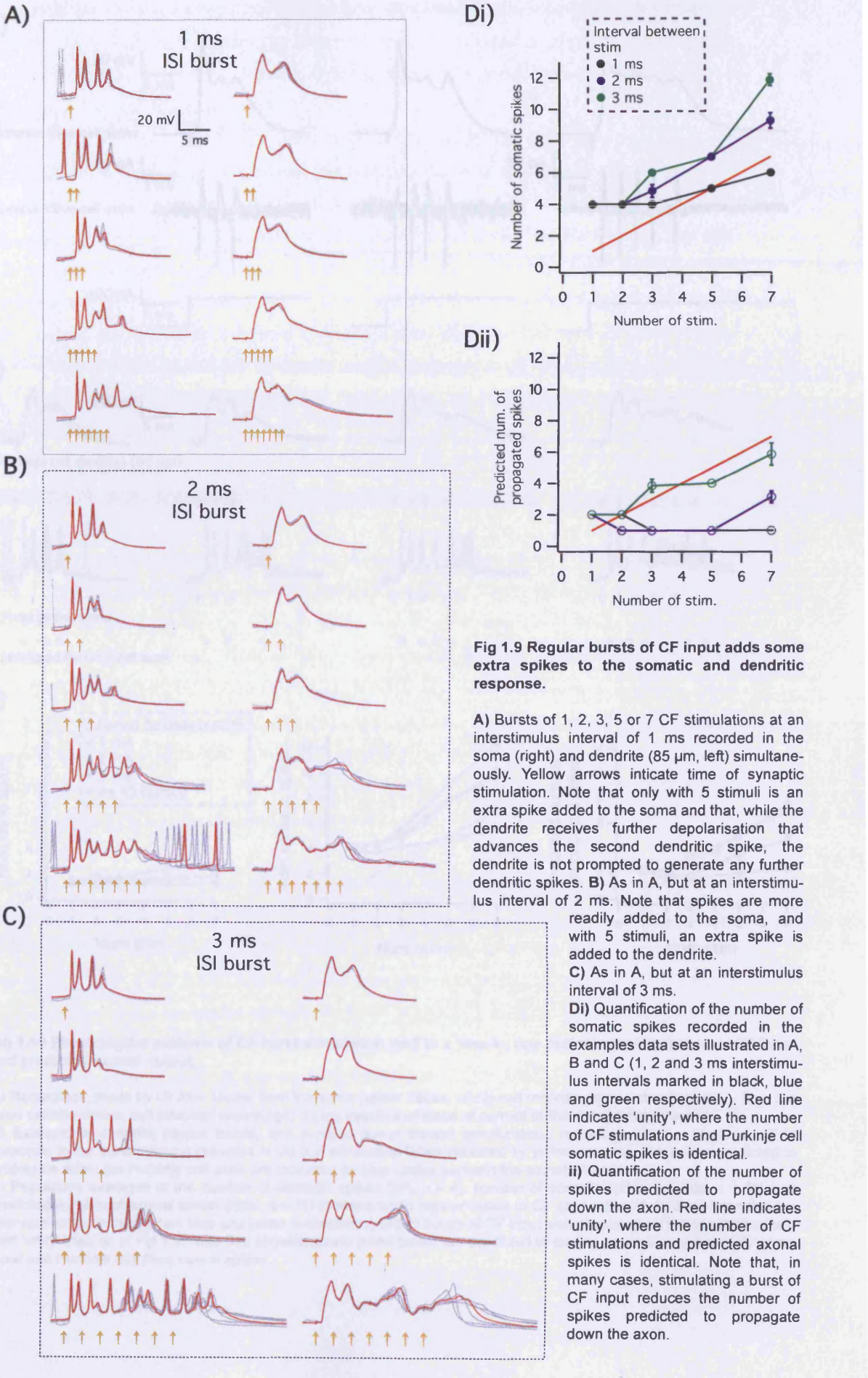

Fig 1.9 Regular bursts of CF input adds some extra spikes to the somatic and dendritic response.

A) Bursts of 1, 2, 3, 5 or 7 CF stimulations at an interstimulus interval of 1 ms recorded in the soma (right) and dendrite (85 µm, left) simultaneously. Yellow arrows inticate time of synaptic stimulation. Note that only with 5 stimuli is an extra spike added to the soma and that, while the dendrite receives further depolarisation that advances the second dendritic spike, the dendrite is not prompted to generate any further dendritic spikes. **B)** As in A, but at an interstimulus interval of 2 ms. Note that spikes are more readily added to the soma, and with 5 stimuli, an extra spike is added to the dendrite.
C) As in A, but at an interstimulus interval of 3 ms.
Di) Quantification of the number of somatic spikes recorded in the examples data sets illustrated in A, B and C (1, 2 and 3 ms interstimulus intervals marked in black, blue and green respectively). Red line indicates 'unity', where the number of CF stimulations and Purkinje cell somatic spikes is identical.
ii) Quantification of the number of spikes predicted to propagate down the axon. Red line indicates 'unity', where the number of CF stimulations and predicted axonal spikes is identical. Note that, in many cases, stimulating a burst of CF input reduces the number of spikes predicted to propagate down the axon.

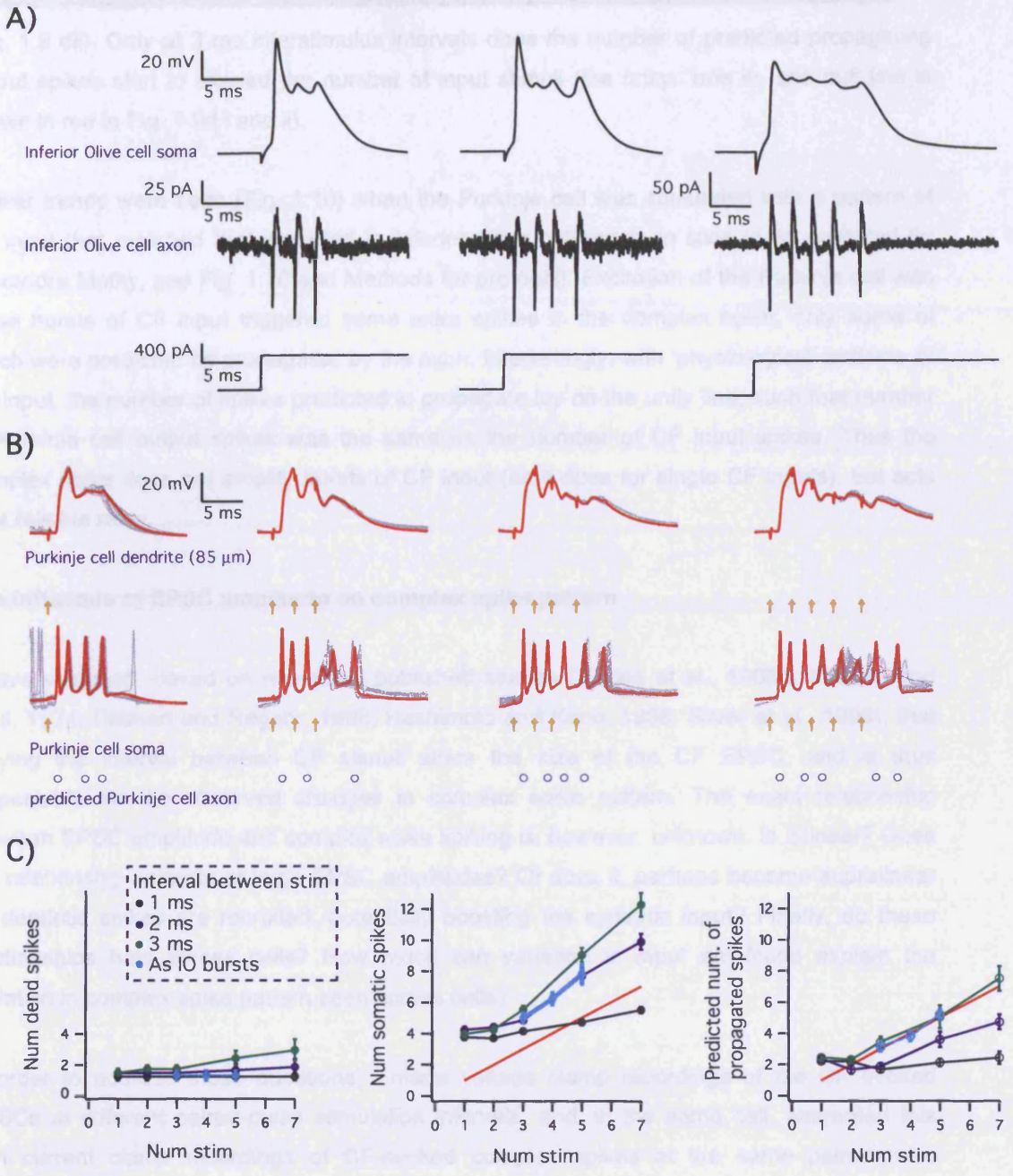

Fig 1.10 Physiological patterns of CF burst stimulation lead to a 'one in, one out' relationship between CF input and predicted axonal output.

A) Recordings, made by Mr Alex Mathy, from the soma (upper traces, whole cell recordings) and simultaneously from the axon (middle traces, cell attached recordings) during injection of steps of current to the soma (lower traces).
B) Example of dendritic (upper traces) and somatic (lower traces) simultaneous recordings from a Purkinje cell in response to the burst patterns recorded in (A) (CF stimulation times indicated by yellow arrows). The spikes predicted to propagate down the Purkinje cell axon are indicated by blue circles beneath the somatic traces.
C) Population averages of the number of dendritic spikes (left, n = 4), number of somatic spikes (middle, n = 11) and predicted number of axonal spikes (right, n = 11) in response to regular bursts of CF stimulation (1, 2, 3 ms interstimulus interval marked in black, dark blue and green respectively) and to bursts of CF input with physiological timings (turquoise). Red 'unity' lines as in Fig 1.9. Note that physiologically timed bursts are predicted to lead to an equal number of CF axon input and Purkinje cell axon output spikes.

(Fig. 1.9 dii). Only at 3 ms interstimulus intervals does the number of predicted propagating output spikes start to exceed the number of input stimuli (the unity, 'one in, one out' line is shown in red in Fig. 1.9d i and ii).

Similar trends were seen (Fig. 1.10) when the Purkinje cell was stimulated with a pattern of CF input that matched that recorded in Inferior Olive cell axons in slice (data collected by Alexandre Mathy, see Fig. 1.10 and Methods for protocol). Excitation of the Purkinje cell with these bursts of CF input triggered some extra spikes in the complex spike, only some of which were predicted be propagated by the axon. Interestingly, with 'physiological' patterns of CF input, the number of spikes predicted to propagate lay on the unity line, such that number of Purkinje cell output spikes was the same as the number of CF input spikes. Thus the complex spike does not amplify bursts of CF input (as it does for single CF inputs), but acts as a reliable relay.

The influence of EPSC amplitude on complex spike pattern

I have assumed, based on numerous published studies (Eccles et al., 1966d; Latham and Paul, 1971; Dittman and Regehr, 1998; Hashimoto and Kano, 1998; Silver et al., 1998), that varying the interval between CF stimuli alters the size of the CF EPSC, and is thus responsible for the observed changes in complex spike pattern. The exact relationship between EPSC amplitude and complex spike spiking is, however, unknown. Is it linear? Does the relationship saturate at large EPSC amplitudes? Or does it, perhaps become supralinear as dendritic spikes are recruited, potentially boosting the synaptic input? Finally, do these relationships hold across cells? How much can variation in input amplitude explain the variation in complex spike pattern seen across cells?

In order to address these questions, I made voltage clamp recordings of the CF evoked EPSCs at different paired-pulse stimulation intervals, and, in the same cell, alternated this with current clamp recordings of CF-evoked complex spikes at the same paired-pulse intervals (Fig. 1.11d). In order to achieve good somatic voltage clamp and current clamp of the CF responses, I made double somatic recordings using a voltage clamp and a current clamp amplifier (an Axopatch 200B and Axoclamp 2B, respectively) (Fig. 1.11a). When recording complex spikes, the voltage clamp amplifier was set to I=0 mode, and thus did not influence the spikes recorded by the current clamp electrode. When EPSCs were recorded in voltage clamp mode, the current clamp electrode was used to monitor the membrane potential at the soma, ensuring good local voltage clamp. In voltage clamp, pipette series resistance compensation was adjusted online until as little voltage escape as possible was recorded with the somatic current clamp electrode (typical values were 80 - 95 % compensation of 5 - 10 MΩ series resistances); the effect of under and over compensating series resistance on the somatic membrane potential and the recorded EPSC is shown in

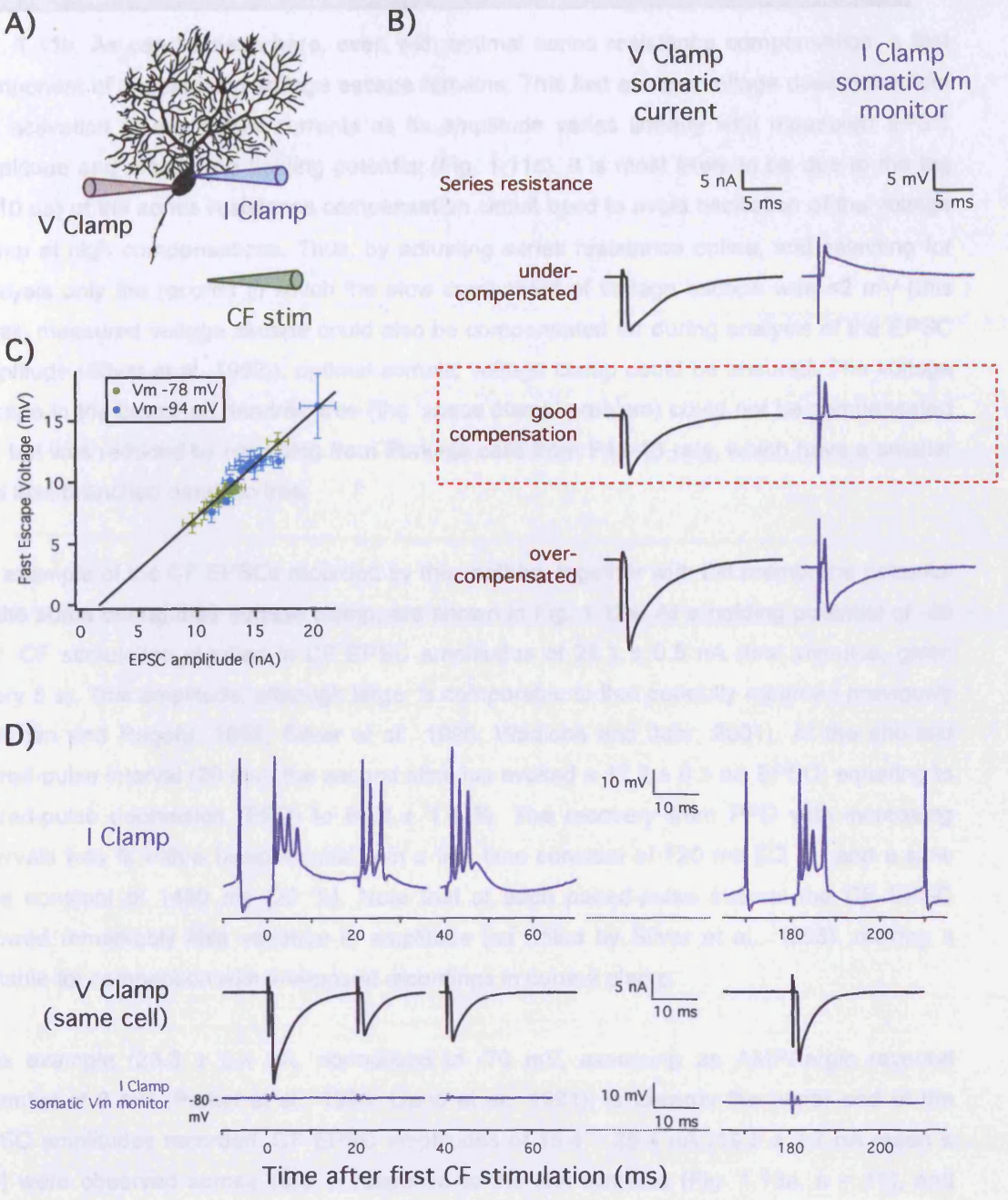

Fig 1.11 Method used to measure complex spikes and their underlying EPSCs

A) Illustration of recording configuration. The soma was patched twice, with one electrode (grey) connected to an Axopatch 200B voltage clamp amplifier and another (blue) to an Axoclamp 2B current clamp amplifier. Paired pulse stimulation of the climbing fibre (green electrode) was recorded in voltage clamp at a Vm of <-70 mV (with the current clamp electrode monitoring the voltage control of the soma) or in current clamp at rest (with the voltage clamp amplifier switched to I=0 mode).

B) Achieving good somatic voltage clamp. By adjusting voltage clamp series resistance compensation, the somatic Vm (right hand column, blue) during the EPSC either deflects positively (under-compensation, top), negatively (over-compensation, bottom) or remains relatively constant (good compensation, middle); the recorded EPSC (left) grew in parallel with increased compensation. Note that the stimulus artefact and a fast positive voltage escape remain, even with good series resistance compensation.

C) Example of relationship between the fast escape voltage (during optimum series resistance compensation) and EPSC amplitude (varied by paired-pulse stimulation of the CF), recorded at two voltages (-78 mV: green markers, and -94 mV: blue markers). Note that the fast voltage escape varies linearly with EPSC amplitude and is reduced at the more depolarised Vm, suggesting that it does not reflect active escape current.

D) By varying the interval between CF paired-pulse stimulations, EPSCs of differing amplitude were evoked (voltage clamp record; middle trace, current clamp monitor; lower trace); at the same intervals, complex spikes of differing waveform were recorded (current clamp; upper traces). As the EPSCs evoked are highly reproducible (see later figures and Silver et al 1998, Dittman Regehr 1998, Hashimoto Kano 1998), it can be concluded that the complex spike waveforms are triggered by the currents recorded at the same intervals, but in separate trials.

Fig. 1.11b. As can be seen here, even with optimal series resistance compensation, a fast component of depolarising voltage escape remains. This fast escape voltage does not reflect the activation of any active currents as its amplitude varies linearly with measured EPSC amplitude and membrane holding potential (Fig. 1.11c). It is most likely to be due to the lag (7-10 μs) of the series resistance compensation circuit used to avoid oscillation of the voltage clamp at high compensations. Thus, by adjusting series resistance online, and selecting for analysis only the records in which the slow component of voltage escape was <2 mV (this small, measured voltage escape could also be compensated for during analysis of the EPSC amplitude (Silver et al. 1998)), optimal somatic voltage clamp could be ensured. The voltage escape in the branched dendritic tree (the 'space clamp' problem) could not be compensated for, but was reduced by recording from Purkinje cells from P12-16 rats, which have a smaller and less branched dendritic tree.

An example of the CF EPSCs recorded by this method, together with the membrane potential at the soma during their voltage clamp, are shown in Fig. 1.12a. At a holding potential of -85 mV, CF stimulation resulted in CF EPSC amplitudes of 28.1 ± 0.5 nA (first stimulus, given every 5 s). This amplitude, although large, is comparable to that carefully recorded previously (Dittman and Regehr, 1998; Silver et al., 1998; Wadiche and Jahr, 2001). At the shortest paired-pulse interval (20 ms), the second stimulus evoked a 17.2 ± 0.3 nA EPSC; equating to paired-pulse depression (PPD) to 60.9 ± 1.4 %. The recovery from PPD with increasing intervals was fit with a biexponential with a fast time constant of 120 ms (23 %) and a slow time constant of 1490 ms (20 %). Note that at each paired-pulse interval the CF EPSC showed remarkably little variation in amplitude (as noted by Silver et al., 1998), making it suitable for comparison with interposed recordings in current clamp.

This example (23.3 ± 0.4 nA, normalised to -70 mV, assuming an AMPAergic reversal potential of 0 mV (Perkel et al., 1990; Llano et al., 1991)) is towards the upper end of the EPSC amplitudes recorded. CF EPSC amplitudes of 15.4 – 25.4 nA (19.5 ± 3.7 nA mean ± SD) were observed across cells in response to the first stimulus (Fig. 1.13a, n = 11), and depressed to 7.4 – 14.9 nA (10.8 ± 2.9, mean ± SD, paired-pulse interval 20 ms), a PPD of between 44 and 61 % (Fig. 1.13b). Recovery from PPD was fitted with an average biexponential curve with τ_{fast} of 15 ms (39 %) and a τ_{slow} of 485 ms (36 %). The wide range of EPSC amplitudes that occur as a result of PPD at this synapse, both within and across cells, together with their trial-to-trial reproducibility, provided an apposite tool with which to investigate the dependence of the complex spike on EPSC amplitude.

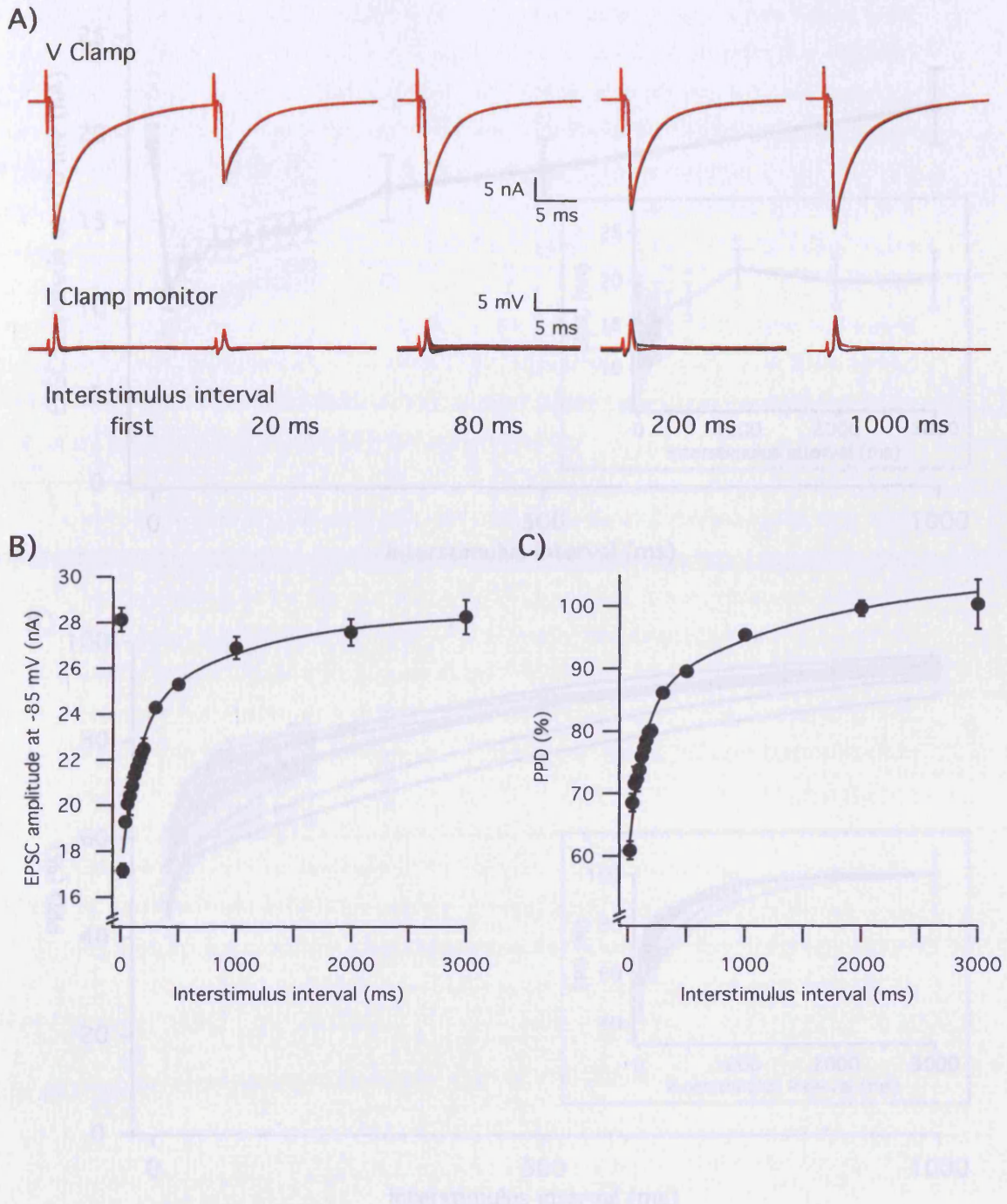

Fig 1.12 Paired pulse depression of CF EPSCs (example)

A) Example recordings of CF EPSCs evoked in a P14 Purkinje cell held in voltage clamp at -85 mV (upper traces; lower traces shown simultaneous current clamp monitor of the somatic voltage. Several traces are overlayed (black) and a single example highlighted in red). CF stimulations at paired pulse intervals of 20 - 500 ms were given every 5 seconds; intervals of 1000 - 3000 ms were given every 8 seconds. Intervals of 20, 80, 200 and 1000 ms are illustrated.
B) Average (± SD) EPSC amplitude at paired-pulse intervals of 20 – 3000 ms. Recovery is fitted with a biexponential (τ_{fast} 142 ms (6 nA), τ_{slow} 1042 ms (4.4 nA)).
C) Average (±SD) paired pulse depression (PPD, second EPSC at a % of first EPSC) of EPSCs. Recovery is fitted with a biexponential (τ_{fast} 120 ms (23 %), τ_{slow} of 1490 ms (20%)).

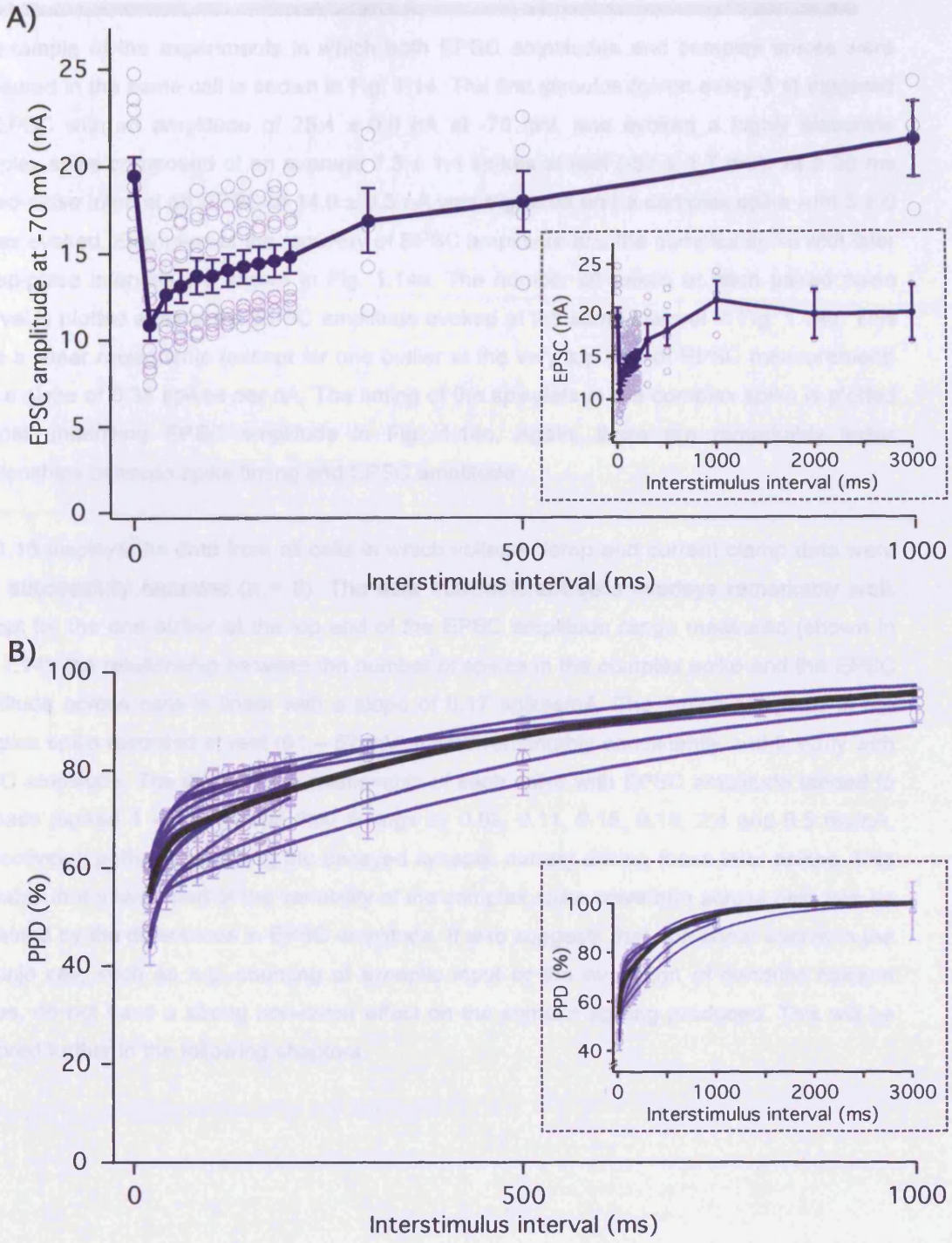

Fig 1.13 Paired pulse depression of CF EPSCs (population average)

A) Average EPSC amplitude recorded in P12-16 Purkinje cells at paired-pulse intervals of 20 – 1000 ms (light blue open circles) (n = 11). Population average ± SEM is overlayed (dark blue filled circles). Inset shows recovery over a longer time scale, 20 – 3000 ms (data 1000 – 3000 ms intervals was collected from fewer cells, n = 3).
B) Average paired pulse depression of EPSCs in the same 11 Purkinje cells (light blue circles). Within each data set, recovery is fitted with a biexponential (dark blue lines); the biexponential described by the average of these fits is overlayed in black (τ_{fast} 15 ms (39 %), τ_{slow} 485 ms (36%)). Again, inset shows recovery on the longer time scale.

An example of the experiments in which both EPSC amplitudes and complex spikes were measured in the same cell is shown in Fig. 1.14. The first stimulus (given every 5 s) triggered an EPSC with an amplitude of 25.4 ± 0.8 nA at -70 mV, and evoked a highly elaborate complex spike composed of on average 7.3 ± 1.4 spikes at rest (-57 ± 1.7 mV). At a 20 ms paired-pulse interval an EPSC of 14.9 ± 0.3 nA was triggered and a complex spike with 3 ± 0 spikes evoked. Examples of the recovery of EPSC amplitude and the complex spike with later paired-pulse intervals are shown in Fig. 1.14a. The number of spikes at each paired pulse interval is plotted against the EPSC amplitude evoked at the same interval in Fig. 1.14b. This gave a linear relationship (except for one outlier at the very top end of EPSC measurement) with a slope of 0.35 spikes per nA. The timing of the spikelets in the complex spike is plotted against underlying EPSC amplitude in Fig. 1.14c. Again, there are remarkably linear relationships between spike timing and EPSC amplitude.

Fig 1.15 displays the data from all cells in which voltage clamp and current clamp data were both successfully recorded (n = 8). The data from different cells overlays remarkably well. Except for the one outlier at the top end of the EPSC amplitude range measured (shown in Fig. 1.14), the relationship between the number of spikes in the complex spike and the EPSC amplitude across cells is linear with a slope of 0.17 spikes/nA. The timing of spikes in the complex spike recorded at rest (61 – 52 mV) varied remarkably consistently and linearly with EPSC amplitude. The slope of the relationship of each spike with EPSC amplitude tended to increase (spikes 1 - 6 advanced their timings by 0.02, 0.11, 0.15, 0.15, 2.4 and 6.5 ms/nA, respectively), perhaps reflecting the decayed synaptic current driving these later spikes. This indicates that a large part of the variability of the complex spike waveform across cells can be explained by the differences in EPSC amplitude. It also suggests that non-linear events in the Purkinje cell, such as e.g. shunting of synaptic input or the evocation of dendritic calcium spikes, do not have a strong non-linear effect on the somatic spiking produced. This will be explored further in the following chapters.

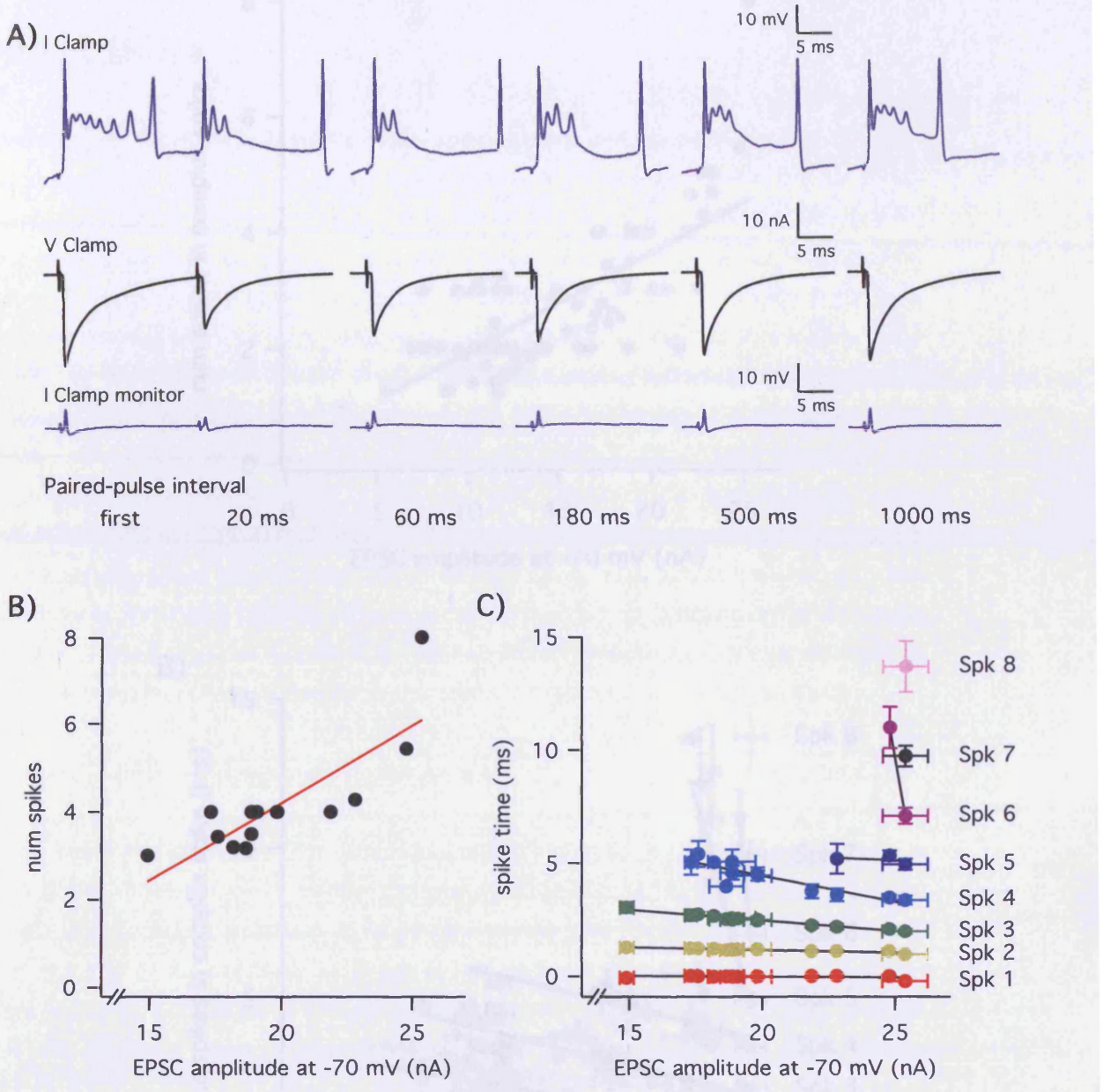

Fig 1.14 Example of complex spike pattern dependence of EPSC amplitude

A) Example responses to paired-pulse CF stimulation recorded in current clamp (top panels) or in voltage clamp (middle panels, current clamp monitor of somatic voltage clamp shown in bottom panels) at the interstimulus intervals marked below the traces (20 - 1000 ms), in a P15 Purkinje cell.
B) Relationship between the number of spikes in the complex spike and the EPSC measured at the same interstimulus interval (normalised to -70 mV), for the cell shown in A.
C) Relationship between time of spikes in the complex spike (coloured according to spike number) and the EPSC measured at the same interstimulus interval (normalised to -70 mV), for cell shown in A.

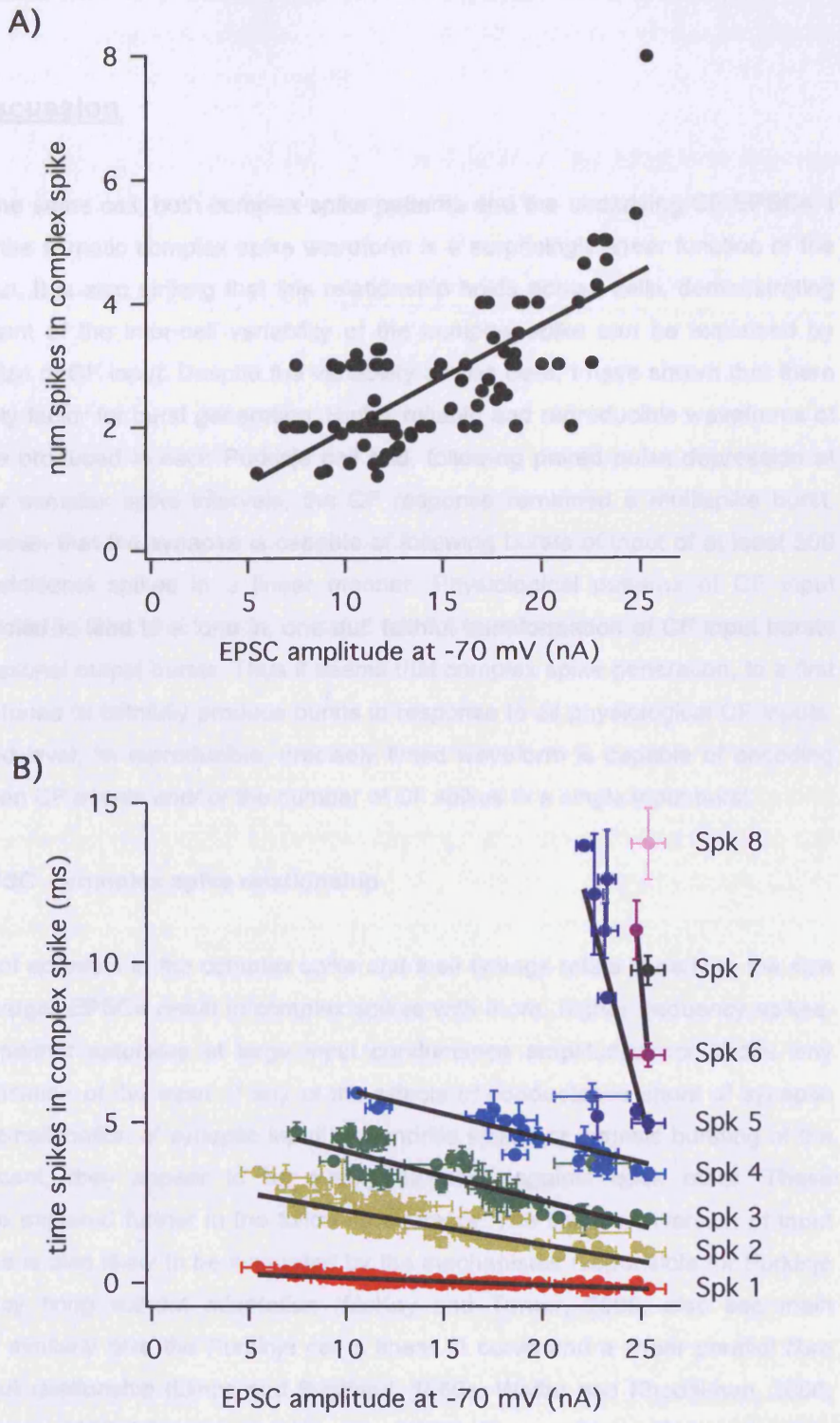

Fig 1.15 Complex spike pattern dependence of EPSC amplitude

A) Average number of spikes in complex spike plotted against the underlying EPSC amplitude recorded at the same paired-pulse stimulation interval (normalised to -70 mV) (n = 8 cells). Black line shows linear fit of the total data, with a slope of 0.17 spikes per nA peak EPSC.

B) Average time of spikes (± SD) in complex spike plotted against the underlying EPSC amplitude (± SD, normalised to -70 mV). Time was measured relative to the average time of the first spike of the complex spike; data from different cells (n = 8) was aligned so that the time of the first spike lay along the same sloping relationship. For each spiklet in the complex spike a line was fitted; spikes were advanced by 0.02, 0.11, 0.15, 0.15, 2.4 and 6.5 ms/ nA peak EPSC for spikes 1 - 6, respectively.

Chapter 1: Discussion

By recording, in the same cell, both complex spike patterns and the underlying CF EPSCs, I have shown that the somatic complex spike waveform is a surprisingly linear function of the CF excitatory input. It is also striking that this relationship holds across cells, demonstrating that a large amount of the inter-cell variability of the complex spike can be explained by variability in the size of CF input. Despite the variability across cells, I have shown that there exists a high safety factor for burst generation. Highly reliable and reproducible waveforms of 2 – 8 spikes were produced in each Purkinje cell and, following paired pulse depression at physiological inter complex spike intervals, the CF response remained a multispike burst. Further, I have shown that the synapse is capable of following bursts of input of at least 500 Hz, generating additional spikes in a linear manner. Physiological patterns of CF input bursting are predicted to lead to a 'one in, one out' faithful transformation of CF input bursts into Purkinje cell axonal output bursts. Thus it seems that complex spike generation, to a first approximation, is tuned to faithfully produce bursts in response to all physiological CF inputs. At a more detailed level, its reproducible, precisely timed waveform is capable of encoding the interval between CF events and/ or the number of CF spikes in a single input burst.

The linear CF EPSC – complex spike relationship

Both the number of spikelets in the complex spike and their timings relate linearly to the size of the CF input. Larger EPSCs result in complex spikes with more, higher frequency spikes. The relationship neither saturates at large input conductance amplitudes nor shows any supralinear amplification of the input. If any of the effects of conductance shunt of synaptic current or active amplification of synaptic input by dendritic spikes or intrinsic bursting of the soma are significant, they appear to be evenly balanced against each other. These possibilities will be explored further in the following chapters. The linear conversion of input into somatic spikes is also likely to be supported by the mechanisms responsible for Purkinje cell high frequency firing without adaptation (McKay and Turner, 2005, also see main Introduction), that similarly give the Purkinje cell a linear f/I curve and a linear parallel fibre input - spike output relationship (Llinas and Sugimori, 1980a; Walter and Khodakhah, 2006; Bekkers and Häusser, 2007; Mittmann and Häusser, 2007). The number or timing of spikes within complex spikes from different cells overlay well when plotted against EPSC amplitude, allowing generalised, linear 'input-output' functions to be made. This shows that, to a large extent, the differences in complex spike pattern across cells are caused by differences in CF input strength. However, there is a fairly large scatter of the data about the these linear fits due to differences between cells, suggesting that inter-cell differences in Purkinje excitability

also contribute to the complex spike pattern generated by a CF input of a certain amplitude; this will also be addressed in the following chapters.

The Purkinje cell excitability, complex spikes and CF EPSCs that I recorded, and drew the above conclusions from, were consistent with previous reports of their characteristics. Spontaneous firing frequencies were similar to those reported in Häusser and Clark, 1997. Somatic complex spikes and dendritic calcium spikes were of similar waveforms to those previously observed *in vivo* (using extracellular recording: Crepel, 1971; Puro and Woodward, 1977; Armstrong and Rawson, 1979; Campbell and Hesslow, 1986a; or intracellular sharp electrode recording: Eccles et al., 1966a; Campbell and Hesslow, 1986a) and at rest *in vitro* (recorded using sharp electrodes: Llinas and Sugimori, 1980b, a; Crepel et al., 1981; Chan et al., 1989; or patch clamp electrodes: Foster et al., 2002; Khaliq et al., 2003). I have here given a quantification of these waveforms. The remarkably large CF EPSC amplitudes (15 – 25 nA, normalised to -70 mV) are similar to the CF EPSC amplitudes reported by some groups (Dittman and Regehr, 1998; Wadiche and Jahr, 2001, reported values normalised to -70 mV), though somewhat larger than the 14 ± 6.4 nA (mean ± SD) EPSCs reported by Silver et al. (1998), who also monitored and corrected for somatic voltage escape. These latter EPSCs were, however, recorded at room temperature: EPSC amplitudes can be increased at more physiological temperatures by a number of factors, including increased receptor channel open probability, more rapid transmitter binding rates and channel kinetics and increases in the size of the vesicle pool (Silver et al., 1996; Micheva and Smith, 2005; Postlethwaite et al., 2007).

The average biexponential fit to EPSC PPD recovery in my data yielded a greater contribution of the fast component, and faster time constants of both the fast and slower components, than measured by Dittman & Regehr in P9-13 Purkinje cells at 34°C (1998):

	τ_1 (ms)	A_1 (%)	τ_2 (ms)	A_2 (%)
My data	17	38	550	35
Dittmann and Regehr's data	44	15	1200	36

The differences observed may be due to the difference in the rate of CF stimulation: I presented pairs of CF stimuli every 5 s, whereas Dittman & Regehr used an interval of at least 10 s between presentations. As Dittman & Regehr found that the fast component of recovery was speeded and increased in amplitude by residual presynaptic calcium, this is a likely cause for my measurement of a larger, more rapid fast component of PPD recovery. The parameters that I recorded are also in close agreement with those measured for recovery of EPSPs in sharp electrode recordings once spiking had decayed (A_1 ~20%, τ_1 ~20 ms, A_1 ~30%, τ_1 ~500 ms; Dittman and Regehr, 1998, taken from Eccles et al., 1966a; Eccles et al.,

1966d, see also Latham and Paul, 1971). It is also possible that there may be a developmental difference in PPD (I recorded from slightly older Purkinje cells, P12-16, rather than P9-13) (Hashimoto and Kano, 2003). Both of these factors may also be, in part, responsible for the differences in paired-pulse depression of the complex spike waveform recorded when presenting pairs of stimuli every 1 s to P18-24 Purkinje cells (see Fig. 1.5).

Voltage clamp recordings were restricted to P12-16 Purkinje cells in order to make more accurate recordings of the CF EPSCs, and somatic membrane potential was simultaneously monitored to control for errors arising from voltage escape. Although I was able to verify good somatic voltage clamp, the passive properties of the highly branched Purkinje cell lead to unavoidable problems of poor space clamp of the dendrites (Spruston et al., 1993; Roth and Häusser, 2001; Williams and Mitchell, 2008). The time taken to charge the membrane capacitance, together with the leak of current through the membrane resistance and the voltage drop across the dendrites axial resistance limit ability of the somatic voltage clamp circuit to control the dendritic voltage; electrically distant synapses can therefore depolarise the local dendritic membrane. This voltage escape in the dendrites could lead to either underestimation or overestimation of the CF EPSC. Passive depolarisation would reduce the synaptic driving force, reducing the recorded EPSC (Spruston et al., 1993; Roth and Häusser, 2001; Williams and Mitchell, 2008) (this may, however, reflect the current that reaches the soma during synaptic input more accurately than that measured given perfect voltage clamp of the dendrites). Depolarisation that leads to a Ca^{2+} spike in the dendrites would generate extra current that would contribute to the 'EPSC' at the soma (though the bulk of this distortion may be limited to the decay, as calcium spikes occur after the peak of the EPSC). Large EPSC amplitudes exacerbate these problems, thus the EPSC-complex spike relationship derived may undersample large CF inputs or those that trigger the largest, unclampable excitable responses. I have attempted to reduce these problems by holding at very hyperpolarised levels (-70 to -90 mV), so that the latter problem of active voltage escape is less likely, and by the restricting recordings to younger Purkinje cells, which are smaller and less branched.

P12-16 Purkinje cells are, however, not fully mature in terms of their dendritic branching pattern (Roth and Häusser, 2001; McKay and Turner, 2005) or their excitability (McKay and Turner, 2005; Fry, 2006). Purkinje cells increase in dendritic width and height with development, only begin to level off after P18 (Berry and Bradley, 1976; McKay and Turner, 2005); over this time they also increase in their excitability (Muller et al., 1998; Cingolani et al., 2002; McKay and Turner, 2005; Fry, 2006). Further, although synaptic properties such as quantal content, vesicular release probability, multivesicular release, post-synaptic receptor density, AMPA receptor properties and synaptic distribution across the main dendrites are mature once mono innervation has been achieved (Palay and Chan-Palay, 1974; Mason et al., 1990; Chedotal and Sotelo, 1992; Tempia et al., 1996; Silver et al., 1998; Hashimoto and

Kano, 2003; Momiyama et al., 2003; Nishiyama and Linden, 2004; Scelfo and Strata, 2005; Tanaka et al., 2005; Masugi-Tokita et al., 2007), it is likely that the total number of synaptic contacts, and thus synaptic conductance, increases somewhat as the Purkinje cell dendritic tree expands to its full extent. Such an increase has been observed empirically (Hashimoto and Kano, 2005; Sugihara, 2006) but has not yet been quantified for direct comparison, perhaps because of the increasing inaccuracy in EPSC measurement introduced by the worsening space clamp problem with age.

With development, complex spike pattern has also been found to alter, decreasing slightly in duration and increasing in spikelet frequency (Crepel, 1971, 1974; Puro and Woodward, 1977). These changes are likely to reflect the increasing excitability of the Purkinje cell (McKay and Turner, 2005; Fry, 2006; Muller et al., 1998; Cingolani et al., 2002) and increasing amplitude of CF input (Hashimoto and Kano, 2005; Sugihara, 2006). The *in vivo*, sensory evoked complex spike has also been found to increase in reproducibility with age (Puro and Woodward, 1977); this might be aided by the aforementioned increases in synaptic amplitude and Purkinje cell excitability, but can be ascribed largely to the loss of CF multi-innervation. My results indicate that the smaller CF inputs to a multiply innervated cell should produce a complex spike of fewer spikes, at a lower frequency than that produced by the largest input; observation of both together in one cell would greatly increase the measure of variability of the response. As I took care to avoid multiply innervated cells, and thus recorded the result of selection of a single strong input, this variability was not seen in my recordings. In addition to this reduction of intracell variability of CF input, there are reasons why the amplitude of CF input might be stabilised with development to produce a response of a certain amplitude after development, reducing intercell variability. For example, excessive CF activity leads to a reduction (LTD) of the CF input (Hansel and Linden, 2000) but some CF activity is required to maintain CF input strength to adult Purkinje cells (Kakizawa et al., 2005). Further, homeostatic feedback, via the activity triggered in the cell, can act both to regulate synaptic activity (Turrigiano, 2007) and postsynaptic excitability (Cerminara and Rawson, 2004; McKay et al., 2007). Indeed, there are suggestions in my data that the complex spike might vary across cells to a greater extent at P12-16 vs P18-24. The intercell variability of EPSC amplitude and complex spikes deserves further exploration at CF identical stimulation frequencies across a continuous range of ages.

Overall, the developmental changes that occurred during my P12-16 recording window (see Results and Crepel, 1971) did not prevent the finding of a common EPSC - complex spike relationship across cells. Further, although some developmental changes continue after P12-16, my recordings of complex spikes in more developed Purkinje cells from older animals (P18-24) do not suggest that there is a fundamental change in the nature of the complex spike pattern or its relationship with paired pulse depression of the CF input.

Reliability of the complex spike pattern

Complex spikes in a single Purkinje cell, generated by the whole range of EPSC sizes measured, whether depressed or not, are highly reproducible. The standard deviation of the total number of spikes was usually <0.5 and that of the spike times was similarly usually <0.5 ms. The timing of later spikes is more variable (although SD was always <1.5 ms) due to an accumulation of timing jitter; throughout the burst the CV of spike timing is usually <10%. Thus, rapid spiking during strong CF input is even more precise than that driven by intrinsic pacemaker currents alone (CV = 10 ± 0.9%, Häusser and Clark, 1997). The reliability of spike timing is probably due to the large conductance, large synaptic release site, sharp onset synaptic input (Silver et al., 1998), in combination with the high density of transient sodium channels available for triggering spikes and of fast potassium channels active between spikes (Kay et al., 1998; Raman and Bean, 1999; McKay et al., 2005; Akemann and Knopfel, 2006; de Ruiter et al., 2006; Fry, 2006; Zagha et al., 2008), all of which are ideal for reducing spike timing jitter (Schneidman et al., 1998; Schreiber et al., 2004; Xu-Friedman and Regehr, 2005)) (though the presence of persistent sodium current (Kay et al., 1998) may act somewhat against these factors, as it increases spike timing jitter of synaptically evoked spikes (Schneidman et al., 1998; Vervaeke et al., 2006)). The increase in spike timing variance throughout the burst is likely to be due to the cumulative actions of noise (from e.g. the stochastic properties of the spike generation mechanisms) randomly perturbing spike generation, especially during its highly non-linear, regenerative initiation (Schneidman et al., 1998). Robinson & Harsch (2002) found (experimentally and theoretically) that, during the suprathreshold period of decreasing current injections, noise uniformly perturbs a stable firing limit cycle of gradually decreasing frequency. This results in a fairly constant accumulation of noise, and a fairly constant CV of spike timing, as seen initially during complex spikes. However, when inputs fall below threshold, noise randomly drives spiking out of the attractor cycle round threshold, triggering spikes at less regular intervals; this results in an increase in spike timing variance (Robinson and Harsch, 2002). These factors may underlie the increases in the CV of spike timing observed in the final phase of the complex spike, where the EPSC - complex spike relationships become more noisy. The amount of time spent in this more noisy phase may be limited by the termination of CF triggered bursts by a variety of potassium and calcium activated potassium conductances in the soma and dendrites, as suggested by Robinson & Harsh (2002) (Edgerton and Reinhart, 2003; McKay et al., 2005; Zagha et al., 2008) and by the fact that the spontaneously firing Purkinje cell is not below threshold even with zero current input (Häusser and Clark, 1997). Thus, the CF input in combination with the intrinsic properties of the Purkinje cell are ideally suited to create a accurately timed, reliable complex spike burst.

Coding with the complex spike pattern

The complex spike generated at the soma is not the final output of the Purkinje cell. Paired axonal and somatic recordings have shown that only spikelets that are sufficiently rapidly

rising, large amplitude and at a sufficient delay after the previous spikelet are successfully propagated by the Purkinje cell axon, to the deep cerebellar nuclei (DCN) (Khaliq and Raman, 2005; Monsivais et al., 2005). Thus the nature of the true input-output curve of the Purkinje cell might be altered. During bursts of input, predictions based on spikelet height and relative timing, suggest that the number of spikes in the Purkinje cell axon might reflect the number of inputs in a burst, carrying this information to the DCN. An *in vivo* pattern of CF activation timing, with inter-activation intervals ranging between 50 ms and several seconds (Eccles et al., 1967; Bell and Grimm, 1969; Armstrong and Rawson, 1979; Maruta et al., 2007), generates a complex spike pattern where spike timing represents the paired pulse depression interval of the CF input. Khaliq et al's (2005) axonal recordings have shown that although some of these spikes fail to propagate down the axon, a constant fraction of the somatic burst is propagated. Campbell and Hesslow (1986b), however find that more spikelets are seen in the axon following paired stimulation at short intervals. Even considering these potential propagation failures in the first and second climbing fibre response, the timing and number of propagated spikes could convey not just the occurrence of a motor error signal or motor coordination command, but the time since the previous such command.

Chapter 2:

The relationship between Purkinje cell geometry and the complex spike

Introduction

While the large, singular connection between the calyx of held and postsynaptic MNTB cell is clasped around the soma, and seems specialised to faithfully and temporally accurately transmit a single spike (Borst et al., 1995; Brew and Forsythe, 1995; Wang et al., 1998; Taschenberger and von Gersdorff, 2000; Gittelman and Tempel, 2006), CF input is distributed across the thick primary branches of the Purkinje cell. It is not yet clear what the functional implications of this distribution are. As outlined in the main introduction, the location of a synapse in the dendrites can strongly influence its effect at the soma. There are a number of reasons why the CF's dendritic, distributed input location might be critical to complex spike burst generation. Firstly, clustering of the enormous ~200 nS synaptic conductance at the <20 MΩ (> 50nS) soma should create a large conductance shunt, which might detrimentally dissipate both the synaptic current and the active currents responsible for burst generation (see main Introduction). Conversely, somatic spiking conductances are themselves large (Raman and Bean, 1999; Khaliq et al., 2003; Swensen and Bean, 2003, 2005), and might detrimentally shunt out somatically injected synaptic current (Häusser et al., 2001). Further, clustering CF input at the soma will generate a large local depolarisation, but a much smaller distributed depolarisation of the dendrites:

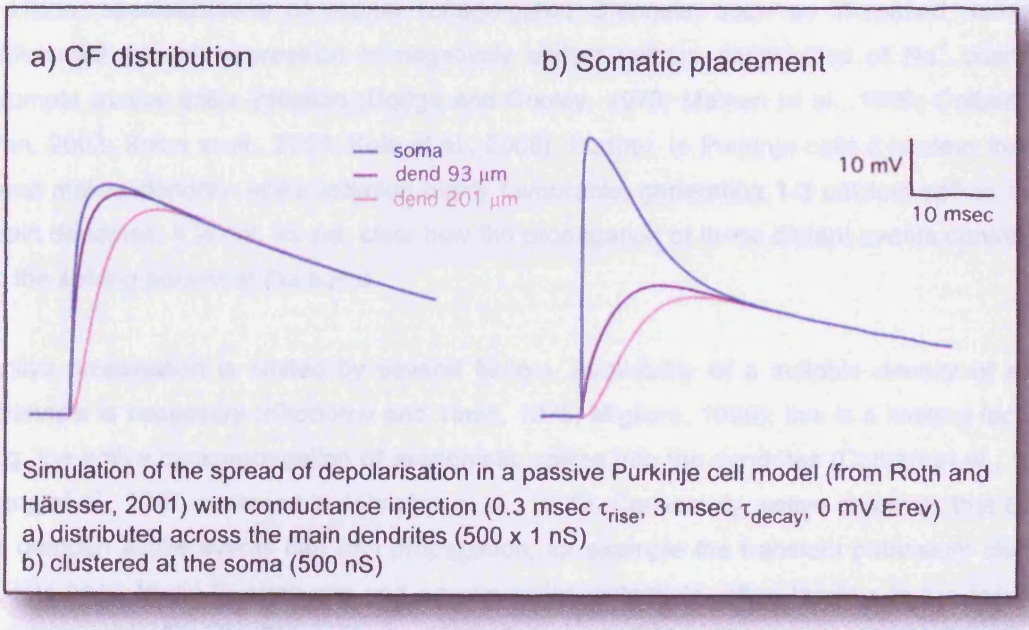

Simulation of the spread of depolarisation in a passive Purkinje cell model (from Roth and Häusser, 2001) with conductance injection (0.3 msec τ_{rise}, 3 msec τ_{decay}, 0 mV Erev)
a) distributed across the main dendrites (500 x 1 nS)
b) clustered at the soma (500 nS)

Active dendritic conductances may therefore be recruited to a much lesser extent and dendritic calcium spikes may not be generated (Callaway and Ross, 1997). Although dendritic calcium spikes are known to cause burst generation in a number of neuronal types

(Llinas and Yarom, 1981a, b; Pinsky and Rinzel, 1994; Mainen and Sejnowski, 1996; Larkum et al., 1999; Magee, 1999; Williams and Stuart, 1999; Larkum et al., 2001; Doiron et al., 2002; Williams and Stuart, 2002), the contribution of dendritic calcium spikes to the generation of the somatic complex spike burst is not yet understood (Schmolesky et al., 2002). By potentially failing to generate dendritic spikes, a clustered somatic CF input may fail to produce a complex spike. In this chapter I have investigated these possibilities by using conductance clamp hardware to artificially inject CF like synaptic conductances into Purkinje cell somata.

It is not only the location of synapses that can have a strong influence on neuronal firing: the site of spike initiation and their subsequent propagation also strongly influences the spiking waveforms produced. The Purkinje cell is a particularly interesting example of this, as axon, soma and dendritic compartments are all electrically excitable (Llinas and Sugimori, 1980b, a), but there are clear limits on propagation both through the dendritic tree (Stuart and Häusser, 1994; Vetter et al., 2001; Rancz and Häusser, 2006) and along the axon (Khaliq and Raman, 2005; Monsivais et al., 2005). As in most neurons, the axon is a highly favourable site for spike initiation (Stuart and Häusser, 1994; Stuart and Sakmann, 1994; Colbert and Johnston, 1996; Stuart et al., 1997a; Stuart et al., 1997b; Clark et al., 2005; Khaliq and Raman, 2006; Palmer and Stuart, 2006; Meeks and Mennerick, 2007; Schmidt-Hieber et al., 2008). This is due in part to its isolation from the capacitative load of the soma and dendrites (Dodge and Cooley, 1973; Mainen et al., 1995; Colbert and Pan, 2002) and its high local impedance and low capacitance, which make it easy to charge and discharge. In addition, specializations of axonal voltage-gated channels, such as increased densities, differential subunit expression or negatively shifted voltage sensitivities of Na^+ channels, promote axonal spike initiation (Dodge and Cooley, 1973; Mainen et al., 1995; Colbert and Pan, 2002; Boiko et al., 2003; Kole et al., 2008). Further, in Purkinje cells it is clear that CF input makes dendritic spike initiation highly favourable, generating 1-3 calcium spikes in the main dendrites. It is not, as yet, clear how the propagation of these distant events contributes to the spiking pattern at the soma.

Active propagation is limited by several factors. Availability of a suitable density of active channels is necessary (Khodorov and Timin, 1975; Migliore, 1996); this is a limiting factor in e.g. the active backpropagation of axosomatic spikes into the dendrites (Colbert et al., 1997; Jung et al., 1997, reviewed in Johnston et al., 1999). Conversely, active channels that curtail or dampen active events can limit propagation, for example the transient potassium channel I_A has been found to attenuate and narrow action potentials, often leading to the failure of active propagation (Hoffman et al., 1997; Cai et al., 2004; Kim et al., 2005; Gentet and Williams, 2007). Further, the conductance shunt caused by strategically placed inhibitory input in the axon or dendrite can cause such a current leak that active propagation past the site becomes impossible (Atwood et al., 1984; Segev, 1990; Lowe, 2002; Xiong and Chen,

2002). Modulation of such active and passive conductances is particularly effective at points at which geometry makes active propagation more unstable, e.g. at branch points or increases in neuronal diameter (one pertinent such widening is the junction between the axon or dendrite and the soma), where the impedance mismatch is unfavourable (Goldstein and Rall, 1974; Parnas and Segev, 1979; Segev and Schneidman, 1999). These constraints can be so strong as to either slow spike propagation, enforce saltatory conduction over the unfavourable section, or to entirely prevent propagation (Segev, 1990; Hoffman et al., 1997; Vetter et al., 2001; Xiong and Chen, 2002; Cai et al., 2004; Engel and Jonas, 2005; Kim et al., 2005; Gentet and Williams, 2007), leaving just the passively propagated 'prepotential' (Katz, 1950; Granit and Phillips, 1956; Coombs et al., 1957a, b; Fuortes et al., 1957; Spencer and Kandel, 1961; Dodge and Cooley, 1973; Stuart et al., 1997b). This can divide a neuron into a number of functional subcompartments which require the favourable coincidence of events (such as appropriately distributed synaptic input (Larkum et al., 1999, 2001; Gasparini et al., 2004; Polsky et al., 2004; Gasparini and Magee, 2006; Losonczy and Magee, 2006; Roth and Häusser, 2007; Losonczy et al., 2008)) in order to interact in a linear or supralinear manner and boost the neuron's output (Chen et al., 1997; Golding and Spruston, 1998; Larkum et al., 1999, 2001; Williams and Stuart, 2002; Ariav et al., 2003; Gasparini et al., 2004).

In this chapter, I have characterised the pattern of the complex spike in detail, in particular the dependence of the amplitude of the spikelets on their timing. I show, using modelling, that the relationships I have demonstrated cannot arise from a spike generation in a single compartment. I have examined the effect altering somatic conductance and active channel availability and have found that the complex spike waveform is easily understood as the result of variable propagation from a distant compartment. The final results chapter will address the role of the dendrites as a possible source of these spikelets; this work, together with direct axonal recording (carried out by Beverley Clark and reported in Davie et al., 2008), demonstrates that the distant source of these spikes is the axon rather than the dendrite.

Chapter 2: Results

The CF input to Purkinje cells triggers an extremely large synaptic conductance (as shown in Chapter 1 and by many other studies (Konnerth et al., 1990; Llano et al., 1991; Dittman and Regehr, 1998; Hashimoto and Kano, 1998; Silver et al., 1998; Foster and Regehr, 2004; McKay et al., 2005)). This conductance is distributed, on stubby, 'thorn'-like spines, across the highly branched main dendrites (Palay and Chan-Palay, 1974; Xu-Friedman et al., 2001). This separation of synapses from each other and from the fast spiking mechanisms of the axon and soma may support the generation of the complex spike rapid burst of spikes and allow the linear relationship between input size and somatic spiking seen in Chapter 1. Further, CF input to the dendrites triggers active spikes, which may contribute to the generation of the complex spike burst at the soma.

The complex spike can be reproduced by a somatic synaptic-like conductance

To determine whether the dendritic distribution of CF synaptic contacts is necessary to generate the distinctive spiking pattern of the complex spike, I examined if concentrating the synaptic conductance at the soma is sufficient to mimic the complex spike waveform. Conductance clamp was used to inject a biexponential conductance (EPSG), based on the physiological CF synaptic conductance (Chapter 1 and Perkel et al., 1990; Llano et al., 1991; Silver et al., 1998; Wadiche and Jahr, 2001), via two somatic patch-clamp electrodes. By adjusting the amplitude of the somatic EPSG (Fig. 2.1d), a remarkably good match could be achieved with the CF-evoked complex spike (Fig. 2.1b). This matching was achievable in most cells, not only in those exhibiting complex spikes consisting of relatively few spikes (e.g. Fig. 2.1b), but also for neurons with elaborate complex spikes consisting of ≥ 5 spikes (Fig. 2.2). The mean value of the 'optimal' synaptic conductance was 170 ± 58 nS (range 80 - 325 nS, n = 40 cells), which is similar to the conductance values measured in Chapter 1 using somatic voltage-clamp recording of CF EPSCs (265 ± 13 nS; p = 0.12). Decreasing the synaptic conductance from the optimal value reduced the number of evoked spikes in the complex spike, while increasing the conductance ultimately led to inactivation of spiking, associated with voltage ripples on top of an envelope of depolarisation. This depolarisation rarely exceeded -30 mV, even at conductance values of 500 nS, thus maintaining a driving force for the synaptic conductance. The 'optimal' synaptic conductance produced a highly quantitative match to the physiological complex spike in the same cells, with the number of spikes being indistinguishable between physiological and synthetic complex spikes (differing by -0.03 ± 0.05 spikes, on average, n = 40 cells, p = 0.62, paired t-test). Furthermore, details of the spike waveform could also be closely matched. In some cells (27/40) a highly accurate match was found, with amplitudes being matched with an average error of only 16.8 ± 2.5 % and times being match with only 10.4 ± 1.3 % error. Even in the

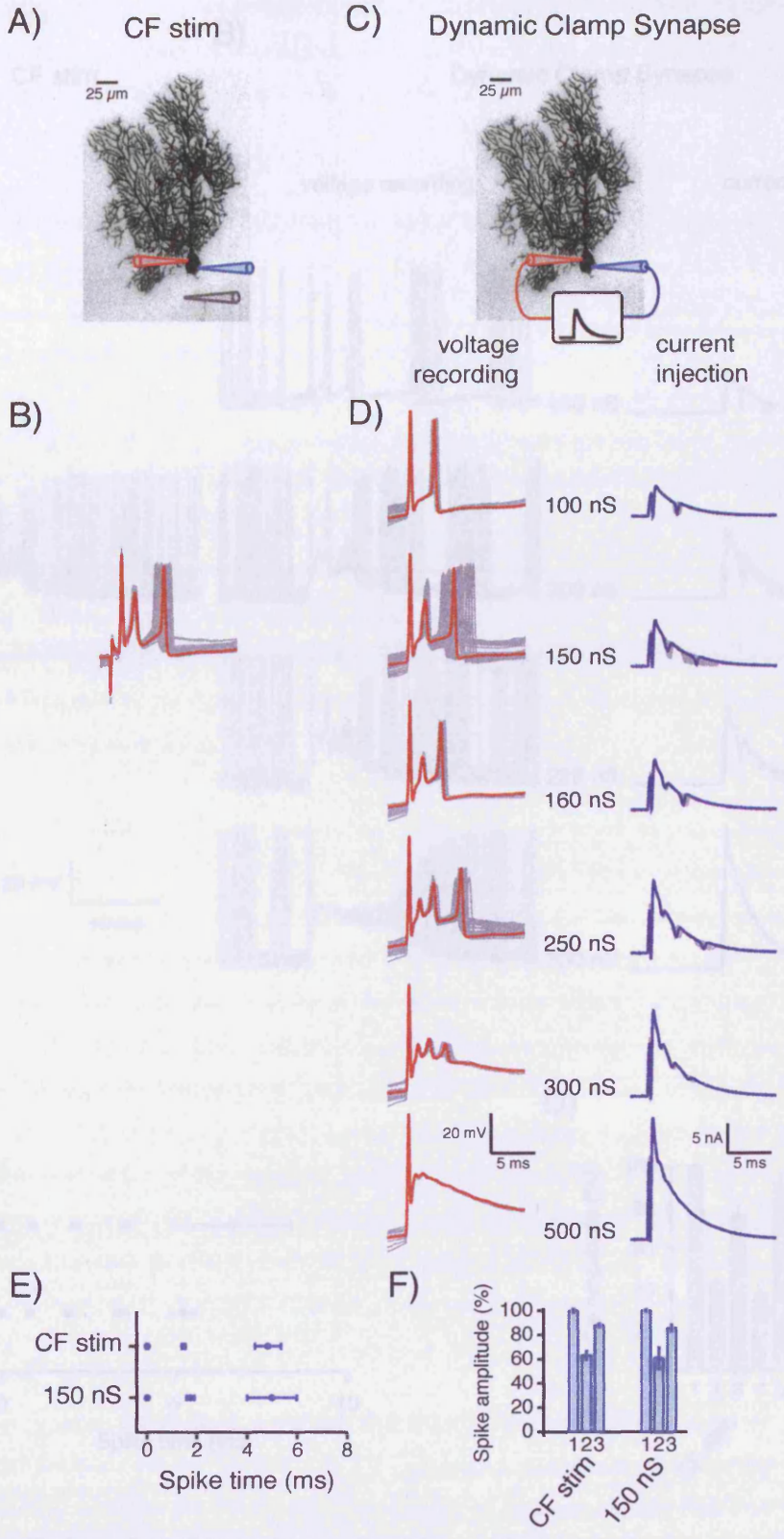

Figure 2.1 CF-evoked complex spikes can be reproduced by somatic dynamic clamp

A) Recording configuration illustrated using an image of a biocytin-filled Purkinje cell. Somatic electrodes (blue), CF stimulating electrode in the granule cell layer (grey). **B)** Complex spike responses of Purkinje cell shown in (A), evoked by 1 Hz stimulation of its CF. Overlay of multiple sweeps (grey) and a single representative example (red). **C)** Simultaneous dual somatic dynamic clamp configuration, with one electrode used to record voltage (red) and the other to inject current (blue). **D)** Responses (left) of the cell shown in A to injection of synaptic-like conductances of increasing amplitude (right, biexponential waveform, τ_{rise} 0.3 ms, τ_{decay} 3 ms, peak amplitudes as indicated beside traces). Note that by choosing the appropriate conductance amplitude (150 nS) the complex spike evoked by CF stimulation could be mimicked. **E)** Timing and **F)** amplitude of spikes (measured with respect to the first spike, for the 1st, 2nd and 3rd spike) within the complex spikes evoked by CF stimulation and by the 150 nS synaptic-like conductance. Spike times differed by <17 %; amplitudes differed by <4 %.

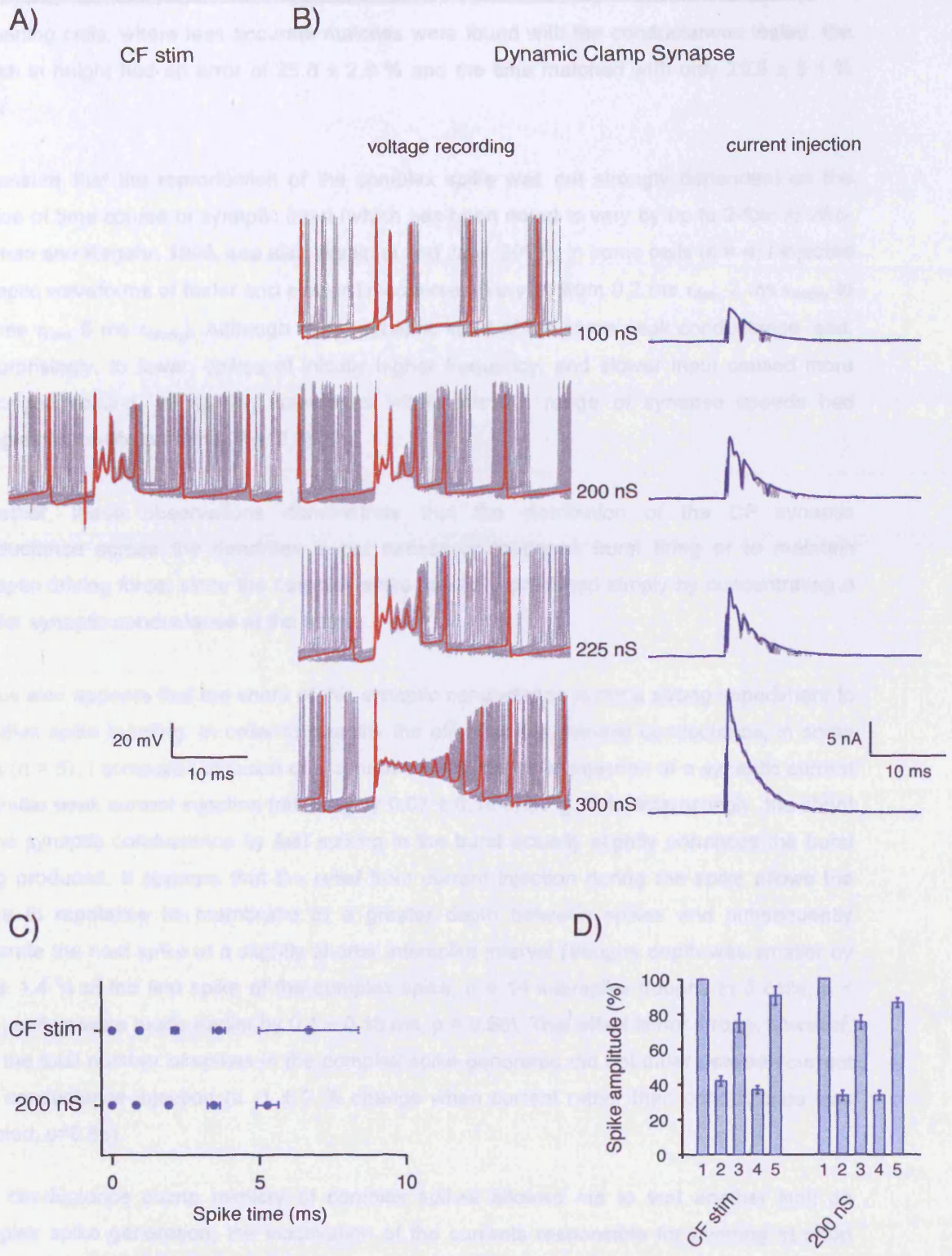

Figure 2.2 Even elaborate complex spikes can be reproduced by somatic dynamic clamp

A) An elaborate complex spike elicited in response to 1 Hz CF stimulation in a Purkinje cell (different cell to that shown in Fig. 1).
B) A range of complex spike-like events evoked by synaptic-like dynamic clamp at the soma of the cell recorded from in (A). Note that the CF-evoked complex spike was mimicked by 200 nS peak conductance injection.
C) Timing and **D)** amplitude of spikes (measured relative to the first spike) within the complex spikes evoked by CF stimulation and 200 nS synaptic-like dynamic clamp. Spike times differed by <12%, amplitudes by <20%.

remaining cells, where less accurate matches were found with the conductances tested, the match in height had an error of 25.6 ± 2.8 % and the time matched with only 20.5 ± 3.1 % error.

To ensure that the reproduction of the complex spike was not strongly dependent on the choice of time course of synaptic input (which has been noted to vary by up to 2-fold in vitro, Dittman and Regehr, 1998, see also Wadiche and Jahr, 2001), in some cells (n = 4) I injected synaptic waveforms of faster and slower timecourses (varying from 0.2 ms τ_{rise}, 2 ms τ_{decay} to 0.5 ms τ_{rise}, 5 ms τ_{decay}). Although faster synaptic input of the same peak conductance lead, unsurprisingly, to fewer, spikes of initially higher frequency, and slower input caused more prolonged spiking, all spiking waveforms within this 2.5 range of synapse speeds had complex spike-like patterns (Fig. 2.3).

Together, these observations demonstrate that the distribution of the CF synaptic conductance across the dendrites is not necessary to permit burst firing or to maintain synaptic driving force, since the complex spike can be reproduced simply by concentrating a similar synaptic conductance at the soma.

It thus also appears that the shunt of this synaptic conductance is not a strong impediment to complex spike bursting. In order to quantify the effect of this somatic conductance, in some cells (n = 5), I compared injection of a synaptic conductance to injection of a synaptic current of similar peak current injection (differing by 0.07 ± 0.18 nA, Fig. 2.4). Interestingly, the shunt of the synaptic conductance by fast spiking in the burst actually slightly enhances the burst firing produced. It appears that the relief from current injection during the spike allows the soma to repolarise its membrane to a greater depth between spikes and subsequently generate the next spike at a slightly shorter interspike interval (troughs depth was smaller by 4.6 ± 1.4 % of the first spike of the complex spike, n = 14 interspike troughs in 5 cells, $p < 0.01$, spikes were made earlier by 0.1 ± 0.16 ms, $p = 0.56$). This effect is not strong, however, and the total number of spikes in the complex spike generated did not differ between current and conductance injection (a -1 ± 2 % change when current rather than conductance was injected, p=0.65).

The conductance clamp mimicry of complex spikes allowed me to test another limit on complex spike generation; the inactivation of the currents responsible for bursting at short interpulse intervals. In Chapter 1 I made use of paired pulse depression at short interstimulus intervals to decrease the size of the synaptic input; at some of the shortest intervals, the reduction in spiking of the second complex spike may be enhanced to some extent by the inactivation of channels during the initial complex spike. To test the extent of this effect, I injected two identical somatic synaptic-like conductances separated by an interval of 20 ms (the shortest interval used in most paired pulse CF stimulation experiments). Two examples

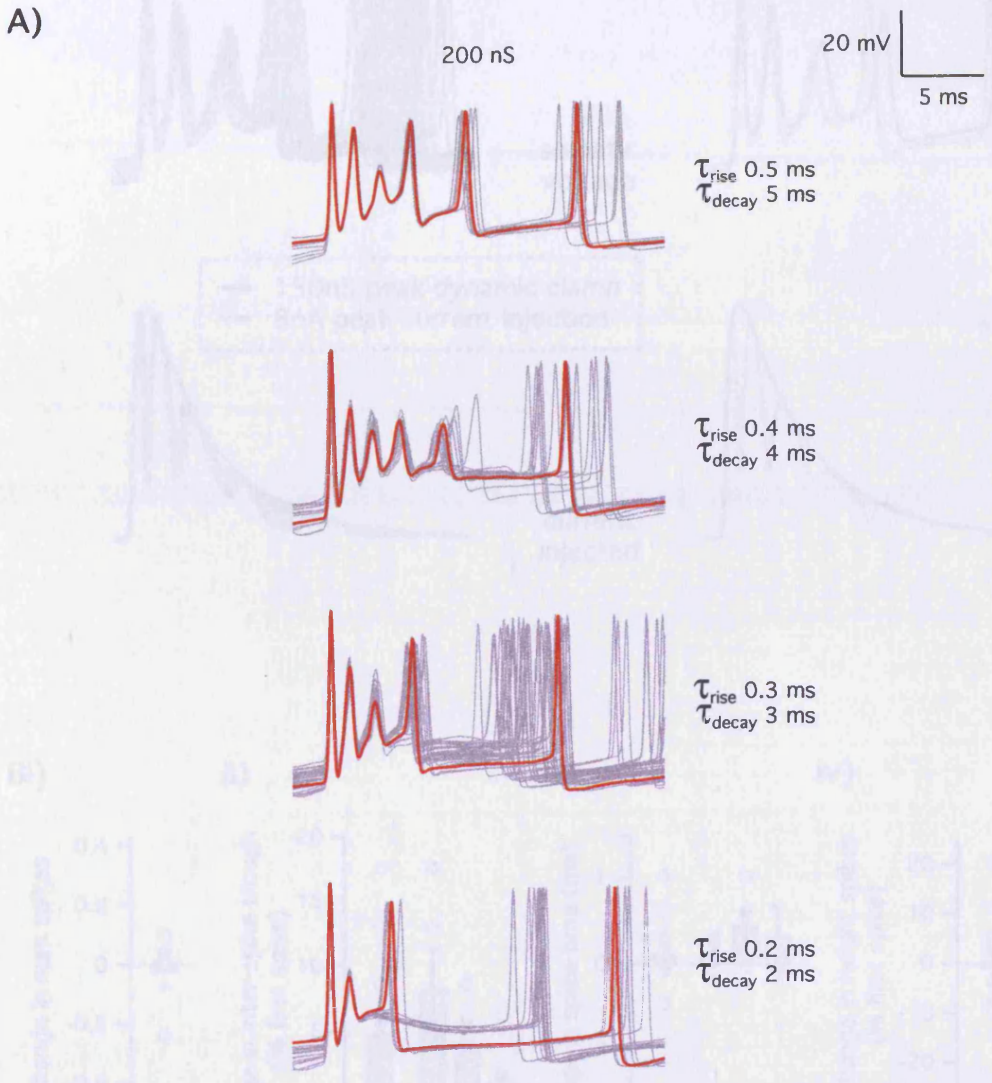

Figure 2.3 Dynamic clamp of different time courses produces complex spike like waveforms

A) Example of injection of 200 nS peak conductance synaptic-like biexponential waveforms of increasingly rapid kinetics. Rise and decay time constants were co-varied from 0.5 ms τ_{rise}, 5 ms τ_{decay} to 0.2 ms τ_{rise}, 2 ms τ_{decay} (the waveform used for the majority of experiments in this thesis was 0.3 ms τ_{rise}, 3 ms τ_{decay}).

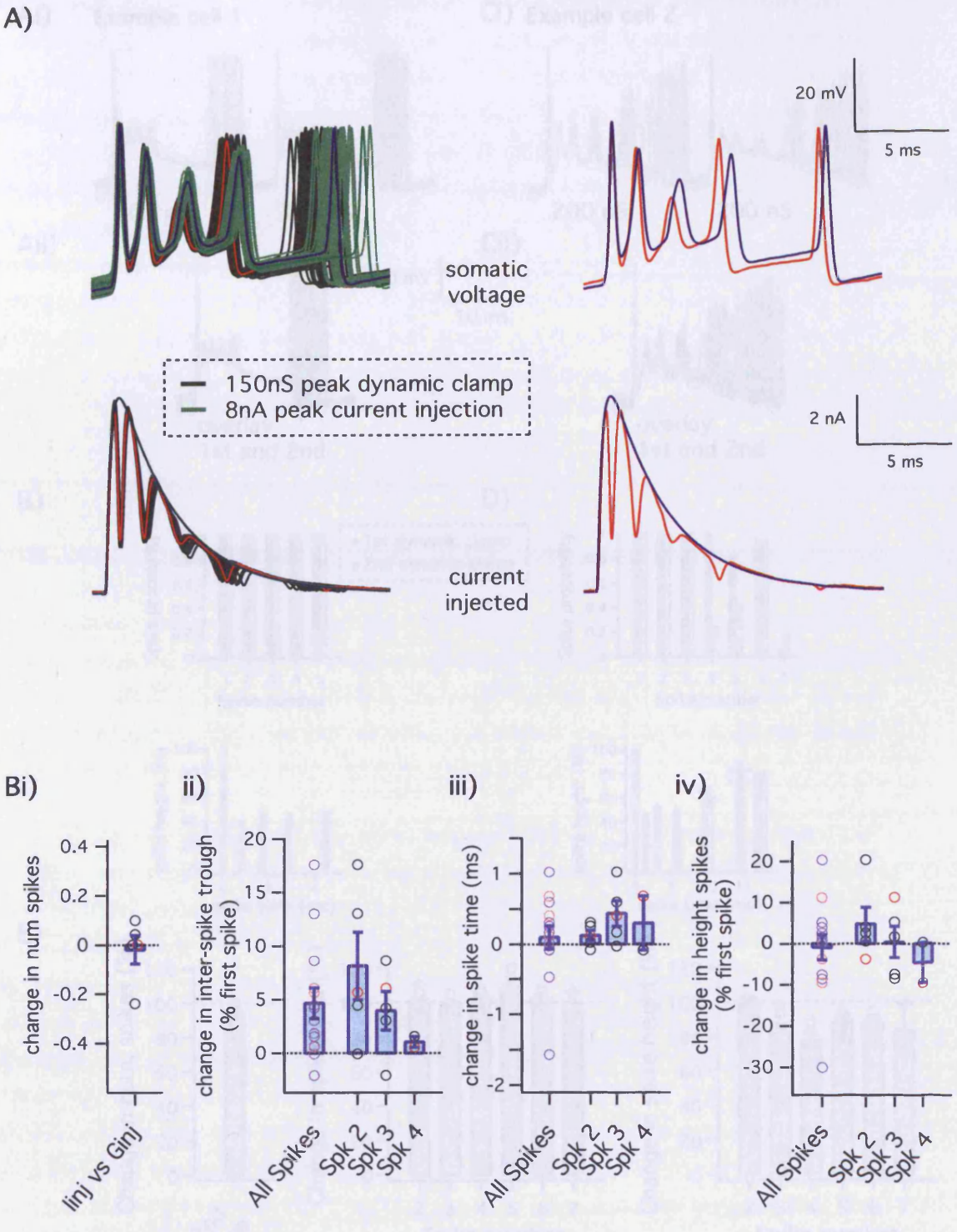

Figure 2.4 Comparison of conductance and current based synaptic-like injections.

A) Example of somatic injection of either a 150 nS peak conductance (black traces and red example trace) or a 8 nA peak current (green traces and blue example trace) synaptic-like waveform. The amplitudes were chosen such that the peak currents injected were similar. Left hand panels show multiple overlayed traces with a single highlighted example; right hand panels show the example traces in isolation. Lower panels show the current injected to the cell, upper traces show the voltage trajectories triggered.
B) Analysis of the change in **(i)** number, **(ii)** interspike trough amplitude, **(iii)** timing and **(iv)** height of spikes, and of the, caused by injection of a synaptic-like current rather than conductance. Data from 5 data sets in 4 cells shown. Red circles indicate analysis of the example shown in A.

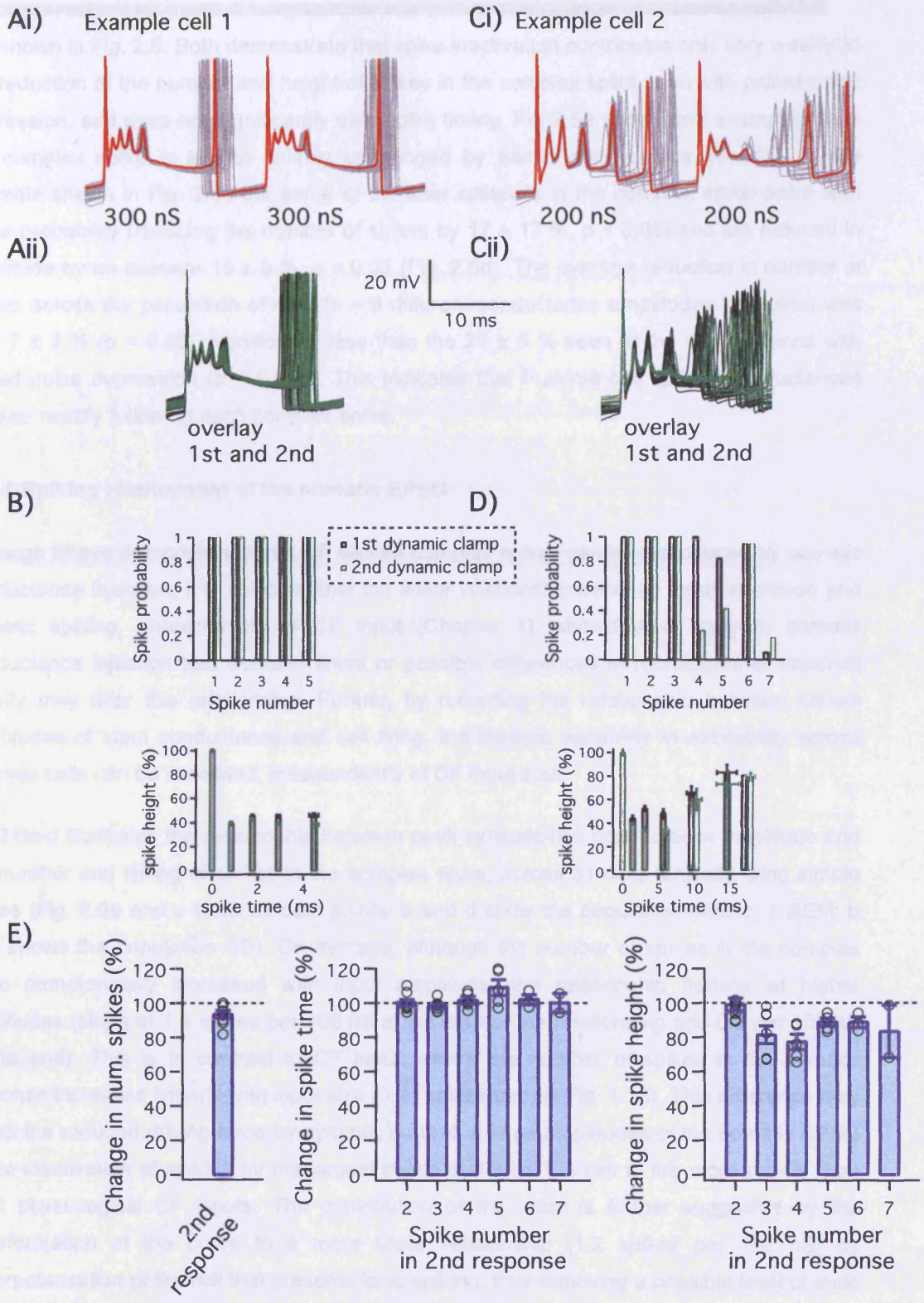

Figure 2.5 'Paired-pulse' injection of two synaptic-like conductances.

A) Example of repeated injection of two 200 nS peak synaptic-like conductances, separated by 20 ms (the shortest interval used in the majority of experiments investigating the paired stimulation of CFs). (i) Several repetitions of this injection (given every 1 s) are shown overlaid (grey, a single example highlighted in red), (ii) first and second injections are overlaid to illustrate that channel inactivation by the first complex spike does strongly affect the second complex spike waveform. **B)** Analysis of the probability of occurrence (upper graph) and the height and time (lower graph) of each spike in the complex spikes evoked by the first and second conductance injections (black and green edged bars, respectively). **C), D)** as A, B, but from a second example cell (two 300 nS peak conductances were presented), where the second complex spike is more affected by the occurrence of a prior complex spike. **E)** Average % change in the number, timing and amplitude of spikes evoked by a second conductance injection of the same amplitude (n = 8 different conductance amplitudes in 4 cells).

are shown in Fig. 2.5. Both demonstrate that spike inactivation contributes only very weakly to the reduction of the number and height of spikes in the complex spike seen with paired pulse depression, and does not significantly alter spike timing. Fig 2.5a shows one example where the complex spike is almost entirely unchanged by paired conductance injection. In the example shown in Fig. 2.5c the some of the later spikelets in the complex spike occur with lower probability (reducing the number of spikes by 17 ± 17 %, $p < 0.05$) and are reduced in amplitude by on average 16 ± 5 %, $p < 0.05$ (Fig. 2.5d). The average reduction in number of spikes across the population of data (n = 8 different conductance amplitudes in 4 cells) was only 7 ± 2 % ($p < 0.05$), significantly less than the 29 ± 5 % seen at the same interval with paired pulse depression ($p < 0.005$). This indicates that Purkinje cell spiking conductances recover rapidly following each complex spike.

Input-Spiking relationship of the somatic EPSG

Although I have demonstrated that CF elicited complex spikes can be reproduced by somatic conductance injection, it is not clear that the linear relationship between input amplitude and somatic spiking, characteristic of CF input (Chapter 1), should also apply to somatic conductance injection too. Somatic shunt or possible differences in recruitment of dendritic activity may alter this relationship. Further, by recording the relationship between known amplitudes of input conductance and cell firing, the intrinsic variability in excitability across Purkinje cells can be assessed, independently of CF input size.

Fig 2.6a-d illustrates the relationship between peak synaptic-like conductance amplitude and the number and timing of spikes in the complex spike, across 31 cells tonically firing simple spikes (Fig. 2.6a and c show all data points; b and d show the population means, ± SEM; b also shows the population SD). On average, although the number of spikes in the complex spike monotonically increased with input amplitude, the relationship flattens at higher amplitudes (slope of 1.6 spikes per 100 nS at the start of the relationship and 0.8 per 100 nS at the end). This is in contrast to CF input, where the number of spikes in the somatic response increases linearly with input size (0.17 spikes per nA Fig. 1.15). This difference may reflect the reduced driving force for synaptic current at large amplitudes of the somatic EPSG or the inactivation of spiking by the largest inputs that drive the cell to fire more rapidly than most physiological CF inputs. The contribution of the latter is further suggested by the transformation of the curve to a more linear relationship (1.2 spikes per 100 nS) by hyperpolarisation of the cell that prevents tonic spiking, thus removing a possible level of tonic inactivation (Fig. 2.6e,f). The relationships between spike timing and input amplitude was also similar for somatic conductance clamp and CF stimulation. Spike latencies decrease monotonically with increasing conductance, but again the rate of decrease flattened out at higher conductances.

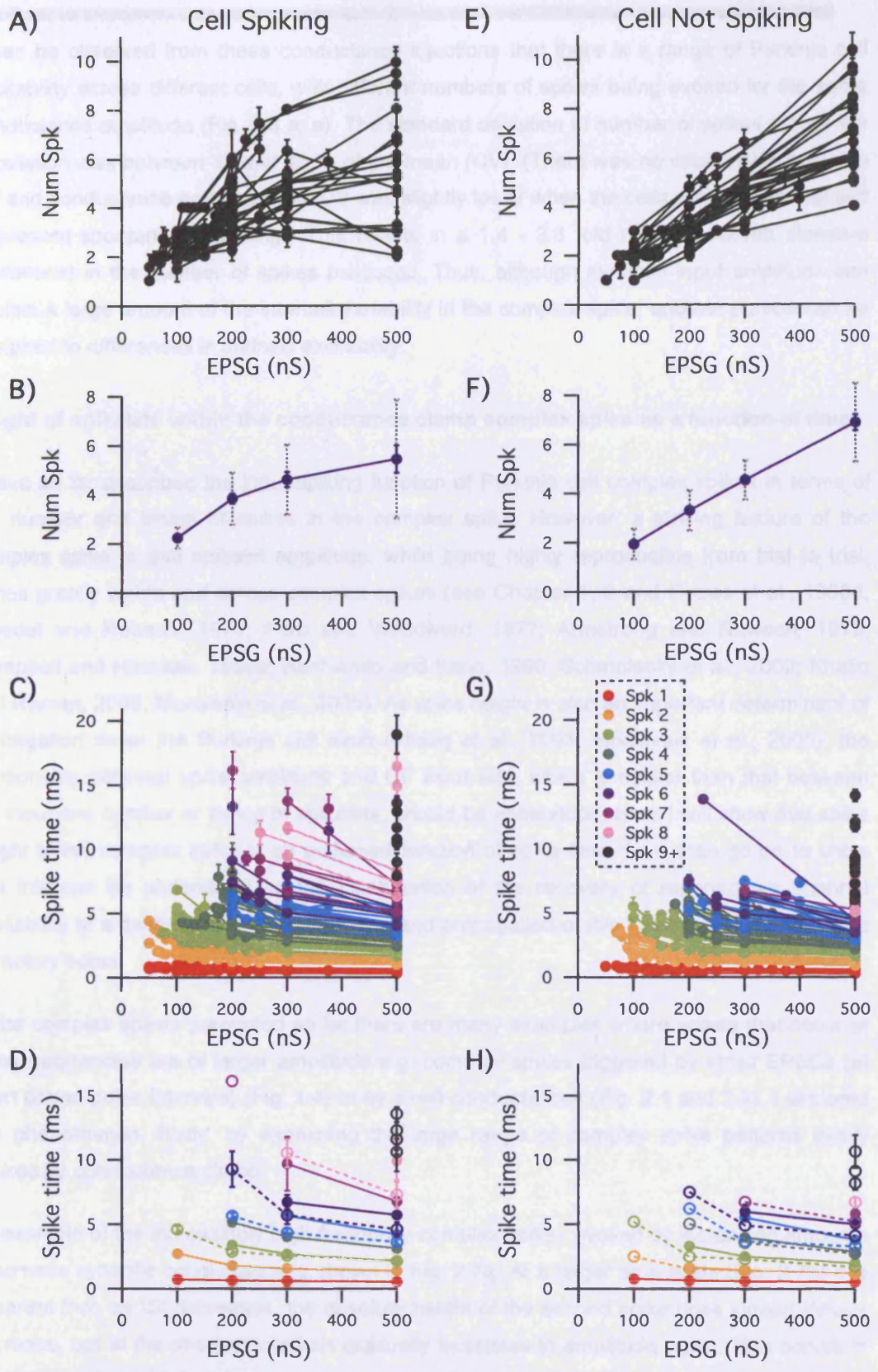

Figure 2.6 Input-output functions of somatic dynamic clamp synapses.

A) Relationship between number of somatic spikes evoked and peak injected somatic synaptic-like conductance (in n = 31 cells) while cells spontaneous firing. Lines connect data points recorded from the same cell. **B)** Mean (± SEM, blue bars; ± SD, gray dashed bars) across all data sets of data in A. **C)** Relationship between spike timing and peak synaptic-like conductance injection in the same data sets as shown in A. **D)** Average (mean ± SEM) across all data sets of data in C. Filled circles show the average of all data, but only for conductances that evoked the spike indicated in the majority cells; open circles show the average of data from the more excitable cells where additional spikes were evoked by lower conductances. **E), F), G), H)** as A, B, C, D, except cells hyperpolarised with tonic current injection to prevent spontaneous firing (n = 33).

It can be observed from these conductance injections that there is a range of Purkinje cell excitability across different cells, with different numbers of spikes being evoked for the same conductance amplitude (Fig. 2.6 a, e). The standard deviation of number of spikes across the population was between 17 and 45 % of the mean (CV). (There was no relationship between CV and conductance amplitude, but CV was slightly lower when the cells were hyperpolarised to prevent spontaneous spiking.) This results in a 1.4 - 2.6 fold range (between standard deviations) in the number of spikes produced. Thus, although synaptic input amplitude can explain a large amount of the intercell variability in the complex spike, another portion can be assigned to differences in intrinsic excitability.

Height of spikelets within the conductance clamp complex spike as a function of time

I have so far described the input-spiking function of Purkinje cell complex spikes in terms of the number and timing of spikes in the complex spike. However, a striking feature of the complex spike is that spikelet amplitude, while being highly reproducible from trial to trial, varies greatly within and across complex spikes (see Chapter 1, 2 and Eccles et al., 1966d; Bloedel and Roberts, 1971; Puro and Woodward, 1977; Armstrong and Rawson, 1979; Campbell and Hesslow, 1986a; Hashimoto and Kano, 1998; Schmolesky et al., 2002; Khaliq and Raman, 2005; Monsivais et al., 2005). As spike height is also an important determinant of propagation down the Purkinje cell axon (Khaliq et al., 2003; Monsivais et al., 2005), the relationship between spike amplitude and CF input size, which is noisier than that between CF input and number or timing of spikelets, should be understood. Here I will show that spike height in the complex spike is an s-shaped function of spike time. I will then go on to show that this can be understood as the combination of the recovery of regenerative channel availability at a distant site of spike initiation and propagation of this spike into a slightly more refractory soma.

In the complex spikes presented so far there are many examples where spikes that occur at lower frequencies are of larger amplitude e.g. complex spikes triggered by small EPSCs (at short paired-pulse intervals) (Fig. 1.4) or by small conductances (Fig. 2.1 and 2.2). I explored this phenomenon, firstly, by examining the large range of complex spike patterns easily evoked by conductance clamp.

An example of the increasingly high frequency complex spikes evoked by increasing amounts of somatic synaptic conductance is shown in Fig. 2.7a. At a larger time scale (Fig. 2.7b) it is apparent that, as ISI decreases, the absolute height of the second spike does indeed initially decrease, but at the shortest intervals gradually increases in amplitude again. This occurs in parallel with an increase in the inter-spike trough height. This trend applies not only the second spike of the complex spike but to later spikes as well (Fig. 2.7ci). A monotonic relationship is however revealed by plotting the spike height as peak amplitude minus the preceding interspike trough depth (Fig. 2.7cii). Such s-shaped relationships were measured

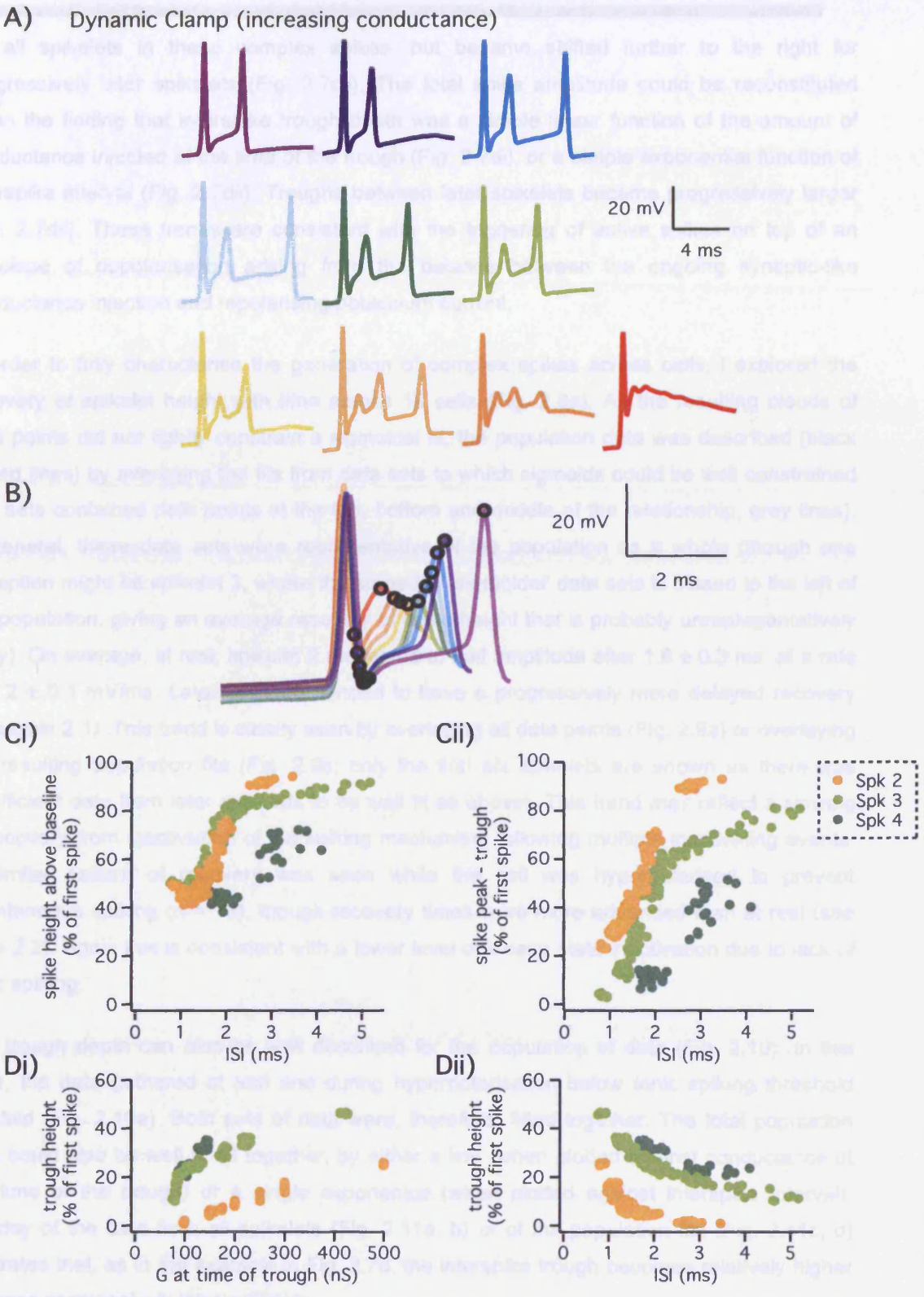

Figure 2.7 Spike height is an s-shaped function of spike time in conductance clamp evoked complex spike.

A) Examples of complex spikes evoked by increasing conductance injection to the same cell as shown in fig 2.1 (from 100 – 500 nS). Note that as conductance amplitude increases and the second spike occurs earlier, its amplitude tends to decrease and the preceding trough tends to increase in height.
B) Overlay of the first two spikes of the traces shown in A, at an expanded time scale. Black circles mark the peak amplitude of the second spike and the depth of the preceding trough.
C) Relationship between spike amplitude and interspike interval, for all complex spike secondary spikes evoked (at rest) by conductance clamp in the cell shown in A (coloured according to spike number within the complex spike). Amplitude was measured as either as **(i)** peak minus baseline Vm, or as **(ii)** peak minus preceding interspike trough.
D) Relationship between interspike trough height and **(i)** conductance injected at the time of the trough minimum or **(ii)** interspike interval (between the spike following the trough and that preceding it).

for all spikelets in these complex spikes, but became shifted further to the right for progressively later spikelets (Fig. 2.7cii). The total spike amplitude could be reconstituted given the finding that interspike trough depth was a simple linear function of the amount of conductance injected at the time of the trough (Fig. 2.7di), or a simple exponential function of interspike interval (Fig. 2.7dii). Troughs between later spikelets became progressively larger (Fig. 2.7dii). These trends are consistent with the triggering of active spikes on top of an envelope of depolarisation arising from the balance between the ongoing synaptic-like conductance injection and repolarising potassium current.

In order to fully characterise the generation of complex spikes across cells, I explored the recovery of spikelet height with time across 16 cells (Fig. 2.8a). As the resulting clouds of data points did not tightly constrain a sigmoidal fit, the population data was described (black dotted lines) by averaging the fits from data sets to which sigmoids could be well constrained (i.e. sets contained data points at the top, bottom and middle of the relationship, grey lines). In general, these data sets were representative of the population as a whole (though one exception might be spikelet 3, where the spread of 'sigmoidal' data sets is biased to the left of the population, giving an average recovery of spike height that is probably unrepresentatively early). On average, at rest, spikelet 2 recovered to half amplitude after 1.6 ± 0.3 ms, at a rate of 0.2 ± 0.1 mV/ms. Later spikelets tended to have a progressively more delayed recovery (see table 2.1). This trend is clearly seen by overlaying all data points (Fig. 2.9a) or overlaying the resulting population fits (Fig. 2.9c; only the first six spikelets are shown as there was insufficient data from later spikelets to be well fit as above). This trend may reflect a slowing of recovery from inactivation of the spiking mechanism following multiple inactivating events. A similar pattern of recovery was seen while the cell was hyperpolarised to prevent spontaneous spiking (n = 13), though recovery times were more advanced than at rest (see table 2.2). Again this is consistent with a lower level of steady-state inactivation due to lack of tonic spiking.

The trough depth can also be well described for the population of data (Fig. 2.10). In this case, the data gathered at rest and during hyperpolarisation below tonic spiking threshold overlaid (Fig. 2.10a). Both sets of data were, therefore, fitted together. The total population data could also be well fit all together, by either a line (when plotted against conductance at the time of the trough) or a single exponential (when plotted against interspike interval). Overlay of the data from all spikelets (Fig. 2.11a, b) or of the population fits (Fig. 2.11c, d) illustrates that, as in the example in Fig. 2.7d, the interspike trough becomes relatively higher between progressively later spikelets.

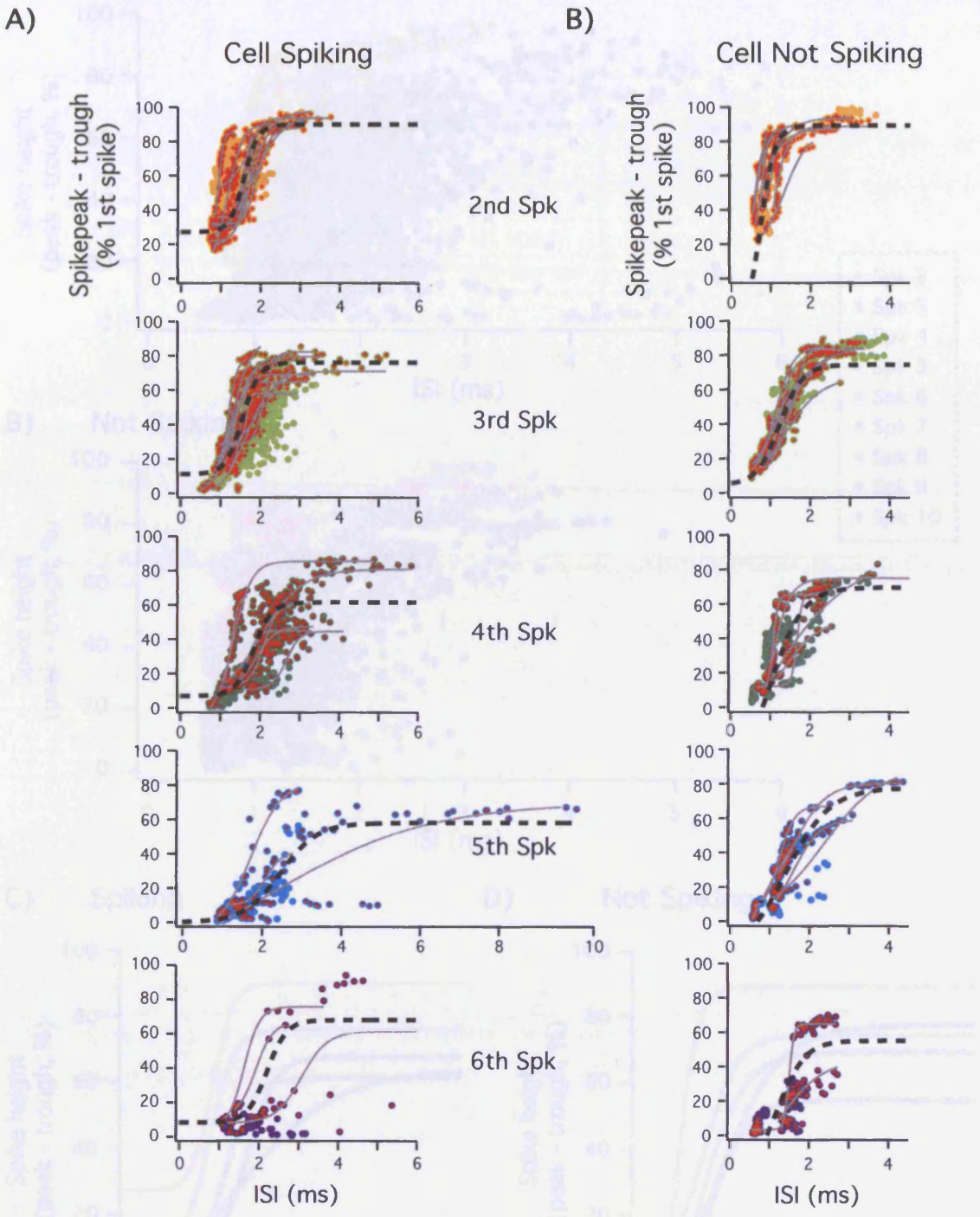

Figure 2.8 Generalised relationships between spike height and time in dynamic clamp evoked complex spikes.

A) Relationship between spike amplitude (peak – trough) and ISI for spikelets 2 – 6 of dynamic clamp evoked complex spikes in 16 cells, at rest, during spontaneous simple spiking. Red crosses mark data points from cells in which the data points from to top, bottom and rising phase of the relationship were evoked, and could thus be fitted with a sigmoid. Grey lines show these sigmoid fits; the population of data is described by a sigmoid (black dashed line) whose coefficients are the average of all these grey individual fits.
B) As in A, but for data collected during tonic somatic current injection to prevent spontaneous spiking (n = 13).

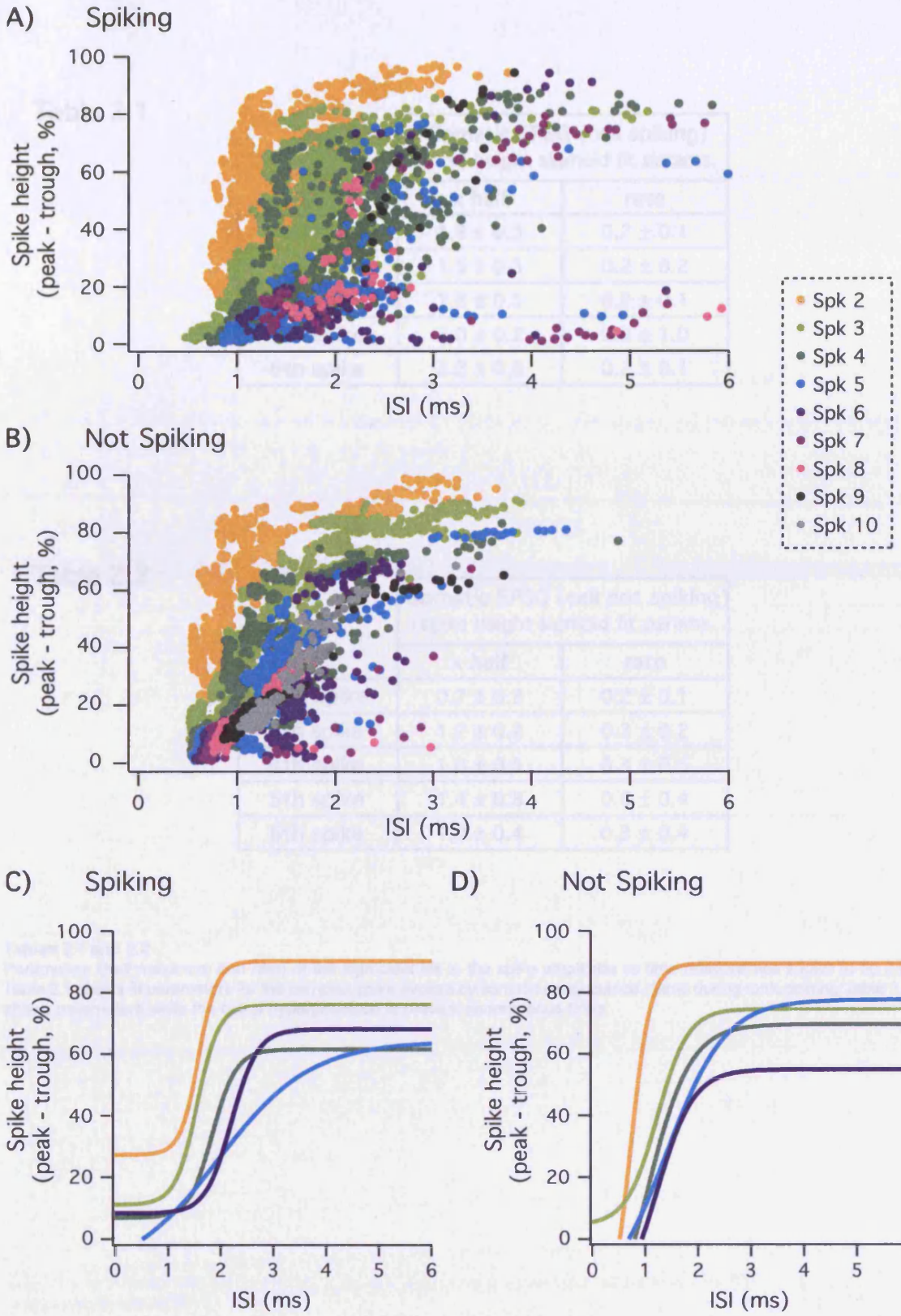

Figure 2.9 Spike height recovers more slowly with respect to ISI in later spikelets of the dynamic clamp evoked complex spike.

A) Overlay of the relationships between spike height (peak - trough) and ISI for all the spikelets (2 – 10) recorded in 16 cells at rest. Points coloured according to spikelets number. Note that the later spikelets tend to occur further to the right of this relationship, having smaller amplitudes for the same ISI. **B)** As in A, but in complex spikes recorded while the cell was hyperpolerised and prevented from firing by tonic somatic current injection (n = 13 cells). **C)** Overlay of the sigmoids that describe the population data shown in A and fig 2.8A, coloured as in A. Note that the sigmoids for the later spikes tend to have a half maximum at a longer ISI. **D)** As in C, but for data gathered at hyperpolarised membrane potentials (shown in B and fig 2.8B).

Table 2.1

	Somatic EPSG (cell spiking) spike height sigmoid fit params.	
	x half	rate
2nd spike	1.6 ± 0.3	0.2 ± 0.1
3rd spike	1.5 ± 0.3	0.2 ± 0.2
4th spike	1.8 ± 0.5	0.2 ± 0.1
5th spike	2.0 ± 0.2	0.9 ± 1.0
6th spike	2.2 ± 0.8	0.2 ± 0.1

Table 2.2

	Somatic EPSG (cell not spiking) spike height sigmoid fit params.	
	x half	rate
2nd spike	0.7 ± 0.3	0.2 ± 0.1
3rd spike	1.2 ± 0.2	0.3 ± 0.2
4th spike	1.0 ± 0.5	0.4 ± 0.5
5th spike	1.4 ± 0.8	0.6 ± 0.4
6th spike	1.2 ± 0.4	0.3 ± 0.4

Tables 2.1 and 2.2
Parameters (half maximum and rate) of the sigmoidal fits to the spike amplitude vs time relationships shown in fig 2.9. Table 2.1 shows fit parameters for the complex spike evoked by somatic conductance clamp during tonic spiking; table 2.2 shows parameters while the cell is hyperpolarised to prevent spontaneous firing.

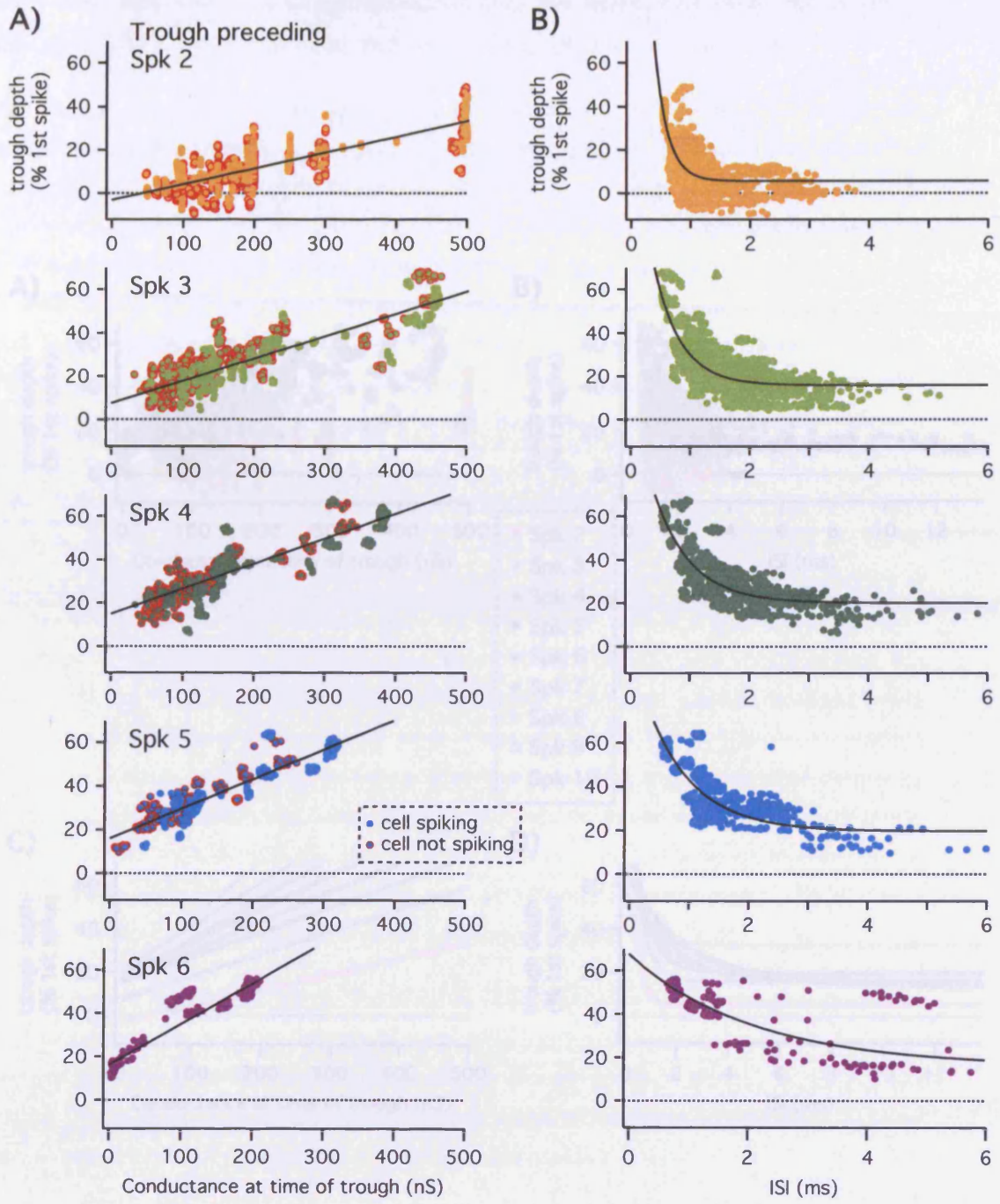

Figure 2.10 Generalised relationships between interspike troughs and conductance or time in dynamic clamp evoked complex spikes.

A) Relationship between the troughs (mV above baseline Vm) preceding spikelets 2 - 6 and the conductance injected at the time of the trough minimum. Data points recorded while the cell was hyperpolarised and prevented from firing spontaneously are outlined in red. As these lay along the same line as those recorded at rest, they were fitted together. For each interspike trough, the population as a whole was fit with a line (black lines).
B) Relationship between troughs and the ISI between the spikelets that surround them (both at rest and while hyperpolarised). For each interspike trough, the population as a whole was fit with an exponential (black lines).

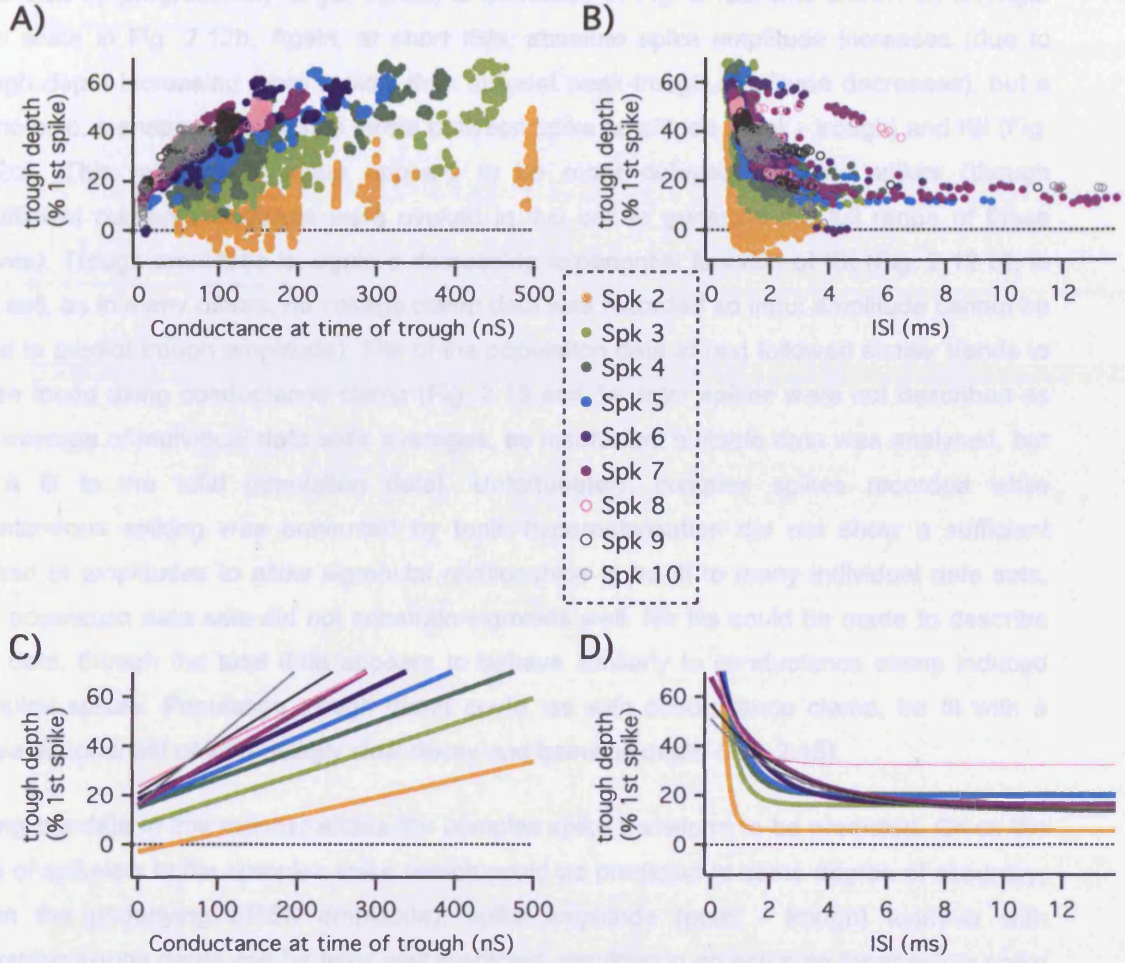

Figure 2.11 Interspike trough depth recovers more slowly with respect to ISI in later spikelets of the dynamic clamp evoked complex spike.

A) Overlay of the relationships between interspike trough and the conductance injected at the time of the trough minimum for all the spikelets (2 – 10) recorded in 18 cells, both at rest and during hyperpolarisation. Points coloured according to spikelets number. Note that the later troughs tend to occur further to the top left of this relationship, having larger amplitudes for the same conductance injection.
B) Overlay of the relationships between interspike trough and ISI. Here later troughs tent to occur further to the upper right of this relationship, having larger amplitudes for the same ISI.
C) Overlay of the lines that describe the population data shown in A and fig 2.10A, coloured as in A. Note that the lines for the later troughs tend to have a steeper slope and larger y intersect.
D) Overlay of the exponentials that describe the population data shown in B and fig 2.10B. Here exponentials for the later troughs tend to decay more slowly and to a higher baseline.

Height of spikelets within the CF evoked complex spike is a function of time

These trends in spike amplitude were found in complex spikes evoked with synaptic-like somatic conductance injection. To ensure similar trends apply to complex spikes evoked by CF stimulation, I analysed the spike amplitudes of complex spikes evoked in 21 cells. An example of a range of complex spikes produced at increasingly long interstimulus intervals (and thus by progressively larger inputs) is illustrated in Fig. 2.12a, and shown on a longer time scale in Fig. 2.12b. Again, at short ISIs, absolute spike amplitude increases (due to trough depth increasing more rapidly than spikelet peak-trough amplitude decreases), but a monotonic, s-shaped relationship exists between spike amplitude (peak - trough) and ISI (Fig. 2.12ci). This relationship again appears to be more delayed for later spikes (though insufficient numbers of spikes were evoked in this cell to generate the full range of these curves). Trough amplitude is, again a decreasing exponential function of ISI (Fig. 2.12 cii; in this cell, as in many others, no voltage clamp data was recorded so input amplitude cannot be used to predict trough amplitude). Fits of the population data at rest followed similar trends to those found using conductance clamp (Fig. 2.13 and 14; later spikes were not described as the average of individual data set's averages, as insufficient suitable data was analysed, but as a fit to the total population data). Unfortunately, complex spikes recorded while spontaneous spiking was prevented by tonic hyperpolarisation did not show a sufficient spread of amplitudes to allow sigmoidal relationships to be fit to many individual data sets, and population data sets did not constrain sigmoids well. No fits could be made to describe this data, though the total data appears to behave similarly to conductance clamp induced complex spikes. Population trough depth could, as with conductance clamp, be fit with a single exponential of increasingly slow decay and baseline depth (Fig. 2.15).

Fitting the data in this manner allows the complex spike waveform to be predicted. Given the time of spikelets in the complex spike (which could be predicted to some degree of accuracy, given the underlying EPSC amplitude), spike amplitude (peak - trough) together with interspike trough depth can be fairly well predicted, resulting in an estimate for absolute spike height. Examples (from 4 different Purkinje cells) are shown in Fig. 2.16.

This analysis has removed some element of the 'mystery' of complex spike waveforms generated by either conductance clamp or CF stimulation; their number and timing of spikes are simple linear or sublinear functions of their input amplitude and intrinsic cell excitability, and their exotic spike amplitudes are a simple function of interspike interval and spikelet number.

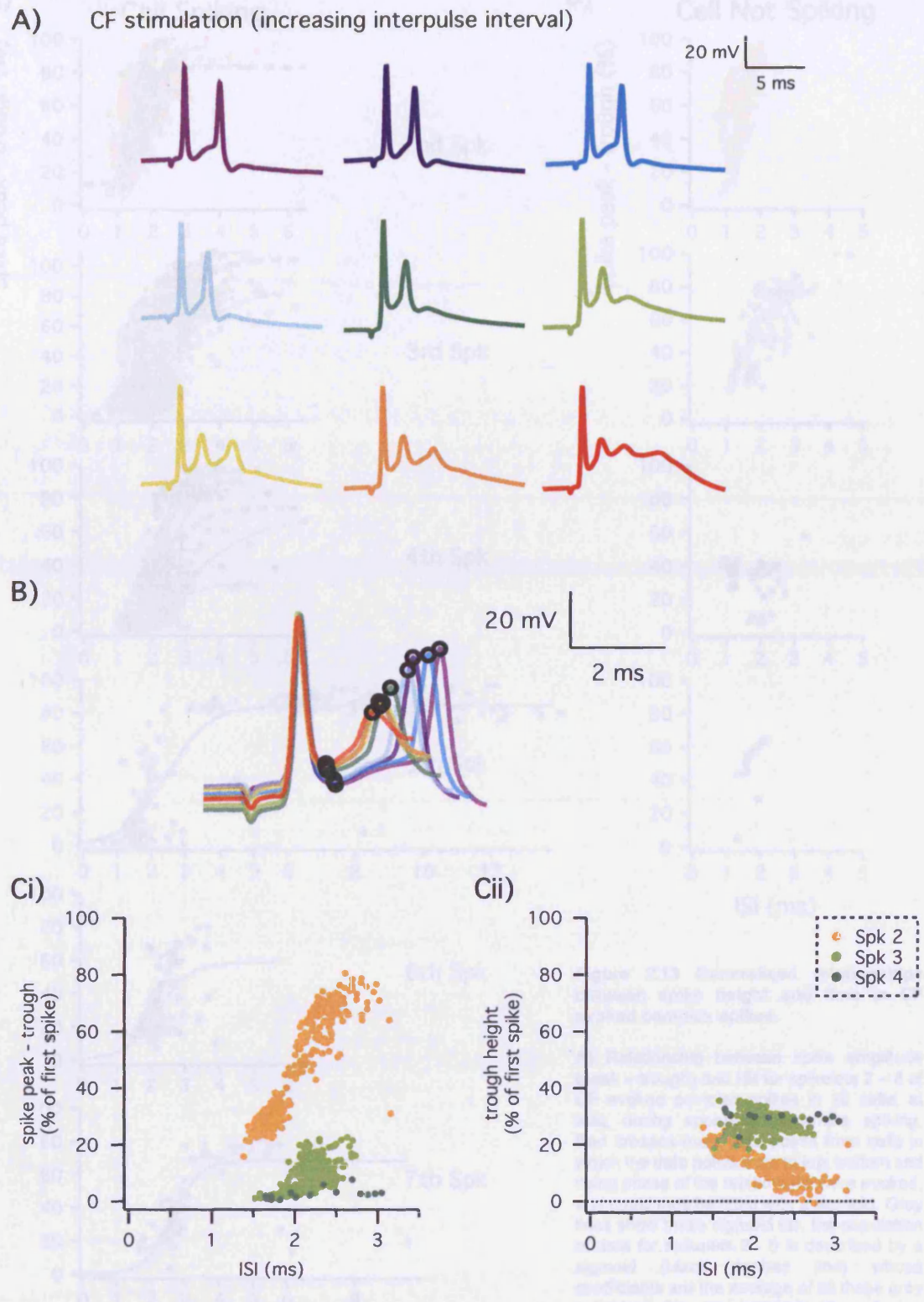

Figure 2.12 Spike height is an s-shaped function of spike time in CF evoked complex spikes.

A) Examples of complex spikes evoked by CF stimuli at increasing paired pulse intervals (from 60 – 5000 msec between stimuli). Note that as the paired pulse interval increases, the second spike occurs earlier (as seen in Fig. 1.4), its amplitude tends to decrease and the preceding trough tends to increase in height, in a similar manner to conductance injection evoked complex spikes.
B) Overlay of the first two spikes of the traces shown in A, at an expanded time scale. Black circles mark the peak amplitude of the second spike and the depth of the preceding trough.
Ci) Relationship between spike amplitude (peak - trough) and interspike interval for all complex spike secondary spikes evoked (at rest) by dynamic clamp in the cell shown in A (coloured according to spike number within the complex spike).
ii) Relationship between interspike trough height (mV above baseline Vm) and interspike interval (msec) between the spike following the trough and that preceding it.

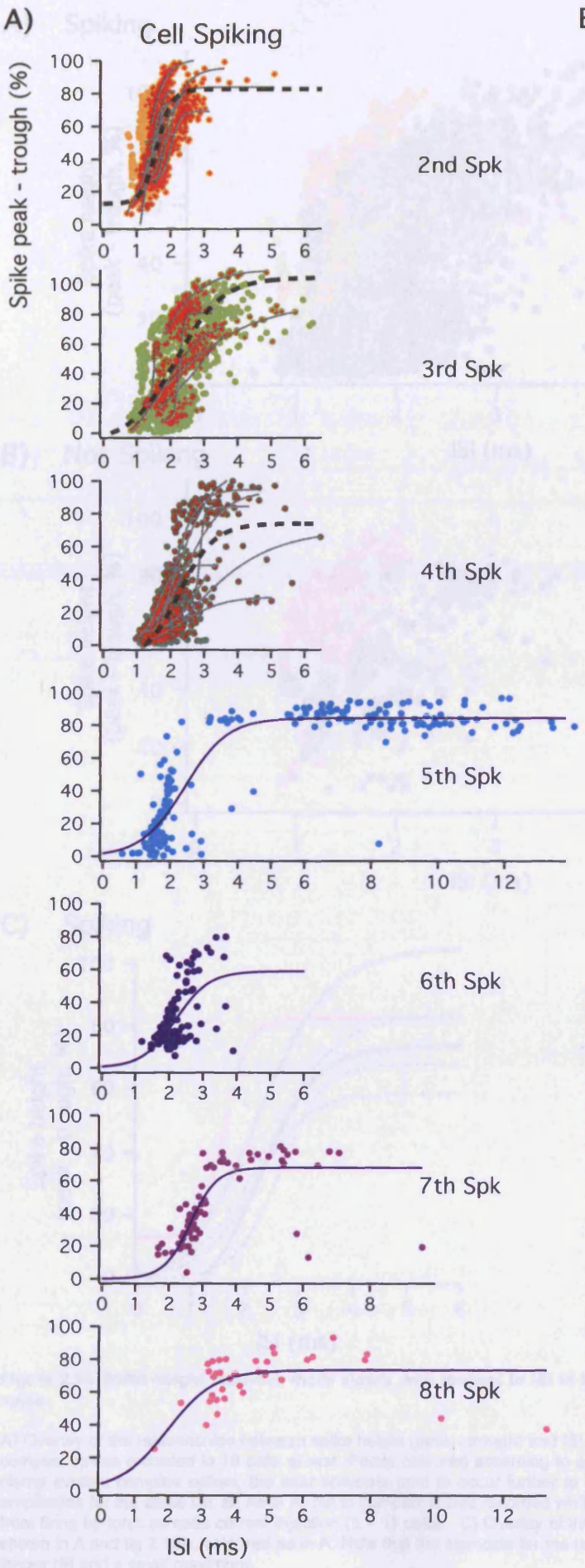

Figure 2.13 Generalised relationships between spike height and time in CF evoked complex spikes.

A) Relationship between spike amplitude (peak – trough) and ISI for spikelets 2 – 8 of CF evoked complex spikes in 19 cells, at rest, during spontaneous simple spiking. Red crosses mark data points from cells in which the data points from to top, bottom and rising phase of the relationship were evoked, and could thus be fitted with a sigmoid. Grey lines show these sigmoid fits; the population of data for spikelets 2 - 5 is described by a sigmoid (black dashed line) whose coefficients are the average of all these grey individual fits. For spikelets 6 – 9 few individual data sets contained a sufficient spread of points to be fitted with a sigmoid, however sigmoidal fits to the population data together constrained to 0 described the data well.

B) As in A, but for data collected during tonic somatic current injection to prevent spontaneous spiking (n = 11). Insufficent spread of data points were available to allow the data to be fit.

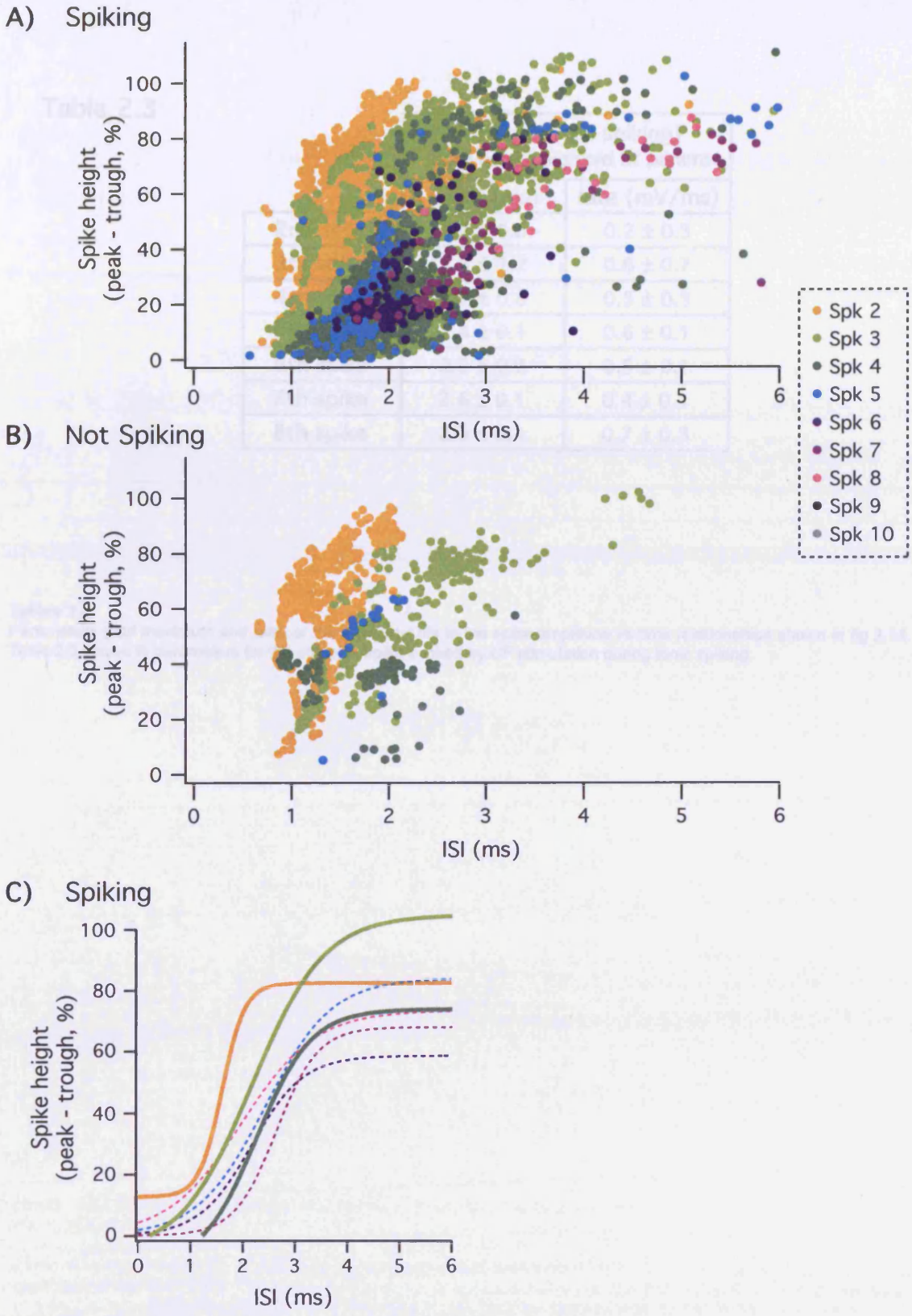

Figure 2.14 Spike height recovers more slowly with respect to ISI in later spikelets of the CF evoked complex spike.

A) Overlay of the relationships between spike height (peak - trough) and ISI for all the spikelets (2 – 10) from CF evoked complex spikes recorded in 19 cells at rest. Points coloured according to spikelets number. Note that, as with dynamic clamp evoked complex spikes, the later spikelets tend to occur further to the right of this relationship, having smaller amplitudes for the same ISI. **B)** As in A, but in complex spikes recorded while the cell was hyperpolerised and prevented from firing by tonic somatic current injection (n = 11 cells). **C)** Overlay of the sigmoids that describe the population data shown in A and fig 2.13A, coloured as in A. Note that the sigmoids for the later spikes tend to have a half maximum at a longer ISI and a small maximum.

Table 2.3

	CF stim. (cell spiking) spike height sigmoid fit params.	
	x half (ms)	rate (mV/ms)
2nd spike	1.6 ± 0.3	0.2 ± 0.3
3rd spike	2.3 ± 1.2	0.6 ± 0.7
4th spike	2.2 ± 0.8	0.5 ± 0.3
5th spike	2.4 ± 0.1	0.6 ± 0.1
6th spike	2.2 ± 0.2	0.5 ± 0.1
7th spike	2.6 ± 0.1	0.4 ± 0.1
8th spike	2.0 ± 0.4	0.7 ± 0.3

Tables 2.3
Parameters (half maximum and rate) of the sigmoidal fits to the spike amplitude vs time relationships shown in fig 2.14. Table 2.3 shows fit parameters for the complex spike evoked by CF stimulation during tonic spiking.

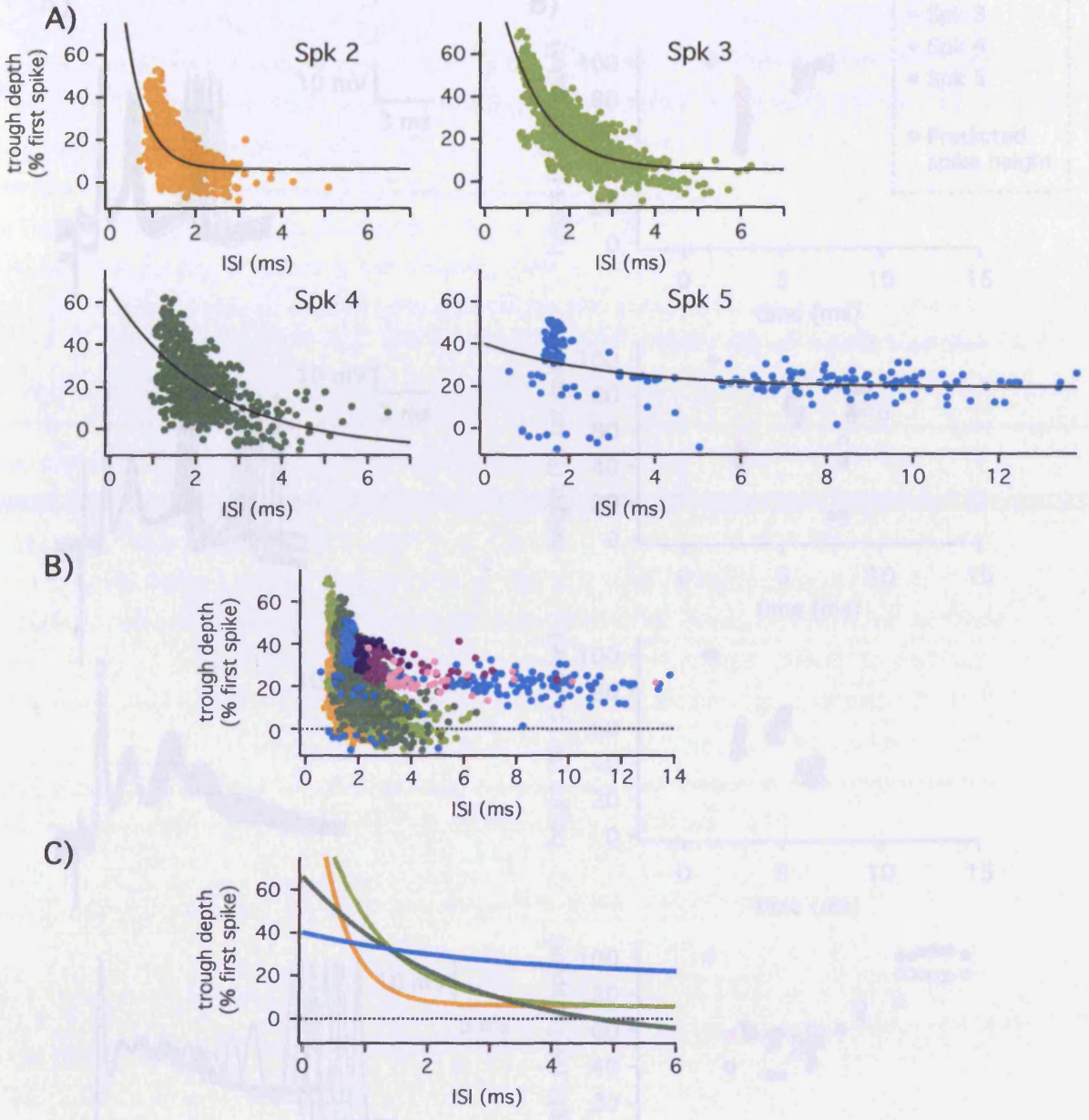

Figure 2.15 Generalised relationships between interspike troughs and conductance or time in CF evoked complex spikes.

A) Relationship between the troughs (mV above baseline Vm) preceding spikelets 2 - 5 and the ISI (ms) between the spikelets that surround them. Data points from complex spikes recorded at rest and during hyperpolarisation overlapped so were plotted and fitted together. For each interspike trough, the population as a whole was fit with a line (black lines).
B) Overlay of the relationships between interspike trough and ISI. Later troughs tent to occur further to the upper right of this relationship, having larger amplitudes for the same ISI.
C) Overlay of the exponentials that describe the population data shown in A and B. Note that exponentials for the later troughs tend to decay more slowly.

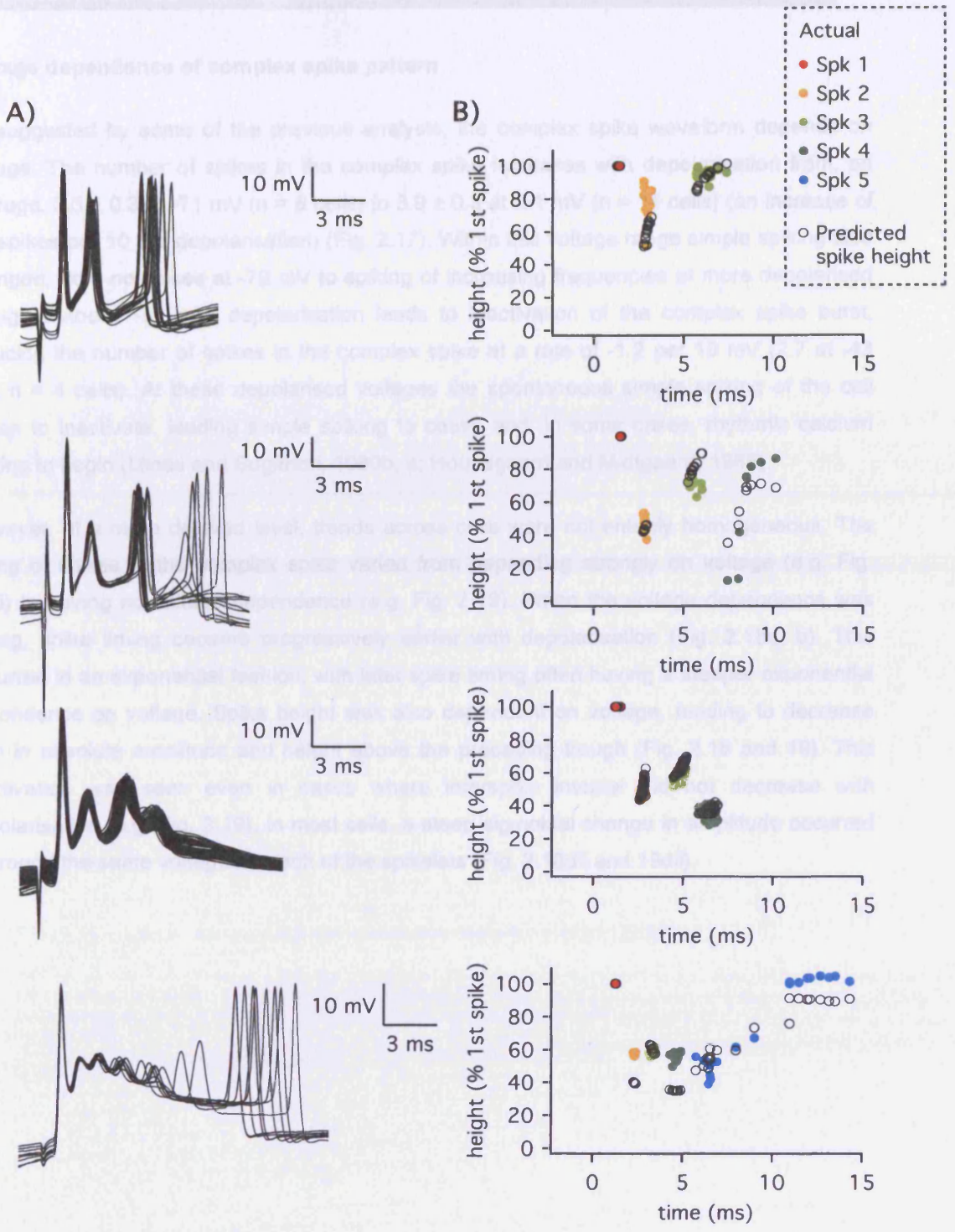

Figure 2.16 Height of spikelets in complex spike predicted from their timing.

A) Example complex spikes in response to 1 Hz CF stimulation in 4 different cells.
B) Height and time of spikelets in the complex spikes shown in A. Actual values shown with filled, coloured circles; values predicted from the relationships shown in fig 2.15 and 2.13 shown open black circles.

Voltage dependence of complex spike pattern

As suggested by some of the previous analysis, the complex spike waveform depends on voltage. The number of spikes in the complex spike increases with depolarisation from, on average, 2.5 ± 0.3 at -71 mV (n = 8 cells) to 3.9 ± 0.3 at -51 mV (n = 14 cells) (an increase of 0.7 spikes per 10 mV depolarisation) (Fig. 2.17). Within this voltage range simple spiking also changed, from no spikes at -70 mV to spiking of increasing frequencies at more depolarised voltages. Above -51 mV, depolarisation leads to inactivation of the complex spike burst, reducing the number of spikes in the complex spike at a rate of -1.2 per 10 mV (2.7 at -43 mV, n = 4 cells). At these depolarised voltages the spontaneous simple spiking of the cell began to inactivate, leading simple spiking to cease and, in soma cases, rhythmic calcium spiking to begin (Llinas and Sugimori, 1980b, a; Hounsgaard and Midtgaard, 1988).

However, at a more detailed level, trends across cells were not entirely homogeneous. The timing of spikes in the complex spike varied from depending strongly on voltage (e.g. Fig. 2.18) to having no voltage dependence (e.g. Fig. 2.19). When the voltage dependence was strong, spike timing became progressively earlier with depolarisation (Fig. 2.18a, b). This occurred in an exponential fashion, with later spike timing often having a steeper exponential dependence on voltage. Spike height was also dependent on voltage, tending to decrease both in absolute amplitude and height above the preceding trough (Fig. 2.18 and 19). This inactivation was seen even in cases where interspike interval did not decrease with depolarisation (e.g. Fig. 2.19). In most cells, a steep sigmoidal change in amplitude occurred at around the same voltage for each of the spikelets (Fig. 2.18dii and 19dii).

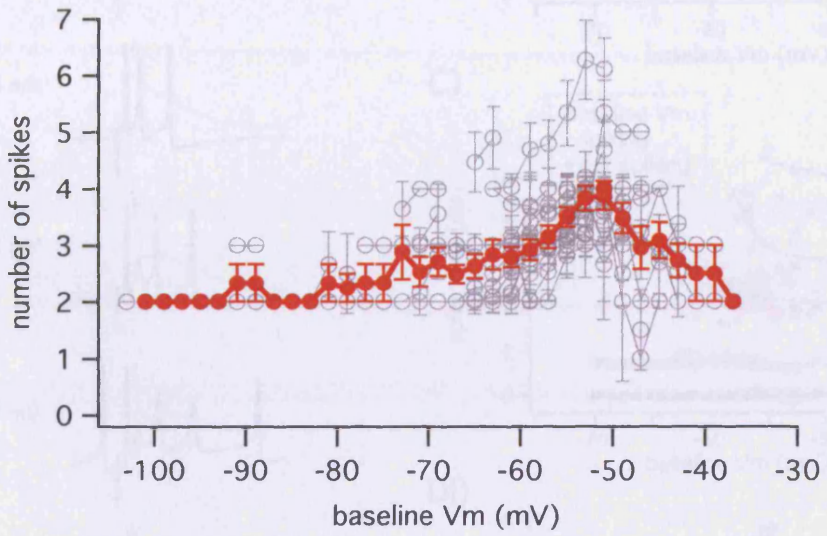

Figure 2.17 Voltage dependence of the number of spikes in the complex spike

Average number of spikes in CF evoked complex spikes recorded from 18 Purkinje cells where average baseline membrane potential (over the 50 ms prior to CF stimulation) was varied by tonic current injection from a second somatic patch electrode. Voltage bin width: 2 mV. Gray traces show individual cell's average ± SD; red trace shows population mean ± SEM.

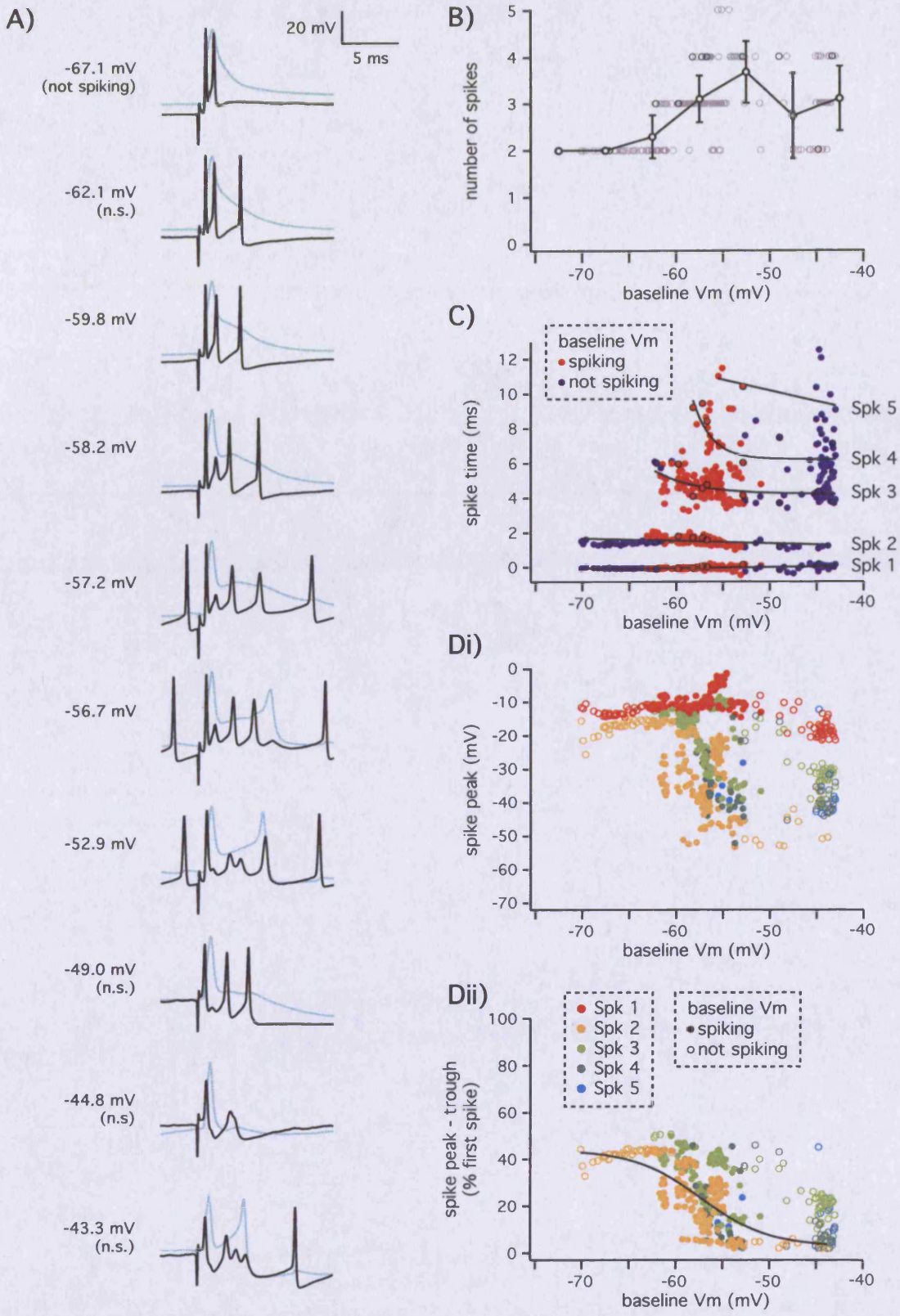

Figure 2.18: Example 1 of voltage dependence of complex spike waveform; spike timing depends on baseline Vm.

A) Examples of CF evoked complex spikes at increasingly more depolarised membrane potentials in the same cell. **B)** Number of spikes in the complex spike at different baseline membrane potentials. Grey circles mark individual complex spikes; black circles with error bars show the mean ± SD of the number of spikes in 5 mV bins **C)** Time (msec after 1st spike at resting Vm) of spikes in the complex spike at different baseline Vms. Red circles mark points at which the cell was spontaneously firing simple spikes; blue circles mark lack of simple spiking. The time of each spikelet in the complex spike vs baseline Vm was fitted with an exponential (black lines). **D)** Height of spikes in the complex spike, measured as either **(i)** peak Vm reached or **(ii)** spike peak minus preceding interspike trough, plotted against baseline membrane potential. The decrease of the second spikelet is fit with a sigmoid with half maximum at -56 mV.

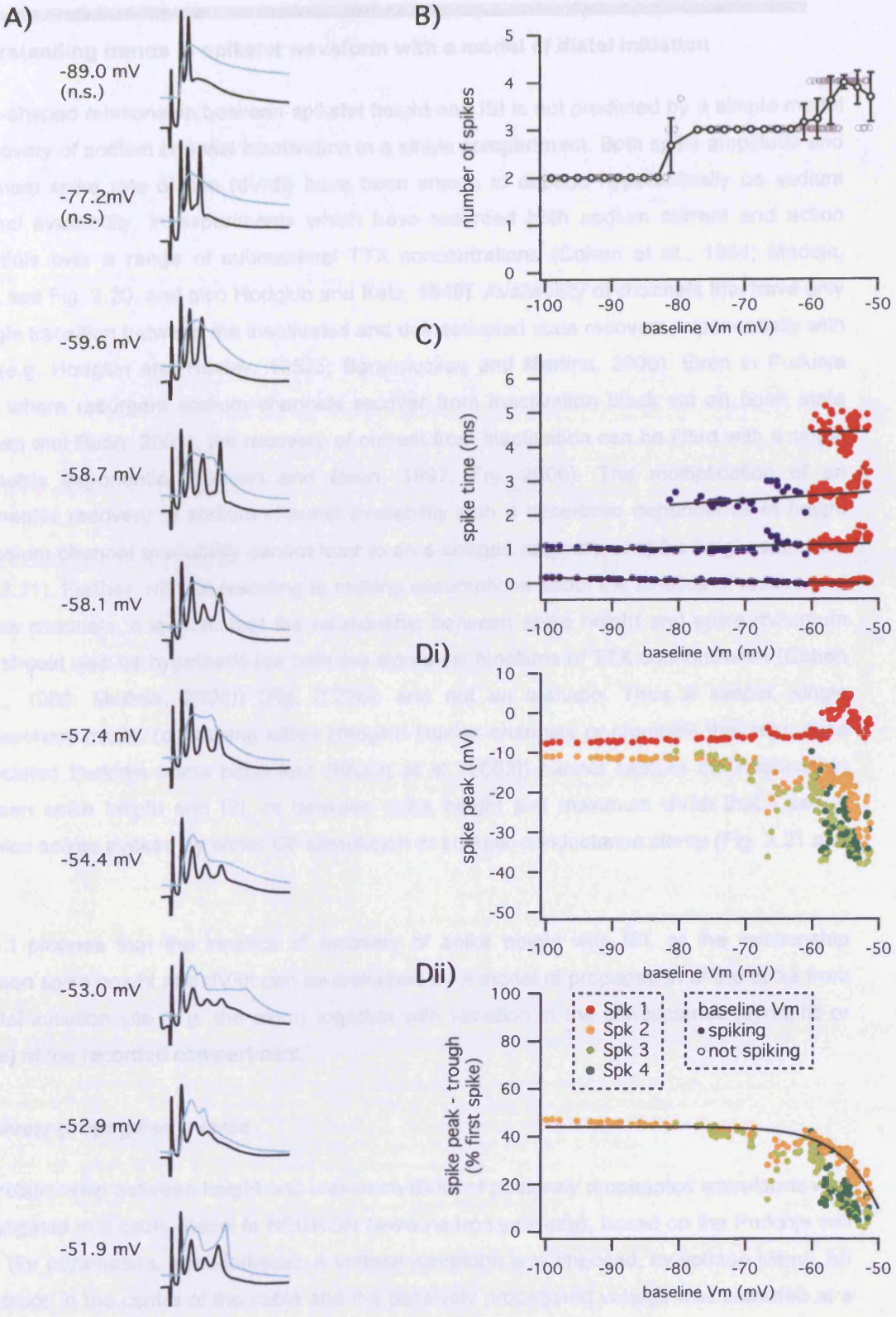

Figure 2.19 Example 2 of voltage dependence of complex spike waveform; spike timing is not dependent on baseline Vm.

A) Examples, in a second sample Purkinje cell, of CF evoked complex spikes at increasingly more depolarised membrane potentials. **B)** Number of spikes in the complex spike at different baseline membrane potentials. Grey circles mark individual complex spikes; black circles with error bars show the mean ± SD of the number of spikes in 2 mV bins. **C)** Time (msec after 1st spike at resting Vm) of spikes in the complex spike at different baseline Vms. Red circles mark points at which the cell was tonically firing; blue circles mark lack of smiplefiring. The time of each spikelet in the complex spike vs baseline Vm was fitted with a line (black lines). **D)** Height of spikes in the complex spike, measured as both **(i)** peak Vm reached or **(ii)** spike peak minus preceding interspike trough, plotted against baseline membrane potential.

Understanding trends in spikelet waveform with a model of distal initiation

The s-shaped relationship between spikelet height and ISI is not predicted by a simple model of recovery of sodium channel inactivation in a single compartment. Both spike amplitude and maximum spike rate of rise (dV/dt) have been shown to depend hyperbolically on sodium channel availability, in experiments which have recorded both sodium current and action potentials over a range of submaximal TTX concentrations (Cohen et al., 1984; Madeja, 2000, see Fig. 2.20, and also Hodgkin and Katz, 1949). Availability of channels that have only a single transition between the inactivated and deinactivated state recovers exponentially with time (e.g. Hodgkin and Huxley, 1952c; Baranauskas and Martina, 2006). Even in Purkinje cells, where resurgent sodium channels recover from inactivation block via an open state (Raman and Bean, 2001), the recovery of current from inactivation can be fitted with a single or double exponential (Raman and Bean, 1997; Fry, 2006). The multiplication of an exponential recovery of sodium channel availability with a hyperbolic dependence of height on sodium channel availability cannot lead to an s-shaped recovery of spike height with time (Fig. 2.21). Further, without resorting to making assumptions about the kinetics of recovery of sodium channels, it is clear that the relationship between spike height and spike maximum dVdt should also be hyperbolic (as both are sigmoidal functions of TTX concentration (Cohen et al., 1984; Madeja, 2000)) (Fig. 2.22b), and not an s-shape. Thus a simple, single compartment model (containing either Hodgkin Huxley channels or channels that reproduce dissociated Purkinje soma behaviour (Khaliq et al., 2003)) cannot capture the relationship between spike height and ISI, or between spike height and maximum dV/dt that I see in complex spikes evoked by either CF stimulation or somatic conductance clamp (Fig. 2.21 and 22).

Here I propose that the kinetics of recovery of spike height with ISI, or the relationship between spike height and dV/dt can be explained by a model of propagation of the spike from a distal initiation site (e.g. the axon) together with variation in the conductance (synaptic or active) of the recorded compartment.

Passively propagated events

The relationship between height and maximum dV/dt of passively propagated waveforms was investigated in a cable model in NEURON (www.neuron.yale.edu), based on the Purkinje cell axon (for parameters, see Methods). A voltage waveform was imposed, by voltage clamp, on a 'hotspot' in the centre of the cable and the passively propagated voltage was recorded at a 'soma' 100 μm away (10000 μm of cable continued on the other side of the 'soma', to avoid the distortion of end effects, see Fig. 2.23a). The effect of varying the conductance of the soma was investigated. The relationship between maximum height and maximum dV/dt in response to a square pulse imposed upon the 'hotspot' (of sufficient duration to allow the 'soma' membrane potential to reach a steady state) had a slight upwards curve; this was

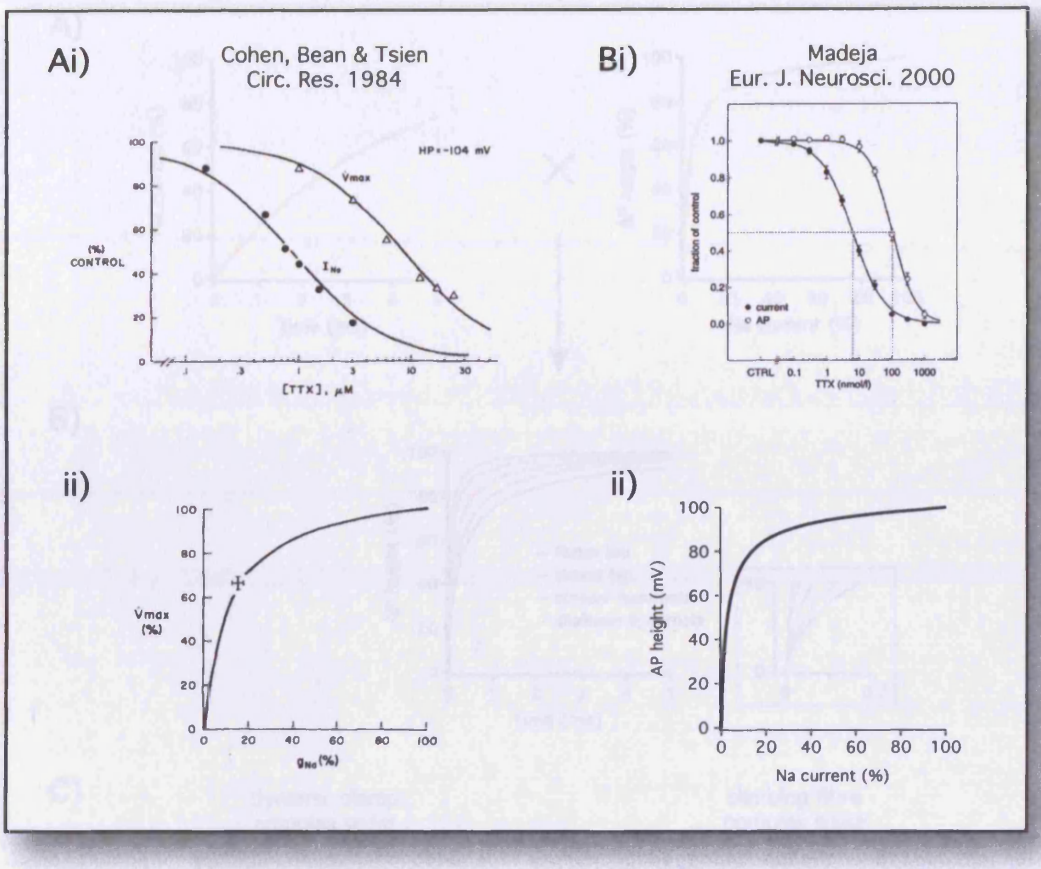

Figure 2.20: Spike height and maximum dV/dt are related hyperbolically to sodium channel availability.

The data shown in this figure are taken from Cohen, Bean & Tsien, 1984 and Madeja, 2000.

Ai) Dose response relationships between sodium current (peak current in response to voltage steps from -104 mV to -44 mV, filled circles) or ˙Vmax (maximum rate of Vm change during upstroke of evoked action potentials, open circles) and TTX concentration in rabbit heart Purkinje fibres (fig 2, Cohen, Bean & Tsien, 1984). Data was fit with equations of the form y = 1 / (1 + [TTX]/KD), where KD = 0.82 μM for sodium current and 8.4 μM for ˙Vmax.
ii) Transformation of data in (A), demonstrating the dependence of maximum action potential dV/dt (˙Vmax) on sodium channel availability (gNa) (taken from fig 3, Cohen, Bean & Tsien, 1984). The hyperbola is obtained by rearranging the equations fitting sodium current and ˙Vmax TTX dose response curves, giving ˙Vmax = 10 gNa / (1 + 9 gNa). Error bars show collected experimental SEM.
Bi) Relationship between sodium current (peak current in response to voltage steps from -80 mV to -20 mV, filled circles) or action potential amplitude (open circles) and TTX concentration in dissociated hippocampal CA1 neurons (fig 1B, Madeja, 2000). Data are fitted with Langmuir equations with IC50 values and Hill coefficients of 6.4 nM and 0.91 for sodium currents and 104 nM and 1.23 for action potential heights.
ii) Transformation of data in C showing the dependence of action potential height of sodium channel availability.

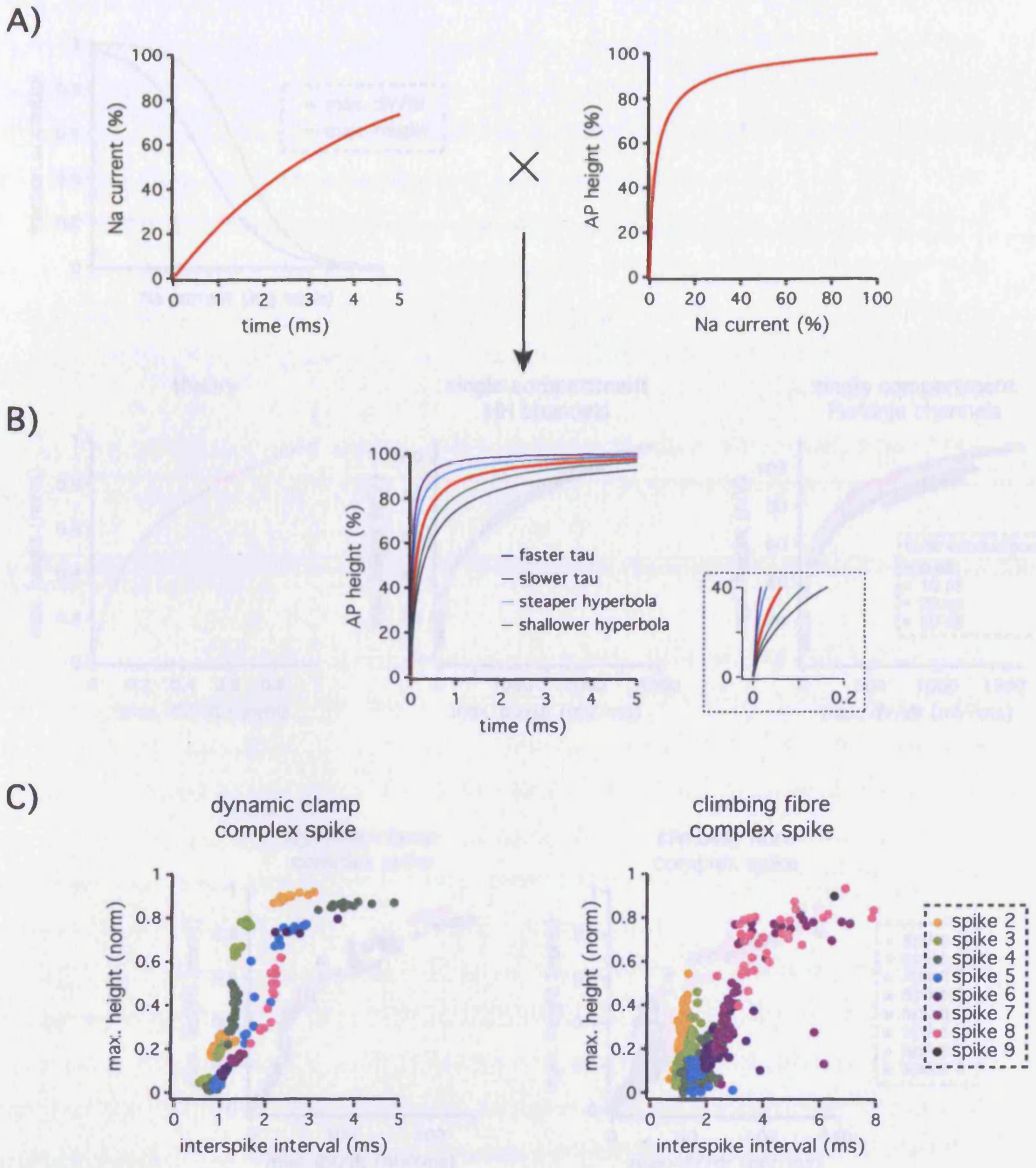

Figure 2.21: Composition of an exponential and a hyperbola cannot explain s-shaped spike height vs time relationship.

A) Illustration of the hypothetical exponential recovery of sodium channel availability with time since an inactivating pulse, and of the hyperbolic increase in action potential height with sodium channel availability.
B) Composition of the two functions shown in A (red trace), generating a relationship between action potential height and time since an inactivating pulse that is not s-shaped. Inset shows the initial rise of the curve at a higher magnification. Altering the time constant of the exponential (dark blue and black traces) or the slope of the hyperbola (light blue and green traces) does not affect the overall shape of the composition.
C) Examples of the real relationships found between spike height and time since a previous action potential in complex spikes generated by dynamic clamp (left) and CF stimulation (right).

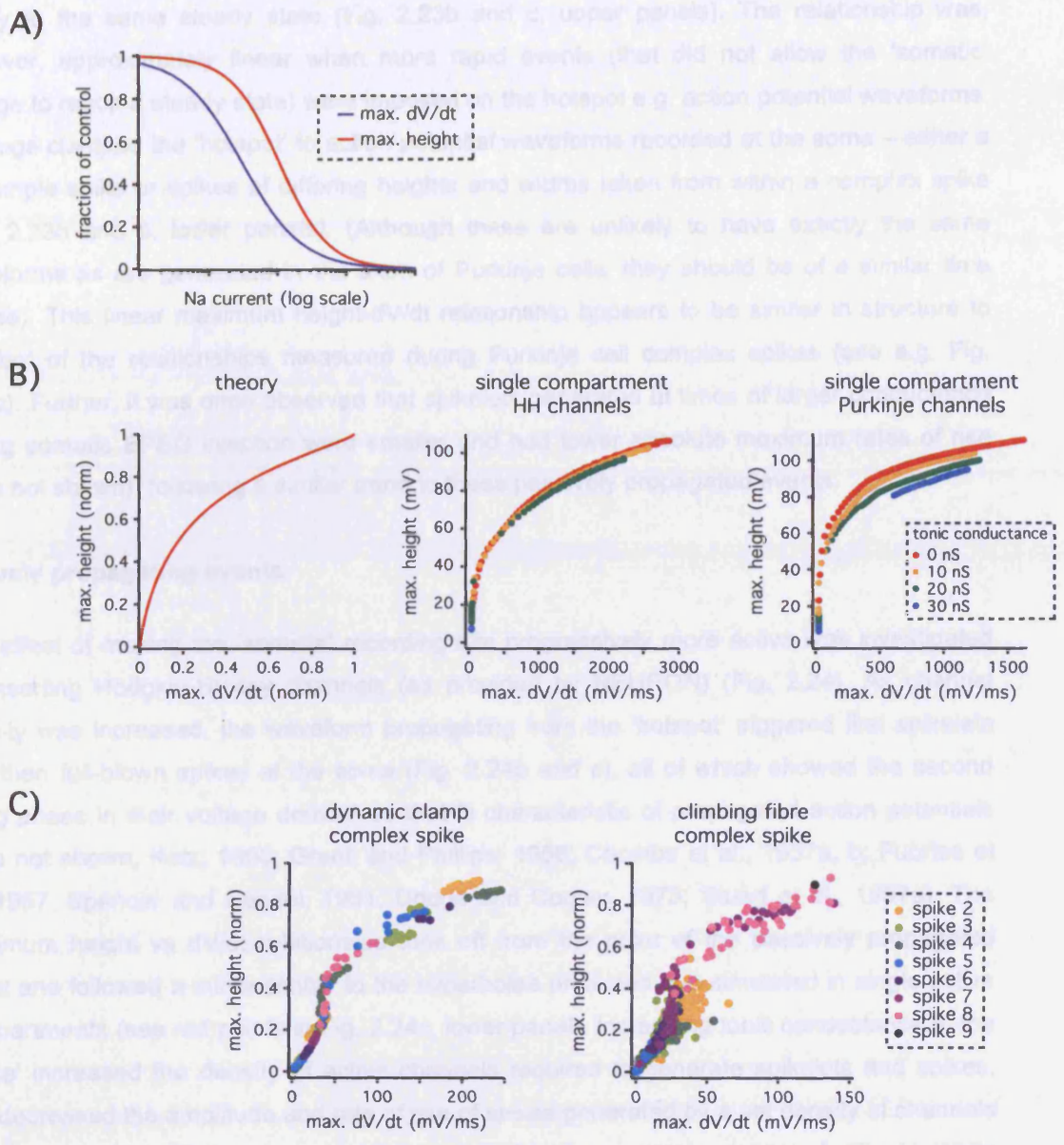

Figure 2.22: Hyperbolic relationship between spike height and maximum dV/dt in a single compartment model.

A) Illustration abstracted dose response relationships between spike height (red) or maximum dV/dt (blue) and sodium channel availability.
B) Relationship between action potential height and maximum dV/dt found by **(i)** transformation of abstracted curves in A **(ii)** simulation, in NEURON, of a single compartment containing standard Hodgkin-Huxley channels at 0 - 8 times standard density, together with a tonic conductance of 0 - 30 nS (red - blue markers) or **(iii)** simulation of a single compartment containing channels that reproduce dissociated Purkinje soma behaviour (Khaliq et al., 2003) at 0 - 8 times standard density, together with a tonic conductance of 0 - 30 nS (red - blue markers).
C) Examples of the real relationships found between spike height and maximum dV/dt in complex spikes generated by dynamic clamp (left) and CF stimulation (right).

more pronounced when the size 'soma' compartment was increased and thus charged more slowly to the same steady state (Fig. 2.23b and c, upper panels). The relationship was, however, approximately linear when more rapid events (that did not allow the 'somatic' voltage to reach a steady state) were imposed on the hotspot e.g. action potential waveforms. I voltage clamped the 'hotspot' to action potential waveforms recorded at the soma – either a full simple spike or spikes of differing heights and widths taken from within a complex spike (Fig. 2.23b and c, lower panels). (Although these are unlikely to have exactly the same waveforms as are generated in the axon of Purkinje cells, they should be of a similar time course). This linear maximum height-dV/dt relationship appears to be similar in structure to the foot of the relationships measured during Purkinje cell complex spikes (see e.g. Fig. 2.22c). Further, it was often observed that spikelets generated at times of larger conductance during somatic EPSG injection were smaller and had lower absolute maximum rates of rise (data not shown), following a similar trend to these passively propagated events.

Actively propagating events

The effect of making the 'somatic' recording site progressively more active was investigated by inserting Hodgkin-Huxley channels (as provided by NEURON) (Fig. 2.24). As channel density was increased, the waveform propagating from the 'hotspot' triggered first spikelets and then full-blown spikes at the soma (Fig. 2.24b and c), all of which showed the second rising phase in their voltage derivatives that is characteristic of propagated action potentials (data not shown, Katz, 1950; Granit and Phillips, 1956; Coombs et al., 1957a, b; Fuortes et al., 1957; Spencer and Kandel, 1961; Dodge and Cooley, 1973; Stuart et al., 1997a). The maximum height vs dV/dt relationship took off from the point of the passively propagated event and followed a curve similar to the hyperbolae predicted and simulated in single active compartments (see red points in Fig. 2.24c, lower panel). Increasing tonic conductance at the 'soma' increased the density of active channels required to generate spikelets and spikes, and decreased the amplitude and rate of rise of spikes generated by a set density of channels (Fig. 2.24b and c). (The tonic conductance applied had a reversal potential of -60 mV. While the reversal potential did not affect the passive relationships seen above, a depolarising reversal potential triggered spontaneous firing, and complicated measures of channel availability. Additional simulations, not shown here, suggest that the reversal potential of the additional conductance does not have a significant effect on the trends observed). The additional tonic conductance did not disrupt the general shape of the active part of the maximum height vs dV/dt relationship, but did add a roughly linear section to the initial part of the relationship, where again passively propagated events were decreased in amplitude and absolute maximal rate of rise. Similar results were seen when the action potential waveform at the 'hotspot' was generated not by voltage clamp but by inserting Hodgkin Huxley channels at the 'hotspot' and applying a current injection (Fig. 2.24d-f). The resulting s-shaped maximum height vs dV/dt relationships were similar to those seen with both conductance clamp and CF evoked complex spikes. This suggests that the relationships seen during the

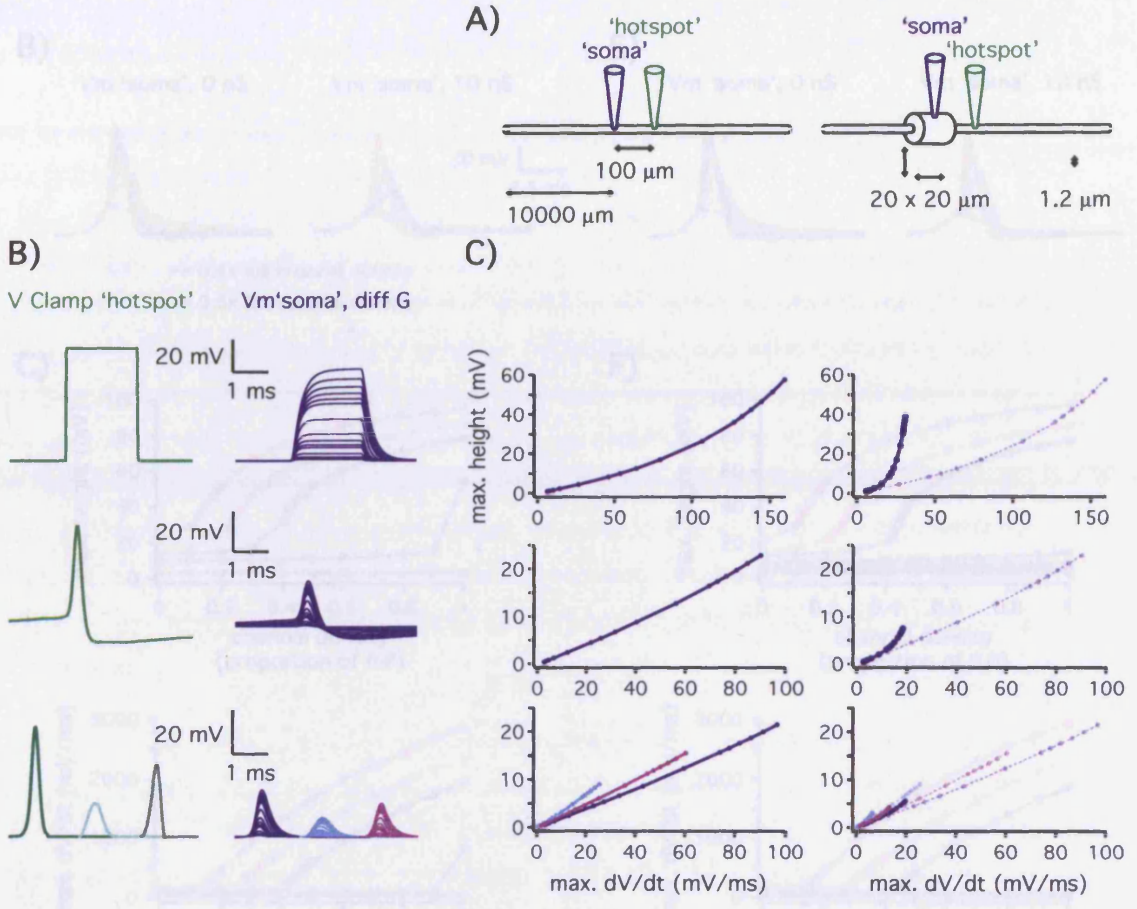

Figure 2.23 Height and maximum dV/dt of passively propagated voltages in a cable.

A) Illustration of the morphologies in which the propagation of a voltage waveform (imposed by voltage clamp at the 'hotspot', green) was recorded (at the 'soma', blue). 'Soma' and 'hotspot' were separated by a 100 µm long, 1.2 µm diameter cable; on the other side of the 'soma' was 10000 µm of sealed end cable. In one set of simulations (left) the morphology was symmetrical about the 'hotspot'; an identical morphology was used in a further set of simulations (right) except that 'soma' compartment was increased from 10 x 1.2 µm to 20 x 20 µm.
Throughout, Ri = 150 Ωcm, Cm = 1 µF/cm^2 and Rm = 20000 Ωcm^2.
B) Voltage clamp waveforms imposed on the 'hotspot' (left) and resulting 'somatic' voltages (right) while 0 - 500 nS of additional tonic conductance was placed the soma. Waveforms are a 2 msec square pulse, a Purkinje cell action potential or spikelets extracted from a complex spike waveform (recorded at the soma, at 34 °C).
C) Relationship measured between spike height an maximum dV/dt while the waveforms shown in B are applied to the morphologies shown in A. For comparison, the results from the uniform cable are superimposed on the results from the cable with enlarged 'soma' compartment (right hand panel, pale lines).

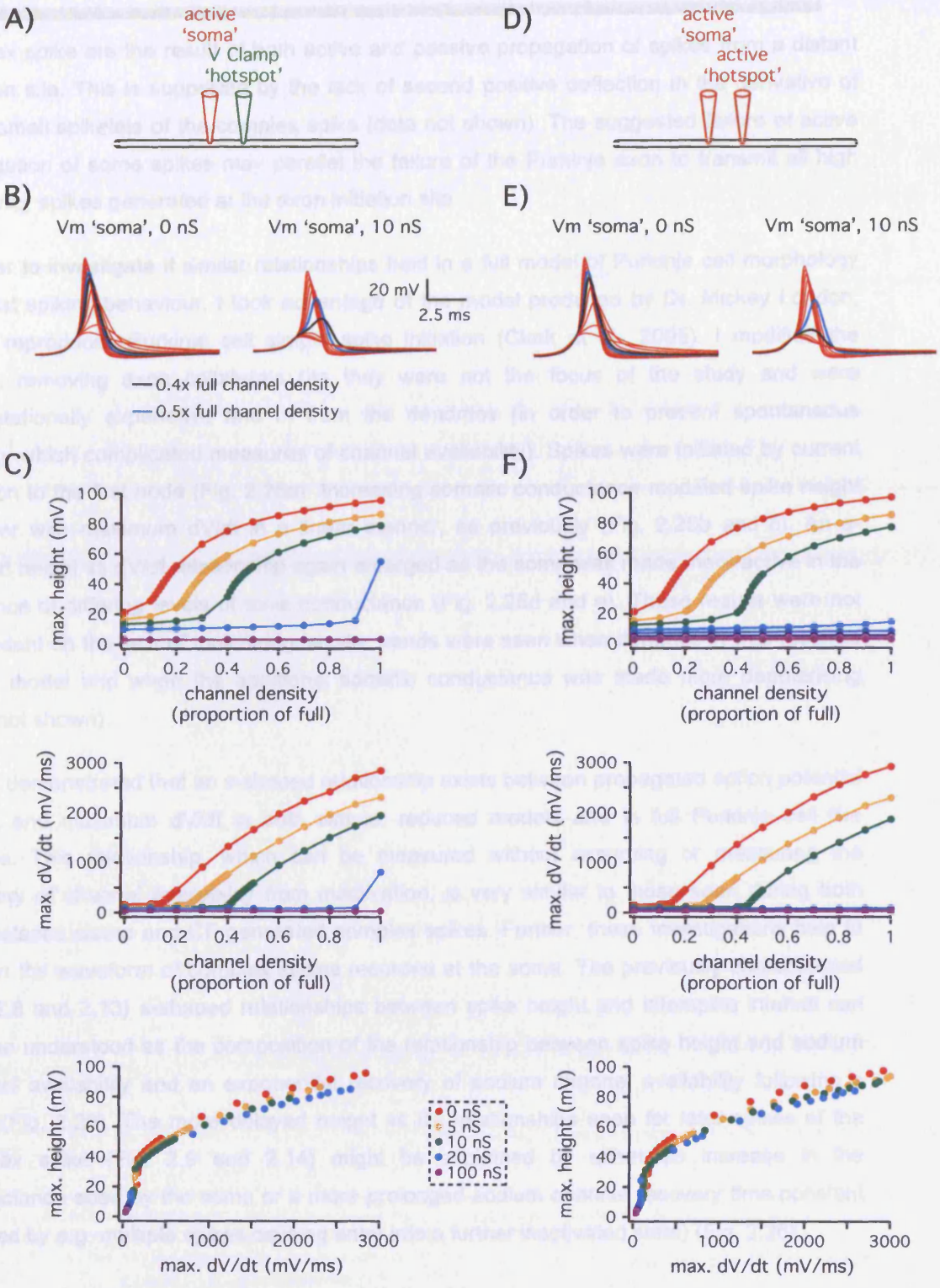

Figure 2.24: Height and maximum dV/dt of actively and passively propagated voltages in a cable.

A) Illustration of the uniform cable morphology used to record propagation of a Hodgkin-Huxley action potential waveform (imposed by voltage clamp at the 'hotspot') while the 'soma' was made increasingly active (0 - 16 times standard density of Hodgkin-Huxley channels) and tonic conductance as varied (0 - 100 nS).
B) Voltage waveforms recorded in the 'soma' as HH channel density was increased from 0 - 1 x full density (steps of 0.1 x) in a background of either no (left) or 10 nS (right) additional tonic conductance at the soma.
C) Relationships measured between spike height and channel density (top), maximum dV/dt and channel density (middle) and between spike height and maximum dV/dt (bottom), in a background of 0 - 100 nS tonic conductance at the soma (red - purple markers, as in legend).
D-F) As in A-C, but action potential waveform at the 'hotspot' evoked by current injection to the compartment (0.4 nA for 0.2 ms), which was made active by addition of Hodgkin-Huxley channels (16 times standard density).

complex spike are the result of both active and passive propagation of spikes from a distant initiation site. This is supported by the lack of second positive deflection in the derivative of some small spikelets of the complex spike (data not shown). The suggested failure of active propagation of some spikes may parallel the failure of the Purkinje axon to transmit all high frequency spikes generated at the axon initiation site.

In order to investigate if similar relationships held in a full model of Purkinje cell morphology and fast spiking behaviour, I took advantage of the model produced by Dr. Mickey London, which reproduces Purkinje cell simple spike initiation (Clark et al., 2005). I modified the model, removing axon collaterals (as they were not the focus of the study and were computationally expensive) and Ih from the dendrites (in order to prevent spontaneous spiking, which complicated measures of channel availability). Spikes were initiated by current injection to the first node (Fig. 2.25a). Increasing somatic conductance modified spike height together with maximum dV/dt in a linear manner, as previously (Fig. 2.25b and c). An s-shaped height vs dV/dt relationship again emerged as the soma was made more active in the presence of differing levels of tonic conductance (Fig. 2.25d and e). These results were not dependent on the lack of tonic firing; similar trends were seen when dendritic Ih was restored to the model and when the additional somatic conductance was made more depolarising (data not shown).

I have demonstrated that an s-shaped relationship exists between propagated action potential height and maximum dV/dt in both simple, reduced models and in full Purkinje cell like models. This relationship, which can be measured without assuming or measuring the recovery of channel availability from inactivation, is very similar to those seen during both conductance clamp and CF generated complex spikes. Further, these investigations help to explain the waveform of complex spikes recorded at the soma. The previously characterised (Fig. 2.8 and 2.13) s-shaped relationships between spike height and interspike interval can thus be understood as the composition of the relationship between spike height and sodium channel availability and an exponential recovery of sodium channel availability following a spike (Fig. 2.26). The more delayed height vs ISI relationships seen for later spikes of the complex spike (Fig. 2.9 and 2.14) might be explained by either an increase in the conductance seen by the soma or a more prolonged sodium channel recovery time constant (caused by e.g. multiple spikes causing entry into a further inactivated state) (Fig. 2.26).

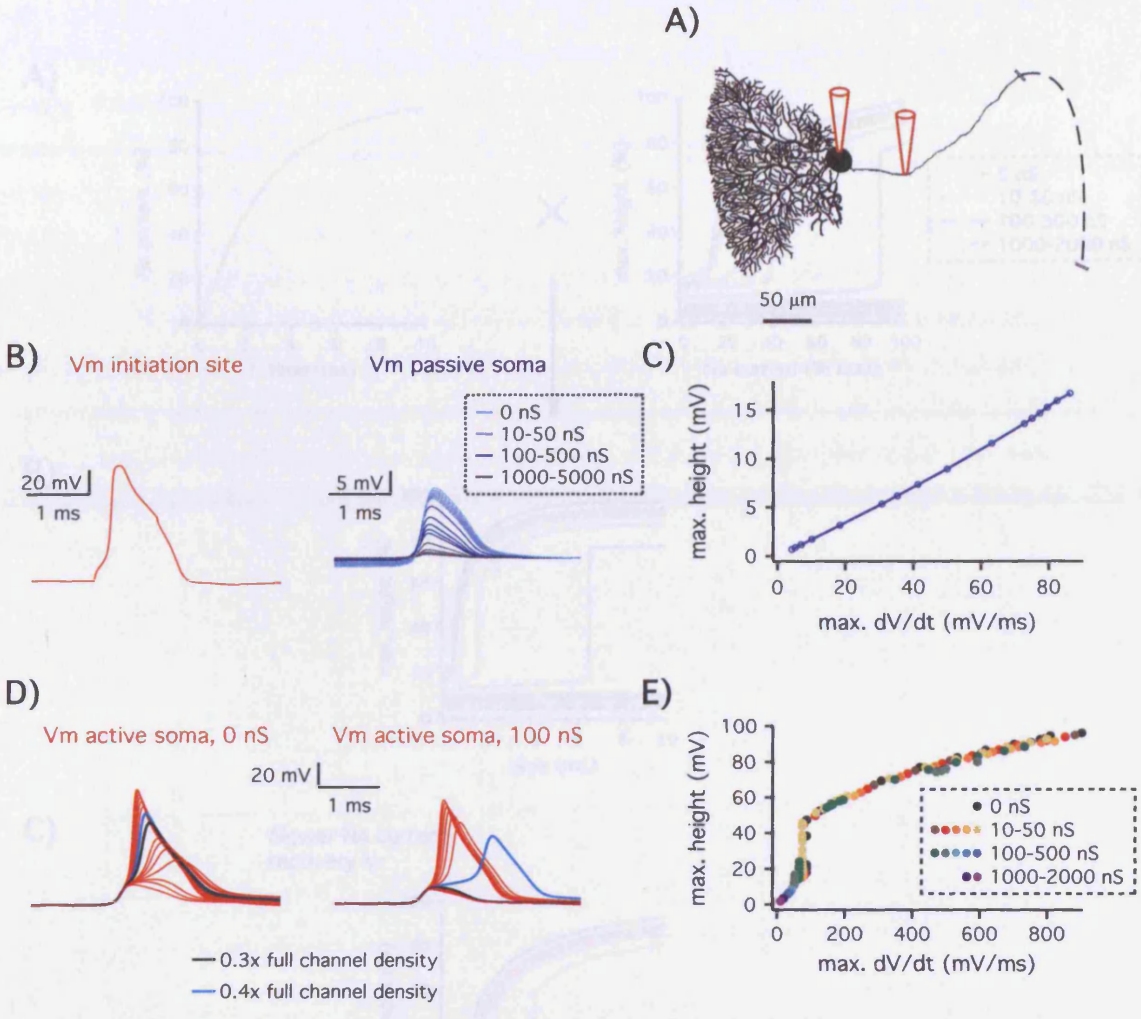

Figure 2.25: Height and maximum dV/dt of actively and passively propagated voltages in a model of the Purkinje cell.

A) Illustration of the P19 Purkinje cell morphology in which active and passive propagation of a spike initiated at the first node (right most electrode) was recorded at the soma (left most electrode). The model is adapted from Clark et al 2005; axonal collaterals were removed, dendritic Ih was omitted, preventing tonic spiking and current injection to the first node (0.2 nA for 1 ms) was used to evoke a spike. Tonic somatic conductance was varied from 0 - 2000 nS and somatic channel density was varied from 0 - 1 times full density.
B) Examples of the action potential initiated at the first node (left) and recorded at the passive soma under increasing amounts of tonic conductance (0 - 5000 nS).
C) Relationship measured at the soma between passively propagated spike height and maximum dV/dt.
D) Examples of the action potentials propagated to the soma as the soma is made increasingly active (0 - 1 x full channel density), in the background of either 0 nS (left) or 100 nS (right) of tonic conductance.
E) S-shaped relationship measured at the soma between actively passively propagated spike height and maximum dV/dt.

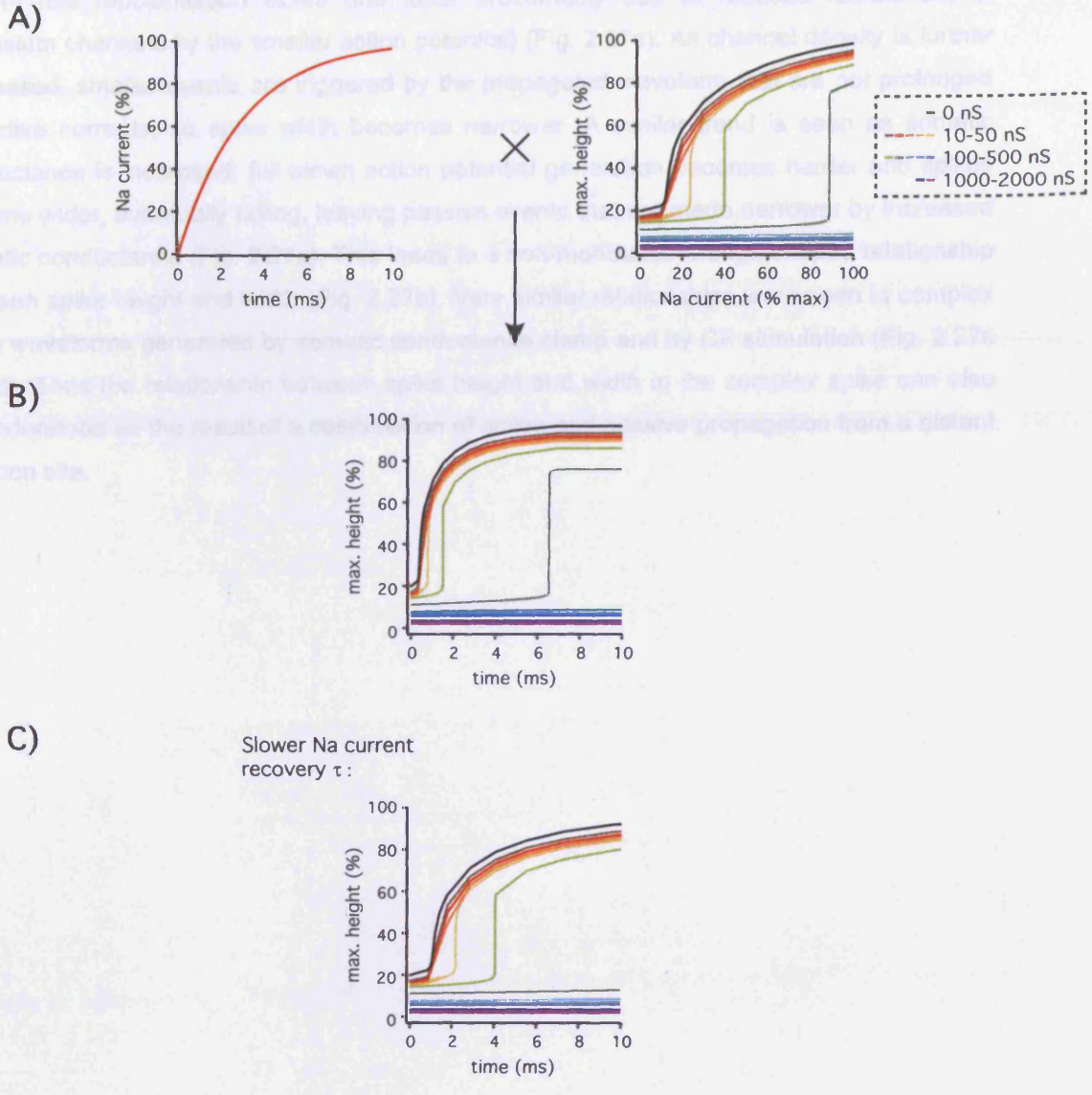

Figure 2.26: Distant spike initiation can explain height vs time relationship.

A) Illustration of the hypothetical exponential recovery of sodium channel availability with time since an inactivating pulse, and of the increase in action potential height with sodium channel availability in a multicompartment model of the Purkinje cell. Differing levels of tonic somatic conductances are shown, coloured as in the legend.
B) Composition of the functions shown in A, generating an s-shaped relationship between action potential height and time since an inactivating.
C) Slowing the time constant of the exponential recovery of sodium channel recovery does not affect the overall shape of the composition, but slows the recovery of action potential amplitude.

Spike width

This model can also help to explain trends in the width of spikelets in the complex spike. As somatic channel density is decreased, action potential amplitude initially increases, as the rate of rise repolarisation slows (the latter presumably due to reduced recruitment of potassium channels by the smaller action potential) (Fig. 2.27a). As channel density is further decreased, smaller events are triggered by the propagated waveform that are not prolonged by active currents, so spike width becomes narrower. A similar trend is seen as somatic conductance is increased; full blown action potential generation becomes harder and spikes become wider, eventually failing, leaving passive events that are made narrower by increased somatic conductance (Fig. 2.27a). This leads to a non-monotonic, wedge shaped relationship between spike height and width (Fig. 2.27b). Very similar relationships were seen in complex spike waveforms generated by somatic conductance clamp and by CF stimulation (Fig. 2.27c and d). Thus the relationship between spike height and width in the complex spike can also be understood as the result of a combination of active and passive propagation from a distant initiation site.

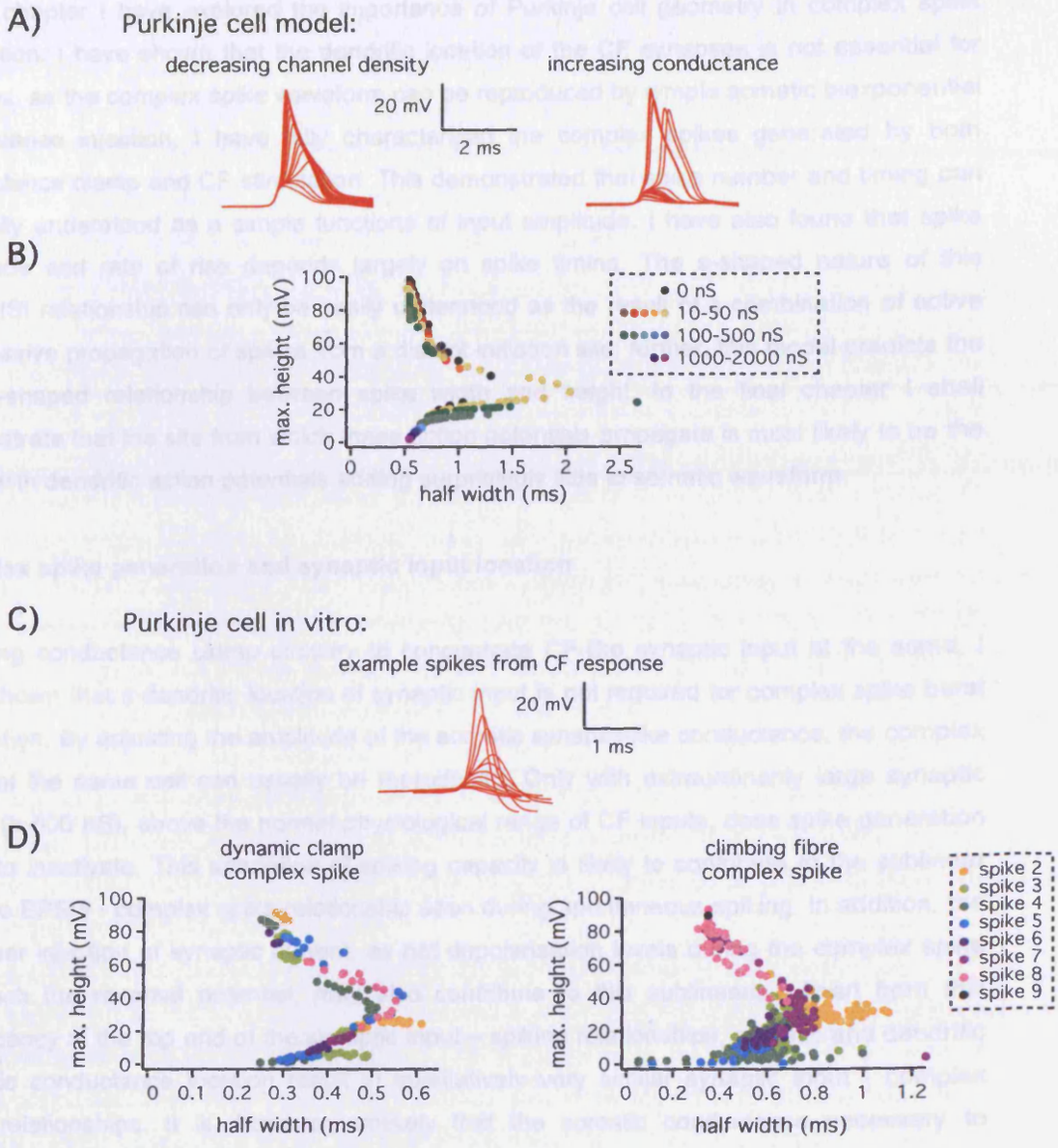

Figure 2.27: Width of actively and passively propagated voltages in a model of the Purkinje cell.

A) Illustration of the way in which propagated spike width is initially increased but then decreased again by decreasing the somatic active channel density (left, 1 - 0 x full density) or increasing the somatic passive conductance (right, 0 - 1000 nS). Purkinje cell model as in Fig 2.25A.
B) Relationship measured at the soma between spike height and spike width as the soma active channel density and passive conductance is varied.
C) Example of spikelets of increasing amplitude taken from the CF evoked complex spikes.
D) Example relationships between somatic spike height and width during complex spikes evoked by dynamic clamp (left) or CF stimulation (right, same cell as in C).

Chapter 2: Discussion

In this chapter I have explored the importance of Purkinje cell geometry in complex spike generation. I have shown that the dendritic location of the CF synapses is not essential for complex, as the complex spike waveform can be reproduced by simple somatic biexponential conductance injection. I have fully characterised the complex spikes generated by both conductance clamp and CF stimulation. This demonstrated that spike number and timing can be easily understood as a simple functions of input amplitude. I have also found that spike amplitude and rate of rise depends largely on spike timing. The s-shaped nature of this height-ISI relationship can only be easily understood as the result of a combination of active and passive propagation of spikes from a distant initiation site; further, this model predicts the wedge-shaped relationship between spike width and height. In the final chapter I shall demonstrate that the site from which these action potentials propagate is most likely to be the axon, with dendritic action potentials adding surprisingly little to somatic waveform.

Complex spike generation and synaptic input location

By using conductance clamp circuitry to concentrate CF-like synaptic input at the soma, I have shown that a dendritic location of synaptic input is not required for complex spike burst generation. By adjusting the amplitude of the somatic synaptic-like conductance, the complex spike of the same cell can usually be reproduced. Only with extraordinarily large synaptic inputs (≥ 500 nS), above the normal physiological range of CF inputs, does spike generation begin to inactivate. This saturation of spiking capacity is likely to contribute to the sublinear somatic EPSG - complex spike relationship seen during spontaneous spiking. In addition, the sublinear injection of synaptic current, as net depolarisation levels during the complex spike approach the reversal potential, may also contribute to this sublinearity. Apart from this discrepancy at the top end of the synaptic input – spiking relationships, somatic and dendritic synaptic conductance location result in qualitatively very similar synaptic input - complex spike relationships. It is, however, unlikely that the somatic conductance necessary to reproduce the complex spike of a particular Purkinje cell is identical to the actual conductance of the CF input. The EPSP caused by somatically concentrated synapses is predicted to be larger than that caused by distributed inputs of the same amplitude, which are attenuated by their propagation through the dendrites (Roth and Häusser, 2001, see also figure in the introduction to Chapter 2). In addition, although the shape of the synaptic input - complex spike relationships were similar for somatic and dendritic synapse locations, the transient conductance of the somatic EPSG may change the gain of the input-output relationship (Chance et al., 2002; Mitchell and Silver, 2003). In order to investigate this possibility, the input - output relationships for somatic current injection and conductance injection should be compared in the same cells, together with knowledge of the cell's input resistance. It is notable, however, that the average somatic conductance injection needed to reproduce the

complex spike was only slightly smaller than the (somatically measured) average conductance of CF input (170 ± 58 nS vs 265 ± 13 nS (as measured in Chapter 1); p = 0.12).

The robustness of the complex spike in the face of somatic conductance reflects a number of Purkinje cell specialisations. Firstly, the timecourse of the physiological CF EPSC does not seem to be strongly affected by its propagation to the soma (Wadiche and Jahr, 2001; timecourses assessed by voltage clamp and voltage jump protocols are similar). This may be due, in part, to its distributed nature, which readily charges the entire proximal dendritic tree, perhaps reducing current flow between dendritic branches; the proximal location of the synapses on the wide main branches of the dendrites may also make the effects of propagation through the dendrites small. The similarity of timecourses assessed by voltage clamp and voltage jump methods helps explain why somatic conductances with timecourses similar to that measured for the dendritic CF EPSG can mimic complex spikes. The rapid spiking of the soma also does not have a strong deleterious effect on somatic input, perhaps partly because the rapid spikes cause only a very brief drop in EPSC driving force, so allowing very similar bursts to be generated by somatic current or conductance injection (see fig 2.4 and McKay et al., 2005). The effect of spike shunting of the excitatory current reaching the soma is therefore also likely to be similar for both the directly somatically injected EPSC and that propagated in from the dendrite (Häusser et al., 2001). The shunt imposed by the somatic synaptic conductance itself appears to be easily accommodated by the Purkinje cell soma, and only inhibits firing at the upper end of the EPSG - complex spike relationship at the depolarised potentials of spontaneous spiking (see Fig. 2.6). This is due in part to the distant initiation site of complex spikelets (suggested in this chapter by modelling, and shown by the experiments in the next chapter and by Dr Beverley Clark (Davie et al., 2008) to be in the axon), which provides electrical isolation from the somatic shunt. Furthermore, the powerful and fast somatic voltage-gated Na^+ conductances in Purkinje cells (Raman and Bean, 1997, 1999), together with the K^+ conductances (Raman and Bean, 1999; Edgerton and Reinhart, 2003; Martina et al., 2003; McKay and Turner, 2004; Zagha et al., 2008), which balance large depolarising currents (Swensen and Bean, 2005; Zagha et al., 2008) and help maintain high-frequency firing, appear to predominate over the synaptic conductance during complex spike generation.

Variation in Purkinje cell intrinsic excitability

As somatic conductance clamp allows the synaptic input amplitude at a controlled location to be systematically manipulated, this method allowed the range of Purkinje cell somatic excitability to be measured independently of CF input. The 1.4 - 2.6 fold variability in the number of somatic spikes in the complex spike in response to a set conductance can help to account for the inter-cell complex spike variability that is not due EPSC size differences. As plasticity of intrinsic excitability has been found to be triggered by large excitatory inputs (both

in Purkinje cells (Cerminara and Rawson, 2004; McKay et al., 2007; Cerminara Rawson 2004, McKay Turner 2007) and other neurons (Desai et al., 1999; Zhang and Linden, 2003), it is likely that these two sources of variability of the complex spike might co-vary. This could have the result of making the response to a CF input of a certain size more similar across cells than might be expected given the population range of excitabilities. This can help explain why the CF input- complex spike relationship holds so well across cells while the parallel fibre- Purkinje cell spike relationships, and the slope of f-I curves differ between Purkinje cells (Llinas and Sugimori, 1980a; Walter and Khodakhah, 2006; Mittmann and Häusser, 2007).

Complex spike pattern and spikelet initiation site

The initiation of spikelets at site distant to the soma appears to play an important role in the complex spike pattern. Neither the s-shaped recovery of spike height with time, the similarly s-shaped relationship between spike height and maximum rate of rise, nor the wedge shaped relationship between spike height and width can be reproduced in a simple single compartment model with classic Hodgkin-Huxley channels, or with Khaliq et al.'s (2003) model of Purkinje somata channels. They can however be readily explained as the result of spike propagation and generation graded by the conductance and active channel availability in the soma. The inactivation of somatic channels in the period following a spikelet, together with the somatic or perisomatic synaptic and active interspike conductances (Raman and Bean, 1999; Swensen and Bean, 2003, 2005) can cause a spike propagated from a distant site to diminish in amplitude and rate of rise and increase in width (Hodgkin and Huxley, 1952b; Engel and Jonas, 2005; Scott et al., 2007). Failed spike propagation leaves its mark at the soma as an isolated 'prepotential' (Katz, 1950; Granit and Phillips, 1956; Coombs et al., 1957a, b; Fuortes et al., 1957; Spencer and Kandel, 1961; Dodge and Cooley, 1973; Stuart et al., 1997b) with only a single component to its voltage derivative. The amplitude, absolute maximum rate of rise and width of this prepotential can be decreased by increase conductance of the somatic recording site. This implies that the soma can follow a lower frequency of firing than the initiation site can generate, in a manner analogous to the failed propagation of some spikelets down the axon (Khaliq and Raman, 2005; Monsivais et al., 2005). There are several reasons why this should be so, some a direct consequence of initiation being favoured at a distant site. Firstly, the soma is a large, wide compartment, and propagation from a distant site (either the axon or the dendrites) will face a significant impedance mismatch, making active propagation liable to failure (Goldstein and Rall, 1974; Parnas and Segev, 1979; Segev and Schneidman, 1999). Secondly, the very specialisations that favour spike initiation (small, isolated, readily charged and discharged compartments, with higher densities of active channels, of specialised subtypes or negatively shifted voltage sensitivities) should also favour higher firing frequencies (Kuba et al., 2006).

Describing the complex spike waveform

The modelling that lead to the prediction that the complex spike pattern is the result of active events, variably propagated from a distant site, to some extent assumes that sodium channel recovery kinetics follow a simple exponential or multiexponential recovery time course that cannot alone account for the s-shaped recovery in spike height with interspike interval. Although there is good evidence that this is a reasonable approximation of Purkinje cell sodium channel behaviour, even considering the open blocked state thought to lead to the resurgent current (Raman and Bean, 1997; Kay et al., 1998; Raman and Bean, 2001; Fry, 2006), the availability of somatic and axon sodium channels throughout the complex spike is not known. One effect that remains to be explained is the slowing of spikelet height recovery with ISI throughout the complex spike; while the second spikelet of the CF evoked complex spike recovers to 50% amplitude by 1.6 ± 0.3 ms (during spontaneous spiking), the fourth spikelet, for example, only recovers by 2.2 ± 0.8 ms. While increased conductance of the soma due e.g. to voltage and/or calcium activated potassium channel activation may account for this slowing (see e.g. Fig. 2.26), another possibility is the progressive increased inactivation of sodium channels, perhaps through entry to a longer lived inactivation state, or the voltage dependence of Purkinje cell sodium channel recovery from inactivation (Colbert et al., 1997; Jung et al., 1997; Raman and Bean, 2001; Vilin and Ruben, 2001; Do and Bean, 2003; Baranauskas and Martina, 2006; Fry, 2006).

The total depolarisation envelope of the complex spike at the soma is the result of propagated action potentials being generated together with a baseline of depolarisation arising from the combination of synaptic current and interspike active channel current. The minimum reached between spikes depends exponentially on interspike interval, and this relationship decays more slowly and to more depolarised baseline levels with spikelet number. This again may be related to channel inactivation (both sodium, potassium and others); somatic conductance clamp allows us to see that for the same amount of external conductance injection at the time of the trough, the depolarisation caused is greater, indicating a greater total somatic resistance. However, we have no definitive measurement of membrane resistance or channel behaviour during the complex spike and currently no models, even those incorporating the best available Purkinje cell channel behaviour data (Khaliq et al., 2003; Clark et al., 2005; De Schutter and Bower, 1994a, c) satisfactorily reproduce the complex spike. Improved models of ionic current during spiking behaviour (generated by e.g. the dynamic IV method of Badel et al., 2008), which should also incorporate a distant site of spike initiation during the complex spike, are required.

My recordings and descriptions of complex spikes evoked by both CF and somatic conductance clamp now allow the pattern of spiking within a cell to be predicted. Given the amplitude of the synaptic input, the number and timing of spikelets in the complex spike can

be predicted. As there is some variability across cells and height depends steeply on inter-spikelet interval, the height of the spikelets within the complex spike can then be predicted once their actual timing is confirmed.

Voltage dependence of the complex spike waveform

These descriptions and predictions apply mostly to the complex spike recorded at rest (no external current injection, allowing spontaneous simple spike firing). However, it has previously been observed that the number of spikes in the complex spike is increased, and that their amplitude is decreased, at depolarised membrane potentials or during fasted simple spike firing periods (Martinez et al., 1971; Gilbert and Thach, 1977; Llinas and Sugimori, 1980a; Chan et al., 1989; Hounsgaard and Midtgaard, 1989; Servais et al., 2004; Khaliq and Raman, 2005; Monsivais et al., 2005). I have described and quantified these effects over a continuous voltage range. The balance between channel activation and inactivation is again likely to underlie these relationships. As the cell is depolarised from hyperpolarised potentials, increase in the number of sodium (and calcium) channels activated by the CF is likely to be responsible for the monotonic increase in the number of spikes in the complex spike seen between -80 mV and -50 mV baseline Vm (Hodgkin and Huxley, 1952b, a, d; Raman and Bean, 1997, 1999; Khaliq et al., 2003; Fry, 2006). Above this point, spiking inactivation, which tends to silence tonic spiking in the cell and lead to the generation of Na^{+}- Ca^{2+} bursts (Llinas and Sugimori, 1980b, a; Hounsgaard and Midtgaard, 1988; McKay and Turner, 2005), causes a decrease in the number of spikelets recorded. Inactivation of both sodium and potassium channels might contribute to this inability to maintain rapid burst firing (Hodgkin and Huxley, 1952c, b; Wang et al., 1991; Raman and Bean, 1997, 2001; Sacco and Tempia, 2002; Martina et al., 2003; Fry, 2006; Sacco et al., 2006). The pattern of spikelet time and height dependence on baseline Vm is not constant across cells, perhaps because it relies on the balance of many different ion channel types in multiple locations, the expression of which may differ somewhat across cells (Goldman et al., 2000; Achard and De Schutter, 2006; Taylor et al., 2006). Often, however, the height of spikelets decreases with depolarisation in a sigmoidal manner, potentially reflecting the progressive inactivation of the somatic sodium channels, and so the decline of the somatic active spike until only the passively propagated 'prepotential' remains (as in e.g. Hodgkin and Huxley, 1952b; Engel and Jonas, 2005; Rancz et al., 2007).

Purkinje cell specialisations

It is clear that the specialisations that cause Purkinje cells to fire bursts in response to their powerful distributed CF input, and MNTB neurons, clasped round their somata by giant calyceal synapses, to fire only single spikes, go far beyond the geometry of their inputs. While the widespread synaptic input to the Purkinje cell seems specialised to produce a global

depolarisation of the Purkinje cell's excitable dendrites, the experiments in this chapter show that this is not the critical element required to support burst generation. A more likely candidate for differentiating between precise single spike firing and reproducible burst firing is the combination of EPSC time course with the complement of ion channels expressed in the cell. EPSCs from the calyx of Held are of extremely rapid time course ($\tau_{decay} \approx 1$ ms), helping to ensure a single precisely timed action potential is generated (Borst et al., 1995; Trussell, 1999; Brenowitz and Trussell, 2001), while CF EPSCs in Purkinje cells are relatively long lasting (Barbour et al., 1994). In addition, the low resting input resistance of MNTB neurons, together with rapidly activating delayed rectifier conductances, ensure a rapid EPSP, and rapid spike repolarisation (reviewed in Trussell, 1999). The strong K_v1 delayed rectifier potassium channel expression also acts to ensure a single, precisely timed action potential is generated in MNTB neurons (Brew and Forsythe, 1995; Dodson et al., 2002; Brew et al., 2003; Gittelman and Tempel, 2006), while high voltage activated K_v3 channels allow repeated single action potential generation to rapidly repeated EPSC input (Wang et al., 1998; Song et al., 2005). In Purkinje cells, K_v1 conductances are not sufficient to prevent multiple spike generation in response to CF input, but curtail the burst, while strong Kv3 expression is required to sustain high frequency bursting in Purkinje cells (Hurlock et al., 2008; Zagha et al., 2008). In addition, the benefits of a distant site of spike initiation in supporting high frequency firing (Kuba et al., 2006; Scott et al., 2007) are likely to be of benefit to both cell types. A direct exploration of relative importance of these variables, through e.g. systematic variation (using modelling and/ or conductance clamp) of synaptic time course and of the different conductances expressed in the two cell types, would further illuminate this conundrum.

Although the role of the dendritic distribution of inputs does not appear to be in burst generation, there may be other reasons for this location. One strong candidate is its potential role in generating dendritic calcium spikes, which, among other roles, are required for associative plasticity in the Purkinje cells, which lack the backpropagating action potentials and NMDA receptors that often subserve this role in other neurons (reviewed in Sjostrom and Nelson, 2002). This, together with the role of dendritic calcium spikes in CF electrical signalling, will be examined in the next chapter.

Chapter 3:

The relationship between CF triggered dendritic calcium spikes and the complex spike.

Introduction

In the previous chapters, I have shown that the complex spike pattern is a linear reflection of input size that does not depend upon the dendritic location of CF synapses for its generation. However, I have also demonstrated that the complex spike waveform can be best understood as the result of spike propagation from a distant initiation site, and Purkinje cells are well known for their conspicuously active dendrites, especially during complex spike generation (Llinas and Nicholson, 1971; Nicholson and Llinas, 1971; Llinas and Sugimori, 1980b; Crepel et al., 1981; Ross and Werman, 1987; Hounsgaard and Midtgaard, 1988; Chan et al., 1989; Miyakawa et al., 1992). Further, in many other neuronal types, dendritic spikes have a strong, amplifying influence on synaptic integration, and can trigger one or even a burst of axo-somatic action potentials (see the main Introduction and Chen et al., 1997; Golding and Spruston, 1998; Larkum et al., 1999, 2001; Williams and Stuart, 2002; Gasparini et al., 2004). Although Purkinje cells were the first neurons in which such dendritic excitability was directly demonstrated (Llinas and Nicholson, 1971), the role of Purkinje cell dendritic spikes in the generation of the somatic burst of action potentials is not yet clear.

In their seminal papers of 1964 and 1966, Eccles, Llinas & Sasaki showed that the complex spike burst could be generated in response to a single CF EPSP (Eccles et al., 1964; Eccles et al., 1966a). This pioneering investigation (Eccles et al., 1966a) also provided evidence, from field electrode recordings at the depth of the dendrites, that the dendrites generate active responses during CF input. Further work proved that Purkinje cell dendrites are capable of generating and actively forward-propagating action potentials in response to parallel fibre stimulation (Llinas et al., 1968; Llinas and Nicholson, 1971; Nicholson and Llinas, 1971), that the electroresponsiveness of the dendrites is mediated by calcium channels (Llinas and Sugimori, 1980b) and that CF stimulation leads to active responses in the dendrites (Fujita, 1968; Llinas and Sugimori, 1980b; Crepel et al., 1981; Chan et al., 1989).

These demonstrations of active dendrites added complexity to the initial suggestions (Granit and Phillips, 1956; Eccles et al., 1966a) that spikelets represented action potentials generated in the axon (while the soma and dendrites were inhibited by excessive depolaristion) which backpropaged into the soma, in a similar manner to simple spike axo-somatic propagation (Granit and Phillips, 1956; Eccles et al., 1966b). Indeed, the similarity between the multiple regenerative potentials seen in the dendrites and the soma following CF stimulation lead Fujita to suggest that each spike in the somatic response might reflect an action potential generated in a separate dendritic subcompartment. Martinez, Crill &

Nicholson (1971) noted that antidromic spikes generated by axonal stimulation appeared not to collide with complex spike spikelets, so suggested that spikelets were not generated in the axon, but in the dendrites (although closer examination of the data presented (Martinez et al. Fig. 8) shows that simulation either failed to produce an antidromic spike, perhaps reflecting axonal collision, or disrupted, rather than just adding to the following complex spike pattern). Campbell and Hesslow (1986b) also examined the secondary spikelets of the complex spike and concluded they were dendritic. They observed (in extracellular recordings) that, during paired pulse stimulation, the secondary spikelets of the complex spike could be manipulated separately from the first, presumably axonal spike. Following the second of two CF stimulations separated by 10 – 150 ms, the amplitudes of the secondary spikelets were increased while the amplitude of the first spike was decreased. They hypothesised that a separate dendritic origin of the later spikelets would allow them to be boosted by dendritic active conductances remaining on following the first CF stimulation. However, as I have shown in Chapters 1 and 2, this effect is readily explained by the paired pulse depression of the second CF response (Eccles et al., 1966d; Latham and Paul, 1971; Dittman and Regehr, 1998; Hashimoto and Kano, 1998; Silver et al., 1998) reducing the frequency of spikelet generation, thus reducing inactivation of the fast spiking mechanism and increasing the amplitude of the later spikelets.

These proposals for dendritic generation of complex spike spikelets have been opposed by more recent manipulations of dendritic spikes (Callaway et al., 1995; Callaway and Ross, 1997). These studies found that inhibition of dendritic spikes appears to have only a weak effect on the somatic complex spike waveform and that somatic bursts of spikes can be triggered without significant dendritic calcium entry. Nevertheless, the contribution of dendritic spikes to the complex spike remains unresolved (Schmolesky et al., 2002).

I have addressed this question through direct recording from the dendrites during complex spike generation. I have shown that dendritic spikes are not necessary for complex spike generation, and that their presence following CF stimulation adds little to the complex spike. I have demonstrated that the depolarisation propagated to the soma is small and often within the axo-somatic refractory period of previous spikelets of the complex spike. I have found that the net effect of calcium conductances during the somatic burst is to reduce excitability, and that the calcium spikes following CF stimulation have a far greater role in prolonging the post-complex spike pause in simple spike firing than in generating the complex spike burst.

Chapter 3: Results

Dendritic calcium spikes are not necessary for complex spike generation

In some cell types, bursts of spikes at the soma are triggered by activation of dendritic calcium spikes (Williams and Stuart, 1999; Larkum et al., 1999; Magee, 1999; Larkum et al., 2001). Physiological CF input typically triggers 1-3 dendritic calcium spikes (Fujita, 1968; Llinas and Sugimori, 1980b; Crepel et al., 1981; Chan et al., 1989; Rancz and Häusser, 2006). It is not clear if these dendritic spikes are necessary to generate the complex spikes. To address this question I made simultaneous dendritic recordings (104 ± 6 µm from the soma) during the 'optimal' somatic EPSG for mimicking the physiological complex spike (Fig. 3.1a). Activation of the CF produced rapidly rising, large amplitude dendritic calcium spikes in addition to the somatic complex spike (Fig. 3.1b; Llinas and Sugimori, 1980b; Crepel et al., 1981; Chan et al., 1989; Rancz and Häusser, 2006). However, the somatic EPSG which mimicked the complex spike in the same cell was not associated with generation of a dendritic calcium spikes (Fig. 3.1c; 13 out of 13 cells): only a small, slow dendritic depolarisation was observed (Fig. 3.1d; peak amplitude 4.6 ± 0.5 mV vs 40.2 mV ± 1.2 mV for the physiological CF input; $p < 10^{-12}$, peak dV/dt 6.3 ± 0.4 mV/ms vs 60.2 mV ± 4.4 mV/ms for the physiological CF input; $p < 10^{-7}$), reflecting in part the passive backpropagation of the somatic spikes (see Fig. 3.1c inset).

A similar result could be seen in all dendritic recordings made during somatic EPSG injection (n = 53, recorded at 110 ± 24 µm). However, on occasion (in 15/53 cells), strong EPSG injection to the soma could eventually trigger dendritic spikes in the dendrites (Fig. 3.2a). These dendritic spikes, nevertheless, always occurred at some considerable delay after the end of somatic burst generation, indicating that they could not be responsible for burst generation (Fig. 3.2b). Their timing was also later than the end of conductance clamp generated bursts in which no dendritic spike was seen at the recorded dendritic location (Fig. 3.2b). This makes it unlikely that dendritic spikes were indeed present (and responsible for somatic burst generation) at some unrecorded dendritic location during successful conductance clamp mimic of the complex spike.

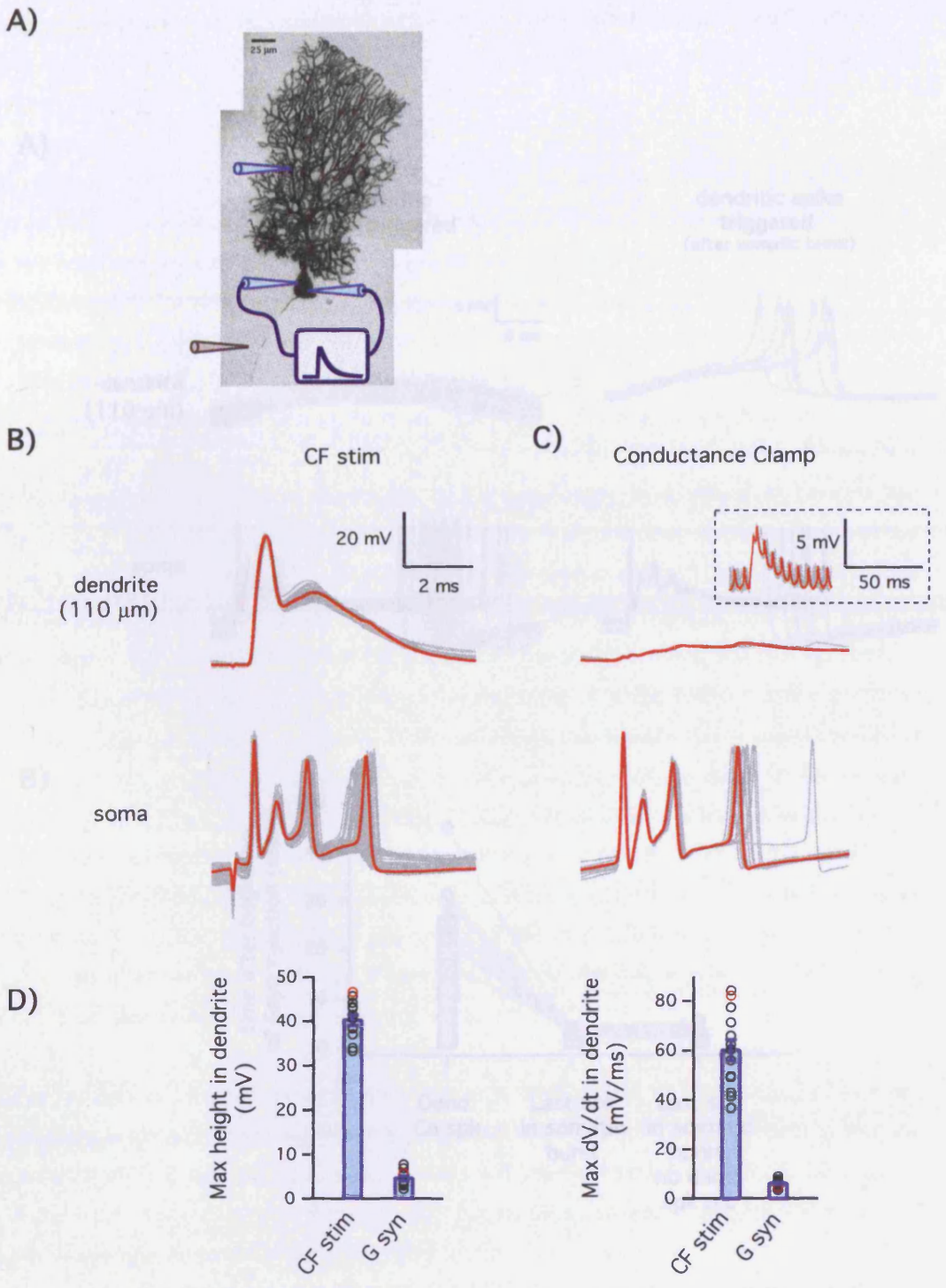

Figure 3.1: Dendritic spikes are not necessary for the generation of the CS

A) The electrode configuration during paired dendritic and somatic patch clamp recording during both climbing fibre stimulation (via the grey electrode) and two electrode synaptic-like conductance injection. Illustrated on an image of the biocytin filled Purkinje cell recorded from in B and C.
B) CF response recorded simultaneously at the soma (lower traces) and 110 µm away in the dendrites (upper traces). CF stimulations evoked CSs in the soma together with characteristic dendritic calcium spikes.
C) Response to 150 nS somatic dynamic clamp in the same cell as shown in A, recorded simultaneously in the soma and dendrites. At the soma, CSs are generated that are well matched to those evoked by CF stimulation (spike times differed by < 18 %, heights by <10 %), but no spikes are recorded in the dendrites.
D) Average height and dV/dt of events recorded in the dendrites in response to CF stimulation or somatic dynamic clamp of an amplitude that matched the CS at the soma (n = 13 cells, significant difference by both measures, $p < 10^{-7}$). Circles show the within-cell averages (averages of the data shown in B and C highlighted in red); bars show the average ± SEM of the total data.

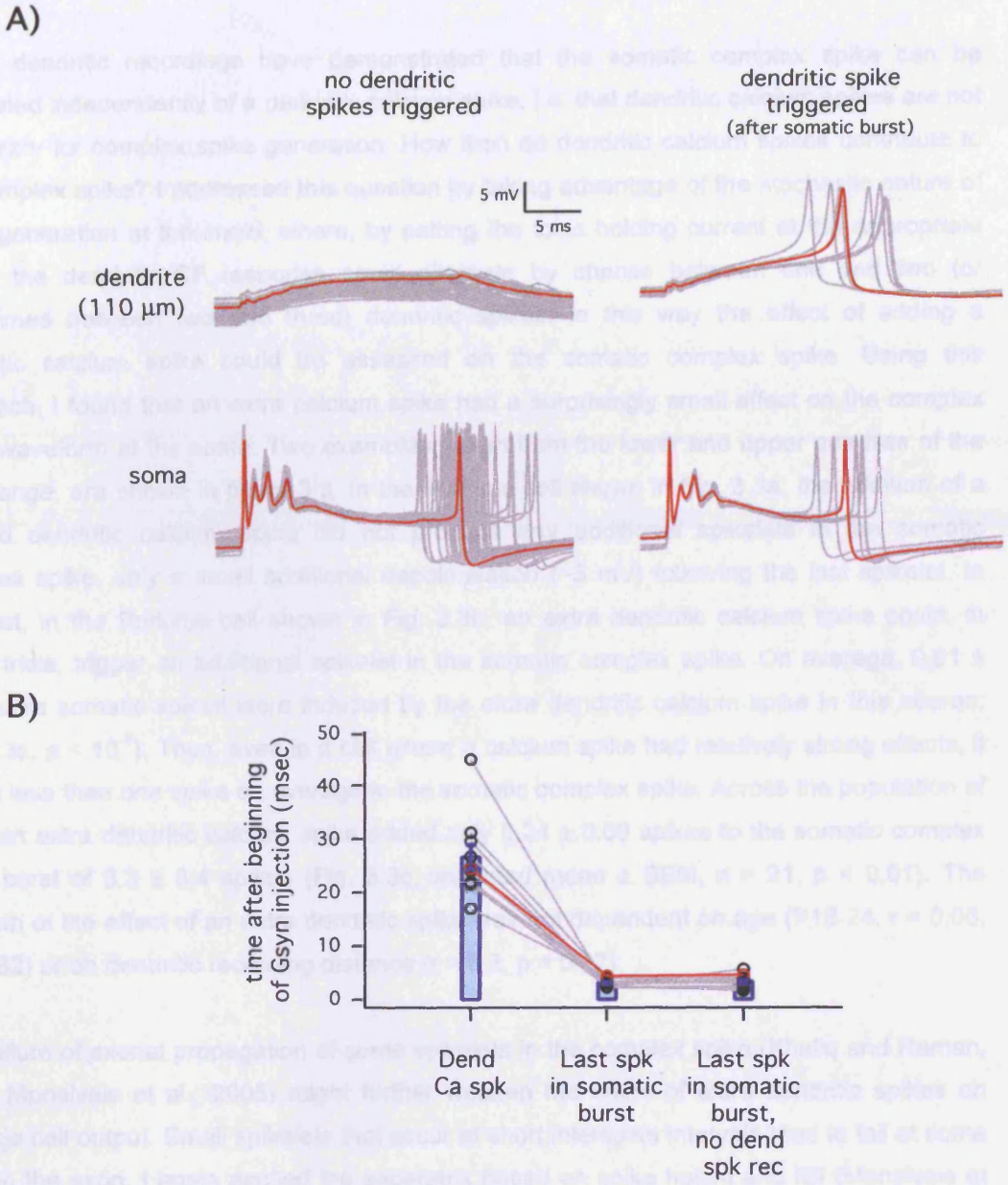

Figure 3.2: Somatic Gsyn occasionally triggers late dendritic spikes, but these are not responsible for somatic CS-like bursts.

A) Example of 300 nS somatic Gsyn which occasion triggered dendritic spikes, simultaneously recorded at the soma (bottom) and 110 µm away in the dendrites (top). Trials where no dendritic spikes were recorded (left) separated from those displaying a dendritic spike (right).
Note that when dendritic spikes were recorded they occurred well after the end of the CS-like bursts (their peak time was later than the end of bursts both in the examples displaying dendritic spikes and those that had no evidence of spikes in the dendritic recordings).
B) Timing of dendritic spikes and the final spikes of somatic bursts (both when dendritic spikes were simultaneously recorded and when they were not) relative to the beginning of somatic Gsyn injection. Black circles and lines; averages from individual data sets (n = 10) (red highlights data from example shown in A), blue bars; population mean ± SEM.

Contribution of dendritic calcium spikes to somatic output during CF triggered complex spikes

These dendritic recordings have demonstrated that the somatic complex spike can be generated independently of a dendritic calcium spike, i.e. that dendritic calcium spikes are not necessary for complex spike generation. How then do dendritic calcium spikes contribute to the complex spike? I addressed this question by taking advantage of the stochastic nature of spike generation at threshold, where, by setting the tonic holding current at the appropriate value, the dendritic CF response could alternate by chance between one and two (or sometimes between two and three) dendritic spikes. In this way the effect of adding a dendritic calcium spike could be assessed on the somatic complex spike. Using this approach, I found that an extra calcium spike had a surprisingly small effect on the complex spike waveform at the soma. Two examples, taken from the lower and upper quartiles of the data range, are shown in figure 3.3. In the Purkinje cell shown in Fig. 3.3a, the addition of a second dendritic calcium spike did not produce any additional spikelets in the somatic complex spike, only a small additional depolarisation (~5 mV) following the last spikelet. In contrast, in the Purkinje cell shown in Fig. 3.3b, an extra dendritic calcium spike could, in some trials, trigger an additional spikelet in the somatic complex spike. On average, 0.81 ± 0.10 extra somatic spikes were induced by the extra dendritic calcium spike in this neuron; Fig. 3.3c, $p < 10^{-6}$). Thus, even in a cell where a calcium spike had relatively strong effects, it added less than one spike on average to the somatic complex spike. Across the population of cells, an extra dendritic calcium spike added only 0.24 ± 0.09 spikes to the somatic complex spike burst of 3.3 ± 0.4 spikes (Fig. 3.3c, weighted mean ± SEM, $n = 21$, $p < 0.01$). The strength of the effect of an extra dendritic spike was not dependent on age (P18-24, $r = 0.05$, $p = 0.82$) or on dendritic recording distance ($r = 0.2$, $p = 0.37$).

The failure of axonal propagation of some spikelets in the complex spike (Khaliq and Raman, 2005; Monsivais et al., 2005) might further weaken the effect of extra dendritic spikes on Purkinje cell output. Small spikelets that occur at short interspike intervals tend to fail at some point in the axon. I again applied the separatrix based on spike height and ISI (Monsivais et al., 2005, see Fig. 1.8) to the events triggered by dendritic spikes (Fig. 3.4a,b). This predicts that only ~25 % of the extra somatic spikelets are tall enough and at a sufficiently long interval after the preceding spike to successfully propagate down the axon.

These experiments demonstrate that, in contrast to the strong influence of the size of the massive CF input (see Chap 1), dendritic spikes have only a weak effect on the somatic complex spike, and an even weaker influence on the axonal burst output.

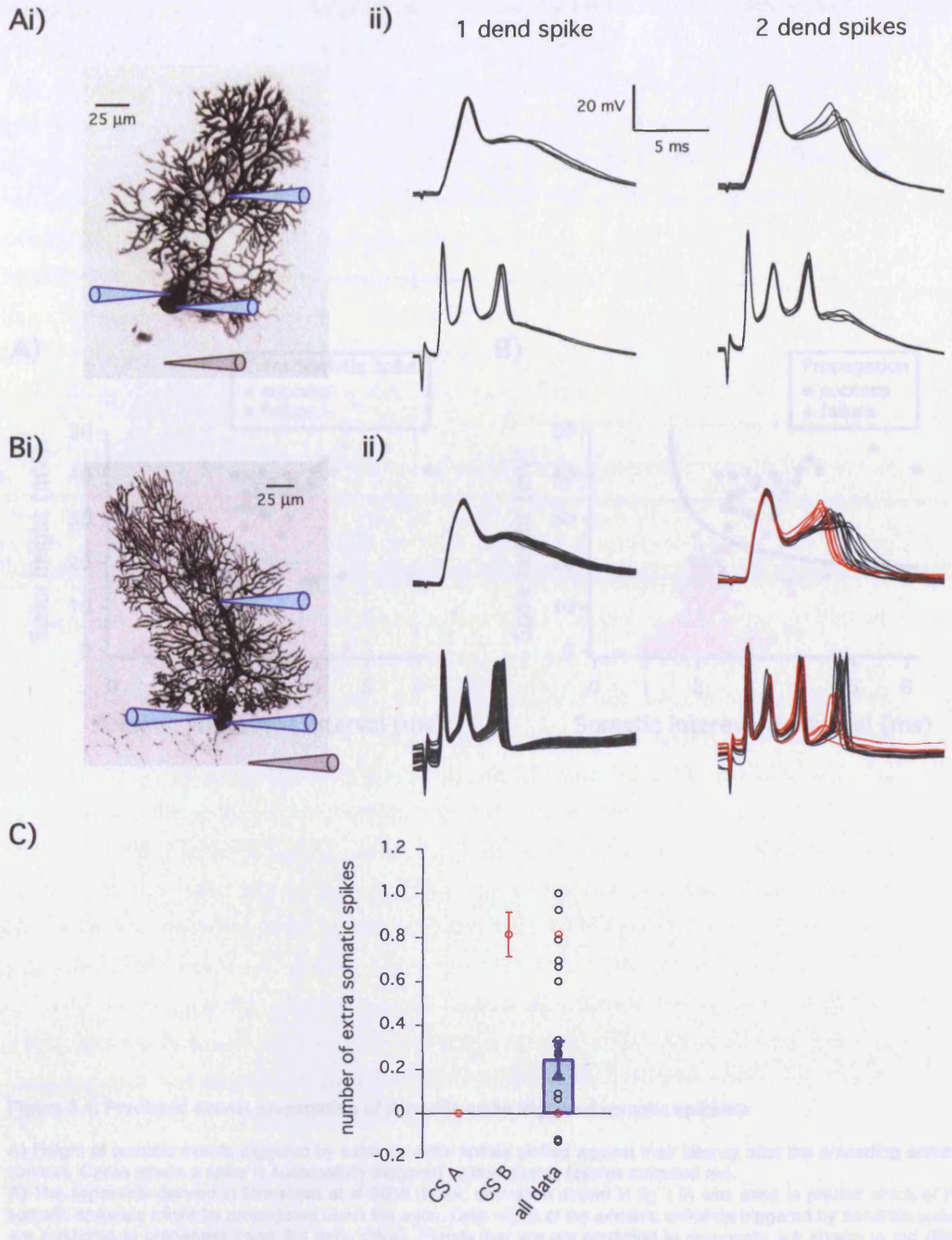

Figure 3.3: Dendritic spikes have only a very weak influence on the somatic CS triggered by CF stimulation

Ai) Recording configuration of experiment. The dendritic recording electrode was 80 µm from the soma. **(ii)** Multiple superimposed CF responses recorded at the soma (bottom) and dendrite (top) of cell in A. Left, responses with one dendritic spike (4 sweeps); right, responses with two dendritic spikes (5 sweeps). Note that in this example, somatic spiking is the same regardless of the number of dendritic spikes, and that the second dendritic spike only produces a small response at the soma.

Bi) A second example where dendritic spikes have a stronger effect on the soma. The dendritic recording electrode was 125 µm from the soma. **(ii)** Threshold for a second dendritic spike occurred when a somatic holding current of -160 pA was applied (left, 1 spike, 29 sweeps; right, 2 spikes, 32 sweeps). In some CF responses, a second dendritic spike triggered an additional somatic spike (0.81 ± 0.10 spikes added). Responses in which the second dendritic spike occurred <2 ms after a somatic spike are shown in red; in these cases, either no further somatic spike, or only a small somatic spikelet occurred. Scale bar in A also applies to B.

C) Average number of somatic spikelets triggered by an extra dendritic spike. "A", "B", mean ± SD of the data shown in A and B; "all data", averages from individual datasets (circles) and weighted mean ± SEM of all datasets (n = 21; bar). On average, 0.24 ± 0.09 additional somatic spikes (significantly different from 0, $p<0.01$) were triggered by an extra dendritic spike.

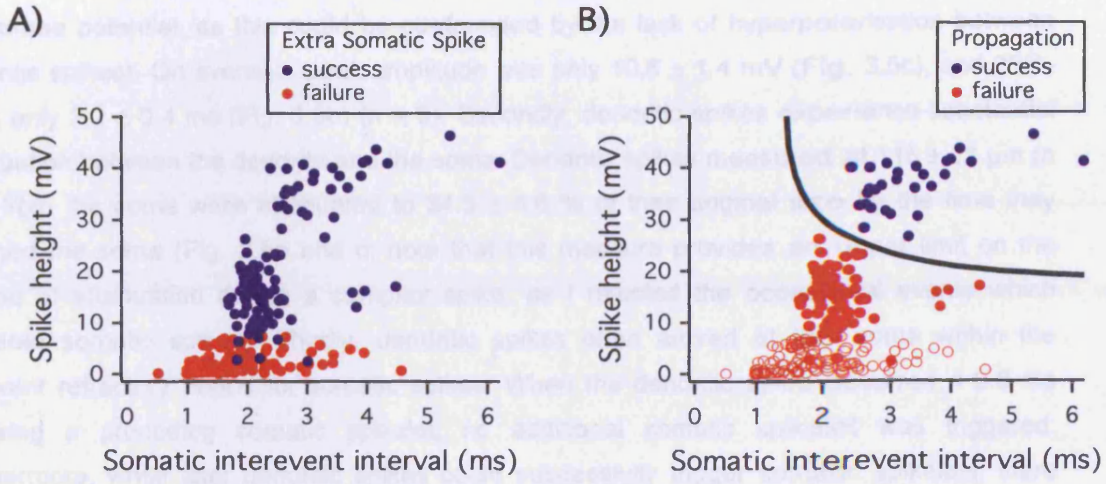

Figure 3.4: Predicted axonal propagation of dendritic spike triggered somatic spikelets

A) Height of somatic events triggered by extra dendritic spikes plotted against their latency after the preceding somatic spikelet. Cases where a spike is successfully triggered coloured blue; failures coloured red.
B) The separatrix derived in Monsivias et al 2005 (black, derivation shown in fig 1.9) was used to predict which of the somatic spikelets might be propagated down the axon. Only ~25% of the somatic spikelets triggered by dendritic spikes are predicted to propagate down the axon (blue). Events that are not predicted to propagate are shown in red (filled circles; somatic spikelets, open circles: somatic subthreshold depolarisations).

Determinants of dendritic spike influence on somatic spiking

Why are dendritic calcium spikes so ineffective at triggering somatic spikelets, given the relatively short distance to the soma and the strong influence of synaptic input size on somatic spiking? There are several reasons for this. Firstly, dendritic spikes in Purkinje cells are relatively small and brief to begin with. I estimated the amplitude of dendritic spikes triggered by CF input relative to just-subthreshold events on alternating trials (Fig. 3.5ai and ii) and measured their width at 20% of their height above the preceding trough (Fig. 3.5ai; this measure was made as an alternative to measuring width at half their height above baseline membrane potential, as this could be confounded by the lack of hyperpolarisation between dendritic spikes). On average, peak amplitude was only 10.6 ± 1.4 mV (Fig. 3.5c), and 20%-width only 3.2 ± 0.4 ms (Fig. 3.5b) (n = 9). Secondly, dendritic spikes experience substantial attenuation between the dendrite and the soma. Dendritic spikes measured at 115 ± 11 µm (n = 9) from the soma were attenuated to 34.5 ± 4.6 % of their original size by the time they reached the soma (Fig. 3.5a and c; note that this measure provides an upper limit on the degree of attenuation during a complex spike, as I rejected the occasional events which triggered somatic spikes). Thirdly, dendritic spikes often arrived at the soma within the apparent refractory period for somatic spikes. When the dendritic spike occurred < 0.8 ms following a preceding somatic spikelet, no additional somatic spikelet was triggered. Furthermore, while later dendritic spikes could successfully trigger somatic spikelets, there was a sigmoidal relationship between the amplitude of these somatic spikelets and the latency of the dendritic spike (as measured in Fig. 3.6a). An example of this is shown in Fig. 3.6b (which corresponds to the data shown in Fig. 3.3b); early dendritic spikes fail to generate any active somatic events, slightly later dendritic spikes trigger small, slowly rising somatic spikelets while the latest dendritic events trigger full-blown spikes at the soma. A similar sigmoidal relationship was seen across all data sets (Fig. 3.6c), with the half-maximum of 1.4 ms. However, even when the dendritic spike occurred well outside the apparent refractory period for a somatic spikelet, it was still often unable to trigger an additional somatic spikelet. This was because the somatic depolarisation caused by the dendritic spike was below threshold for generating a somatic spikelet (Fig. 3.6e, $p < 0.03$, paired t-test).

Together, these characteristics explain why dendritic spikes have a relatively weak influence on somatic spikelet generation. As a consequence, there was not a consistent temporal relationship between a dendritic spike and the somatic spikelets within the complex spike. Specifically, the peaks of individual dendritic spikes could either occur both before or after a the somatic complex spikelet that they triggered (Fig. 3.7a). This indicates that somatic spikelets are not simply reflections of forward propagated dendritic spikes. In fact, the timing of the extra somatic spike appears to be strongly influenced by intrinsic axosomatic properties. The later a dendritic spike occurs after the penultimate somatic spike, the earlier the extra spike occurs relative to the dendritic spike (Fig. 3.7b). If the somatic ISI was independent of the dendritic Ca^{2+} spike time, the slope of this relationship would be -1 (conversely, if it was entirely dependent on the Ca^{2+} spike time, the slope would be 0):

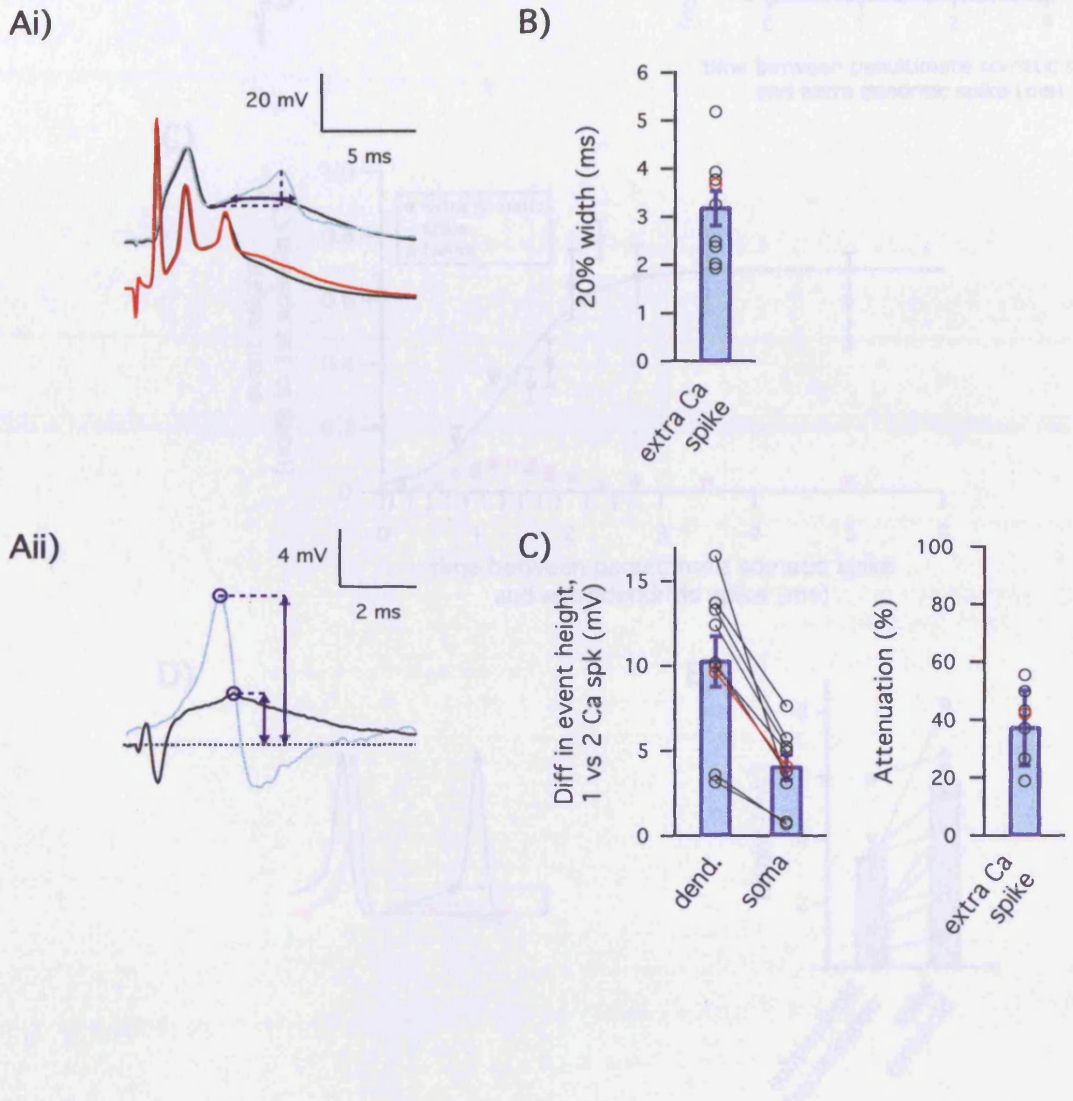

Figure 3.5: Dendritic spikes during the CS are small, brief and highly attenuated.

A) Illustration of the method used to measure the duration, amplitude and attenuation of dendritic spikes during the complex spike.
i) Example of an event with an extra dendritic spike recorded simultaneously in the dendrite (light blue) and soma (red), together with the dendritic and somatic averages of events that lacked extra dendritic spikes but had a similar somatic firing pattern (black). Spike width was measured at 20% of the height of the dendritic spike above the preceding trough (blue arrow). To measure the amplitude of individual extra dendritic spikes and the somatic depolarisations they cause, the 'no extra spike' dendritic and somatic averages, respectively, were subtracted. The peak differences in depolarisation (blue circles) were measured (blue arrows). The somatic height as a percentage of dendritic height yielded attenuation.
B) Average extra spike width at 20% height. Individual data set averages; black circles (red circle highlights data set shown in A, population average ± SEM (n=9).
C) Average extra dendritic spike and somatic depolarisation height above 'no extra spike' events (left) and extra dendritic spike attenuation (right).

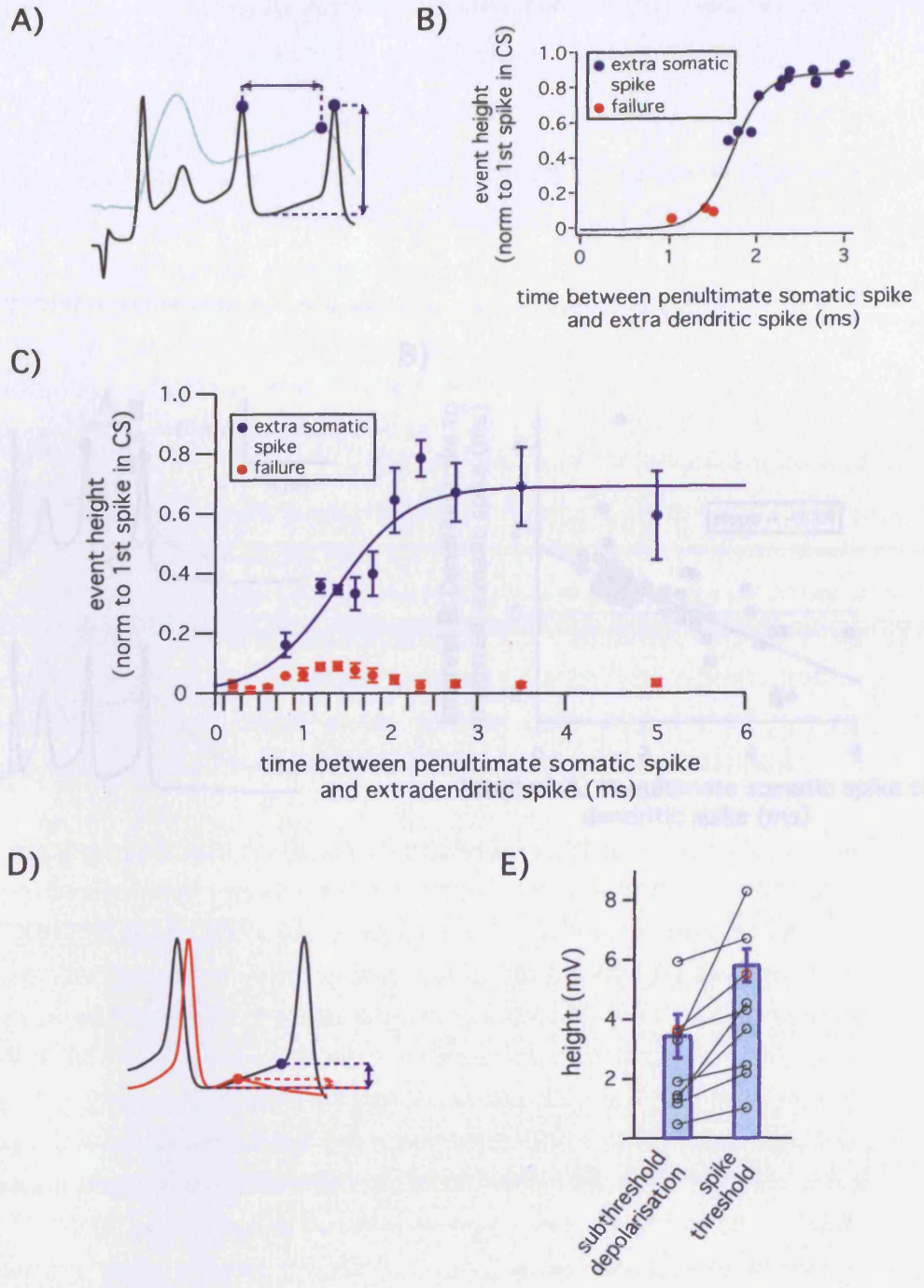

Figure 3.6 Dendritic spikes are often within a refractory period or below threshold for triggering a somatic spike in the CS.

A) Illustration of the measurements made of dendritic spike time and resulting somatic event height. Horizontal arrow: time between the extra dendritic spike and the spike preceding the somatic event. Vertical arrow: somatic event height, measured as difference between preceding trough minimum and event maximum; this height is normalised by the height (above average baseline Vm) of the first spike of the CS.

B) Dependence of somatic event height on dendritic spike time, measured as shown in A, for the data shown in (fig 3.3 Bii). Red points: cases where an extra dendritic spike failed to trigger a spike, generating only a subthreshold depolarisation; blue points: cases where an extra spike triggered a somatic spike. Refractory trend highlighted by sigmoidal fit (black); half maximum was at 1.7 ms.

C) Dependence of somatic event height on dendritic spike time, total data from 19 data sets plotted together, binned according to the time intervals marked by the x axis ticks. Red and blue points as in C. Refractory trend highlighted by sigmoidal fit to blue points, constrained to a baseline height of 0; half maximum was at 1.4 ms.

D) Illustration of the measurements made in order to compare the amplitude of events where no somatic spikes were triggered (red) to the threshold for generating somatic spikes in the same cell (blue). See methods for details of threshold location. Amplitude was calculated by subtracting the preceding trough's minimum from the peak of spike failure 'bumps' or from the voltage at threshold.

E) Height of spike failures compared to spike threshold in the same cell. Red circles highlight averages from the data-set illustrated in (fig 3.3 Bii). Bars show total data average ± SEM (n = 7, sig. diff $p < 0.03$, paired t-test).

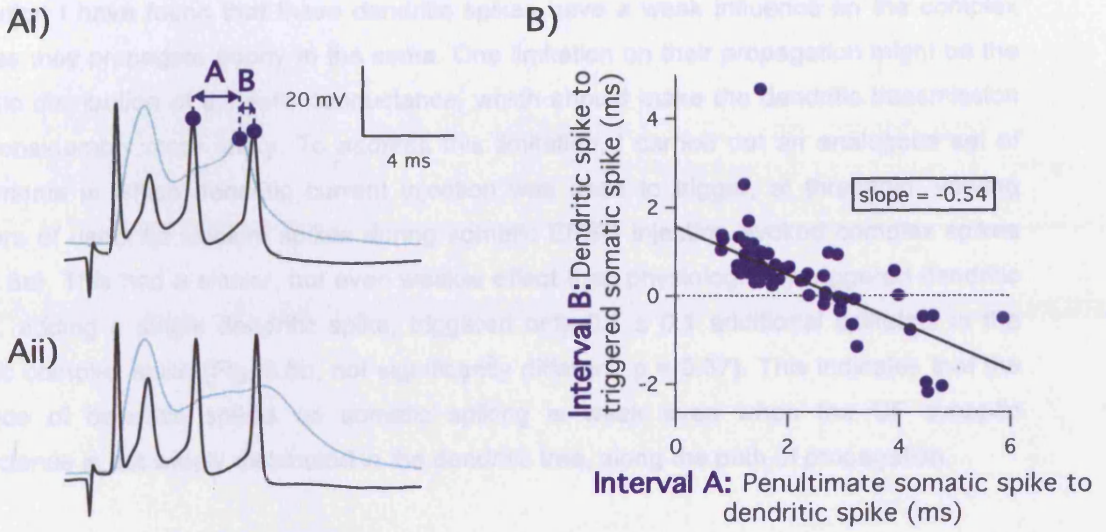

Figure 3.7: Lack of temporal relationship between dendritic spikes and somatic spikelets

Ai) Illustration of measurements made to investigate temporal relationship between extra dendritic spikes and the somatic spikelets they succeed in triggering. Left-most arrow, interval A: time between the penultimate somatic spike and the extra dendritic spike; right-most arrow, interval B: time between the extra dendritic spike and somatic spike it triggers.
ii) Example of a complex spike in which the triggered somatic spike occurs before the peak of the dendritic spike.
B) Relationship between the latency of triggered somatic spikes (interval B) and dendritic spike latency (interval A). Note that the somatic spikes neither occur at a consistent latency after the dendritic spikes (as would be expected if the somatic spikes were direct reflections of dendritic spikes) nor in an inverse latency relationship with a slope of -1 (as would be expected if the somatic firing interval was unaffected by the timing of the dendritic spike). The slope of -0.5 indicates that somatic spike timing was influenced, but not wholly determined by dendritic spike time.

I find a slope of -0.54, indicating that the somatic spike timing was influenced, but not wholly determined, by the dendritic spike time.

Effect of dendritic spikes on somatic spike generation during somatic conductance injection

By recording the chance occurrence of extra dendritic calcium spikes during climbing fibre stimulation I have found that these dendritic spikes have a weak influence on the complex spike as they propagate poorly to the soma. One limitation on their propagation might be the dendritic distribution of synaptic conductance, which should make the dendritic transmission path considerably more leaky. To address this limitation, I carried out an analogous set of experiments in which dendritic current injection was used to trigger, at threshold, varying numbers of dendritic calcium spikes during somatic EPSG injection evoked complex spikes (Fig. 3.8a). This had a similar, but even weaker effect than physiologically-triggered dendritic spikes; adding a single dendritic spike, triggered only 0.1 ± 0.1 additional spikelets in the somatic complex spike (Fig. 3.8b, not significantly different, $p = 0.37$). This indicates that the influence of dendritic spikes on somatic spiking is weak even when the CF synaptic conductance is not widely distributed in the dendritic tree, along the path of propagation.

Similarly, dendritic spikes generated during somatic conductance clamp failed to trigger extra somatic spikes as they too often arrived within the somatic refractory period or were below spike threshold (Fig. 3.9a and b). There was again a sigmoidal relationship between triggered somatic spike amplitude and dendritic spike latency (Fig. 3.9a), indicating that only if the dendritic spike occurred sufficiently long after the previous somatic spike could it generate and extra somatic spike. In combination with this, the somatic depolarisations caused by extra dendritic spikes were often below somatic spike threshold (Fig. 3.9b, $p < 0.04$, paired t-test). Further, any extra somatic spikelets were again not direct reflections of dendritic spikes, occurring both before and after the extra dendritic spikes. Within most data sets there was a negative relationship (of a similar slope to that seen during CF stimulation) between dendritic spike timing (latency after the previous somatic spike) and somatic spike timing (relative to the dendritic spike) (Fig. 3.9c). The lack of a single relationship between dendritic and somatic spike timing across the population of experiments is likely to be because dendritic spikes occurred at a much more variable latency after somatic spikes. The timing of these spikes were determined by inputs of unrelated amplitude, whereas, following CF stimulation the common underlying synaptic input is likely to influence the timing of both dendritic and somatic spikes.

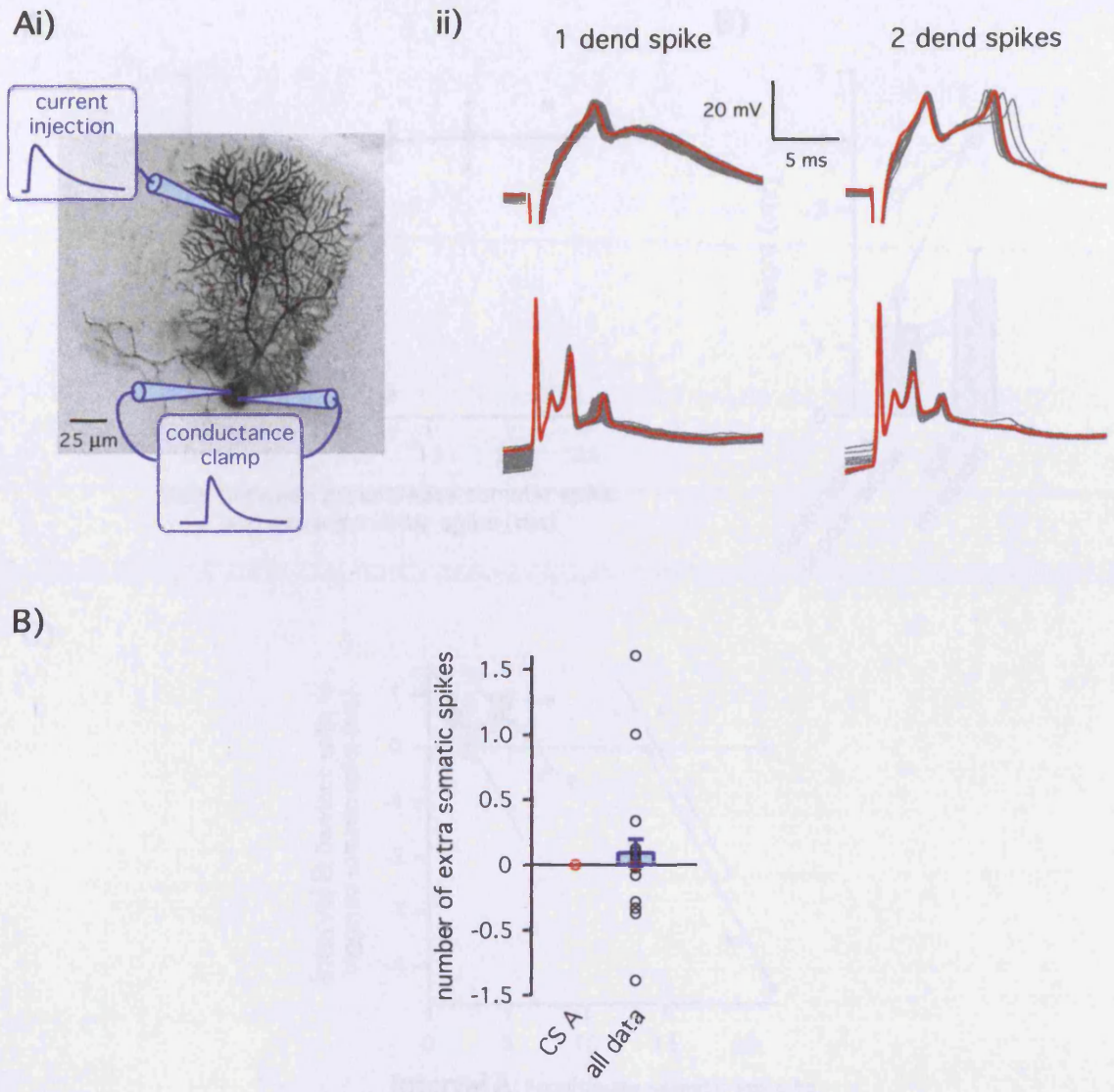

Figure 3.8: Dendritic spikes have a very weak influence on the somatic CS triggered by somatic conductance injection.

Ai) Biocytin staining of a Purkinje cell illustrating the experimental setup. Two somatic patch clamp electrodes (blue) were used for two-electrode dynamic clamp injection of synaptic-like conductance (τ_{rise} 0.3 ms, τ_{decay} 3 ms), a dendritic electrode (125 µm from the soma, in this case) was used to inject current a phasic biexponential of τ_{rise} 0.5 ms and τ_{decay} 5 ms, which triggered dendritic calcium spikes, together with a tonic current adjusted to take the cell to threshold for triggering a second dendritic spike.
ii) Recordings made from the cell shown in Ai while injecting 200 nS peak synaptic-like conductance to the soma, together with 3 nA peak phasic current and 80 pA tonic current to the dendrite. This took the cell to threshold for generating a second dendritic calcium spike. Layout as in (fig 3.3 Aii). The second dendritic spike (right hand column) triggered no further somatic spikelets.
B) Average number of somatic spikelets triggered by an extra dendritic spike during somatic dynamic clamp. Average ± SD of the data shown in Aii labelled 'CSA'; individual data-set averages (circles) and weighted mean ± SEM of all data sets (bar) (n = 19) labelled 'all data'. On average, 0.1 ± 0.1 somatic spikes (not sig. diff. to zero, p = 0.37) were triggered by an extra dendritic spike.

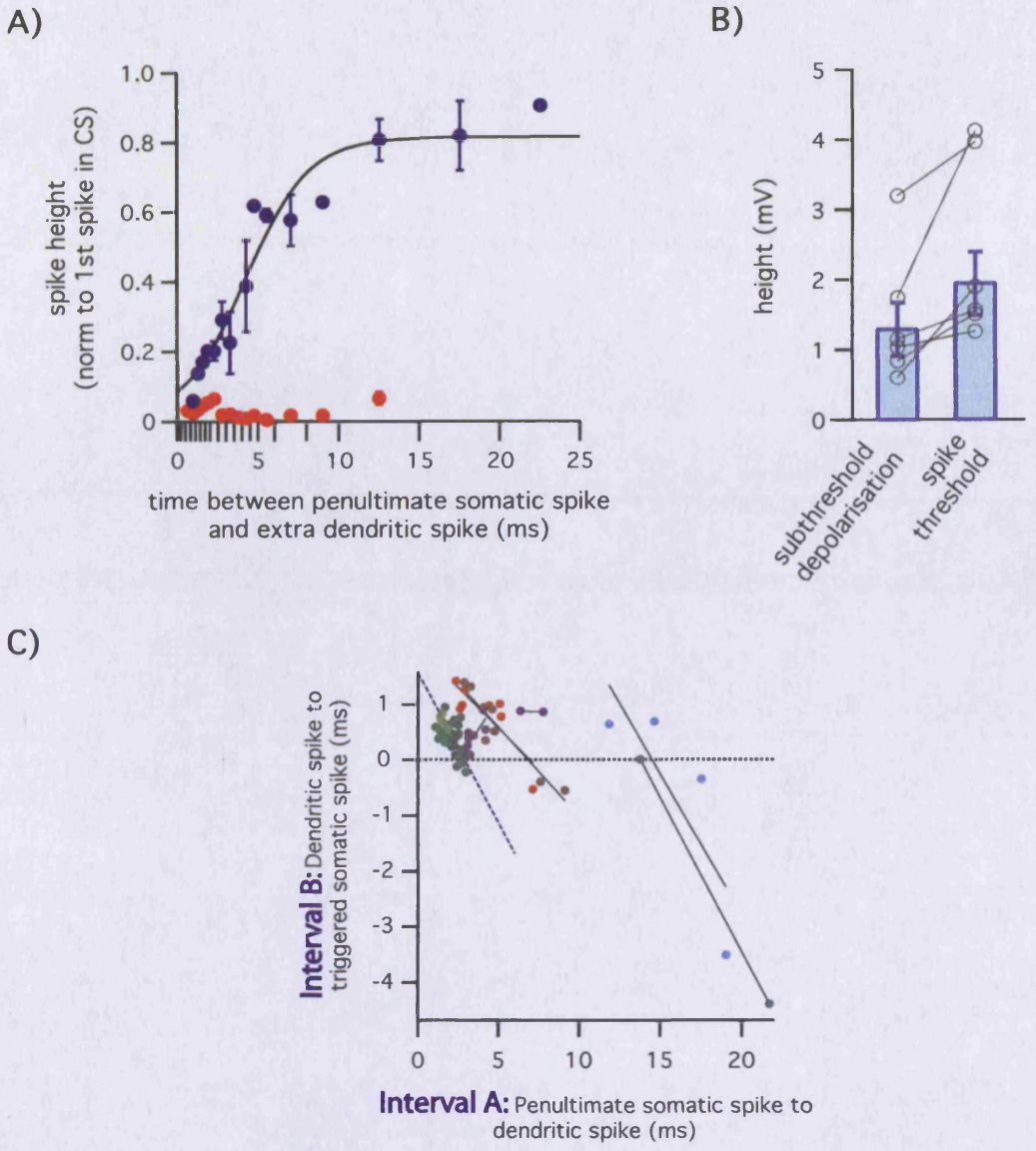

Figure 3.9: Dendritic spikes are often within the somatic refractory period during somatic dynamic clamp generated CSs.

A) Dependence of somatic event height on dendritic spike time, measured as shown in (Fig. 3.6 A). Red points: cases where an extra dendritic spike failed to trigger a spike, generating only a subthreshold depolarisation; blue points: cases where an extra spike triggered a somatic spike. Refractory trend highlighted by sigmoidal fit to blue points, constrained to a baseline height of 0.
B) Height of spike failures compared to spike threshold in the same cell (measured as in (fig 3.6 D)). Red circles highlight averages from the data-set illustrated in (aii). Bars show total data average ± SEM (n = 6, sig. diff $p < 0.04$, paired t-test).
C) Relationship between timing of somatic spikes triggered by extra dendritic spikes and dendritic spike time. Individual data sets coloured and fit separately. Fit from (fig 3.7 B) appended in blue for comparison. The negative relationships between these two timings illustrates that the spikes triggered at the soma are not direct reflections of dendritic spikes; that slopes are <-1, however, indicates that somatic spike timing was not entirely independent of dendritic spike timing.

Net effect of calcium channels on complex spike generation during somatic conductance injection

The experiments presented so far in this chapter have demonstrated that dendritic calcium spikes are not required for complex spike generation and indeed are poor promoters of somatic spiking when they are present (regardless of the distribution of synaptic input). One further method is available to assess the net effect of Purkinje cell calcium conductances on the somatic EPSG triggered complex spike; as this does not rely on synaptic transmission, calcium channels can be pharmacologically blocked. This was achieved by washing in sufficient concentration of $CdCl_2$ to block the CF stimulation evoked EPSP (400 μM). $CdCl_2$ wash-in lead to depolarisation of the cells resting membrane potential to ~40 mV, and thus to inactivation of spontaneous spiking: tonic holding current (-50 to -500 pA) was therefore used to hyperpolarise to cell to ~-65 mV both before and during $CdCl_2$ application. I found that, under these conditions, blocking calcium channels surprisingly lead a more excited complex spike (n = 10 cells). Spikelets in the complex spike occurred at a higher frequency, and continued for a longer time following somatic EPSG injection, both factors contributing to an increase in the number of spikelets in the complex spike (Fig. 3.10a and b). On average (across all amplitudes of EPSG injection, n = 20; increases were similar for injections of 100, 200, 250, 300 and 500 nS peak synaptic-like conductance injection), the frequency of spikelets (measured in the initial four spikelets) increased by 132 ± 54 %, the duration of spiking by 1023 ± 254 % and the total number of spikes by 637 ± 125 %.

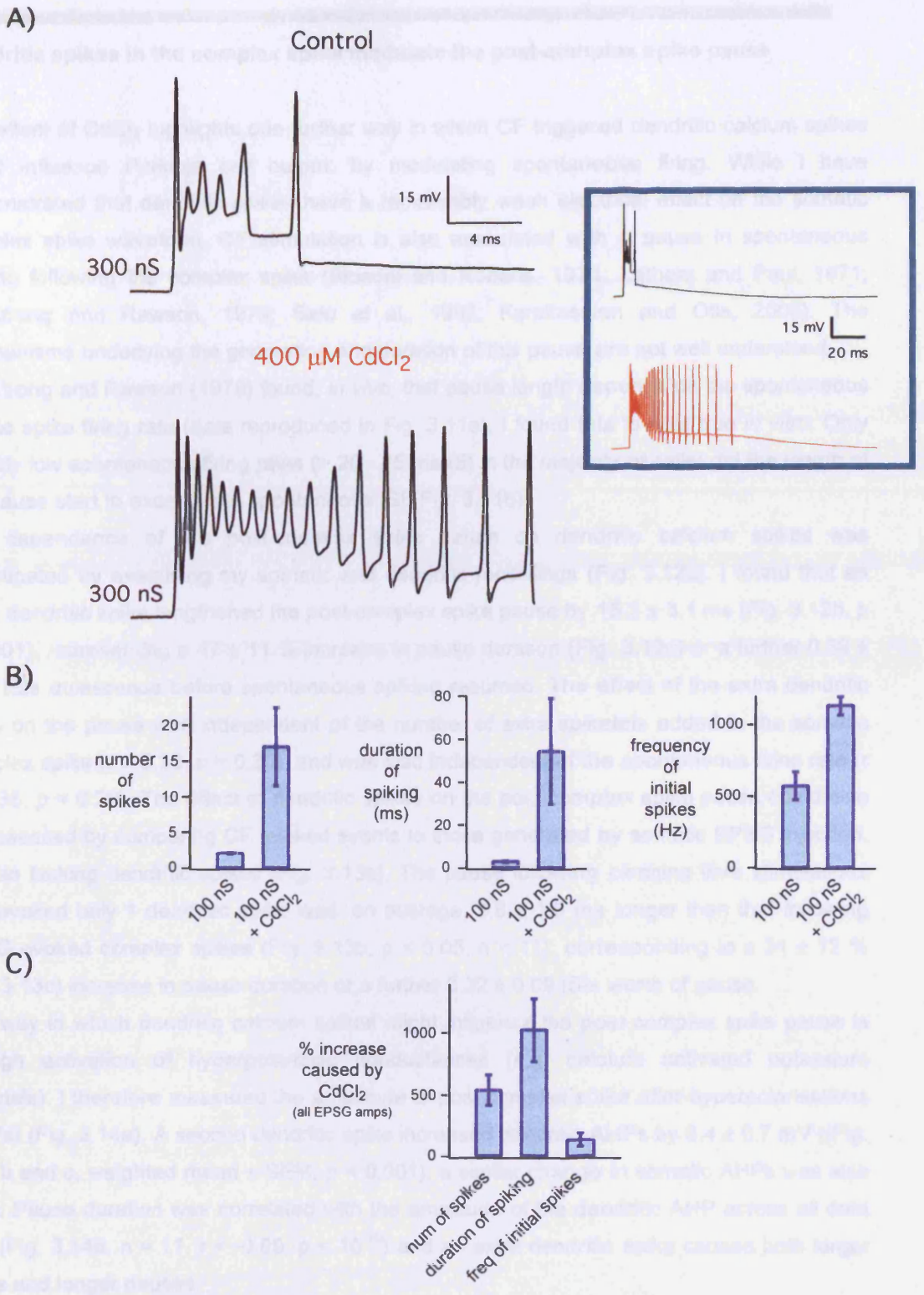

Figure 3.10: Blocking Ca2+ channels enhances excitable response to Gsyn

A) Example of responses of a Purkinje cell to a 300 nS EPSG before (top) and after (bottom) calcium channels were blocked with 400 µM $CdCl_2$. Tonic current injection was used to hold the cell at ~ -65 mV as $CdCl_2$ changed the resting membrane potential. Inset (right) shows same data on a longer time scale in order to illustrate not just the increase in firing frequency in $CdCl_2$, but the increased duration of the response, which together lead to an increased number of spikes in the complex spike.

B) Average number of spikes, duration of spiking and firing frequency of the response to a 100 nS EPSG (at -65 mV) before and after addition of 400 µM $CdCl_2$ (n = 7 cells). Average firing frequency calculated from the first four spikes in the complex spike.

C) Average % increase in number of spikes, duration of spiking and firing frequency in response to all EPSG amplitudes (a selection from 100, 200, 250, 300 and 500 nS in each of 7 cells). All increases are significantly above 0 ($p < 0.0005$, $p < 0.001$, $p < 0.05$ respectively).

Dendritic spikes in the complex spike modulate the post-complex spike pause

The effect of $CdCl_2$ highlights one further way in which CF triggered dendritic calcium spikes might influence Purkinje cell output: by modulating spontaneous firing. While I have demonstrated that dendritic spikes have a remarkably weak electrical effect on the somatic complex spike waveform, CF stimulation is also associated with a pause in spontaneous spiking following the complex spike (Bloedel and Roberts, 1971; Latham and Paul, 1971; Armstrong and Rawson, 1979; Sato et al., 1992; Karakossian and Otis, 2005). The mechanisms underlying the generation and duration of this pause are not well understood.

Armstrong and Rawson (1979) found, *in vivo*, that pause length depends on the spontaneous simple spike firing rate (data reproduced in Fig. 3.11a); I found this to hold true *in vitro*. Only at fairly low spontaneous firing rates (> 20 - 25 ms ISI in the majority of cells) did the length of the pause start to exceed one spontaneous ISI (Fig. 3.11b).

The dependence of the post-complex spike pause on dendritic calcium spikes was investigated by examining my somatic and dendritic recordings (Fig. 3.12a). I found that an extra dendritic spike lengthened the post-complex spike pause by 15.3 ± 3.1 ms (Fig. 3.12b, $p < 0.001$), representing a 47 ± 11 % increase in pause duration (Fig. 3.12c) or a further 0.59 ± 0.14 ISIs quiescence before spontaneous spiking resumed. The effect of the extra dendritic spike on the pause was independent of the number of extra spikelets added to the somatic complex spike ($r = 0.36$, $p = 0.30$), and was also independent of the spontaneous firing rate ($r = -0.35$, $p = 0.29$). The effect of dendritic spikes on the post-complex spike pause could also be assessed by comparing CF evoked events to those generated by somatic EPSG injection, and so lacking dendritic spikes (Fig. 3.13a). The pause following climbing fibre stimulations that evoked only 1 dendritic spike was, on average, 3.8 ± 1.6 ms longer than that following EPSG evoked complex spikes (Fig. 3.13b, $p < 0.05$, $n = 11$), corresponding to a 31 ± 12 % (Fig. 3.13c) increase in pause duration or a further 0.22 ± 0.09 ISIs worth of pause.

One way in which dendritic calcium spikes might influence the post-complex spike pause is through activation of hyperpolarizing conductances (e.g. calcium activated potassium channels). I therefore measured the amplitude of post-complex spike after-hyperpolarisations (AHPs) (Fig. 3.14a). A second dendritic spike increased dendritic AHPs by 3.4 ± 0.7 mV ((Fig. 3.14 b and c, weighted mean ± SEM, $p < 0.001$); a similar change in somatic AHPs was also seen. Pause duration was correlated with the amplitude of the dendritic AHP across all data sets (Fig. 3.14d, $n = 11$, $r = -0.89$, $p < 10^{-16}$) and an extra dendritic spike caused both larger AHPs and longer pauses.

These data suggest that, from the point of view of the postsynaptic deep cerebellar nuclei (DCN) neurons, the most salient effect of dendritic spikes may be to increase the pause following the complex-spike rather than the number and timing of spikelets in the complex spikes themselves.

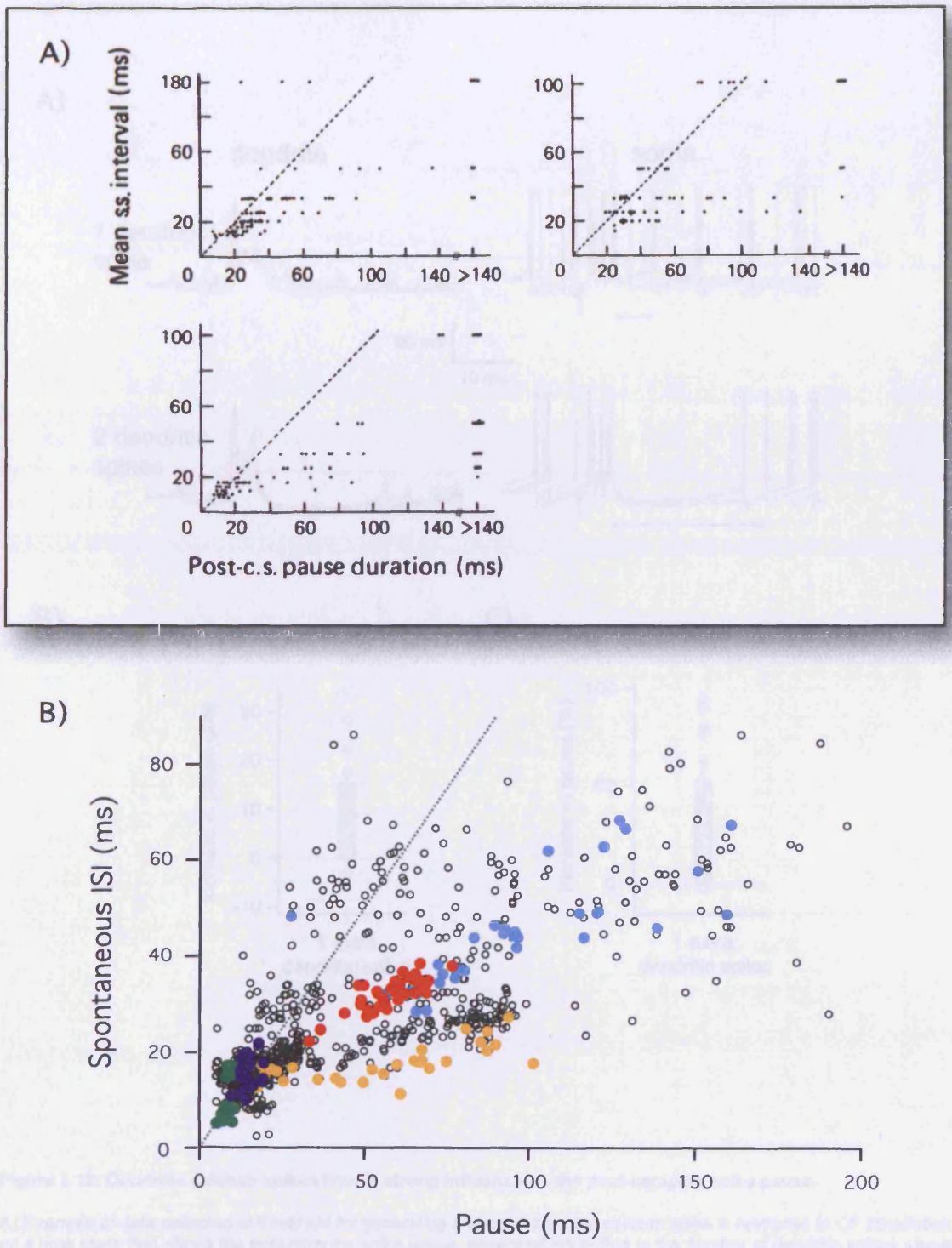

Figure 3.11: Post-complex spike pause duration depends on spontaneous firing rate

A) Data from Armstrong & Rawson, 1979 demonstrating the relationship between spontaneous simple spike firing and post-CS pause duration in vivo. The unity line, where the post-CS pause is identical to one spontaneous ISI, is shown (dotted line). These examples (n = 3 cells) were used to illustrate their observation that pauses only tended to exceed one spontaneous ISI when the firing rate was low; "less than 40-50/s".
B) Relationship between spontaneous firing and the post-CS pause duration in vitro (n = 17 cells, colours highlight data from 5 individual cells). Dotted line: unity line. Note that the trend is similar to that found in vivo, and the generalisation that pauses only exceed one spontaneous ISI when spontaneous firing rates are below 40-50/s applies to most cells.

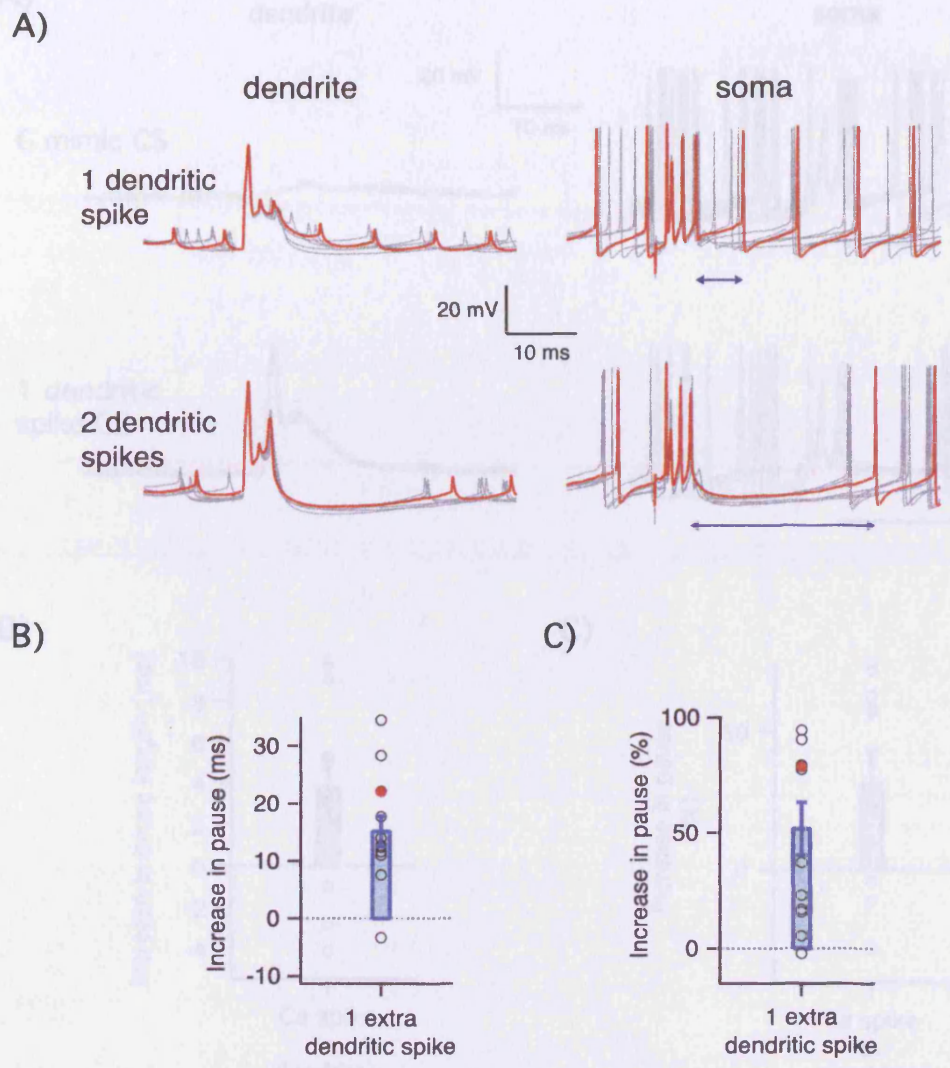

Figure 3.12: Dendritic calcium spikes have a strong influence on the post-complex spike pause.

A) Example of data collected at threshold for generating a second dendritic calcium spike in response to CF stimulation, on a time scale that shows the post-complex spike pause, separated according to the number of dendritic spikes. Upper panels: one dendritic spike, lower panels: two dendritic spikes; left panels: dendritic recordings (60 µm from the soma), right panels: somatic recordings. Arrows indicate pause length measurement (time between the last spikelets in the complex spike and the next spontaneous spike) made in the red example traces. An extra dendritic spike increased the pause from 28.0 ± 17.9 ms to 50.0 ± 12.7 ms ($p < 0.01$).
B) Average increase in pause length triggered by an extra dendritic calcium spike (in msec). Circles show averages of individual datasets (dataset shown in (A) highlighted in red), bar indicates weighted mean ± SEM of the population data ($n = 11$, significantly different from 0, $p < 0.0005$).
C) Average increase in pause length triggered by an extra dendritic calcium spike (as % of pause length without extra dendritic calcium spike). Circles and bars as in (B) ($n = 15$, significantly different from 0, $p < 0.005$).

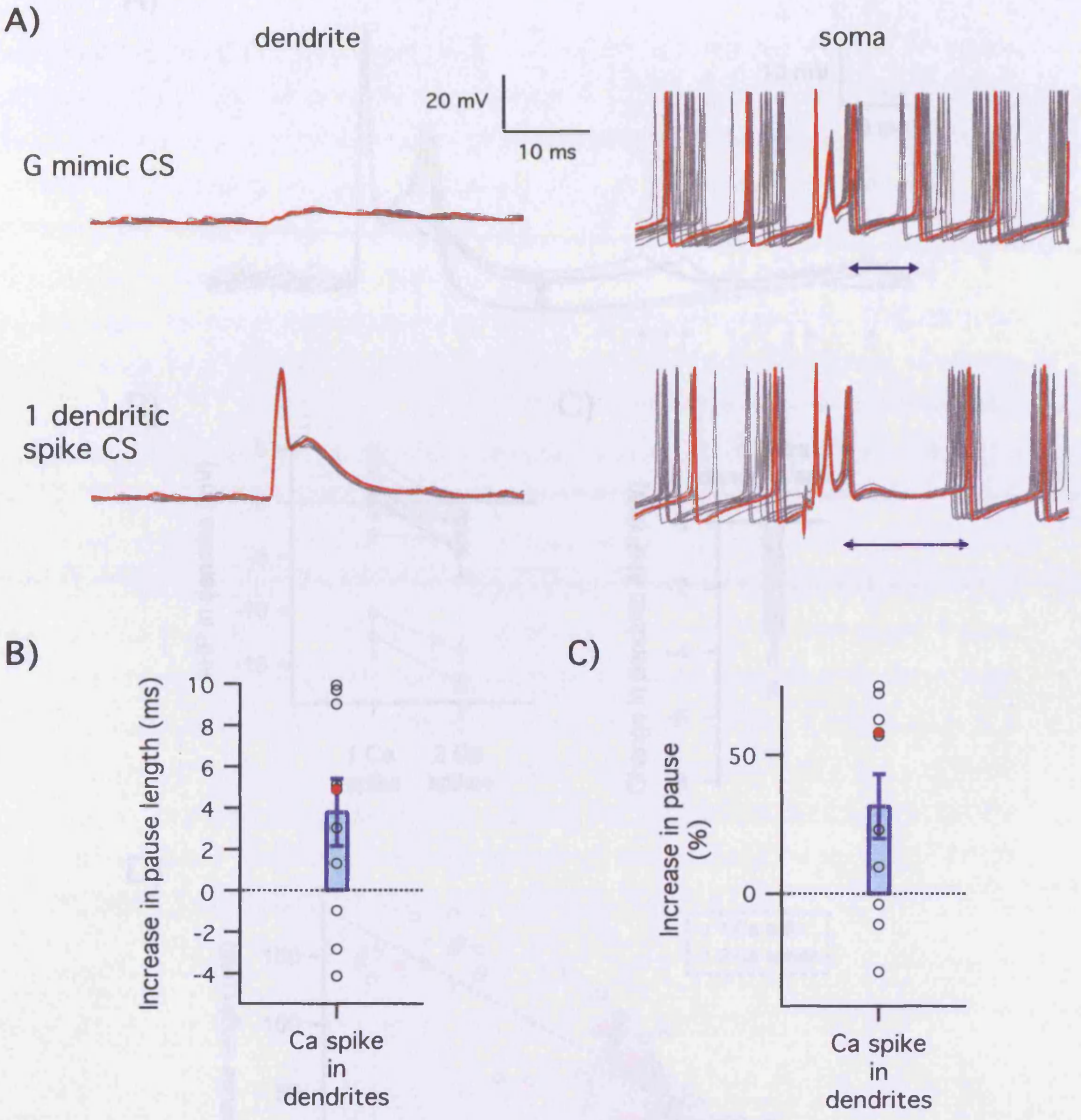

Figure 3.13: Dendritic calcium spikes have a strong influence on the post-complex spike pause.

A) Example experiment where somatic EPSG injection was tuned to match the somatic firing pattern, shown on a longer time scale to illustrate the length of the post-complex spike pause. Upper panels, 100 nS somatic EPSG (hence no dendritic spikes), lower panels, 1 Hz CF stimulation stimulating one dendritic spike; left hand panels dendritic recordings (110 µm from the soma), right hand side, somatic recordings. Arrows indicate pause length measurement (time between the last CS spikelets and the next spontaneous spike) made in the red example traces. The presence of a dendritic spike lengthened the pause from 8.4 ± 1.3 ms to 13.3 ± 1.1 ms ($p < 10^{-10}$).
B) Average pause length increase following CF stimulation above that following somatic EPSG injection (in ms). Circles show averages of individual data sets (data set shown in A highlighted in red), bar indicates mean ± SEM of the population data (n = 12, sig diff from 0, $p < 0.05$).
C) Average pause length increase following CF stimulation above that following somatic EPSG injection (as % of pause length without extra dendritic calcium spike). Circles and bars as in B (n = 12, sig diff from 0, $p < 0.05$).

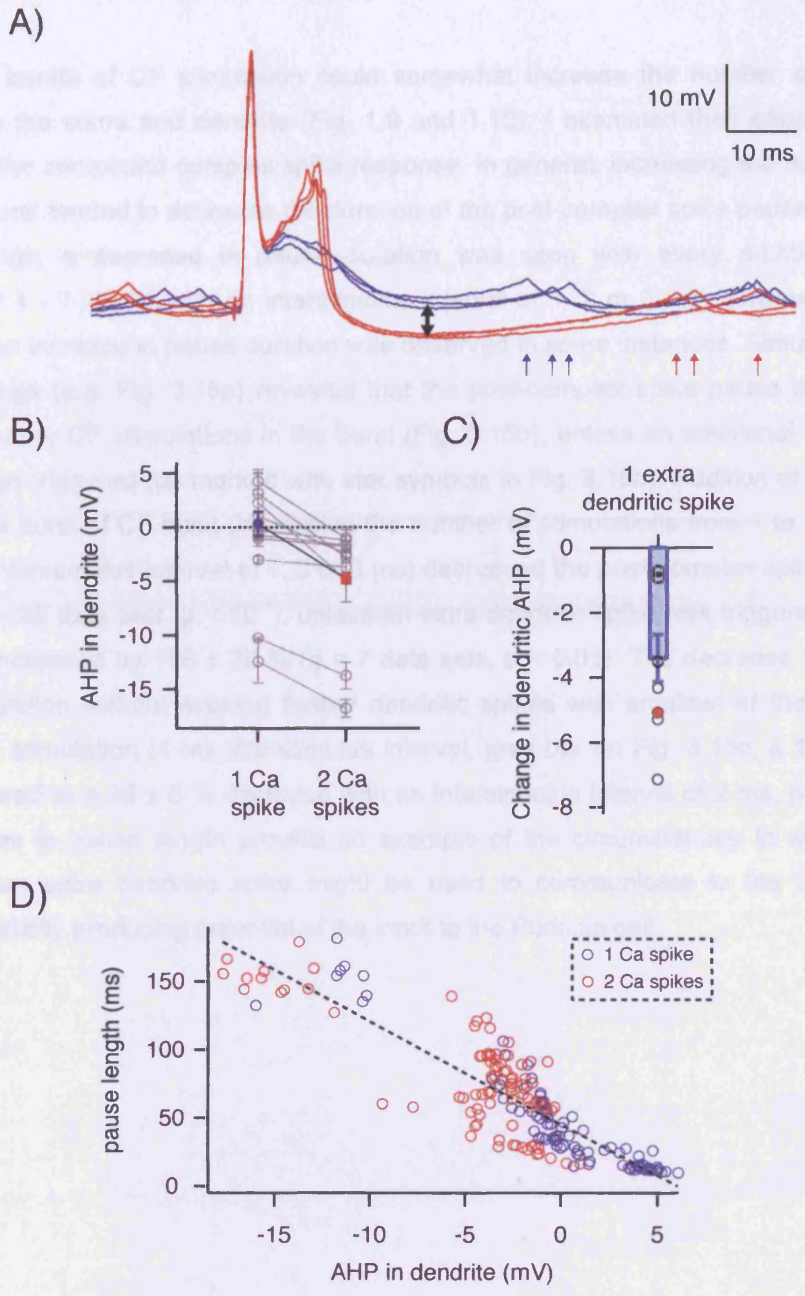

Figure 3.14: Dendritic spikes regulate the AHP following the complex spike

A) Dendritic recording (155 µm from the soma) of responses to CF stimulation collected at threshold for generating a second dendritic calcium spike (blue: one dendritic spike, red: two dendritic spikes). The black arrow indicates the measured difference in AHP amplitude; red and blue arrows mark the time of somatic action potentials (reflected as small depolarisations in the dendritic recording) that terminate the post-complex spike pause in the one and two dendritic spike traces, respectively.
B) Average dendritic AHP (minimum dendritic membrane potential reached during the pause minus average baseline dendritic membrane potential preceding CF stimulation) following CF stimulation that evokes, at threshold, 1 or 2 dendritic calcium spikes. Lines connect 1 and 2 spike data from the same set; the data set shown in A is highlighted in colour.
C) Average change in AHP amplitude caused by an extra dendritic spike. Circles show averages of individual datasets (dataset shown in A highlighted in red), bar indicates weighted mean ± SEM of the population data (n = 11, significantly different from 0, $p < 0.001$).
D) Relationship between post-complex spike pause duration and dendritic AHP amplitude. Each datapoint represents a single measurement made following CF stimulation at threshold for generating an extra dendritic spike (n = 11 cells; blue symbols: sweeps with 1 dendritic spike trials, red symbols: sweeps with 2 dendritic spikes). Black line indicates the negative correlation between pause length and AHP depth ($r = -0.89$, $p < 10^{-16}$).

Modulation of post-complex spike pausing by bursts of CF stimulation

As I found that bursts of CF stimulation could somewhat increase the number of spikes triggered in both the soma and dendrite (Fig. 1.9 and 1.10), I examined their effect on the pause following the compound complex spike response. In general, increasing the number of CF stimuli in a burst tended to decrease the duration of the post-complex spike pause. In 4/10 somatic recordings, a decrease in pause duration was seen with every additional CF stimulation (over 1 - 7 stimuli with an interstimulus interval of 1, 2 or 3 ms); however in the remaining cells an increase in pause duration was observed in some instances. Simultaneous dendritic recordings (e.g. Fig. 3.15a) revealed that the post-complex spike pause tended to decrease with further CF stimulations in the burst (Fig. 3.15b), unless an additional dendritic calcium spike was triggered (as marked with star symbols in Fig. 3.15b). Addition of an extra two stimuli to the burst of CF input (increasing the number of stimulations from 1 to 3, 3 to 5 or 5 to 7, at an interstimulus interval of 1, 2 or 3 ms) decreased the post-complex spike pause by 31 ± 4 % ($n = 29$ data sets, $p < 10^{-7}$), unless an extra dendritic spike was triggered, when the pause was increased by 106 ± 26 % ($n = 7$ data sets, $p < 0.01$). The decrease following further CF stimulation without evoking further dendritic spikes was smallest at the highest frequency of CF stimulation (1 ms interstimulus interval, grey bar on Fig. 3.15c; a 18 ± 5 % decrease compared to a 38 ± 6 % decrease with an interstimulus interval of 2 ms, $p < 0.05$). These differences in pause length provide an example of the circumstances in which the appearance of an extra dendritic spike might be used to communicate to the DCN the strength and plasticity producing potential of the input to the Purkinje cell.

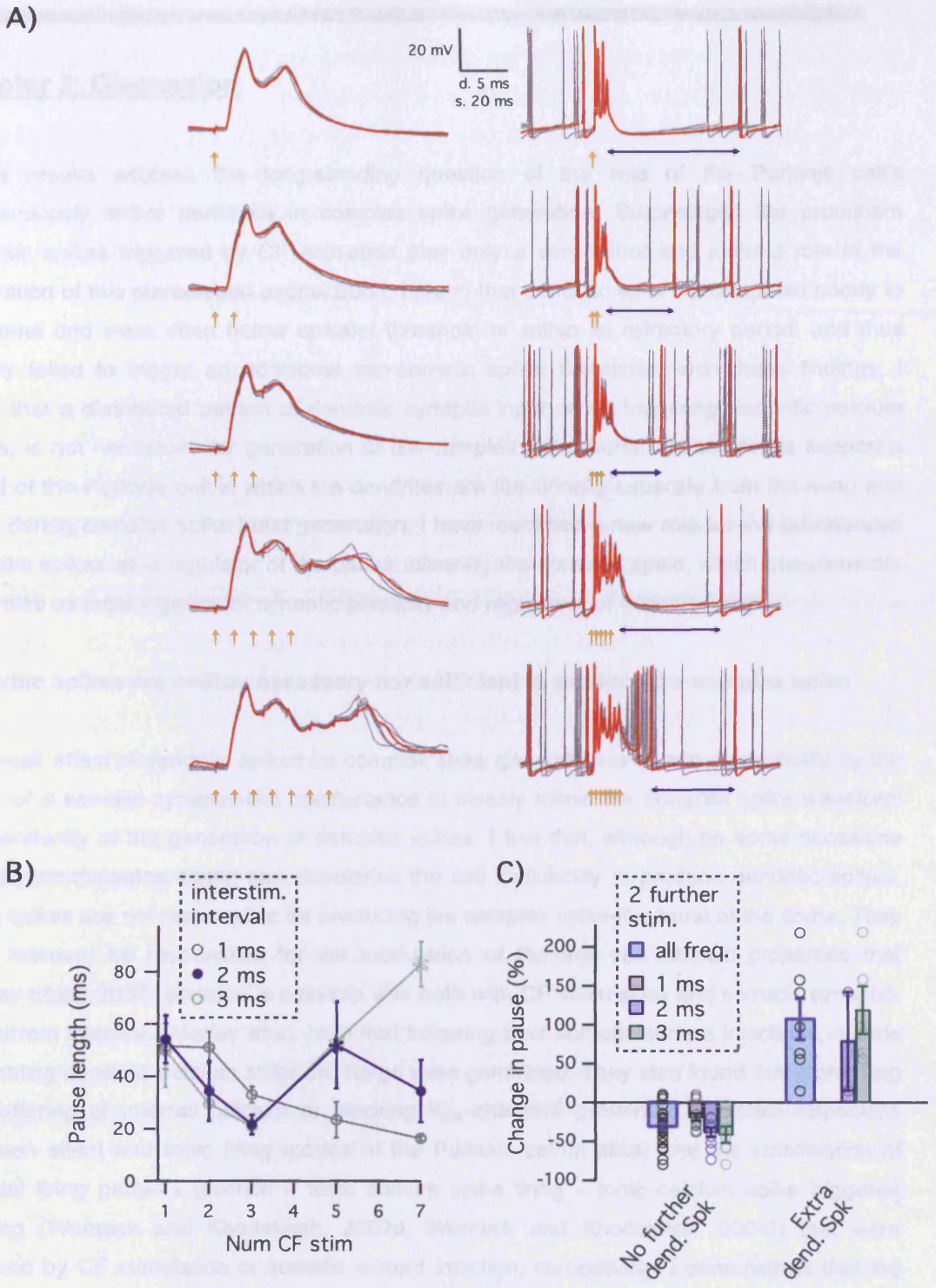

Figure 3.15: The pause following bursts of CF input

A) Example of data recorded simultaneously from the dendrite (left 85 µm) and the soma during bursts of CF stimulation. Dendrite shown on a larger time scale to show the number of dendritic spikes evoked. The cell's CF was stimulated 1, 2, 3, 5 or 7 times (top to bottom) every 2 ms (yellow arrows). Post-CS pauses of red example traces highlighted by blue arrows. Note that pause duration decreases with increasing number of CF-stimulations, except in the when further dendritic calcium spikes are also evoked, when pause duration increases.

B) Average pause duration vs number of CF stimulations for the data shown in (A) (blue); pauses resulting from bursts of CF stimulation at higher and lower frequencies in the same cell also shown (grey and green). Responses where further dendritic calcium spikes were evoked marked by *.

C) Change in pause duration following addition of two CF stimulations to the burst of input (n = 4 data sets). When no further dendritic spike was evoked (left), additional CF stimulation shortened the length of the post-CS pause; when extra dendritic spikes were stimulated, pause length increased (right). Data separated according to burst frequency (grey, dark blue and green bars) or at all stimulation frequencies (light blue bar).

Chapter 3: Discussion

These results address the long-standing question of the role of the Purkinje cell's conspicuously active dendrites in complex spike generation. Surprisingly, the prominent dendritic spikes triggered by CF activation play only a very minor and indirect role in the generation of this stereotyped axonal burst. I found that dendritic spikes propagated poorly to the soma and were often below spikelet threshold or within its refractory period, and thus usually failed to trigger an additional axo-somatic spike. Consistent with these findings, I found that a distributed pattern of dendritic synaptic input, while triggering dendritic calcium spikes, is not necessary for generation of the complex spike burst. These results support a model of the Purkinje cell in which the dendrites are functionally separate from the axon and soma during complex spike burst generation. I have identified a new role for the pronounced dendritic spikes as a regulator of the pause following the complex spike, which complements their roles as local triggers for synaptic plasticity and regulators of intrinsic firing.

Dendritic spikes are neither necessary nor sufficient to produce the complex spike

The weak effect of dendritic spikes on complex spike generation is shown dramatically by the ability of a somatic synaptic-like conductance to closely mimic the complex spike waveform independently of the generation of dendritic spikes. I find that, although on some occasions somatic conductance clamp can depolarise the cell sufficiently to produce dendritic spikes, these spikes are not responsible for producing the complex spike-like burst at the soma. They may, however be responsible for the modulation of Purkinje cell intrinsic properties that (McKay et al., 2007) observe is possible with both with CF stimulation and somatic synaptic-like current injection. McKay et al. note that following their somatic current injections, events resembling dendritic calcium spike discharge were generated. They also found that increasing the buffering of internal calcium or blocking K_{Ca} channels prevented the state transitions (between silent and tonic firing modes of the Purkinje cell in slice) and the stabilisation of trimodal firing patterns (silence – tonic sodium spike firing – tonic calcium spike triggered bursting (Womack and Khodakhah, 2002a; Womack and Khodakhah, 2004)) that were triggered by CF stimulation or somatic current injection, respectively. I demonstrate that the Ca^{2+} spikes that appear to be necessary for intrinsic firing regulation, and for synaptic plasticity (reviewed in Ito, 2002) are not an integral part of complex spike generation. Furthermore, I have found that they are far more readily evoked by CF stimulation than by somatic conductance injection. This is likely to be because dendritically distributed synaptic input effectively depolarises the dendrites to calcium spike threshold (Roth and Häusser, 2001, see also Introduction to Chap 2), whereas somatic EPSG injection results in a burst of rapid somatic spikes, which are poorly backpropagated (Stuart and Sakmann, 1994), together with a slower, small increase in baseline depolarisation, which is more effectively

backpropagated, but usually of insufficient amplitude to trigger dendritic calcium spikes (Fig 3.1). In addition, the isolation of the dendrites from the fast spiking conductances of the soma allows sufficiently large input to trigger full blown, slower time course calcium spikes. I propose that it is this reliable generation of calcium spikes, necessary for modulation of spontaneous firing and intrinsic and synaptic plasticity, that is the limiting factor on the positioning of CF inputs on the Purkinje cell, rather than the generation of the complex spike burst.

The calcium spikes that are triggered after somatic conductance injection also illustrate the fact that they are not sufficient to generate the complex spike: they do not on their own trigger this characteristic burst of firing (see e.g. Fig. 3.2). This is true of the many other situations in which spikes are triggered in Purkinje cell dendrites e.g. strong parallel fibre stimulation (Llinas and Nicholson, 1971; Callaway and Ross, 1997; Rancz and Häusser, 2006; Walter and Khodakhah, 2006; Mittmann and Häusser, 2007; Steuber et al., 2007) depolarising current injection to the soma or dendrites (Llinas and Sugimori, 1980b, a; Hounsgaard and Midtgaard, 1988) or during the bursting phase of the trimodal firing pattern sometimes seen in Pukinje cells in slice (Womack and Khodakhah, 2002a; Womack and Khodakhah, 2004). In all these situations dendritic spikes can accelerate somatic firing, but in none is the characteristic burst of the complex spike reproduced. Dendritic spikes are therefore neither necessary nor sufficient to generate the complex spike.

Propagation of dendritic spikes

Our simultaneous somatic and dendritic recordings directly demonstrate that the dendritic spikes triggered by CF input do not directly trigger somatic spikelets in the complex spike. Rather, by manipulating the number of dendritic spikes, I have shown that they have a surprisingly weak influence on the somatic complex spike, only generating a fraction of an extra spike at the soma. These findings parallel the relatively weak effect of local suppression of the dendritic complex spike by dendritic inhibition on the somatic complex spike (Callaway et al., 1995).

The irrelevance of dendritic spikes for somatic spiking during the complex spike may initially seem puzzling given the relatively short dendrites of the Purkinje cell, their predominantly large calibre, and the widespread nature of dendritic spikes during the complex spike. However, I have demonstrated that the weak efficacy of dendritic spikes in these neurons is due to a combination of factors. Dendritic spikes in Purkinje cells are relatively brief and of small amplitude, in striking contrast to the ~80 mV, ~60 ms dendritic Ca^{2+} spikes recorded in layer 5 pyramidal cells (Zhu, 2000). This alone reduces their spike triggering potency. Further, the propagation of dendritic spikes to the soma and axon is associated with substantial attenuation in Purkinje cells. This is due in part to the unfavourable impedance mismatches

associated with the highly branched geometry of the Purkinje cell dendritic tree; this is particularly unfavourable to the forward propagation of brief, active events (Vetter et al., 2001, see also Main Introduction). Additionally, the strong synaptic and voltage-gated shunting conductances active during the climbing fibre response may also enhance attenuation (indeed the attenuation may be greater during later dendritic spikes, due to the activation of active conductances by previous spikes, as suggested in Llinas and Nicholson, 1971). However, isolated dendritic spikes, generated in the absence of distributed CF stimulation of the Purkinje cell, are attenuated to a similar, or indeed more severe, extent (see Fig. 3.8 and Rancz and Häusser, 2006). This suggests that the widespread nature of dendritic spike initiation during the complex spike may actually aid propagation to the soma, by reducing the axial current between branches and thus partially mitigating the impedance mismatch. The last point at which further attenuation may occur is in the soma itself, where the conductances underlying fast spikelet generation may shunt out the propagated depolarisation (Häusser et al., 2001). These conductances are large (Raman and Bean, 1999; Swensen and Bean, 2003, 2005), and unpublished data (Christensen, 2002) has found that dialysis of the sodium channel blocker QX-314 reveals somatic spiking very similar to that of the dendritic calcium spike, suggesting axo-somatic conductances could indeed significantly shunt out a propagated dendritic calcium spike. Finally, I have demonstrated that the highly attenuated somatic counterpart of the small dendritic spike is usually subthreshold, or within the refractory period of the previous spikelet. These factors acting in concert explain why dendritic spikes in Purkinje cells have a far weaker influence on axonal spiking than in cortical and hippocampal pyramidal neurons (Schiller et al., 1997; Golding and Spruston, 1998; Larkum et al., 1999, 2001) where a calcium spike can trigger 2.5 axonal spikes (Williams and Stuart, 2002).

Pyramidal-cell like sequence of dendritic spike propagation

Although I have found that Purkinje cell dendritic spikes are worse triggers of somatic spikes than the dendritic sodium and calcium spikes of other cell types, their mode of propagation and spike triggering does not appear to fundamentally differ. In layer 5 pyramidal cells it has been found that even a dendritically initiated forward propagating spike triggers a spike first in the axon which then backpropagates into the soma (Stuart et al., 1997a; Stuart et al., 1997b). A similar scenario is predicted to occur in mitral cells (Shen et al., 1999) and, by analogy, CA1 pyramidal cells (Colbert and Johnston, 1996; Golding and Spruston, 1998). In Purkinje cells, at room temperature, the first spike of the complex spike occurs first in the axon (Stuart and Häusser, 1994). Direct proof that all spikelets initiate in the axon has been found by Dr Beverly Clark, who has made cell-attached recordings from the proximal axon (≤ 75 μm) and has found that every spikelet of the complex spike occurs first in the axon (in Davie et al., 2008). This confirms that spikelets of the complex spike do not directly reflect dendritic spikes. It also implies that even when a dendritic spike does promote an extra somatic spike, (which

can occur either before or after the dendritic spike, see e.g. Fig. 3.7), axonal spiking precedes somatic spiking; thus the pyramidal cell-like pattern of spike initiation is maintained.

That the axon continues to be the most favourable site of spike initiation throughout the complex spike, despite the enormous CF-triggered current that charges the soma and proximal dendrites, highlights the specialisations that make it the site of initiation even during high frequency spontaneous spiking (Stuart and Häusser, 1994; Clark et al., 2005; Khaliq and Raman, 2006). The axon's narrow diameter aids initiation as it bestows both a high axial resistance, isolating it from the conductance and capacitance of the soma and dendrites, and a small, readily charged surface area (Dodge and Cooley, 1973; Mainen et al., 1995; Colbert and Pan, 2002). Further, specialisations of axonal voltage-gated ion channels, such as increased densities, specific subunit expression or negatively shifted voltage sensitivities of sodium channels, can also help to account for a lower axonal threshold (Wollner and Catterall, 1986; Mainen et al., 1995; Jenkins and Bennett, 2001; Colbert and Pan, 2002; Boiko et al., 2003; Meeks and Mennerick, 2007; Ogiwara et al., 2007; Kole et al., 2008). In fact, the very specialisations that lead to axonal initiation make it likely that the initiation site can follow higher firing frequencies than soma, or indeed the distal axon. As is predicted in Chapter 2, some spikelets may not fully actively invade the soma, particularly at the shortest ISIs within the complex spike; this parallels the failure of small, slowly rising spikelets generated at short ISIs to propagate down the Purkinje cell axon (Khaliq and Raman, 2005; Monsivais et al., 2005).

Functional role of dendritic calcium spikes triggered by CF inputs

The net effect of perisomatic calcium conductance activation by the complex spike appears to be inhibitory. Their blockage by $CdCl_2$ causes an increase in the number and frequency of spikes in the complex spike generated by somatic conductance injection. This paradoxical effect is most likely to be the result of reduced activation of K_{Ca} channels, both during the complex spike and tonically, due to removal of the calcium influx necessary to activate these channels. This finding is consistent with the trends of initially increased firing frequency in Purkinje cells in slice and prolonged, more rapid spiking in response to a brief current injection in dissociated cells (Edgerton and Reinhart, 2003; Swensen and Bean, 2003).
In the experiments in this thesis, the $CdCl_2$ concentration added was high (400 μM) and potentially may have had non-specific effects e.g. mM $CdCl_2$ concentrations are known to block neuronal sodium channels (Frelin et al., 1986; Swensen and Bean, 2003), and more pertinently, it has recently been found that both I_A and delayed rectifier potassium channels in pyramidal cells are blocked by $CdCl_2$, with IC_{50}s of 500 - 800 μM (Wang et al., 2008). However, the concentration was chosen empirically as that required to block the calcium dependent CF EPSP. Indeed the effective concentration of $CdCl_2$ in solution is likely to have been lower than calculated, due to precipitation with the phosphate used as a pH buffer in the

ACSF. Experiments with lower $CdCl_2$ concentrations (in e.g. HEPES buffered ACSF) or more specific channel blockers (e.g. the P-type calcium channel blocker ω-Agatoxin IVA) would ensure the reported result was indeed not due to non-specific effects.

The increased excitability observed here is likely to be due to both an increase in input resistance and a reduction of hyperpolarising post-spike currents. One indication that tonic channel activation was altered by $CdCl_2$ wash-in was the depolarisation of resting membrane potential, as has previously been observed by Edgerton and Reinhart (2003) (using 100 μM $CdCl_2$). During tonic spontaneous spiking, calcium channels, BK and SK channels are all activated (Cingolani et al., 2002; Womack and Khodakhah, 2002; Edgerton and Reinhart, 2003; Swensen and Bean, 2003; McKay and Turner, 2004; Swensen and Bean, 2005; Walter et al., 2006) and indeed the net current through Ca^{2+} and K_{Ca} channels together is outward during this simple spiking (Raman and Bean, 1999; Swensen and Bean, 2003, 2005). At the hyperpolarised voltage at which these experiments were carried out (-65 mV), BK and P-type calcium channels are not expected to be open, but an outward calcium sensitive current carried by SK channels may remain, due to their lack of voltage sensitivity and their greater calcium sensitivity (Raman and Bean, 1999; Womack and Khodakhah, 2002; Khaliq et al., 2003; Stocker, 2004). The absolute amplitude of the input resistance change was regrettably not quantified in these experiments. However, it is unlikely that an increase in input resistance alone is responsible for the increased excitably of the complex spike response to somatic conductance injection. Firstly, it is known that additional calcium and K_{Ca} conductances are recruited by Purkinje cell spiking, especially in rapid bursts (Edgerton and Reinhart, 2003; Swensen and Bean, 2003; McKay and Turner, 2004; Swensen and Bean, 2005; Walter et al., 2006). Further, our experiments found that the original complex spike patterns could not be restored by simply injecting smaller conductances, as might be expected if a higher input resistance caused only a greater voltage deflection in response to somatic EPSGs (data not shown). At similar initial firing frequencies, spike amplitudes were larger and the total duration of spiking was prolonged. This first observation was reflected in analyses of the spike height vs ISI (as in chapter 2), which still showed s-shaped relationships, but recovered more rapidly under $CdCl_2$. Both observations are consistent with the removal of spike activated K_{Ca} hyperpolarising currents. Curiously, the peak depth of the AHP following e.g. the first spike of the complex spike pattern was not greatly altered (a similar result was observed by Edgerton and Reinhart (2003)). Changes in AHPs of slower timecourses could not be easily quantified as they were accluded by the rapid spiking evoked under $CdCl_2$. There are several ways in which the source of the increased excitability of the complex spike under calcium channel block might be further investigated. Differences in channel activation could be investigated by voltage clamp, using either classical techniques or the 'spike clamp' method (Raman and Bean, 1999, 2001; Swensen and Bean, 2003, 2005). Additionally, alterations in the amplitude and time course conductances activated following spikes could be assessed using the recently described dynamic IV method (Badel et al., 2008). Dynamic clamp could also be

engaged further; the isolated effect of removing conductances of particular kinetics (e.g. BK, SK or P-type calcium conductances) could be mimicked (Lien and Jonas, 2003; Vervaeke et al., 2006), or the difference in input resistance under $CdCl_2$ compensated by injection of tonic baseline conductance.

Although these experiments do not tell us anything about the influence of dendritic spikes on somatic spiking (as dendritic spikes are not usually generated by somatic EPSG injection), they do highlight an additional route by which calcium spikes during the complex spike might, through the activation of K_{Ca} channels, effect the final output of the Purkinje cell.

I have demonstrated a new functional role for dendritic spikes in Purkinje cells: regulation of the pause in spiking following the complex spike. This pause is a well-known feature of the complex spike *in vivo* (Bloedel and Roberts, 1971; Latham and Paul, 1971; Sato et al., 1992), but its underlying mechanisms are unknown. My findings suggest that the calcium entry elicited by CF input-triggered dendritic spikes (Ross and Werman, 1987; Miyakawa et al., 1992) may activate calcium-dependent potassium conductances (Hounsgaard and Midtgaard, 1989; Rancz and Häusser, 2006) causing a prolonged pause before the resumption of spontaneous firing, analogous to the recently described pause in spiking triggered by strong parallel fibre input (Steuber et al., 2007). This is supported by the finding that disruption of calcium buffering in Purkinje cells (Schiffmann et al., 1999; Servais et al., 2005), or of calcium channel expression (Hoebeek et al., 2005), alters the post-complex spike pause duration.

The greatly reduced pause in the absence of dendritic calcium spikes (when the complex spike is evoked by somatic EPSG injection) is consistent with a much lower total K_{Ca} outward current, due to lack of dendritic channel activation. Similarly, the $CdCl_2$ block of any remaining calcium dependent conductances during somatic EPSG injection removed the hyperpolarisation that terminated the complex spike, causing it to flow, without pause, into repeated, full amplitude spikes. However, the increase in pause duration seen when comparing 0 to 1 dendritic calcium spikes (somatic conductance clamp vs CF stimulation evoking 1 dendritic spike) was less than the increase between 1 and 2 spikes (CF stimulation at threshold for generating an extra dendritic spike), and, further, a single dendritic spike does not always generate a large dendritic AHP (blue points in Fig. 3.14d; in fact in some cases, the minimum dendritic voltage during the pause was not less than baseline Vm). This may be due to a threshold (voltage and/or calcium concentration) for the activation of the conductances responsible for this AHP. If calcium spikes are not of sufficient amplitude or duration, the calcium influx and presumed subsequent K_{Ca} activation may not provide adequate outward current to arrest intrinsic simple spike generation, especially at high baseline firing frequencies (Fig. 3.11). The BK conductance, with its requirement for the depolarised voltages and high calcium concentrations (several μM, Womack and Khodakhah, 2002) evoked by strong calcium spike evoking stimuli (0.5 - 30 μM, Eilers et al., 1995; Maeda

et al., 1999), is well placed to create such a threshold. However, BK conductances close rapidly after depolarising events (Khaliq et al., 2003; Swensen and Bean, 2003) and the pause can last for 10s of ms. SK conductances show a more prolonged timecourse (~100 ms at room temperature, Cingolani et al., 2002, see also Swensen and Bean, 2003), and although they carry some resting current, the steepest part of their activation is expected to be at the concentrations seen following CF stimulation (EC_{50} of ~0.6 μM, Xia et al., 1998; Hirschberg et al., 1999; Stocker, 2004). It is possible that the two conductances act in consort to initiate and then prolong the pause. As both these conductances are altered in density by development (Muller et al., 1998; Cingolani et al., 2002), together with an increase in the calcium buffering of the cell (Fierro and Llano, 1996), the relative contribution of each conductance and the calcium influx required to generate the pause might differ with development. In order to understand the conductances responsible for the post-complex spike pause at each stage of development, careful pharmacological experiments are required, together with the characterisation of the post-complex spike change in somatic and dendritic conductances (e.g. using the dynamic IV method (Badel et al., 2008)), and accurate modelling of the Purkinje cell calcium current, intracellular calcium buffering and K_{Ca} channel activation.

The CF input's location in the dendrites is well placed to recruit the currents that create the post-complex spike pause. Firstly, the dendrites are isolated from fast action potential generation, allowing calcium spike generation. Further, the CFs distributed nature also ensures a large, global dendritic calcium response; similar dendritic spike waveforms are evoked simultaneously at electrically distant points on the main dendrites (Christensen, 2002) and calcium influx is seen across the cell (Ross and Werman, 1987; Miyakawa et al., 1992; Callaway et al., 1995; Eilers et al., 1995), aided by the distribution of P-type calcium channels in all compartments of the cell (Westenbroek et al., 1995). Calcium activated potassium channels (both BK and SK) are, however, concentrated in the main dendrites and soma (Knaus et al., 1996; Cingolani et al., 2002), well placed to react to CF input and complex spike generation. Their apparent lower concentration in finer dendrites raises the possibility that there might be some non-uniformity in the dendritic recruitment of conductances. There are indications that CF stimulated calcium concentrations may differ in the spiny branchlets (Miyakawa et al., 1992; Callaway et al., 1995; Eilers et al., 1995, though careful ratiometric studies are required) and the downstream physiological effect of CF evoked calcium spikes differs from that evoked by parallel fibre simulation or local current injection (Rancz and Hausser, 2006). To investigate if the spiny dendrites might play a different role in the generation of the pause, pharmacological agents could be applied specifically to the distal dendrites, where spiny dendrites predominate, or to the proximal dendrites, where the main dendrites are located.

I have found that the balance of currents following the complex spike is also modulated by the number of CF inputs stimulated. The greater the number of CF stimulations, the shorter the pause. Such a decrease in the length of the pause is likely to reflect the increase in excitatory current provided by further CF inputs. This decreasing trend continues until the point where further calcium spikes are added, when pause length is again increased. The duration of the pause thus reports the number of dendritic spikes triggered by CF input, both when a single CF input is triggered or during bursts of CF activation. The further modulation, by bursts of CF input, of both the pause length and the number of axonally propagated spikes in the complex spike (see Chapter 1) adds a further layer of information to the transmitted spiking pattern.

The pause is likely to be a potent signal to downstream DCN neurons, perhaps more so than the complex spike itself, which is often poorly propagated down the axon (Khaliq and Raman, 2005; Monsivais et al., 2005). The relief of DCN cells from persistent inhibition triggers rebound firing (Aizenman and Linden, 1999; Sekirnjak and du Lac, 2002; McKay et al., 2006), which is both a salient electrical signal and a trigger for plasticity at the DCN (Aizenman et al., 1998; Nelson et al., 2003; Pugh and Raman, 2006).

This new role for dendritic spikes in regulating the post-complex spike pause complements their already well-known role in triggering prominent dendritic calcium signals (Ross and Werman, 1987; Miyakawa et al., 1992). In particular, the calcium influx associated with CF-induced dendritic spikes can trigger LTD of CF input and plays an important role in short-term and long-term regulation of parallel fibre and inhibitory synaptic strength (Hansel et al., 2001; Brenowitz and Regehr, 2005). Further, CF stimulation also regulates intrinsic firing behaviours in ways likely to involve calcium influx, e.g. triggering bistability (Loewenstein et al., 2005; McKay et al., 2007) and modulating spontaneous firing rate and pattern (Colin et al., 1980; Cerminara and Rawson, 2004; McKay et al., 2007).

Thus, the finding that dendritic calcium spikes regulate Purkinje cell spiking, not during the complex spike, but during the post-complex spike pause, illuminates a mechanism linking the plasticity and the spiking output of the cerebellum.

General Discussion

Purkinje cell functional compartments

The work in this thesis suggests a new framework for considering the behaviour of the Purkinje cell following CF input. During complex spike generation the Purkinje cell is composed of (at least) 3 functional compartments; soma, axon and dendrites. The proximal axon initiates all spikelets (Davie et al., 2008), which propagate, with differing degrees of success, to the soma to form the distinctive, reproducible complex spike; the separation of these two compartments is required to explain the details of complex spikelet height and width. The dendrites, meanwhile, because of their relative electrical isolation from the soma and axon, are able to generate one or more calcium spikes in response to the CF input they receive. Backpropagating somatic action potentials fail to actively invade the dendrites (Stuart and Häusser, 1994), and dendritic calcium spikes propagate forwards poorly, having very little impact on burst generation in the axon and soma. Further functional compartments that might be considered are the distal axon, which selectively propagates only sufficiently fully formed spikelets of the complex spike (Clark et al., 2005; Khaliq and Raman, 2005), and potentially the many spiny branchlets which, though veiled by lack of direct patch-clamp recordings, have been shown by imaging studies to act separately, according to the concomitant parallel fibre or inhibitory input (Eccles et al., 1966d; Eccles et al., 1967; Callaway et al., 1995; Wang et al., 2000; Brenowitz and Regehr, 2005; Isope and Murphy, 2005; Rancz and Häusser, 2006).

During the post-complex spike pause, the soma, dendrites and axon become less functionally separated. The AHP promoted by dendritic calcium spikes is more effectively spread through the cell, probably because of its slower timecourse (Rall, 1967; Jack et al., 1983; Spruston et al., 1994; Roth and Häusser, 2001), and so contributes to the pause in axonally generated spontaneous spiking (Stuart and Häusser, 1994; Clark et al., 2005; Khaliq and Raman, 2006).

Simultaneous dendritic spike and somatic burst production

The transiently separated compartments of the Purkinje cell allow for two of its principal characteristics, rapid spike firing and dendritic calcium spike generation, to occur in parallel following CF input. This mirrors the role of CF input of providing both a timing signal for online motor control (Welsh and Llinas, 1997; Kitazawa et al., 1998) and an error signal enabling synaptic plasticity at parallel fibre and mossy fibre-DCN synapses (Gilbert and Thach, 1977; Gellman et al., 1985; Kitazawa et al., 1998; Pugh and Raman, 2006).

Dendritic calcium spikes are reliably generated by distributed CF input to the dendrites. The distributed EPSC readily charges the dendritic membrane above threshold, and the extensive branching and lack of sodium channels in the dendrites efficiently isolates both synaptic and active currents from the shunt associated with the Purkinje cell's specialized high-frequency firing mechanisms (Stuart and Häusser, 1994; Raman and Bean, 1999; Häusser et al., 2001). Where mechanisms for both calcium spike and sodium spike generation coexist in the same compartment, as in the soma, rapid spiking can prevent slower calcium spike generation: block of sodium channels with QX-314 reveals a somatic CF very similar to that of the dendrites (Christensen, 2002). The mutual isolation of the soma and dendrites also allows the number of dendritic calcium spikes – and the resulting downstream effects of dendritic activity following CF input – to be modulated by parallel fibre or inhibitory input without strongly influencing the burst pattern at the soma (Callaway et al., 1995). The slow electrical effect of dendritic spikes on the post-complex spike pause provides a link between excitability and plasticity in the Purkinje cell dendritic tree, the regulation of Purkinje cell output, and plasticity in its downstream DCN targets.

The axo-somatic complex spike burst is also highly reliably generated in response to CF input and linearly represents CF input strength. This linearity may be a reflection of the weak effect that dendritic calcium spikes (recruited by larger inputs in paired pulse depression experiments) have on the somatic complex spike. Alternatively, any small sublinearity that might be caused by reduced dendritic driving force for larger inputs, or increased conductance shunt, might be compensated for by the appearance of dendritic spikes. This small, but measurable effect of dendritic calcium spikes may also be the reason that some complex spikes were more accurately reproduced by somatic conductance clamp than others (see Chapter 2).

Although there is a clear linear relationship between input strength (either CF synaptic input or somatic EPSG injection) and the complex spike burst produced, there is some variability in these relationships, due to differences in the intrinsic excitability of the cells (Figs 1.15 and 2.6). One source of these difference is input resistance variability. Synaptic input to a cell of smaller input resistance would be expected to produce a smaller driving voltage for spike production, and so a complex spike burst of fewer spikes and lower frequency. Across the ages used in these studies (P12-24), input resistance is known to decrease, from 58-111 MΩ (depending on cell morphology) at P12, to 16 ± 1 MΩ after P18 (McKay and Turner, 2005). However, across a similar age range, intrinsic excitability is known to increase (McKay and Turner, 2005; Fry, 2006), due to changes in channel expression (e.g. increases in sodium channel density (Fry, 2006), see also Main Introduction). Changes in input resistance and channel expression may act in consort to maintain similar complex spike patterns across cells, but both may clearly contribute to differences in intrinsic excitability and complex spike pattern. Input resistance was not measured in these studies and could have been used, together with e.g. generation of steady state firing f-I curves, to help explain differences in

complex spikes seen across cells, both within age groups and across age groups. As discussed in Chapter 3, knowledge of input resistance could also aid understanding of the increased excitability under $CdCl_2$ application. Further, measurement of dendritic and somatic input resistance, their electrotonic transfer responses, and reconstruction of neuronal morphology could have increased understanding of dendritic spike propagation using neuronal modelling.

Reliable burst production

CF triggered complex spike burst generation occurs with a high safety factor. Mechanisms appear to be in place to maintain burst generation at hyperpolarised or depolarised membrane potentials, and at short inter-IO event intervals, where both the size of CF input and the number of stimuli in the CF burst are decreased (Dittman and Regehr, 1998; Hashimoto and Kano, 1998; Silver et al., 1998; Maruta et al., 2007). At the same time, the systematic, linear variation of the complex spike with input amplitude and number (and so input timing) appears capable of encoding some information other than the simple occurrence of CF input. As reliable, graded burst generation is not the inevitable outcome of a large input onto a high frequency firing cell, as demonstrated by e.g. the calyx of Held to MNTB neuron synapse, the potential role of the Purkinje cell complex spike burst in the cerebellar circuit should be considered.

Implications for cerebellar circuit behaviour

The neurons of the DCN receive convergent input from at least 30 Purkinje cells, mostly onto their somata (Chan-Palay, 1977). *In vivo*, even after considering the bisability of Purkinje cells (Loewenstein et al., 2005), the tonic spiking of multiple Purkinje cell inputs should lead to a tonic inhibitory input to the tonically spiking DCN. Thus, the only Purkinje cell signal available at the DCN to differentiate between spontaneous firing and CF input is the brevity of the ISI, and the variable occurrence of a post-complex spike pause. Therefore the reliable generation of a burst of Purkinje cell spikes is essential to convey CF occurrence. It would appear that the system is designed not to 'lose' CF signals, even when they occur at brief intervals or in weakly excitable Purkinje cells with small CF inputs.

The graded nature of the somatic complex spike and the propagated axonal signal with CF input size and the number of CF inputs in a burst (this thesis and Khaliq and Raman, 2005), both of which increase with inter-CF event interval (Dittman and Regehr, 1998; Hashimoto and Kano, 1998; Silver et al., 1998; Maruta et al., 2007), may serve to 'downplay' the importance of CF signals generated at brief intervals. Both reduced input number and reduced interspike interval may make short-interval CF input a less salient signal. This would tend to damp any oscillation set up in the olivo-cerebellar loop (see Introduction and Kistler

and De Zeeuw, 2003), especially within groups of synchronously activated, so perhaps synchronously depressed Purkinje cells that converge onto similar areas of the DCN. As aberrant repeated CF activation, due partially to reverberant IO activation, is associated with the poorly timed motor learning exhibited by connexin-36 knockout mice (Van Der Giessen et al., 2008), this dampening could serve as a safety mechanism. Similarly, the voltage dependence of complex spike pattern may serve as a feedback mechanism to help control the average level of IO input to the cerebellar cortex; the reduced excitability of Purkinje cells due to increased levels of CF input (Colin et al., 1980; Cerminara and Rawson, 2004; McKay et al., 2007) should result in fewer spikelets in the complex spike and thus less recurrent input to the IO. More importantly, both the voltage and timing dependence of the complex spike is likely to result in a similar dependence of the motor output signal of the DCN. This could help damp the tendency of the olivocerebellar system to produce motor tremor, both physiological and harmaline induced (Llinas and Volkind, 1973).

The effect of post-complex spike pause modulation on the DCN is easier to envisage. Although the timing, amplitude and duration of inhibitory input to the DCN influences the strength of the rebound burst that follows (Aizenman and Linden, 1999; Sekirnjak and du Lac, 2002), the expression of increased DCN firing should be strictly controlled by the duration of any post-complex spike pause. The power of this burst-pause signal will be greatly enhanced by the synchronous convergence of multiple Purkinje cell inputs (Chan-Palay, 1977). The anatomy of the olivocerebellar loop gives CF input a distinct advantage, in this respect, over the burst-pause sequence that can be generated by strong parallel fibre input to the Purkinje cell (Steuber et al., 2007). As dendritic calcium spike generation is more labile than complex spike burst generation, and the post-complex spike pause is likely to be influenced by both intrinsic Purkinje cell properties and cortical inhibitory input (Murphy and Sabah, 1970; Bloedel and Roberts, 1971; Sato et al., 1992; Barmack and Yakhnitsa, 2008) its potential to encode the general excitatory state of the cerebellar cortex is greater. The occurrence of the post-complex spike pause in a large proportion of the Purkinje cells converging on a DCN neuron would produce a greatly more salient signal both for spiking output and motor control and for plasticity in the DCN (Aizenman et al., 1998; Nelson et al., 2003; Pugh and Raman, 2006).

The only way to be sure of the effect of complex spike like patterns of input to the DCN is to test it. The effect of paired pulse depression of the Purkinje cell to DCN synapse (Telgkamp and Raman, 2002), of relative contribution of IPSP conductance shunt or hyperpolarisation following temporally clustered input, the importance of spike timing and reproducibility of input to the spiking pattern produced etc cannot be entirely predicted given current data. Further, the effect of IO excitatory input, which should occur shortly before complex spike inhibitory input (as it arises from CF axon collaterals thought to project topographically to the appropriate DCN area (Ruigrok, 1997)), is also not clear (though see McDevitt et al., 1987; Rowland and Jaeger, 2008). It is also likely that there are a variety of responses to such input

displayed by the heterogeneous populations of DCN neurons, which include both feedback inhibitory outputs and feedforward excitatory outputs, as well as local interneurons (Sekirnjak and du Lac, 2002; Aizenman et al., 2003; Sekirnjak et al., 2003; McKay et al., 2006; Molineux et al., 2006; Gittis and du Lac, 2007, 2008). These parameters could be explored in slice, perhaps more easily with artificial somatic conductance or current injections that with extracellular stimulation, as the appropriate axons are hard to isolate in the more amorphous DCN structure. In short, in order to get one further step closer understanding to the motor output of the cerebellum, the input-output function of the neurons one further step closer to the motor system must be characterised.

References:

Achard P, De Schutter E (2006) Complex parameter landscape for a complex neuron model. PLoS Comput Biol 2:e94.

Ahlijanian MK, Westenbroek RE, Catterall WA (1990) Subunit structure and localization of dihydropyridine-sensitive calcium channels in mammalian brain, spinal cord, and retina. Neuron 4:819-832.

Aizenman CD, Linden DJ (1999) Regulation of the rebound depolarization and spontaneous firing patterns of deep nuclear neurons in slices of rat cerebellum. J Neurophysiol 82:1697-1709.

Aizenman CD, Manis PB, Linden DJ (1998) Polarity of long-term synaptic gain change is related to postsynaptic spike firing at a cerebellar inhibitory synapse. Neuron 21:827-835.

Aizenman CD, Huang EJ, Linden DJ (2003) Morphological correlates of intrinsic electrical excitability in neurons of the deep cerebellar nuclei. J Neurophysiol 89:1738-1747.

Akemann W, Knopfel T (2006) Interaction of Kv3 potassium channels and resurgent sodium current influences the rate of spontaneous firing of Purkinje neurons. J Neurosci 26:4602-4612.

Albus JS (1971) A theory of cerebellar function. Math Biosci 10:25-61.

Altman J (1972) Postnatal development of the cerebellar cortex in the rat. II. Phases in the maturation of Purkinje cells and of the molecular layer. J Comp Neurol 145:399-463.

Andersson G, Armstrong DM (1987) Complex spikes in Purkinje cells in the lateral vermis (b zone) of the cat cerebellum during locomotion. J Physiol 385:107-134.

Angelo K, London M, Christensen SR, Häusser M (2007) Local and global effects of I(h) distribution in dendrites of mammalian neurons. J Neurosci 27:8643-8653.

Ariav G, Polsky A, Schiller J (2003) Submillisecond precision of the input-output transformation function mediated by fast sodium dendritic spikes in basal dendrites of CA1 pyramidal neurons. J Neurosci 23:7750-7758.

Armstrong BD, Harvey RJ (1966) Responses in the inferior olive to stimulation of the cerebellar and cerebral cortices in the cat. J Physiol 187:553-574.

Armstrong DM, Rawson JA (1979) Activity patterns of cerebellar cortical neurones and climbing fibre afferents in the awake cat. J Physiol 289:425-448.

Armstrong DM, Eccles JC, Harvey RJ, Matthews PB (1968) Responses in the dorsal accessory olive of the cat to stimulation of hind limb afferents. J Physiol 194:125-145.

Attwell PJ, Ivarsson M, Millar L, Yeo CH (2002) Cerebellar mechanisms in eyeblink conditioning. Ann N Y Acad Sci 978:79-92.

Atwood HL, Stevens JK, Marin L (1984) Axoaxonal synapse location and consequences for presynaptic inhibition in crustacean motor axon terminals. J Comp Neurol 225:64-74.

Auger C, Attwell D (2000) Fast removal of synaptic glutamate by postsynaptic transporters. Neuron 28:547-558.

Badel L, Lefort S, Brette R, Petersen CC, Gerstner W, Richardson MJ (2008) Dynamic I-V curves are reliable predictors of naturalistic pyramidal-neuron voltage traces. J Neurophysiol 99:656-666.

Baker MR, Edgley SA (2006) Non-uniform olivocerebellar conduction time in the vermis of the rat cerebellum. J Physiol 570:501-506.

Baranauskas G, Martina M (2006) Sodium currents activate without a Hodgkin-and-Huxley-type delay in central mammalian neurons. J Neurosci 26:671-684.

Barbour B, Keller BU, Llano I, Marty A (1994) Prolonged presence of glutamate during excitatory synaptic transmission to cerebellar Purkinje cells. Neuron 12:1331-1343.

Barmack NH, Yakhnitsa V (2008) Functions of interneurons in mouse cerebellum. J Neurosci 28:1140-1152.

Baude A, Molnar E, Latawiec D, McIlhinney RA, Somogyi P (1994) Synaptic and nonsynaptic localization of the GluR1 subunit of the AMPA-type excitatory amino acid receptor in the rat cerebellum. J Neurosci 14:2830-2843.

Bekkers JM, Häusser M (2007) Targeted dendrotomy reveals active and passive contributions of the dendritic tree to synaptic integration and neuronal output. Proc Natl Acad Sci U S A 104:11447-11452.

Bell CC, Grimm RJ (1969) Discharge properties of Purkinje cells recorded on single and double microelectrodes. J Neurophysiol 32:1044-1055.

Bengtsson F, Hesslow G (2006) Cerebellar control of the inferior olive. Cerebellum 5:7-14.

Berger T, Larkum ME, Luscher HR (2001) High I(h) channel density in the distal apical dendrite of layer V pyramidal cells increases bidirectional attenuation of EPSPs. J Neurophysiol 85:855-868.

Bergles DE, Dzubay JA, Jahr CE (1997) Glutamate transporter currents in bergmann glial cells follow the time course of extrasynaptic glutamate. Proc Natl Acad Sci U S A 94:14821-14825.

Bergmann M, Fox PA, Grabs D, Post A, Schilling K (1996) Expression and subcellular distribution of glutamate receptor subunits 2/3 in the developing cerebellar cortex. J Neurosci Res 43:78-86.

Berry M, Bradley P (1976) The growth of the dendritic trees of Purkinje cells in the cerebellum of the rat. Brain Res 112:1-35.

Betz WJ (1970) Depression of transmitter release at the neuromuscular junction of the frog. J Physiol 206:629-644.

Bland JM, Kerry SM (1998) Statistics notes. Weighted comparison of means. Bmj 316:129.

Blenkinsop TA, Lang EJ (2006) Block of inferior olive gap junctional coupling decreases Purkinje cell complex spike synchrony and rhythmicity. J Neurosci 26:1739-1748.

Bloedel JR, Roberts WJ (1971) Action of climbing fibers in cerebellar cortex of the cat. J Neurophysiol 34:17-31.

Bloedel JR, Bracha V (1998) Current concepts of climbing fiber function. Anat Rec 253:118-126.

Boiko T, Van Wart A, Caldwell JH, Levinson SR, Trimmer JS, Matthews G (2003) Functional specialization of the axon initial segment by isoform-specific sodium channel targeting. J Neurosci 23:2306-2313.

Borst JG, Helmchen F, Sakmann B (1995) Pre- and postsynaptic whole-cell recordings in the medial nucleus of the trapezoid body of the rat. J Physiol 489 (Pt 3):825-840.

Bower JM, Beeman D (1998) The book of GENESIS: exploring realistic neural models with the GEneral NEural SImulation System. New York: Springer-Verlag.

Bowie D, Mayer ML (1995) Inward rectification of both AMPA and kainate subtype glutamate receptors generated by polyamine-mediated ion channel block. Neuron 15:453-462.

Braitenberg V (1961) Functional interpretation of cerebellar histology. Nature 190:539-540.

Brasnjo G, Otis TS (2004) Isolation of glutamate transport-coupled charge flux and estimation of glutamate uptake at the climbing fiber-Purkinje cell synapse. Proc Natl Acad Sci U S A 101:6273-6278.

Brenowitz S, Trussell LO (2001) Maturation of synaptic transmission at end-bulb synapses of the cochlear nucleus. J Neurosci 21:9487-9498.

Brenowitz SD, Regehr WG (2005) Associative short-term synaptic plasticity mediated by endocannabinoids. Neuron 45:419-431.

Brew HM, Forsythe ID (1995) Two voltage-dependent K+ conductances with complementary functions in postsynaptic integration at a central auditory synapse. J Neurosci 15:8011-8022.

Brew HM, Hallows JL, Tempel BL (2003) Hyperexcitability and reduced low threshold potassium currents in auditory neurons of mice lacking the channel subunit Kv1.1. J Physiol 548:1-20.

Brorson JR, Zhang Z, Vandenberghe W (1999) Ca(2+) permeation of AMPA receptors in cerebellar neurons expressing glu receptor 2. J Neurosci 19:9149-9159.

Brunel N, Hakim V, Isope P, Nadal JP, Barbour B (2004) Optimal information storage and the distribution of synaptic weights: perceptron versus Purkinje cell. Neuron 43:745-757.

Cai X, Liang CW, Muralidharan S, Kao JP, Tang CM, Thompson SM (2004) Unique roles of SK and Kv4.2 potassium channels in dendritic integration. Neuron 44:351-364.

Callaway JC, Ross WN (1997) Spatial distribution of synaptically activated sodium concentration changes in cerebellar Purkinje neurons. J Neurophysiol 77:145-152.

Callaway JC, Lasser-Ross N, Ross WN (1995) IPSPs strongly inhibit climbing fiber-activated [Ca2+]i increases in the dendrites of cerebellar Purkinje neurons. J Neurosci 15:2777-2787.

Calvin WH, Hellerstein D (1969) Dendritic spikes versus cable properties. Science 163:96-97.

Campbell NC, Hesslow G (1986a) The secondary spikes of climbing fibre responses recorded from Purkinje cell somata in cat cerebellum. J Physiol 377:207-224.

Campbell NC, Hesslow G (1986b) The secondary spikes of climbing fibre responses recorded from Purkinje cell axons in cat cerebellum. J Physiol 377:225-235.

Cash S, Yuste R (1998) Input summation by cultured pyramidal neurons is linear and position-independent. J Neurosci 18:10-15.

Cash S, Yuste R (1999) Linear summation of excitatory inputs by CA1 pyramidal neurons. Neuron 22:383-394.

Cavelier P, Pouille F, Desplantez T, Beekenkamp H, Bossu JL (2002a) Control of the propagation of dendritic low-threshold Ca(2+) spikes in Purkinje cells from rat cerebellar slice cultures. J Physiol 540:57-72.

Cavelier P, Beekenkamp H, Shin HS, Jun K, Bossu JL (2002b) Cerebellar slice cultures from mice lacking the P/Q calcium channel: electroresponsiveness of Purkinje cells. Neurosci Lett 333:64-68.

Cerminara NL, Rawson JA (2004) Evidence that climbing fibers control an intrinsic spike generator in cerebellar Purkinje cells. J Neurosci 24:4510-4517.

Chan CY, Hounsgaard J, Midtgaard J (1989) Excitatory synaptic responses in turtle cerebellar Purkinje cells. J Physiol 409:143-156.

Chan-Palay V (1971) The recurrent collaterals of Purkinje cell axons: a correlated study of the rat's cerebellar cortex with electron microscopy and the Golgi method. Z Anat Entwicklungsgesch 134:200-234.

Chan-Palay V (1977) Cerebellar dentate nucleus. Organization, cytology, and transmitters. Berlin: Springer.

Chance FS, Abbott LF, Reyes AD (2002) Gain modulation from background synaptic input. Neuron 35:773-782.

Chaudhry FA, Lehre KP, van Lookeren Campagne M, Ottersen OP, Danbolt NC, Storm-Mathisen J (1995) Glutamate transporters in glial plasma membranes: highly differentiated localizations revealed by quantitative ultrastructural immunocytochemistry. Neuron 15:711-720.

Chaudhuri D, Alseikhan BA, Chang SY, Soong TW, Yue DT (2005) Developmental activation of calmodulin-dependent facilitation of cerebellar P-type Ca2+ current. J Neurosci 25:8282-8294.

Chaudhuri D, Chang SY, DeMaria CD, Alvania RS, Soong TW, Yue DT (2004) Alternative splicing as a molecular switch for Ca2+/calmodulin-dependent facilitation of P/Q-type Ca2+ channels. J Neurosci 24:6334-6342.

Chen WR, Midtgaard J, Shepherd GM (1997) Forward and backward propagation of dendritic impulses and their synaptic control in mitral cells. Science 278:463-467.

Chedotal A, Sotelo C (1992) Early Development of Olivocerebellar Projections in the Fetal Rat Using CGRP Immunocytochemistry. Eur J Neurosci 4:1159-1179.

Christensen SR (2002) Synaptic integration and dendritic excitability in cerebellar Purkinje neurons. In. London: University College London.

Christie JM, Westbrook GL (2003) Regulation of backpropagating action potentials in mitral cell lateral dendrites by A-type potassium currents. J Neurophysiol 89:2466-2472.

Chung SH, Lee KY, Kim KH, Kim CT, Lee NS, Sawada K, Haga H, Lee BC, Fukui Y, Rhee MH, Jeong YG (2002) Immunohistochemistry of voltage-gated calcium channel alpha1B subunit in mouse cerebellum. J Vet Sci 3:175-178.

Chung YH, Kim HS, Shin CM, Kim MJ, Cha CI (2001) Immunohistochemical study on the distribution of voltage-gated K(+) channels in rat brain following transient focal ischemia. Neurosci Lett 308:157-160.

Cingolani LA, Gymnopoulos M, Boccaccio A, Stocker M, Pedarzani P (2002) Developmental regulation of small-conductance Ca2+-activated K+ channel expression and function in rat Purkinje neurons. J Neurosci 22:4456-4467.

Clark BA, Barbour B (1997) Currents evoked in Bergmann glial cells by parallel fibre stimulation in rat cerebellar slices. J Physiol 502 (Pt 2):335-350.

Clark BA, Monsivais P, Branco T, London M, Häusser M (2005) The site of action potential initiation in cerebellar Purkinje neurons. Nat Neurosci 8:137-139.

Coetzee WA, Amarillo Y, Chiu J, Chow A, Lau D, McCormack T, Moreno H, Nadal MS, Ozaita A, Pountney D, Saganich M, Vega-Saenz de Miera E, Rudy B (1999) Molecular diversity of K+ channels. Ann N Y Acad Sci 868:233-285.

Cohen CJ, Bean BP, Tsien RW (1984) Maximal upstroke velocity as an index of available sodium conductance. Comparison of maximal upstroke velocity and voltage clamp measurements of sodium current in rabbit Purkinje fibers. Circ Res 54:636-651.

Colbert CM, Johnston D (1996) Axonal action-potential initiation and Na+ channel densities in the soma and axon initial segment of subicular pyramidal neurons. J Neurosci 16:6676-6686.

Colbert CM, Pan E (2002) Ion channel properties underlying axonal action potential initiation in pyramidal neurons. Nat Neurosci 5:533-538.

Colbert CM, Magee JC, Hoffman DA, Johnston D (1997) Slow recovery from inactivation of Na+ channels underlies the activity-dependent attenuation of dendritic action potentials in hippocampal CA1 pyramidal neurons. J Neurosci 17:6512-6521.

Colin F, Manil J, Desclin JC (1980) The olivocerebellar system. I. Delayed and slow inhibitory effects: an overlooked salient feature of cerebellar climbing fibers. Brain Res 187:3-27.

Coombs JS, Curtis DR, Eccles JC (1957a) The generation of impulses in motoneurones. J Physiol 139:232-249.

Coombs JS, Curtis DR, Eccles JC (1957b) The interpretation of spike potentials of motoneurones. J Physiol 139:198-231.

Crepel F (1971) Maturation of climbing fiber responses in the rat. Brain Res 35:272-276.

Crepel F (1974) Excitatory and inhibitory processes acting upon cerebellar Purkinje cells during maturation in the rat; influence of hypothyroidism. Exp Brain Res 20:403-420.

Crepel F, Penit-Soria J (1986) Inward rectification and low threshold calcium conductance in rat cerebellar Purkinje cells. An in vitro study. J Physiol 372:1-23.

Crepel F, Dhanjal SS, Garthwaite J (1981) Morphological and electrophysiological characteristics of rat cerebellar slices maintained in vitro. J Physiol 316:127-138.

Crill WE, Kennedy TT (1967) Inferior olive of the cat: intracellular recording. Science 157:716-718.

Davie JT, Clark BA, Häusser M (2008) The origin of the complex spike in cerebellar Purkinje cells. J Neurosci 28:7599-7609.

Davie JT, Kole MH, Letzkus JJ, Rancz EA, Spruston N, Stuart GJ, Häusser M (2006) Dendritic patch-clamp recording. Nat Protoc 1:1235-1247.

Davison IG, Boyd JD, Delaney KR (2004) Dopamine inhibits mitral/tufted--> granule cell synapses in the frog olfactory bulb. J Neurosci 24:8057-8067.

de Ruiter MM, De Zeeuw CI, Hansel C (2006) Voltage-gated sodium channels in cerebellar Purkinje cells of mormyrid fish. J Neurophysiol 96:378-390.

De Schutter E, Bower JM (1994a) An active membrane model of the cerebellar Purkinje cell II. Simulation of synaptic responses. J Neurophysiol 71:401-419.

De Schutter E, Bower JM (1994b) Simulated responses of cerebellar Purkinje cells are independent of the dendritic location of granule cell synaptic inputs. Proc Natl Acad Sci U S A 91:4736-4740.

De Schutter E, Bower JM (1994c) An active membrane model of the cerebellar Purkinje cell. I. Simulation of current clamps in slice. J Neurophysiol 71:375-400.

De Zeeuw CI, Simpson JI, Hoogenraad CC, Galjart N, Koekkoek SK, Ruigrok TJ (1998) Microcircuitry and function of the inferior olive. Trends Neurosci 21:391-400.

De Zeeuw CI, Chorev E, Devor A, Manor Y, Van Der Giessen RS, De Jeu MT, Hoogenraad CC, Bijman J, Ruigrok TJ, French P, Jaarsma D, Kistler WM, Meier C, Petrasch-Parwez E, Dermietzel R, Sohl G, Gueldenagel M, Willecke K, Yarom Y (2003) Deformation of network connectivity in the inferior olive of connexin 36-deficient mice is compensated by morphological and electrophysiological changes at the single neuron level. J Neurosci 23:4700-4711.

Dean I, Robertson SJ, Edwards FA (2003) Serotonin drives a novel GABAergic synaptic current recorded in rat cerebellar purkinje cells: a Lugaro cell to Purkinje cell synapse. J Neurosci 23:4457-4469.

Dean I, Harper NS, McAlpine D (2005) Neural population coding of sound level adapts to stimulus statistics. Nat Neurosci 8:1684-1689.

Desai NS, Rutherford LC, Turrigiano GG (1999) Plasticity in the intrinsic excitability of cortical pyramidal neurons. Nat Neurosci 2:515-520.

Deschenes M, Paradis M, Roy JP, Steriade M (1984) Electrophysiology of neurons of lateral thalamic nuclei in cat: resting properties and burst discharges. J Neurophysiol 51:1196-1219.

Destexhe A, Rudolph M, Pare D (2003) The high-conductance state of neocortical neurons in vivo. Nat Rev Neurosci 4:739-751.

Devor A (2002) The great gate: control of sensory information flow to the cerebellum. Cerebellum 1:27-34.

Devor A, Yarom Y (2002a) Generation and propagation of subthreshold waves in a network of inferior olivary neurons. J Neurophysiol 87:3059-3069.

Devor A, Yarom Y (2002b) Electrotonic coupling in the inferior olivary nucleus revealed by simultaneous double patch recordings. J Neurophysiol 87:3048-3058.

Diana MA, Otsu Y, Maton G, Collin T, Chat M, Dieudonne S (2007) T-type and L-type Ca2+ conductances define and encode the bimodal firing pattern of vestibulocerebellar unipolar brush cells. J Neurosci 27:3823-3838.

DiGregorio DA, Rothman JS, Nielsen TA, Silver RA (2007) Desensitization properties of AMPA receptors at the cerebellar mossy fiber granule cell synapse. J Neurosci 27:8344-8357.

Dittman JS, Regehr WG (1998) Calcium dependence and recovery kinetics of presynaptic depression at the climbing fiber to Purkinje cell synapse. J Neurosci 18:6147-6162.

Dittman JS, Kreitzer AC, Regehr WG (2000) Interplay between facilitation, depression, and residual calcium at three presynaptic terminals. J Neurosci 20:1374-1385.

Do MT, Bean BP (2003) Subthreshold sodium currents and pacemaking of subthalamic neurons: modulation by slow inactivation. Neuron 39:109-120.

Dodge FA, Cooley JW (1973) Action Potential of Motor-Neuron. Ibm Journal of Research and Development 17:219-229.

Dodson PD, Barker MC, Forsythe ID (2002) Two heteromeric Kv1 potassium channels differentially regulate action potential firing. J Neurosci 22:6953-6961.

Doiron B, Laing C, Longtin A, Maler L (2002) Ghostbursting: a novel neuronal burst mechanism. J Comput Neurosci 12:5-25.

Dolphin AC (2006) A short history of voltage-gated calcium channels. Br J Pharmacol 147 Suppl 1:S56-62.

Donato R, Page KM, Koch D, Nieto-Rostro M, Foucault I, Davies A, Wilkinson T, Rees M, Edwards FA, Dolphin AC (2006) The ducky(2J) mutation in Cacna2d2 results in reduced spontaneous Purkinje cell activity and altered gene expression. J Neurosci 26:12576-12586.

Dzubay JA, Otis TS (2002) Climbing fiber activation of metabotropic glutamate receptors on cerebellar purkinje neurons. Neuron 36:1159-1167.

Eccles J, Llinas R, Sasaki K (1964) Excitation of Cerebellar Purkinje Cells by the Climbing Fibres. Nature 203:245-246.

Eccles JC, Llinas R, Sasaki K (1966a) The excitatory synaptic action of climbing fibres on the purinje cells of the cerebellum. J Physiol 182:268-296.

Eccles JC, Llinas R, Sasaki K (1966b) The action of antidromic impulses on the cerebellar Purkinje cells. J Physiol 182:316-345.

Eccles JC, Llinas R, Sasaki K (1966c) Intracellularly recorded responses of the cerebellar Purkinje cells. Exp Brain Res 1:161-183.

Eccles JC, Ito M, Szenthagothai J (1967) The cerebellum as a neuronal machine. Berlin Heidelberg New York: Springer-Verlag.

Eccles JC, Llinas R, Sasaki K, Voorhoeve PE (1966d) Interaction experiments on the responses evoked in Purkinje cells by climbing fibres. J Physiol 182:297-315.

Edgerton JR, Reinhart PH (2003) Distinct contributions of small and large conductance Ca2+-activated K+ channels to rat Purkinje neuron function. J Physiol 548:53-69.

Eilers J, Callewaert G, Armstrong C, Konnerth A (1995) Calcium signaling in a narrow somatic submembrane shell during synaptic activity in cerebellar Purkinje neurons. Proc Natl Acad Sci U S A 92:10272-10276.

Ekerot CF, Oscarsson O (1981) Prolonged depolarization elicited in Purkinje cell dendrites by climbing fibre impulses in the cat. J Physiol 318:207-221.

Engel D, Jonas P (2005) Presynaptic action potential amplification by voltage-gated Na+ channels in hippocampal mossy fiber boutons. Neuron 45:405-417.

Farrant M, Cull-Candy SG (1991) Excitatory amino acid receptor-channels in Purkinje cells in thin cerebellar slices. Proc Biol Sci 244:179-184.

Felts PA, Yokoyama S, Dib-Hajj S, Black JA, Waxman SG (1997) Sodium channel alpha-subunit mRNAs I, II, III, NaG, Na6 and hNE (PN1): different expression patterns in developing rat nervous system. Brain Res Mol Brain Res 45:71-82.

Fernandez FR, Engbers JD, Turner RW (2007) Firing dynamics of cerebellar purkinje cells. J Neurophysiol 98:278-294.

Fernandez FR, Mehaffey WH, Molineux ML, Turner RW (2005) High-threshold K+ current increases gain by offsetting a frequency-dependent increase in low-threshold K+ current. J Neurosci 25:363-371.

Fierro L, Llano I (1996) High endogenous calcium buffering in Purkinje cells from rat cerebellar slices. J Physiol 496 (Pt 3):617-625.

Flourens P (1824) *Recherches experimentales sur les proprietes et les fonctions du systeme nerveux dans les animaux vertebres*. Arch Gen Med 2:321-370.

Foster KA, Regehr WG (2004) Variance-mean analysis in the presence of a rapid antagonist indicates vesicle depletion underlies depression at the climbing fiber synapse. Neuron 43:119-131.

Foster KA, Kreitzer AC, Regehr WG (2002) Interaction of postsynaptic receptor saturation with presynaptic mechanisms produces a reliable synapse. Neuron 36:1115-1126.

Frelin C, Cognard C, Vigne P, Lazdunski M (1986) Tetrodotoxin-sensitive and tetrodotoxin-resistant Na+ channels differ in their sensitivity to Cd2+ and Zn2+. Eur J Pharmacol 122:245-250.

Fry M (2006) Developmental expression of Na+ currents in mouse Purkinje neurons. Eur J Neurosci 24:2557-2566.

Fujita Y (1968) Activity of dendrites of single Purkinje cells and its relationship to so-called inactivation response in rabbit cerebellum. J Neurophysiol 31:131-141.

Fuortes MG, Frank K, Becker MC (1957) Steps in the production of motoneuron spikes. J Gen Physiol 40:735-752.

Gasparini S, Magee JC (2006) State-dependent dendritic computation in hippocampal CA1 pyramidal neurons. J Neurosci 26:2088-2100.

Gasparini S, Migliore M, Magee JC (2004) On the initiation and propagation of dendritic spikes in CA1 pyramidal neurons. J Neurosci 24:11046-11056.

Geiger JR, Bischofberger J, Vida I, Frobe U, Pfitzinger S, Weber HJ, Haverkampf K, Jonas P (2002) Patch-clamp recording in brain slices with improved slicer technology. Pflugers Arch 443:491-501.

Gellman R, Gibson AR, Houk JC (1985) Inferior olivary neurons in the awake cat: detection of contact and passive body displacement. J Neurophysiol 54:40-60.

Gentet LJ, Williams SR (2007) Dopamine gates action potential backpropagation in midbrain dopaminergic neurons. J Neurosci 27:1892-1901.

Gibb AJ, Edwards FA (1994) Patch clamp recording in sliced tissue preparations. In: Microelectrode Techniques. The Plymouth Workshop Handbook (Ogden D, ed), pp 255-274. Cambridge, UK: The Company of Biologists Ltd.

Gilbert PF, Thach WT (1977) Purkinje cell activity during motor learning. Brain Res 128:309-328.

Gittelman JX, Tempel BL (2006) Kv1.1-containing channels are critical for temporal precision during spike initiation. J Neurophysiol 96:1203-1214.

Gittis AH, du Lac S (2007) Firing properties of GABAergic versus non-GABAergic vestibular nucleus neurons conferred by a differential balance of potassium currents. J Neurophysiol 97:3986-3996.

Gittis AH, du Lac S (2008) Similar properties of transient, persistent, and resurgent Na currents in GABAergic and non-GABAergic vestibular nucleus neurons. J Neurophysiol 99:2060-2065.

Golding NL, Spruston N (1998) Dendritic sodium spikes are variable triggers of axonal action potentials in hippocampal CA1 pyramidal neurons. Neuron 21:1189-1200.

Golding NL, Jung HY, Mickus T, Spruston N (1999) Dendritic calcium spike initiation and repolarization are controlled by distinct potassium channel subtypes in CA1 pyramidal neurons. J Neurosci 19:8789-8798.

Goldman MS, Golowasch J, Marder E, Abbott LF (2000) Dependence of firing pattern on intrinsic ionic conductances: Sensitive and insensitive combinations. Neurocomputing 32:141-146.

Goldman-Wohl DS, Chan E, Baird D, Heintz N (1994) Kv3.3b: a novel Shaw type potassium channel expressed in terminally differentiated cerebellar Purkinje cells and deep cerebellar nuclei. J Neurosci 14:511-522.

Goldstein SS, Rall W (1974) Changes of action potential shape and velocity for changing core conductor geometry. Biophys J 14:731-757.

Grammer K (1993) 5-Alpha-Androst-16en-3-Alpha-on - a Male Pheromone - a Brief Report. Ethology and Sociobiology 14:201-207.

Granit R, Phillips CG (1956) Excitatory and inhibitory processes acting upon individual Purkinje cells of the cerebellum in cats. J Physiol 133:520-547.

Grieco TM, Raman IM (2004) Production of resurgent current in NaV1.6-null Purkinje neurons by slowing sodium channel inactivation with beta-pompilidotoxin. J Neurosci 24:35-42.

Grieco TM, Afshari FS, Raman IM (2002) A role for phosphorylation in the maintenance of resurgent sodium current in cerebellar purkinje neurons. J Neurosci 22:3100-3107.

Grieco TM, Malhotra JD, Chen C, Isom LL, Raman IM (2005) Open-channel block by the cytoplasmic tail of sodium channel beta4 as a mechanism for resurgent sodium current. Neuron 45:233-244.

Gruol DL, Jacquin T, Yool AJ (1991) Single-channel K+ currents recorded from the somatic and dendritic regions of cerebellar Purkinje neurons in culture. J Neurosci 11:1002-1015.

Gruol DL, Netzeband JG, Schneeloch J, Gullette CE (2006) L-type Ca2+ channels contribute to current-evoked spike firing and associated Ca2+ signals in cerebellar Purkinje neurons. Cerebellum 5:146-154.

Gulledge AT, Kampa BM, Stuart GJ (2005) Synaptic integration in dendritic trees. J Neurobiol 64:75-90.

Haghdoust H, Janahmadi M, Behzadi G (2007) Physiological role of dendrotoxin-sensitive K+ channels in the rat cerebellar Purkinje neurons. Physiol Res 56:807-813.

Hansel C, Linden DJ (2000) Long-term depression of the cerebellar climbing fiber--Purkinje neuron synapse. Neuron 26:473-482.

Hansel C, Linden DJ, D'Angelo E (2001) Beyond parallel fiber LTD: the diversity of synaptic and non-synaptic plasticity in the cerebellum. Nat Neurosci 4:467-475.

Harrison J, Jahr CE (2003) Receptor occupancy limits synaptic depression at climbing fiber synapses. J Neurosci 23:377-383.

Hashimoto K, Kano M (1998) Presynaptic origin of paired-pulse depression at climbing fibre-Purkinje cell synapses in the rat cerebellum. J Physiol 506 (Pt 2):391-405.

Hashimoto K, Kano M (2003) Functional differentiation of multiple climbing fiber inputs during synapse elimination in the developing cerebellum. Neuron 38:785-796.

Hashimoto K, Kano M (2005) Postnatal development and synapse elimination of climbing fiber to Purkinje cell projection in the cerebellum. Neurosci Res 53:221-228.

Hatten ME, Heintz N (1995) Mechanisms of neural patterning and specification in the developing cerebellum. Annu Rev Neurosci 18:385-408.

Häusser M, Roth A (1997a) Estimating the time course of the excitatory synaptic conductance in neocortical pyramidal cells using a novel voltage jump method. J Neurosci 17:7606-7625.

Häusser M, Roth A (1997b) Dendritic and somatic glutamate receptor channels in rat cerebellar Purkinje cells. J Physiol 501 (Pt 1):77-95.

Häusser M, Clark BA (1997) Tonic synaptic inhibition modulates neuronal output pattern and spatiotemporal synaptic integration. Neuron 19:665-678.

Häusser M, Mel B (2003) Dendrites: bug or feature? Curr Opin Neurobiol 13:372-383.

Häusser M, Spruston N, Stuart GJ (2000) Diversity and dynamics of dendritic signaling. Science 290:739-744.

Häusser M, Major G, Stuart GJ (2001) Differential shunting of EPSPs by action potentials. Science 291:138-141.

Higashima M, Kinoshita H, Koshino Y (1998) Contribution of T-type calcium channels to afterdischarge generation in rat hippocampal slices. Brain Res 781:127-134.

Hirschberg B, Maylie J, Adelman JP, Marrion NV (1999) Gating properties of single SK channels in hippocampal CA1 pyramidal neurons. Biophys J 77:1905-1913.

Hines ML, Carnevale NT (1997) The NEURON simulation environment. Neural Comput 9:1179-1209.

Hodgkin AL, Katz B (1949) The effect of sodium ions on the electrical activity of the giant axon of the squid. J Physiol 108:37-77.

Hodgkin AL, Huxley AF (1952a) Currents carried by sodium and potassium ions through the membrane of the giant axon of Loligo. J Physiol 116:449-472.

Hodgkin AL, Huxley AF (1952b) A quantitative description of membrane current and its application to conduction and excitation in nerve. J Physiol 117:500-544.

Hodgkin AL, Huxley AF (1952c) The dual effect of membrane potential on sodium conductance in the giant axon of Loligo. J Physiol 116:497-506.

Hodgkin AL, Huxley AF (1952d) The components of membrane conductance in the giant axon of Loligo. J Physiol 116:473-496.

Hoebeek FE, Stahl JS, van Alphen AM, Schonewille M, Luo C, Rutteman M, van den Maagdenberg AM, Molenaar PC, Goossens HH, Frens MA, De Zeeuw CI (2005) Increased noise level of purkinje cell activities minimizes impact of their modulation during sensorimotor control. Neuron 45:953-965.

Hoffman DA, Magee JC, Colbert CM, Johnston D (1997) K+ channel regulation of signal propagation in dendrites of hippocampal pyramidal neurons. Nature 387:869-875.

Holmes G (1917) The symptoms of acute cerebellar injuries due to gunshot injuries. Brain 40:461-535.

Holt GR, Koch C (1997) Shunting inhibition does not have a divisive effect on firing rates. Neural Comput 9:1001-1013.

Hore J, Timmann D, Watts S (2002) Disorders in timing and force of finger opening in overarm throws made by cerebellar subjects. Ann N Y Acad Sci 978:1-15.

Hounsgaard J, Midtgaard J (1988) Intrinsic determinants of firing pattern in Purkinje cells of the turtle cerebellum in vitro. J Physiol 402:731-749.

Hounsgaard J, Midtgaard J (1989) Synaptic control of excitability in turtle cerebellar Purkinje cells. J Physiol 409:157-170.

Hsu YH, Huang HY, Tsaur ML (2003) Contrasting expression of Kv4.3, an A-type K+ channel, in migrating Purkinje cells and other post-migratory cerebellar neurons. Eur J Neurosci 18:601-612.

Hurlock EC, McMahon A, Joho RH (2008) Purkinje-cell-restricted restoration of Kv3.3 function restores complex spikes and rescues motor coordination in Kcnc3 mutants. J Neurosci 28:4640-4648.

Isope P, Barbour B (2002) Properties of unitary granule cell-->Purkinje cell synapses in adult rat cerebellar slices. J Neurosci 22:9668-9678.

Isope P, Murphy TH (2005) Low threshold calcium currents in rat cerebellar Purkinje cell dendritic spines are mediated by T-type calcium channels. J Physiol 562:257-269.

Ito M (2002) The molecular organization of cerebellar long-term depression. Nat Rev Neurosci 3:896-902.

Ito M, Kano M (1982) Long-lasting depression of parallel fiber-Purkinje cell transmission induced by conjunctive stimulation of parallel fibers and climbing fibers in the cerebellar cortex. Neurosci Lett 33:253-258.

Izhikevich EM (2003) Simple model of spiking neurons. IEEE Trans Neural Netw 14:1569-1572.

Izhikevich EM (2004) Which model to use for cortical spiking neurons? IEEE Trans Neural Netw 15:1063-1070.

Jack JJB, Noble D, Tsien RW (1983) Electrical current flow in excitable cells. Oxford: Oxford University Press.

Jacquin TD, Gruol DL (1999) Ca2+ regulation of a large conductance K+ channel in cultured rat cerebellar Purkinje neurons. Eur J Neurosci 11:735-739.

Jaeger D, De Schutter E, Bower JM (1997) The role of synaptic and voltage-gated currents in the control of Purkinje cell spiking: a modeling study. J Neurosci 17:91-106.

Jahnsen H, Llinas R (1984) Ionic basis for the electro-responsiveness and oscillatory properties of guinea-pig thalamic neurones in vitro. J Physiol 349:227-247.

Jenkins SM, Bennett V (2001) Ankyrin-G coordinates assembly of the spectrin-based membrane skeleton, voltage-gated sodium channels, and L1 CAMs at Purkinje neuron initial segments. J Cell Biol 155:739-746.

Johnston D, Wu SM-S (1995) Foundations of cellular neurophysiology. Cambridge, Massachusetts: The MIT Press.

Johnston D, Hoffman DA, Colbert CM, Magee JC (1999) Regulation of back-propagating action potentials in hippocampal neurons. Curr Opin Neurobiol 9:288-292.

Jonas P, Burnashev N (1995) Molecular mechanisms controlling calcium entry through AMPA-type glutamate receptor channels. Neuron 15:987-990.

Jun K, Piedras-Renteria ES, Smith SM, Wheeler DB, Lee SB, Lee TG, Chin H, Adams ME, Scheller RH, Tsien RW, Shin HS (1999) Ablation of P/Q-type Ca(2+) channel currents, altered synaptic transmission, and progressive ataxia in mice lacking the alpha(1A)-subunit. Proc Natl Acad Sci U S A 96:15245-15250.

Jung HY, Mickus T, Spruston N (1997) Prolonged sodium channel inactivation contributes to dendritic action potential attenuation in hippocampal pyramidal neurons. J Neurosci 17:6639-6646.

Kalume F, Yu FH, Westenbroek RE, Scheuer T, Catterall WA (2007) Reduced sodium current in Purkinje neurons from Nav1.1 mutant mice: implications for ataxia in severe myoclonic epilepsy in infancy. J Neurosci 27:11065-11074.

Kamboj SK, Swanson GT, Cull-Candy SG (1995) Intracellular spermine confers rectification on rat calcium-permeable AMPA and kainate receptors. J Physiol 486 (Pt 2):297-303.

Kanumilli S, Tringham EW, Payne CE, Dupere JR, Venkateswarlu K, Usowicz MM (2006) Alternative splicing generates a smaller assortment of CaV2.1 transcripts in cerebellar Purkinje cells than in the cerebellum. Physiol Genomics 24:86-96.

Karakossian MH, Otis TS (2005) Which stimuli engage hyperpolarization-activated cation channels in Purkinje neurons? In: Society for Neuroscience, p Program No. 728.715. Washington, DC.

Katz B (1950) Action potentials from a sensory nerve ending. J Physiol 111:248-260.

Katz B (1966) Nerve, muscle and synapse. New York: McGraw-Hill.

Kay AR, Sugimori M, Llinas R (1998) Kinetic and stochastic properties of a persistent sodium current in mature guinea pig cerebellar Purkinje cells. J Neurophysiol 80:1167-1179.

Kazama H, Wilson RI (2008) Homeostatic matching and nonlinear amplification at identified central synapses. Neuron 58:401-413.

Keating JG, Thach WT (1995) Nonclock behavior of inferior olive neurons: interspike interval of Purkinje cell complex spike discharge in the awake behaving monkey is random. J Neurophysiol 73:1329-1340.

Kepecs A, Wang XJ, Lisman J (2002) Bursting neurons signal input slope. J Neurosci 22:9053-9062.

Khaliq ZM, Raman IM (2005) Axonal propagation of simple and complex spikes in cerebellar Purkinje neurons. J Neurosci 25:454-463.

Khaliq ZM, Raman IM (2006) Relative contributions of axonal and somatic Na channels to action potential initiation in cerebellar Purkinje neurons. J Neurosci 26:1935-1944.

Khaliq ZM, Gouwens NW, Raman IM (2003) The contribution of resurgent sodium current to high-frequency firing in Purkinje neurons: an experimental and modeling study. J Neurosci 23:4899-4912.

Khavandgar S, Walter JT, Sageser K, Khodakhah K (2005) Kv1 channels selectively prevent dendritic hyperexcitability in rat Purkinje cells. J Physiol 569:545-557.

Khodorov BI, Timin EN (1975) Nerve impulse propagation along nonuniform fibres. Prog Biophys Mol Biol 30:145-184.

Kakizawa S, Miyazaki T, Yanagihara D, Iino M, Watanabe M, Kano M (2005) Maintenance of presynaptic function by AMPA receptor-mediated excitatory postsynaptic activity in adult brain. Proc Natl Acad Sci U S A 102:19180-19185.

Kim J, Wei DS, Hoffman DA (2005) Kv4 potassium channel subunits control action potential repolarization and frequency-dependent broadening in rat hippocampal CA1 pyramidal neurones. J Physiol 569:41-57.

Kim J, Jung SC, Clemens AM, Petralia RS, Hoffman DA (2007) Regulation of dendritic excitability by activity-dependent trafficking of the A-type K+ channel subunit Kv4.2 in hippocampal neurons. Neuron 54:933-947.

Kirov SA, Sorra KE, Harris KM (1999) Slices have more synapses than perfusion-fixed hippocampus from both young and mature rats. J Neurosci 19:2876-2886.

Kistler WM, De Zeeuw CI (2003) Time windows and reverberating loops: a reverse-engineering approach to cerebellar function. Cerebellum 2:44-54.

Kistler WM, van Hemmen JL, De Zeeuw CI (2000) Time window control: a model for cerebellar function based on synchronization, reverberation, and time slicing. Prog Brain Res 124:275-297.

Kistler WM, De Jeu MT, Elgersma Y, Van Der Giessen RS, Hensbroek R, Luo C, Koekkoek SK, Hoogenraad CC, Hamers FP, Gueldenagel M, Sohl G, Willecke K, De Zeeuw CI (2002) Analysis of Cx36 knockout does not support tenet that olivary gap junctions are required for complex spike synchronization and normal motor performance. Ann N Y Acad Sci 978:391-404.

Kitazawa S, Kimura T, Yin PB (1998) Cerebellar complex spikes encode both destinations and errors in arm movements. Nature 392:494-497.

Knaus HG, Schwarzer C, Koch RO, Eberhart A, Kaczorowski GJ, Glossmann H, Wunder F, Pongs O, Garcia ML, Sperk G (1996) Distribution of high-conductance Ca(2+)-activated K+ channels in rat brain: targeting to axons and nerve terminals. J Neurosci 16:955-963.

Kole MH, Ilschner SU, Kampa BM, Williams SR, Ruben PC, Stuart GJ (2008) Action potential generation requires a high sodium channel density in the axon initial segment. Nat Neurosci 11:178-186.

Kollo M, Holderith NB, Nusser Z (2006) Novel subcellular distribution pattern of A-type K+ channels on neuronal surface. J Neurosci 26:2684-2691.

Konnerth A, Llano I, Armstrong CM (1990) Synaptic currents in cerebellar Purkinje cells. Proc Natl Acad Sci U S A 87:2662-2665.

Kuba H, Ishii TM, Ohmori H (2006) Axonal site of spike initiation enhances auditory coincidence detection. Nature 444:1069-1072.

Kupper J, Prinz AA, Fromherz P (2002) Recombinant Kv1.3 potassium channels stabilize tonic firing of cultured rat hippocampal neurons. Pflugers Arch 443:541-547.

Lambolez B, Audinat E, Bochet P, Crepel F, Rossier J (1992) AMPA receptor subunits expressed by single Purkinje cells. Neuron 9:247-258.

Lang EJ, Sugihara I, Welsh JP, Llinas R (1999) Patterns of spontaneous purkinje cell complex spike activity in the awake rat. J Neurosci 19:2728-2739.

Larkum ME, Zhu JJ, Sakmann B (1999) A new cellular mechanism for coupling inputs arriving at different cortical layers. Nature 398:338-341.

Larkum ME, Zhu JJ, Sakmann B (2001) Dendritic mechanisms underlying the coupling of the dendritic with the axonal action potential initiation zone of adult rat layer 5 pyramidal neurons. J Physiol 533:447-466.

Latham A, Paul DH (1971) Spontaneous activity of cerebellar Purkinje cells and their responses to impulses in climbing fibres. J Physiol 213:135-156.

Letzkus JJ, Kampa BM, Stuart GJ (2006) Learning rules for spike timing-dependent plasticity depend on dendritic synapse location. J Neurosci 26:10420-10429.

Levin SI, Khaliq ZM, Aman TK, Grieco TM, Kearney JA, Raman IM, Meisler MH (2006) Impaired motor function in mice with cell-specific knockout of sodium channel Scn8a (NaV1.6) in cerebellar purkinje neurons and granule cells. J Neurophysiol 96:785-793.

Leznik E, Makarenko V, Llinas R (2002) Electrotonically mediated oscillatory patterns in neuronal ensembles: an in vitro voltage-dependent dye-imaging study in the inferior olive. J Neurosci 22:2804-2815.

Lien CC, Jonas P (2003) Kv3 potassium conductance is necessary and kinetically optimized for high-frequency action potential generation in hippocampal interneurons. J Neurosci 23:2058-2068.

Llano I, Marty A, Armstrong CM, Konnerth A (1991) Synaptic- and agonist-induced excitatory currents of Purkinje cells in rat cerebellar slices. J Physiol 434:183-213.

Llinas R, Nicholson C (1971) Electrophysiological properties of dendrites and somata in alligator Purkinje cells. J Neurophysiol 34:532-551.

Llinas R, Volkind RA (1973) The olivo-cerebellar system: functional properties as revealed by harmaline-induced tremor. Exp Brain Res 18:69-87.

Llinas R, Sugimori M (1980a) Electrophysiological properties of in vitro Purkinje cell somata in mammalian cerebellar slices. J Physiol 305:171-195.

Llinas R, Sugimori M (1980b) Electrophysiological properties of in vitro Purkinje cell dendrites in mammalian cerebellar slices. J Physiol 305:197-213.

Llinas R, Yarom Y (1981a) Properties and distribution of ionic conductances generating electroresponsiveness of mammalian inferior olivary neurones in vitro. J Physiol 315:569-584.

Llinas R, Yarom Y (1981b) Electrophysiology of mammalian inferior olivary neurones in vitro. Different types of voltage-dependent ionic conductances. J Physiol 315:549-567.

Llinas R, Yarom Y (1986) Oscillatory properties of guinea-pig inferior olivary neurones and their pharmacological modulation: an in vitro study. J Physiol 376:163-182.

Llinas R, Sasaki K (1989) The Functional Organization of the Olivo-Cerebellar System as Examined by Multiple Purkinje Cell Recordings. Eur J Neurosci 1:587-602.

Llinas R, Nicholson C, Precht W (1969a) Preferred centripetal conduction of dendritic spikes in alligator Purkinje cells. Science 163:184-187.

Llinas R, Bloedel JR, Hillman DE (1969b) Functional characterization of neuronal circuitry of frog cerebellar cortex. J Neurophysiol 32:847-870.

Llinas R, Nicholson C, Freeman JA, Hillman DE (1968) Dendritic spikes and their inhibition in alligator Purkinje cells. Science 160:1132-1135.

Llinas R, Nicholson C, Freeman JA, Hillman DE (1969c) Dendritic spikes versus cable properties. Science 163:97.

Llinas R, Sugimori M, Lin JW, Cherksey B (1989) Blocking and isolation of a calcium channel from neurons in mammals and cephalopods utilizing a toxin fraction (FTX) from funnel-web spider poison. Proc Natl Acad Sci U S A 86:1689-1693.

Loewenstein Y, Mahon S, Chadderton P, Kitamura K, Sompolinsky H, Yarom Y, Häusser M (2005) Bistability of cerebellar Purkinje cells modulated by sensory stimulation. Nat Neurosci 8:202-211.

Loftis JL, King DD, Colbert CM (2003) Kinase-dependent loss of Na+ channel slow-inactivation in rat CA1 hippocampal pyramidal cell dendrites after brief exposure to convulsants. Eur J Neurosci 18:1029-1032.

Lohof AM, Mariani J, Sherrard RM (2005) Afferent-target interactions during olivocerebellar development: transcommissural reinnervation indicates interdependence of Purkinje cell maturation and climbing fibre synapse elimination. Eur J Neurosci 22:2681-2688.

London M, Häusser M (2005) Dendritic computation. Annu Rev Neurosci 28:503-532.

Long MA, Deans MR, Paul DL, Connors BW (2002) Rhythmicity without synchrony in the electrically uncoupled inferior olive. J Neurosci 22:10898-10905.

Losonczy A, Magee JC (2006) Integrative properties of radial oblique dendrites in hippocampal CA1 pyramidal neurons. Neuron 50:291-307.

Losonczy A, Makara JK, Magee JC (2008) Compartmentalized dendritic plasticity and input feature storage in neurons. Nature 452:436-441.

Lowe G (2002) Inhibition of backpropagating action potentials in mitral cell secondary dendrites. J Neurophysiol 88:64-85.

Madeja M (2000) Do neurons have a reserve of sodium channels for the generation of action potentials? A study on acutely isolated CA1 neurons from the guinea-pig hippocampus. Eur J Neurosci 12:1-7.

Maeda H, Ellis-Davies GC, Ito K, Miyashita Y, Kasai H (1999) Supralinear Ca2+ signaling by cooperative and mobile Ca2+ buffering in Purkinje neurons. Neuron 24:989-1002.

Magee JC (1999) Dendritic Ih normalizes temporal summation in hippocampal CA1 neurons. Nat Neurosci 2:508-514.

Magee JC (2000) Dendritic integration of excitatory synaptic input. Nat Rev Neurosci 1:181-190.

Magee JC, Johnston D (2005) Plasticity of dendritic function. Curr Opin Neurobiol 15:334-342.

Mainen ZF, Sejnowski TJ (1996) Influence of dendritic structure on firing pattern in model neocortical neurons. Nature 382:363-366.

Mainen ZF, Joerges J, Huguenard JR, Sejnowski TJ (1995) A model of spike initiation in neocortical pyramidal neurons. Neuron 15:1427-1439.

Mariani J, Changeux JP (1981) Ontogenesis of olivocerebellar relationships. I. Studies by intracellular recordings of the multiple innervation of Purkinje cells by climbing fibers in the developing rat cerebellum. J Neurosci 1:696-702.

Marr D (1969) A theory of cerebellar cortex. J Physiol 202:437-470.

Martina M, Yao GL, Bean BP (2003) Properties and functional role of voltage-dependent potassium channels in dendrites of rat cerebellar Purkinje neurons. J Neurosci 23:5698-5707.

Martina M, Metz AE, Bean BP (2007) Voltage-dependent potassium currents during fast spikes of rat cerebellar Purkinje neurons: inhibition by BDS-I toxin. J Neurophysiol 97:563-571.

Martinez FE, Crill WE, Kennedy TT (1971) Electrogenesis of cerebellar Purkinje cell responses in cats. J Neurophysiol 34:348-356.

Maruta J, Hensbroek RA, Simpson JI (2007) Intraburst and interburst signaling by climbing fibers. J Neurosci 27:11263-11270.

Mason CA, Christakos S, Catalano SM (1990) Early climbing fiber interactions with Purkinje cells in the postnatal mouse cerebellum. J Comp Neurol 297:77-90.

Masugi-Tokita M, Tarusawa E, Watanabe M, Molnar E, Fujimoto K, Shigemoto R (2007) Number and density of AMPA receptors in individual synapses in the rat cerebellum as revealed by SDS-digested freeze-fracture replica labeling. J Neurosci 27:2135-2144.

McDevitt CJ, Ebner TJ, Bloedel JR (1987) Changes in the responses of cerebellar nuclear neurons associated with the climbing fiber response of Purkinje cells. Brain Res 425:14-24.

McDonough SI, Bean BP (1998) Mibefradil inhibition of T-type calcium channels in cerebellar purkinje neurons. Mol Pharmacol 54:1080-1087.

McKay BE, Turner RW (2004) Kv3 K+ channels enable burst output in rat cerebellar Purkinje cells. Eur J Neurosci 20:729-739.

McKay BE, Turner RW (2005) Physiological and morphological development of the rat cerebellar Purkinje cell. J Physiol 567:829-850.

McKay BE, Molineux ML, Mehaffey WH, Turner RW (2005) Kv1 K+ channels control Purkinje cell output to facilitate postsynaptic rebound discharge in deep cerebellar neurons. J Neurosci 25:1481-1492.

McKay BE, McRory JE, Molineux ML, Hamid J, Snutch TP, Zamponi GW, Turner RW (2006) Ca(V)3 T-type calcium channel isoforms differentially distribute to somatic and dendritic compartments in rat central neurons. Eur J Neurosci 24:2581-2594.

McKay BE, Engbers JD, Mehaffey WH, Gordon GR, Molineux ML, Bains JS, Turner RW (2007) Climbing fiber discharge regulates cerebellar functions by controlling the intrinsic characteristics of purkinje cell output. J Neurophysiol 97:2590-2604.

McMahon A, Fowler SC, Perney TM, Akemann W, Knopfel T, Joho RH (2004) Allele-dependent changes of olivocerebellar circuit properties in the absence of the voltage-gated potassium channels Kv3.1 and Kv3.3. Eur J Neurosci 19:3317-3327.

Medina JF, Mauk MD (2000) Computer simulation of cerebellar information processing. Nat Neurosci 3 Suppl:1205-1211.

Meeks JP, Mennerick S (2007) Action potential initiation and propagation in CA3 pyramidal axons. J Neurophysiol 97:3460-3472.

Mehaffey WH, Doiron B, Maler L, Turner RW (2005) Deterministic multiplicative gain control with active dendrites. J Neurosci 25:9968-9977.

Micheva KD, Smith SJ (2005) Strong effects of subphysiological temperature on the function and plasticity of mammalian presynaptic terminals. J Neurosci 25:7481-7488.

Midtgaard J (1995) Spatial synaptic integration in Purkinje cell dendrites. J Physiol Paris 89:23-32.

Midtgaard J, Lasser-Ross N, Ross WN (1993) Spatial distribution of Ca2+ influx in turtle Purkinje cell dendrites in vitro: role of a transient outward current. J Neurophysiol 70:2455-2469.

Migliore M (1996) Modeling the attenuation and failure of action potentials in the dendrites of hippocampal neurons. Biophys J 71:2394-2403.

Migliore M, Shepherd GM (2002) Emerging rules for the distributions of active dendritic conductances. Nat Rev Neurosci 3:362-370.

Mintz IM, Adams ME, Bean BP (1992) P-type calcium channels in rat central and peripheral neurons. Neuron 9:85-95.

Mitchell SJ, Silver RA (2003) Shunting inhibition modulates neuronal gain during synaptic excitation. Neuron 38:433-445.

Mittmann W, Häusser M (2007) Linking synaptic plasticity and spike output at excitatory and inhibitory synapses onto cerebellar Purkinje cells. J Neurosci 27:5559-5570.

Miyakawa H, Lev-Ram V, Lasser-Ross N, Ross WN (1992) Calcium transients evoked by climbing fiber and parallel fiber synaptic inputs in guinea pig cerebellar Purkinje neurons. J Neurophysiol 68:1178-1189.

Molineux ML, McRory JE, McKay BE, Hamid J, Mehaffey WH, Rehak R, Snutch TP, Zamponi GW, Turner RW (2006) Specific T-type calcium channel isoforms are associated with distinct burst phenotypes in deep cerebellar nuclear neurons. Proc Natl Acad Sci U S A 103:5555-5560.

Momiyama A, Silver RA, Häusser M, Notomi T, Wu Y, Shigemoto R, Cull-Candy SG (2003) The density of AMPA receptors activated by a transmitter quantum at the climbing fibre-Purkinje cell synapse in immature rats. J Physiol 549:75-92.

Monsivais P, Clark BA, Roth A, Häusser M (2005) Determinants of action potential propagation in cerebellar Purkinje cell axons. J Neurosci 25:464-472.

Morara S, van der Want JJ, de Weerd H, Provini L, Rosina A (2001) Ultrastructural analysis of climbing fiber-Purkinje cell synaptogenesis in the rat cerebellum. Neuroscience 108:655-671.

Mouginot D, Bossu JL, Gahwiler BH (1997) Low-threshold Ca2+ currents in dendritic recordings from Purkinje cells in rat cerebellar slice cultures. J Neurosci 17:160-170.

Muller YL, Reitstetter R, Yool AJ (1998) Regulation of Ca2+-dependent K+ channel expression in rat cerebellum during postnatal development. J Neurosci 18:16-25.

Murphy JT, Sabah NH (1970) The inhibitory effect of climbing fiber activation on cerebellar purkinje cells. Brain Res 19:486-490.

Napper RM, Harvey RJ (1988) Number of parallel fiber synapses on an individual Purkinje cell in the cerebellum of the rat. J Comp Neurol 274:168-177.

Nelson AB, Krispel CM, Sekirnjak C, du Lac S (2003) Long-lasting increases in intrinsic excitability triggered by inhibition. Neuron 40:609-620.

Nevian T, Larkum ME, Polsky A, Schiller J (2007) Properties of basal dendrites of layer 5 pyramidal neurons: a direct patch-clamp recording study. Nat Neurosci 10:206-214.

Nicholson C, Llinas R (1971) Field potentials in the alligator cerebellum and theory of their relationship to Purkinje cell dendritic spikes. J Neurophysiol 34:509-531.

Nicholson DA, Freeman JH, Jr. (2003a) Developmental changes in evoked Purkinje cell complex spike responses. J Neurophysiol 90:2349-2357.

Nicholson DA, Freeman JH, Jr. (2003b) Addition of inhibition in the olivocerebellar system and the ontogeny of a motor memory. Nat Neurosci 6:532-537.

Nishiyama H, Linden DJ (2004) Differential maturation of climbing fiber innervation in cerebellar vermis. J Neurosci 24:3926-3932.

Nitz D, Tononi G (2002) Tonic rhythmic activity of rat cerebellar neurons. Exp Brain Res 146:265-270.

Nolan MF, Malleret G, Lee KH, Gibbs E, Dudman JT, Santoro B, Yin D, Thompson RF, Siegelbaum SA, Kandel ER, Morozov A (2003) The hyperpolarization-activated HCN1 channel is important for motor learning and neuronal integration by cerebellar Purkinje cells. Cell 115:551-564.

Nusbaum MP, Blitz DM, Swensen AM, Wood D, Marder E (2001) The roles of co-transmission in neural network modulation. Trends Neurosci 24:146-154.

Nusser Z, Mulvihill E, Streit P, Somogyi P (1994) Subsynaptic segregation of metabotropic and ionotropic glutamate receptors as revealed by immunogold localization. Neuroscience 61:421-427.

O'Leary JL, Dunsker SB, Smith JM, Inukai J, O'Leary M (1970) Termination of the olivocerebellar system in the cat. Arch Neurol 22:193-206.

Ogiwara I, Miyamoto H, Morita N, Atapour N, Mazaki E, Inoue I, Takeuchi T, Itohara S, Yanagawa Y, Obata K, Furuichi T, Hensch TK, Yamakawa K (2007) Na(v)1.1 localizes to axons of parvalbumin-positive inhibitory interneurons: a circuit basis for epileptic seizures in mice carrying an Scn1a gene mutation. J Neurosci 27:5903-5914.

Orduz D, Llano I (2007) Recurrent axon collaterals underlie facilitating synapses between cerebellar Purkinje cells. Proc Natl Acad Sci U S A 104:17831-17836.

Otis TS, Kavanaugh MP, Jahr CE (1997) Postsynaptic glutamate transport at the climbing fiber-Purkinje cell synapse. Science 277:1515-1518.

Ovsepian SV, Friel DD (2008) The leaner P/Q-type calcium channel mutation renders cerebellar Purkinje neurons hyper-excitable and eliminates Ca2+-Na+ spike bursts. Eur J Neurosci 27:93-103.

Palay SL, Chan-Palay V (1974) Cerebellar Cortex. New York: Springer-Verlag.

Palmer LM, Stuart GJ (2006) Site of action potential initiation in layer 5 pyramidal neurons. J Neurosci 26:1854-1863.

Palmer LM, Stuart GJ (2007) Imaging electrical coupling between spines and dendrites. In: Society for Neuroscience. San Diego.

Parnas I, Segev I (1979) A mathematical model for conduction of action potentials along bifurcating axons. J Physiol 295:323-343.

Patneau DK, Vyklicky L, Jr., Mayer ML (1993) Hippocampal neurons exhibit cyclothiazide-sensitive rapidly desensitizing responses to kainate. J Neurosci 13:3496-3509.

Perez-Garci E, Gassmann M, Bettler B, Larkum ME (2006) The GABAB1b isoform mediates long-lasting inhibition of dendritic Ca2+ spikes in layer 5 somatosensory pyramidal neurons. Neuron 50:603-616.

Perez-Reyes E (2003) Molecular physiology of low-voltage-activated t-type calcium channels. Physiol Rev 83:117-161.

Perkel DJ, Hestrin S, Sah P, Nicoll RA (1990) Excitatory synaptic currents in Purkinje cells. Proc Biol Sci 241:116-121.

Petralia RS, Zhao HM, Wang YX, Wenthold RJ (1998) Variations in the tangential distribution of postsynaptic glutamate receptors in Purkinje cell parallel and climbing fiber synapses during development. Neuropharmacology 37:1321-1334.

Pinsky PF, Rinzel J (1994) Intrinsic and network rhythmogenesis in a reduced Traub model for CA3 neurons. J Comput Neurosci 1:39-60.

Piochon C, Irinopoulou T, Brusciano D, Bailly Y, Mariani J, Levenes C (2007) NMDA receptor contribution to the climbing fiber response in the adult mouse Purkinje cell. J Neurosci 27:10797-10809.

Poirazi P, Brannon T, Mel BW (2003) Pyramidal neuron as two-layer neural network. Neuron 37:989-999.

Polsky A, Mel BW, Schiller J (2004) Computational subunits in thin dendrites of pyramidal cells. Nat Neurosci 7:621-627.

Postlethwaite M, Hennig MH, Steinert JR, Graham BP, Forsythe ID (2007) Acceleration of AMPA receptor kinetics underlies temperature-dependent changes in synaptic strength at the rat calyx of Held. J Physiol 579:69-84.

Pouille F, Cavelier P, Desplantez T, Beekenkamp H, Craig PJ, Beattie RE, Volsen SG, Bossu JL (2000) Dendro-somatic distribution of calcium-mediated electrogenesis in purkinje cells from rat cerebellar slice cultures. J Physiol 527 Pt 2:265-282.

Prinz AA, Bucher D, Marder E (2004) Similar network activity from disparate circuit parameters. Nat Neurosci 7:1345-1352.

Pugh JR, Raman IM (2006) Potentiation of mossy fiber EPSCs in the cerebellar nuclei by NMDA receptor activation followed by postinhibitory rebound current. Neuron 51:113-123.

Puro DG, Woodward DJ (1977) Maturation of evoked climbing fiber input to rat cerebellar purkinje cells (I.). Exp Brain Res 28:85-100.

Rall W (1959) Branching dendritic trees and motoneuron membrane resistivity. Exp Neurol 1:491-527.

Rall W (1964) Theoretical significance of dendritic trees for neuronal input-output relations. In: Neural theory and modeling (Reiss RF, ed). Palo Alto: Stanford University Press.

Rall W (1967) Distinguishing theoretical synaptic potentials computed for different soma-dendritic distributions of synaptic input. J Neurophysiol 30:1138-1168.

Rall W (1969) Time constants and electrotonic length of membrane cylinders and neurons. Biophys J 9:1483-1508.

Ramakers GM, Storm JF (2002) A postsynaptic transient K(+) current modulated by arachidonic acid regulates synaptic integration and threshold for LTP induction in hippocampal pyramidal cells. Proc Natl Acad Sci U S A 99:10144-10149.

Raman IM, Bean BP (1997) Resurgent sodium current and action potential formation in dissociated cerebellar Purkinje neurons. J Neurosci 17:4517-4526.

Raman IM, Bean BP (1999) Ionic currents underlying spontaneous action potentials in isolated cerebellar Purkinje neurons. J Neurosci 19:1663-1674.

Raman IM, Bean BP (2001) Inactivation and recovery of sodium currents in cerebellar Purkinje neurons: evidence for two mechanisms. Biophys J 80:729-737.

Raman IM, Sprunger LK, Meisler MH, Bean BP (1997) Altered subthreshold sodium currents and disrupted firing patterns in Purkinje neurons of Scn8a mutant mice. Neuron 19:881-891.

Ramón y Cajal S (1888) Sobre las fibras nerviosas de la capa molecular del cerebelo. Rev Trim Histol Normal Patol 1:33-49.

Ramón y Cajal S (1911) Histologie du Systeme Nerveux de l'Homme et des Vertébrés. Paris: Maloine.

Rancz EA, Häusser M (2005) Dendritic spikes clamp somatic spike output in cerebellar Purkinje cells. In: Society for Neuroscience Meeting, p Program No. 738.710. Washington D.C.

Rancz EA, Häusser M (2006) Dendritic calcium spikes are tunable triggers of cannabinoid release and short-term synaptic plasticity in cerebellar Purkinje neurons. J Neurosci 26:5428-5437.

Rancz EA, Ishikawa T, Duguid I, Chadderton P, Mahon S, Häusser M (2007) High-fidelity transmission of sensory information by single cerebellar mossy fibre boutons. Nature 450:1245-1248.

Rapp M, Segev I, Yarom Y (1994) Physiology, morphology and detailed passive models of guinea-pig cerebellar Purkinje cells. J Physiol 474:101-118.

Rashid AJ, Dunn RJ, Turner RW (2001) A prominent soma-dendritic distribution of Kv3.3 K+ channels in electrosensory and cerebellar neurons. J Comp Neurol 441:234-247.

Raymond JL, Lisberger SG, Mauk MD (1996) The cerebellum: a neuronal learning machine? Science 272:1126-1131.

Regan LJ (1991) Voltage-dependent calcium currents in Purkinje cells from rat cerebellar vermis. J Neurosci 11:2259-2269.

Rettig J, Heinemann SH, Wunder F, Lorra C, Parcej DN, Dolly JO, Pongs O (1994) Inactivation properties of voltage-gated K+ channels altered by presence of beta-subunit. Nature 369:289-294.

Rinzel J, Rall W (1974) Transient response in a dendritic neuron model for current injected at one branch. Biophys J 14:759-790.

Rinzel J, Ermentrout B (1998) Analysis of neural excitability and oscillations. In: Methods in neuronal modeling (Koch C, Segev I, eds). Cambridge, Massachusetts: The MIT Press.

Ripellino JA, Neve RL, Howe JR (1998) Expression and heteromeric interactions of non-N-methyl-D-aspartate glutamate receptor subunits in the developing and adult cerebellum. Neuroscience 82:485-497.

Robinson HP, Kawai N (1993) Injection of digitally synthesized synaptic conductance transients to measure the integrative properties of neurons. J Neurosci Methods 49:157-165.

Robinson HP, Harsch A (2002) Stages of spike time variability during neuronal responses to transient inputs. Phys Rev E Stat Nonlin Soft Matter Phys 66:061902.

Rolando L (1809) *Saggio sopra la vera structtura del cervello dell'uomo e degli animali sopra le funzioni del sinstema nervoso.* Stemperia di S S R M Privilegiata, Sassari.

Ross WN, Werman R (1987) Mapping calcium transients in the dendrites of Purkinje cells from the guinea-pig cerebellum in vitro. J Physiol 389:319-336.

Roth A, Häusser M (2001) Compartmental models of rat cerebellar Purkinje cells based on simultaneous somatic and dendritic patch-clamp recordings. J Physiol 535:445-472.

Roth A, Häusser M (2004) Morphological determinants of dendritic spike initiation. In: Society for Neuroscience. Washington DC.

Roth A, Häusser M (2007) Cooperativity of synapses contributing to initiation of local dendritic spikes depends on dendritic morphology. In: Society for Neuroscience, p Program No. 251.219. San Diego.

Rothman JS, Manis PB (2003) The roles potassium currents play in regulating the electrical activity of ventral cochlear nucleus neurons. J Neurophysiol 89:3097-3113.

Rowland NC, Jaeger D (2008) Responses to tactile stimulation in deep cerebellar nucleus neurons result from recurrent activation in multiple pathways. J Neurophysiol 99:704-717.

Rudy B, McBain CJ (2001) Kv3 channels: voltage-gated K+ channels designed for high-frequency repetitive firing. Trends Neurosci 24:517-526.

Ruff RL (2003) Neurophysiology of the neuromuscular junction: overview. Ann N Y Acad Sci 998:1-10.

Ruigrok TJ (1997) Cerebellar nuclei: the olivary connection. Prog Brain Res 114:167-192.

Sacco T, Tempia F (2002) A-type potassium currents active at subthreshold potentials in mouse cerebellar Purkinje cells. J Physiol 543:505-520.

Sacco T, De Luca A, Tempia F (2006) Properties and expression of Kv3 channels in cerebellar Purkinje cells. Mol Cell Neurosci 33:170-179.

Salkoff L, Butler A, Ferreira G, Santi C, Wei A (2006) High-conductance potassium channels of the SLO family. Nat Rev Neurosci 7:921-931.

Sato Y, Miura A, Fushiki H, Kawasaki T (1992) Short-term modulation of cerebellar Purkinje cell activity after spontaneous climbing fiber input. J Neurophysiol 68:2051-2062.

Sausbier M, Hu H, Arntz C, Feil S, Kamm S, Adelsberger H, Sausbier U, Sailer CA, Feil R, Hofmann F, Korth M, Shipston MJ, Knaus HG, Wolfer DP, Pedroarena CM, Storm JF, Ruth P (2004) Cerebellar ataxia and Purkinje cell dysfunction caused by Ca2+-activated K+ channel deficiency. Proc Natl Acad Sci U S A 101:9474-9478.

Scelfo B, Strata P (2005) Correlation between multiple climbing fibre regression and parallel fibre response development in the postnatal mouse cerebellum. Eur J Neurosci 21:971-978.

Schaefer AT, Larkum ME, Sakmann B, Roth A (2003) Coincidence detection in pyramidal neurons is tuned by their dendritic branching pattern. J Neurophysiol 89:3143-3154.

Schaller KL, Caldwell JH (2003) Expression and distribution of voltage-gated sodium channels in the cerebellum. Cerebellum 2:2-9.

Schiffmann SN, Cheron G, Lohof A, d'Alcantara P, Meyer M, Parmentier M, Schurmans S (1999) Impaired motor coordination and Purkinje cell excitability in mice lacking calretinin. Proc Natl Acad Sci U S A 96:5257-5262.

Schiller J, Schiller Y (2001) NMDA receptor-mediated dendritic spikes and coincident signal amplification. Curr Opin Neurobiol 11:343-348.

Schiller J, Schiller Y, Stuart G, Sakmann B (1997) Calcium action potentials restricted to distal apical dendrites of rat neocortical pyramidal neurons. J Physiol 505 (Pt 3):605-616.

Schiller J, Major G, Koester HJ, Schiller Y (2000) NMDA spikes in basal dendrites of cortical pyramidal neurons. Nature 404:285-289.

Schmidt H, Brown EB, Schwaller B, Eilers J (2003) Diffusional mobility of parvalbumin in spiny dendrites of cerebellar Purkinje neurons quantified by fluorescence recovery after photobleaching. Biophys J 84:2599-2608.

Schmidt-Hieber C, Jonas P, Bischofberger J (2008) Action potential initiation and propagation in hippocampal mossy fibre axons. J Physiol 586:1849-1857.

Schmolesky MT, Weber JT, De Zeeuw CI, Hansel C (2002) The making of a complex spike: ionic composition and plasticity. Ann N Y Acad Sci 978:359-390.

Schneidman E, Freedman B, Segev I (1998) Ion channel stochasticity may be critical in determining the reliability and precision of spike timing. Neural Comput 10:1679-1703.

Schonewille M, Khosrovani S, Winkelman BH, Hoebeek FE, De Jeu MT, Larsen IM, Van der Burg J, Schmolesky MT, Frens MA, De Zeeuw CI (2006) Purkinje cells in awake behaving animals operate at the upstate membrane potential. Nat Neurosci 9:459-461; author reply 461.

Schreiber S, Fellous JM, Tiesinga P, Sejnowski TJ (2004) Influence of ionic conductances on spike timing reliability of cortical neurons for suprathreshold rhythmic inputs. J Neurophysiol 91:194-205.

Schreurs BG, Tomsic D, Gusev PA, Alkon DL (1997) Dendritic excitability microzones and occluded long-term depression after classical conditioning of the rabbit's nictitating membrane response. J Neurophysiol 77:86-92.

Schreurs BG, Gusev PA, Tomsic D, Alkon DL, Shi T (1998) Intracellular correlates of acquisition and long-term memory of classical conditioning in Purkinje cell dendrites in slices of rabbit cerebellar lobule HVI. J Neurosci 18:5498-5507.

Scott LL, Hage TA, Golding NL (2007) Weak action potential backpropagation is associated with high-frequency axonal firing capability in principal neurons of the gerbil medial superior olive. J Physiol 583:647-661.

Segev I (1990) Computer study of presynaptic inhibition controlling the spread of action potentials into axonal terminals. J Neurophysiol 63:987-998.

Segev I, Rall W (1988) Computational study of an excitable dendritic spine. J Neurophysiol 60:499-523.

Segev I, Rall W (1998) Excitable dendrites and spines: earlier theoretical insights elucidate recent direct observations. Trends Neurosci 21:453-460.

Segev I, Burke RE (1998) Compartmental models of complex neurons. In: Mothos in neuronal modeling: from ions to networks (Koch C, Segev I, eds). Cambidge, Massachusetts: The MIT Press.

Segev I, Schneidman E (1999) Axons as computing devices: basic insights gained from models. J Physiol Paris 93:263-270.

Segev I, London M (2000) Untangling dendrites with quantitative models. Science 290:744-750.

Sekirnjak C, du Lac S (2002) Intrinsic firing dynamics of vestibular nucleus neurons. J Neurosci 22:2083-2095.

Sekirnjak C, Vissel B, Bollinger J, Faulstich M, du Lac S (2003) Purkinje cell synapses target physiologically unique brainstem neurons. J Neurosci 23:6392-6398.

Serodio P, Rudy B (1998) Differential expression of Kv4 K+ channel subunits mediating subthreshold transient K+ (A-type) currents in rat brain. J Neurophysiol 79:1081-1091.

Servais L, Bearzatto B, Hourez R, Dan B, Schiffmann SN, Cheron G (2004) Effect of simple spike firing mode on complex spike firing rate and waveform in cerebellar Purkinje cells in non-anesthetized mice. Neurosci Lett 367:171-176.

Servais L, Bearzatto B, Schwaller B, Dumont M, De Saedeleer C, Dan B, Barski JJ, Schiffmann SN, Cheron G (2005) Mono- and dual-frequency fast cerebellar oscillation in mice lacking parvalbumin and/or calbindin D-28k. Eur J Neurosci 22:861-870.

Shah BS, Stevens EB, Pinnock RD, Dixon AK, Lee K (2001) Developmental expression of the novel voltage-gated sodium channel auxiliary subunit beta3, in rat CNS. J Physiol 534:763-776.

Sharp AA, O'Neil MB, Abbott LF, Marder E (1993) Dynamic clamp: computer-generated conductances in real neurons. J Neurophysiol 69:992-995.

Shen GY, Chen WR, Midtgaard J, Shepherd GM, Hines ML (1999) Computational analysis of action potential initiation in mitral cell soma and dendrites based on dual patch recordings. J Neurophysiol 82:3006-3020.

Silver RA, Cull-Candy SG, Takahashi T (1996) Non-NMDA glutamate receptor occupancy and open probability at a rat cerebellar synapse with single and multiple release sites. J Physiol 494 (Pt 1):231-250.

Silver RA, Momiyama A, Cull-Candy SG (1998) Locus of frequency-dependent depression identified with multiple-probability fluctuation analysis at rat climbing fibre-Purkinje cell synapses. J Physiol 510 (Pt 3):881-902.

Sjostrom PJ, Nelson SB (2002) Spike timing, calcium signals and synaptic plasticity. Curr Opin Neurobiol 12:305-314.

Sjostrom PJ, Häusser M (2006) A cooperative switch determines the sign of synaptic plasticity in distal dendrites of neocortical pyramidal neurons. Neuron 51:227-238.

Song P, Yang Y, Barnes-Davies M, Bhattacharjee A, Hamann M, Forsythe ID, Oliver DL, Kaczmarek LK (2005) Acoustic environment determines phosphorylation state of the Kv3.1 potassium channel in auditory neurons. Nat Neurosci 8:1335-1342.

Southan AP, Robertson B (2000) Electrophysiological characterization of voltage-gated K(+) currents in cerebellar basket and purkinje cells: Kv1 and Kv3 channel subfamilies are present in basket cell nerve terminals. J Neurosci 20:114-122.

Spencer WA, Kandel ER (1961) Electrophysiology of hippocampal neurons. IV. Fast prepotentials. J Neurophysiol 24:272-285.

Spruston N (2003) Branching out: a new idea for dendritic function. Focus on "Coincidence detection in pyramidal neurons is tuned by their dendritic branching pattern". J Neurophysiol 89:2887-2888.

Spruston N, Jaffe DB, Johnston D (1994) Dendritic attenuation of synaptic potentials and currents: the role of passive membrane properties. Trends Neurosci 17:161-166.

Spruston N, Stuart GJ, Häusser M (2008) Dendritic integration. In: Dendrites (Stuart GJ, Spruston N, Häusser M, eds). Oxford: Oxford University Press.

Spruston N, Jaffe DB, Williams SH, Johnston D (1993) Voltage- and space-clamp errors associated with the measurement of electrotonically remote synaptic events. J Neurophysiol 70:781-802.

Spruston N, Schiller Y, Stuart G, Sakmann B (1995) Activity-dependent action potential invasion and calcium influx into hippocampal CA1 dendrites. Science 268:297-300.

Steuber V, Mittmann W, Hoebeek FE, Silver RA, De Zeeuw CI, Häusser M, De Schutter E (2007) Cerebellar LTD and pattern recognition by Purkinje cells. Neuron 54:121-136.

Stocker M (2004) Ca(2+)-activated K+ channels: molecular determinants and function of the SK family. Nat Rev Neurosci 5:758-770.

Stocker M, Pedarzani P (2000) Differential distribution of three Ca(2+)-activated K(+) channel subunits, SK1, SK2, and SK3, in the adult rat central nervous system. Mol Cell Neurosci 15:476-493.

Storm JF (1988) Temporal integration by a slowly inactivating K+ current in hippocampal neurons. Nature 336:379-381.

Stuart G, Häusser M (1994) Initiation and spread of sodium action potentials in cerebellar Purkinje cells. Neuron 13:703-712.

Stuart G, Schiller J, Sakmann B (1997a) Action potential initiation and propagation in rat neocortical pyramidal neurons. J Physiol 505 (Pt 3):617-632.

Stuart G, Spruston N, Sakmann B, Häusser M (1997b) Action potential initiation and backpropagation in neurons of the mammalian CNS. Trends Neurosci 20:125-131.

Stuart GJ, Sakmann B (1994) Active propagation of somatic action potentials into neocortical pyramidal cell dendrites. Nature 367:69-72.

Stuart GJ, Häusser M (2001) Dendritic coincidence detection of EPSPs and action potentials. Nat Neurosci 4:63-71.

Stuart GJ, Dodt HU, Sakmann B (1993) Patch-clamp recordings from the soma and dendrites of neurons in brain slices using infrared video microscopy. Pflugers Arch 423:511-518.

Sugihara I (2005) Microzonal projection and climbing fiber remodeling in single olivocerebellar axons of newborn rats at postnatal days 4-7. J Comp Neurol 487:93-106.

Sugihara I (2006) Organization and remodeling of the olivocerebellar climbing fiber projection. Cerebellum 5:15-22.

Sugihara I, Shinoda Y (2004) Molecular, topographic, and functional organization of the cerebellar cortex: a study with combined aldolase C and olivocerebellar labeling. J Neurosci 24:8771-8785.

Sugihara I, Quy PN (2007) Identification of aldolase C compartments in the mouse cerebellar cortex by olivocerebellar labeling. J Comp Neurol 500:1076-1092.

Sugihara I, Wu HS, Shinoda Y (2001) The entire trajectories of single olivocerebellar axons in the cerebellar cortex and their contribution to Cerebellar compartmentalization. J Neurosci 21:7715-7723.

Sugihara I, Marshall SP, Lang EJ (2007) Relationship of complex spike synchrony bands and climbing fiber projection determined by reference to aldolase C compartments in crus IIa of the rat cerebellar cortex. J Comp Neurol 501:13-29.

Swensen AM, Bean BP (2003) Ionic mechanisms of burst firing in dissociated Purkinje neurons. J Neurosci 23:9650-9663.

Swensen AM, Bean BP (2005) Robustness of burst firing in dissociated purkinje neurons with acute or long-term reductions in sodium conductance. J Neurosci 25:3509-3520.

Takahashi M, Kovalchuk Y, Attwell D (1995) Pre- and postsynaptic determinants of EPSC waveform at cerebellar climbing fiber and parallel fiber to Purkinje cell synapses. J Neurosci 15:5693-5702.

Takahashi M, Sarantis M, Attwell D (1996) Postsynaptic glutamate uptake in rat cerebellar Purkinje cells. J Physiol 497 (Pt 2):523-530.

Takatsuru Y, Takayasu Y, Iino M, Nikkuni O, Ueda Y, Tanaka K, Ozawa S (2006) Roles of glial glutamate transporters in shaping EPSCs at the climbing fiber-Purkinje cell synapses. Neurosci Res 54:140-148.

Takayasu Y, Iino M, Kakegawa W, Maeno H, Watase K, Wada K, Yanagihara D, Miyazaki T, Komine O, Watanabe M, Tanaka K, Ozawa S (2005) Differential roles of glial and neuronal glutamate transporters in Purkinje cell synapses. J Neurosci 25:8788-8793.

Tanaka J, Ichikawa R, Watanabe M, Tanaka K, Inoue Y (1997) Extra-junctional localization of glutamate transporter EAAT4 at excitatory Purkinje cell synapses. Neuroreport 8:2461-2464.

Tanaka J, Matsuzaki M, Tarusawa E, Momiyama A, Molnar E, Kasai H, Shigemoto R (2005) Number and density of AMPA receptors in single synapses in immature cerebellum. J Neurosci 25:799-807.

Tank DW, Sugimori M, Connor JA, Llinas RR (1988) Spatially resolved calcium dynamics of mammalian Purkinje cells in cerebellar slice. Science 242:773-777.

Taschenberger H, von Gersdorff H (2000) Fine-tuning an auditory synapse for speed and fidelity: developmental changes in presynaptic waveform, EPSC kinetics, and synaptic plasticity. J Neurosci 20:9162-9173.

Taylor AL, Hickey TJ, Prinz AA, Marder E (2006) Structure and visualization of high-dimensional conductance spaces. J Neurophysiol 96:891-905.

Telgkamp P, Raman IM (2002) Depression of inhibitory synaptic transmission between Purkinje cells and neurons of the cerebellar nuclei. J Neurosci 22:8447-8457.

Tempia F, Kano M, Schneggenburger R, Schirra C, Garaschuk O, Plant T, Konnerth A (1996) Fractional calcium current through neuronal AMPA-receptor channels with a low calcium permeability. J Neurosci 16:456-466.

Thach WT, Jr. (1967) Somatosensory receptive fields of single units in cat cerebellar cortex. J Neurophysiol 30:675-696.

Tringham EW, Payne CE, Dupere JR, Usowicz MM (2007) Maturation of rat cerebellar Purkinje cells reveals an atypical Ca2+ channel current that is inhibited by omega-agatoxin IVA and the dihydropyridine (-)-(S)-Bay K8644. J Physiol 578:693-714.

Trussell LO (1997) Cellular mechanisms for preservation of timing in central auditory pathways. Curr Opin Neurobiol 7:487-492.

Trussell LO (1999) Synaptic mechanisms for coding timing in auditory neurons. Annu Rev Physiol 61:477-496.

Tsaur ML, Chou CC, Shih YH, Wang HL (1997) Cloning, expression and CNS distribution of Kv4.3, an A-type K+ channel alpha subunit. FEBS Lett 400:215-220.

Turrigiano G (2007) Homeostatic signaling: the positive side of negative feedback. Curr Opin Neurobiol 17:318-324.

Turner RW, Lemon N, Doiron B, Rashid AJ, Morales E, Longtin A, Maler L, Dunn RJ (2002) Oscillatory burst discharge generated through conditional backpropagation of dendritic spikes. J Physiol Paris 96:517-530.

Usowicz MM, Sugimori M, Cherksey B, Llinas R (1992) P-type calcium channels in the somata and dendrites of adult cerebellar Purkinje cells. Neuron 9:1185-1199.

Van Der Giessen RS, Koekkoek SK, van Dorp S, De Gruijl JR, Cupido A, Khosrovani S, Dortland B, Wellershaus K, Degen J, Deuchars J, Fuchs EC, Monyer H, Willecke K, De Jeu MT, De Zeeuw CI (2008) Role of olivary electrical coupling in cerebellar motor learning. Neuron 58:599-612.

Vargas G, Yeh TY, Blumenthal DK, Lucero MT (1999) Common components of patch-clamp internal recording solutions can significantly affect protein kinase A activity. Brain Res 828:169-173.

Vega-Saenz de Miera EC, Rudy B, Sugimori M, Llinas R (1997) Molecular characterization of the sodium channel subunits expressed in mammalian cerebellar Purkinje cells. Proc Natl Acad Sci U S A 94:7059-7064.

Veh RW, Lichtinghagen R, Sewing S, Wunder F, Grumbach IM, Pongs O (1995) Immunohistochemical localization of five members of the Kv1 channel subunits: contrasting subcellular locations and neuron-specific co-localizations in rat brain. Eur J Neurosci 7:2189-2205.

Vervaeke K, Hu H, Graham LJ, Storm JF (2006) Contrasting effects of the persistent Na+ current on neuronal excitability and spike timing. Neuron 49:257-270.

Vetter P, Roth A, Häusser M (2001) Propagation of action potentials in dendrites depends on dendritic morphology. J Neurophysiol 85:926-937.

Vilin YY, Ruben PC (2001) Slow inactivation in voltage-gated sodium channels: molecular substrates and contributions to channelopathies. Cell Biochem Biophys 35:171-190.

Voogd J, Glickstein M (1998) The anatomy of the cerebellum. Trends Neurosci 21:370-375.

Wadiche JI, Jahr CE (2001) Multivesicular release at climbing fiber-Purkinje cell synapses. Neuron 32:301-313.

Walter JT, Khodakhah K (2006) The linear computational algorithm of cerebellar Purkinje cells. J Neurosci 26:12861-12872.

Walter JT, Alvina K, Womack MD, Chevez C, Khodakhah K (2006) Decreases in the precision of Purkinje cell pacemaking cause cerebellar dysfunction and ataxia. Nat Neurosci 9:389-397.

Wang D, Schreurs BG (2006) Characteristics of IA currents in adult rabbit cerebellar Purkinje cells. Brain Res 1096:85-96.

Wang LY, Gan L, Forsythe ID, Kaczmarek LK (1998) Contribution of the Kv3.1 potassium channel to high-frequency firing in mouse auditory neurones. J Physiol 509 (Pt 1):183-194.

Wang S, Xing TR, Tang ML, Yong W, Li CC, Chen L, Wang HL, Tang JL, Ruan DY (2008) Effects of Cd2+ on transient outward and delayed rectifier potassium currents in acutely isolated rat hippocampal CA1 neurons. Naunyn Schmiedebergs Arch Pharmacol 377:245-253.

Wang SS, Denk W, Häusser M (2000) Coincidence detection in single dendritic spines mediated by calcium release. Nat Neurosci 3:1266-1273.

Wang Y, Strahlendorf JC, Strahlendorf HK (1991) A transient voltage-dependent outward potassium current in mammalian cerebellar Purkinje cells. Brain Res 567:153-158.

Watt A, Cuntz H, Mori M, Nusser Z, Sjostrom J, Häusser M (*In review*) Traveling waves in juvenile cerebellar cortex mediated by directed synaptic connections between Purkinje cells. Nat Neurosci.

Wei DS, Mei YA, Bagal A, Kao JP, Thompson SM, Tang CM (2001) Compartmentalized and binary behavior of terminal dendrites in hippocampal pyramidal neurons. Science 293:2272-2275.

Weiser M, Vega-Saenz de Miera E, Kentros C, Moreno H, Franzen L, Hillman D, Baker H, Rudy B (1994) Differential expression of Shaw-related K+ channels in the rat central nervous system. J Neurosci 14:949-972.

Welsh JP, Llinas R (1997) Some organizing principles for the control of movement based on olivocerebellar physiology. Prog Brain Res 114:449-461.

Welsh JP, Lang EJ, Suglhara I, Llinas R (1995) Dynamic organization of motor control within the olivocerebellar system. Nature 374:453-457.

Westenbroek RE, Hell JW, Warner C, Dubel SJ, Snutch TP, Catterall WA (1992) Biochemical properties and subcellular distribution of an N-type calcium channel alpha 1 subunit. Neuron 9:1099-1115.

Westenbroek RE, Sakurai T, Elliott EM, Hell JW, Starr TV, Snutch TP, Catterall WA (1995) Immunochemical identification and subcellular distribution of the alpha 1A subunits of brain calcium channels. J Neurosci 15:6403-6418.

Widmer HA, Rowe IC, Shipston MJ (2003) Conditional protein phosphorylation regulates BK channel activity in rat cerebellar Purkinje neurons. J Physiol 552:379-391.

Williams SR (2004) Spatial compartmentalization and functional impact of conductance in pyramidal neurons. Nat Neurosci 7:961-967.

Williams SR, Stuart GJ (1999) Mechanisms and consequences of action potential burst firing in rat neocortical pyramidal neurons. J Physiol 521 Pt 2:467-482.

Williams SR, Stuart GJ (2000) Site independence of EPSP time course is mediated by dendritic I(h) in neocortical pyramidal neurons. J Neurophysiol 83:3177-3182.

Williams SR, Stuart GJ (2002) Dependence of EPSP efficacy on synapse location in neocortical pyramidal neurons. Science 295:1907-1910.

Williams SR, Stuart GJ (2003) Role of dendritic synapse location in the control of action potential output. Trends Neurosci 26:147-154.

Williams SR, Mitchell SJ (2008) Direct measurement of somatic voltage clamp errors in central neurons. Nat Neurosci 11:790-798.

Williams SR, Christensen SR, Stuart GJ, Häusser M (2002) Membrane potential bistability is controlled by the hyperpolarization-activated current I(H) in rat cerebellar Purkinje neurons in vitro. J Physiol 539:469-483.

Wollner DA, Catterall WA (1986) Localization of sodium channels in axon hillocks and initial segments of retinal ganglion cells. Proc Natl Acad Sci U S A 83:8424-8428.

Womack M, Khodakhah K (2002a) Active contribution of dendrites to the tonic and trimodal patterns of activity in cerebellar Purkinje neurons. J Neurosci 22:10603-10612.

Womack MD, Khodakhah K (2002b) Characterization of large conductance Ca2+-activated K+ channels in cerebellar Purkinje neurons. Eur J Neurosci 16:1214-1222.

Womack MD, Khodakhah K (2003) Somatic and dendritic small-conductance calcium-activated potassium channels regulate the output of cerebellar purkinje neurons. J Neurosci 23:2600-2607.

Womack MD, Khodakhah K (2004) Dendritic control of spontaneous bursting in cerebellar Purkinje cells. J Neurosci 24:3511-3521.

Womack MD, Chevez C, Khodakhah K (2004) Calcium-activated potassium channels are selectively coupled to P/Q-type calcium channels in cerebellar Purkinje neurons. J Neurosci 24:8818-8822.

Xia XM, Fakler B, Rivard A, Wayman G, Johnson-Pais T, Keen JE, Ishii T, Hirschberg B, Bond CT, Lutsenko S, Maylie J, Adelman JP (1998) Mechanism of calcium gating in small-conductance calcium-activated potassium channels. Nature 395:503-507.

Xiong W, Chen WR (2002) Dynamic gating of spike propagation in the mitral cell lateral dendrites. Neuron 34:115-126.

Xu-Friedman MA, Regehr WG (2004) Structural contributions to short-term synaptic plasticity. Physiol Rev 84:69-85.

Xu-Friedman MA, Regehr WG (2005) Dynamic-clamp analysis of the effects of convergence on spike timing. I. Many synaptic inputs. J Neurophysiol 94:2512-2525.

Xu-Friedman MA, Harris KM, Regehr WG (2001) Three-dimensional comparison of ultrastructural characteristics at depressing and facilitating synapses onto cerebellar Purkinje cells. J Neurosci 21:6666-6672.

Yamada KA, Tang CM (1993) Benzothiadiazides inhibit rapid glutamate receptor desensitization and enhance glutamatergic synaptic currents. J Neurosci 13:3904-3915.

Yokoyama CT, Westenbroek RE, Hell JW, Soong TW, Snutch TP, Catterall WA (1995) Biochemical properties and subcellular distribution of the neuronal class E calcium channel alpha 1 subunit. J Neurosci 15:6419-6432.

Yunker AM, Sharp AH, Sundarraj S, Ranganathan V, Copeland TD, McEnery MW (2003) Immunological characterization of T-type voltage-dependent calcium channel CaV3.1 (alpha 1G) and CaV3.3 (alpha 1I) isoforms reveal differences in their localization, expression, and neural development. Neuroscience 117:321-335.

Zagha E, Lang EJ, Rudy B (2008) Kv3.3 channels at the Purkinje cell soma are necessary for generation of the classical complex spike waveform. J Neurosci 28:1291-1300.

Zhang L, Weiner JL, Valiante TA, Velumian AA, Watson PL, Jahromi SS, Schertzer S, Pennefather P, Carlen PL (1994) Whole-cell recording of the Ca(2+)-dependent slow

afterhyperpolarization in hippocampal neurones: effects of internally applied anions. Pflugers Arch 426:247-253.

Zhang W, Linden DJ (2003) The other side of the engram: experience-driven changes in neuronal intrinsic excitability. Nat Rev Neurosci 4:885-900.

Zhu JJ (2000) Maturation of layer 5 neocortical pyramidal neurons: amplifying salient layer 1 and layer 4 inputs by Ca2+ action potentials in adult rat tuft dendrites. J Physiol 526 Pt 3:571-587.